Angular Correlation of Electrons Emitted by Double Auger Decay of K-Shell Ionized Neon

by

Matthew Philip Jones

A dissertation submitted to the Graduate Faculty of
Auburn University
in partial fulfillment of the
requirements for the Degree of
Doctor of Philosophy

Auburn, Alabama
August 06, 2011

Keywords: Neon, Double, Auger, Angular, Correlation, COLTRIMS, PCI, PDI, K-Shell, core-ion

Approved by

Allen L. Landers, Chairman, Associate Professor of Physics
Mike Fogle, Assistant Professor of Physics
Stuart Loch, Associate Professor of Physics
Terry Austin, Affiliated Professor of Physics

Abstract

We have investigated in detail the 4-body continuum state produced when core-ionized neon undergoes Double-Auger (DA) decay, using COLd Target Recoil Ion Momentum Spectroscopy (COLTRIMS). We conducted the experiment at the Lawrence Berkeley National Laboratory's Advanced Light Source (LBNL-ALS) beamline 11.0.2. The synchrotron operated in 2-bunch mode and outputted an elliptically polarized, pulsed photon beam ($h\nu$=872.9eV), sufficient to K-shell ionize neon just above threshold.

Our analysis supports research showing that Auger electrons tend to share energy asymmetrically. We qualitatively compared this result to Photo-Double Ionization (PDI) of helium. Further, we confirm research that shows how Auger electrons that share energy symmetrically can be modeled by the elastic-like knock-out process plus Post-Collision Interaction (PCI) effects.

New observations include the angular correlation between the photo-electron and each respective Auger electron, for specific ranges of energy sharing. We identify a broad feature in the asymmetric case that shows a level of interaction between electrons that until recently, has disagreed with theory. Additionally, we consider the angular correlation between the photo-electron and the momentum sum of the Auger electrons. We observe that the angular correlation between this sum and the photo-electron in the highly asymmetric case is nearly identical to the correlation between just the fast-Auger and the photo-electron - as expected. In the case of symmetric energy sharing, the sum momentum vector appears to be isotropic, particularly for small angles of interaction.

Finally, we acknowledge two novel methods of calibration. The first, uses well known line-energies to calibrate the spectrometer. These lines correspond to the decay channels of core-excited neon, $Ne(1s^{-1}3p)$. The second, describes a method to statistically weight list-mode data in order to calibrate it to well known physical features (e.g., isotropic distributions).

Acknowledgments

Some three decades ago, I began an academic journey. Along the way, I have reached many milestones, each of which has inspired me to press ahead to the next. The dissertation presented here represents a special marker along a long road of scholarship. From this vantage point I look ahead with eager anticipation of future destinations. I also take time to look back on fond memories, important lessons learned and most of all, those influential people who have helped me arrive at this special place in my life - the view from here is most beautiful. To my parents, Phil and Nancy, words are insufficient to express my thanks for your unwavering devotion and encouragement throughout my life. I am very grateful to have been given such good direction so early on in my journey. Thanks also to the many who have provided me assistance, advice and opportunity along the way. A special thanks goes to my advisor, Allen L. Landers for his role in equiping me for my future travels.

Table of Contents

List of Figures

List of Tables

Chapter 1

INTRODUCTION

The Auger decay process has been the subject of extensive research ever since it became the namesake of its discoverer in 1925. [1][1] In this atomic process, a bound electron undergoes an exoergic transition, which results in the placement of a second electron into the continuum. Conservation requires that the energy of an Auger electron represent its respective element. This identifying characteristic has been exploited in various techniques such as Auger Electron Spectroscopy (AES), Scanning Auger Microscopy (SAM) and X-ray Photo-electron Spectroscopy (XPS)[8]. Of course, a further understanding of the Auger decay process is not to the exclusive benefit of the applied physics community; it additionally affords researchers considerable insight into the inner-shell structure of atoms - as evidenced by the experimental and theoretical results which have been gathered over the decades since Pierre Auger first submitted his findings.[4][6][10][11][12][13][40]

We begin this chapter by considering the decay channels that result when neon is core-excited to the $3p$ state (Eq1.1). Of particular interest is the rich spectrum of line energies that make up the Ne^{2+} charge state.[21][34] Despite our initial interest in the angular correlation between these emitted electrons, we later realized that the series of line energies could be utilized as a precise means of spectrometer calibration. Accordingly, we briefly introduce some of the pertinent details that lead us to this new method.

Next, attention turns to the decay channels that relate to the core-ionization of neon, just above threshold (Eq.1.2). We compare theoretical channels with experimental data. We briefly comment on each charge state and its role within this body of research. Special attention is given to the single Auger decay mechanism that is associated with the Ne^{2+} charge state since these details have

[1] While the credit of discovery goes to Auger, it was Lise Meitner who first observed this process in 1922.

provided much of the motivation for this work.[40] Further, we provide a comprehensive review of published results that pertains to the single-Auger decay mechanism.[6][9][28][29][36][37][40]

The details of single-Auger physics lead into a discussion of the Double-Auger, DA decay mechanism. We present an overview of published work on the subject, specifically with regard to the angular correlation between continuum electrons.[2][3][5][15][17][19][20][24][27][25][29][39] A comparison is drawn between the DA decay of core ionized neon and the seemingly different phenomenon, the Photo Double Ionization, PDI of helium.[23][30][33][22]

Having identified the decay channels of interest, we investigate specific relaxation dynamics that are associated with the core-ionized target. We discuss Post-Collision-Interaction, PCI, which is later observed in the many-body Coulomb break-up of the target atom.[18][35] Additionally, we provide calculations that describe the method we used to select the photon energy at the beamline. The chapter concludes with a description of the shake-off model and the knock-out picture.[9][39] Each of these topics are used within the Atomic Molecular & Optical (AMO) physics community to facilitate the communication of specific quantum mechanical details, associated with the aforementioned atomic processes.

1.1 The Decay Channels of K-Excited Neon

Over the course of eight days ($03/04/09 - 03/11/09$), a small battery of COLd Target Recoil Ion Momentum Spectroscopy (COLTRIMS) experiments were conducted at the LBNL-ALS beamline 11.0.2. While the primary objective throughout the beam time was to investigate the K-ionization of neon, we also collected a few smaller, tangential data sets; it has become standard practice among group members to probe around a bit on side projects in order to better prepare for future beam times. It was in this spirit that a small data set was recorded on $03/11/09$. The pulsed photon energy at the beamline was specified to produce the initial $3p$-state,

$$Ne + \gamma(867\text{eV}) \rightarrow Ne(1s2s^2 2p^6 3p) \tag{1.1}$$

The subsequent decay of this state produces numerous channels. The published work shown in Figure 1.1 reveals the spectrum of lines that results when the initial state relaxes.[21] We show later in Chapter 3 how these lines can be used to calibrate our spectrometer. For now, we will provide a short summary of this published work.

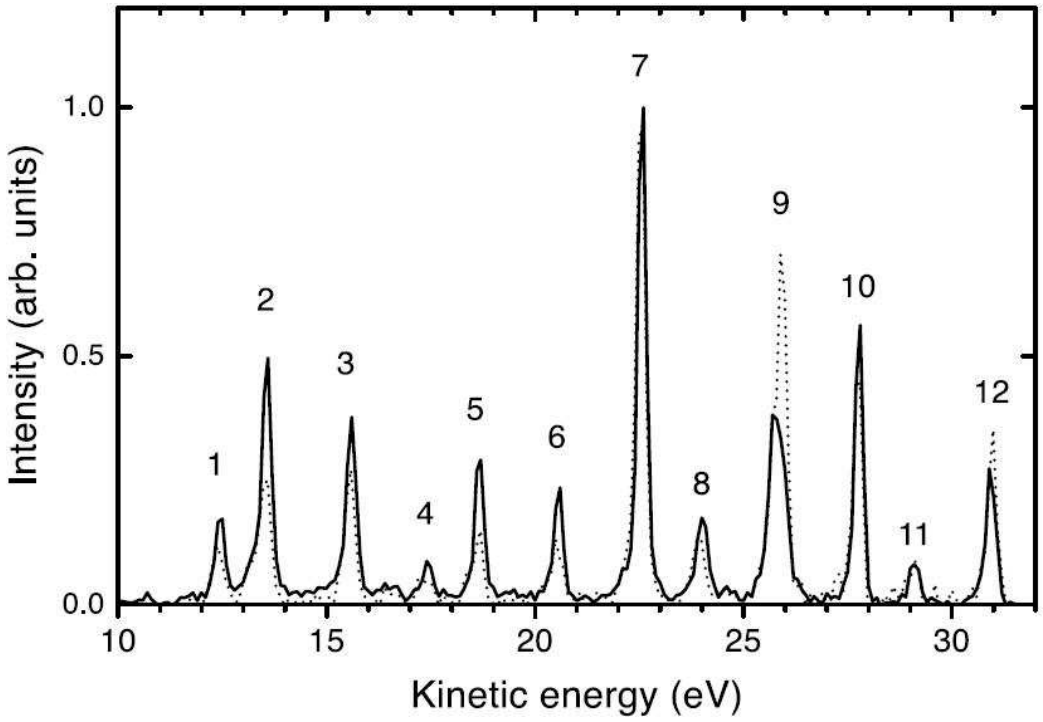

Figure 1.1: A segment of the second-step Auger spectrum that results from the transition between the initial $Ne(1s^{-1}3p)$ state and final Ne^{2+} states. The two curves are representative of the recorded angle relative to the photon polarization axis. Each curve was normalized by the photon beam intensity. We use this span of line energies to calibrate the spectrometer.

1.1.1 Specifics on the Line Energies

The cited work by Yoshida *et al.* was conducted at SPring-8 (Japan), during two-bunch mode operation[21]. A photon energy of 867eV was specified in order to populate neon to the $3p$ core-excited state. The method of experiment incorporated two angle-resolving TOF spectrometers. The analyzers were mounted inside a rotating chamber, in a plane that was perpendicular to the pulsed beam. This setup allowed for the precise measurement of both the kinetic energy and direction

of electron emission. The enumerated peaks shown in Figure 1.1 are identified in the table below (Tab.1.2).

Table 1.1: Selected Transition Energies as Reported by Yoshida

Line No.	Transition	KE (eV)
1	$2s^1 2p^5(^3P)3p \rightarrow 2s^2 2p^4(^1D_2)$	12.6
2	$2s^0 2p^6(^1S)3p \rightarrow 2s^1 2p^5(^1P_1)$	13.6
3	$2s^1 2p^5(^3P)3p \rightarrow 2s^2 2p^4(^3P)$	15.7
4	$2s^1 2p^5(^3P)4p \rightarrow 2s^2 2p^4(^1D_2)$	17.4
5	$2s^0 2p^6(^1S)4p \rightarrow 2s^1 2p^5(^1P_1)$	18.7
6	$2s^1 2p^5(^3P)4p \rightarrow 2s^2 2p^4(^3P)$	20.6
7	$2s^1 2p^5(^1P)3p \rightarrow 2s^2 2p^4(^1D_2)$	22.6
8	$2s^0 2p^6(^1S)3p \rightarrow 2s^1 2p^5(^3P)$	24.1
9	$2s^1 2p^5(^1P)3p \rightarrow 2s^2 2p^4(^3P)$	25.7
10	$2s^1 2p^5(^1P)4p \rightarrow 2s^2 2p^4(^1D_2)$	27.8
11	$2s^0 2p^6(^1S)4p \rightarrow 2s^1 2p^5(^3P)$	29.1
12	$2s^1 2p^5(^1P)4p \rightarrow 2s^2 2p^4(^3P)$	30.9

Table 1.2: The enumerated transition energies correspond to the peaks shown in Figure 1.1. Also provided is the kinetic energy of the respective electron.[21].

1.1.2 A Novel Method of Calibration

As mentioned earlier, we first considered investigating the rich spectrum of decay channels that result from the core-excitation of Ne^{2+} out of an interest in furthering our understanding of the respective electron-electron correlations. While our preliminary analysis did not indicate this to be a fruitful pursuit, we did recognize a use for the data set. Refering to Figure 1.1, we note the range of energy shown spans thirty electron-volts! We take advantage of this broad band feature to calibrate the spectrometer.[2]

The design of a COLTRIMS-style spectrometer enables us to measure the Time-Of-Flight (TOF) of a charged particle. We can determine the momentum of such a particle provided we can measure

[2]Details of the spectrometer are provided in Chapter 2 and the calibration method is described in detail in Chapter 3.

the magnitude of the applied electric field and the distance the particle travels (i.e., the length of the acceleration region). It is these parameters that are related to the TOF of the particle (i.e., the particle is influenced by these parameters). As will be shown in Chapter 3, the magnitude of electric field is **directly** proportional to the TOF whereas, the length of the acceleration region is **inversely** proportional to the TOF. Therefore, we can use these well known lines[21] to calibrate the spectrometer; lines of high-energy are used to calibrate the electric field and lines of low-energy, to calibrate the length of the acceleration region (Fig.1.1). We can then carry these parameters over to the next analysis (K-ionization of neon), confident of their accuracy.

1.2 The Decay Channels of K-Ionized Neon

While a small data set was taken with regard to the K-excitation of neon, the majority of beam time was devoted to investigating the K-*ionization* of neon. Specifically, we were interested in observing the angular correlation between electrons that are launched into the continuum by way of DA decay. The motivation for such work is rooted in questions that arise out of a similar, single-Auger decay analysis. In each case we begin with the same initial state of neon, core-ionized just above threshold:

$$Ne + \gamma(872.9\text{eV}) \rightarrow Ne(1s2s^2 2p^6)^+ + e_\gamma^- \tag{1.2}$$

Many decay channels can be calculated from this initial state. Figure 1.2 represents a diagram of the energetically allowed states.[3] This representation was particularly useful in ruling out a cascade effect for the production of the Ne^{3+} charge state (i.e., it is energetically forbidden for the initial state to intermediately decay into Ne^{2+} on its way to Ne^{3+}). Therefore, single photon interactions that lead to Ne^{3+} by way of 1*s* core-ionization *must* be due to DA decay.

We also observe that decay channels within a specific charge state are sufficiently close in energy to be resolved by our spectrometer. Therefore, we must consider the overall contribution

[3]Special thanks goes to M. Pindzola for his calculation of the $Ne^{1s^{-1}}$ decay channels.

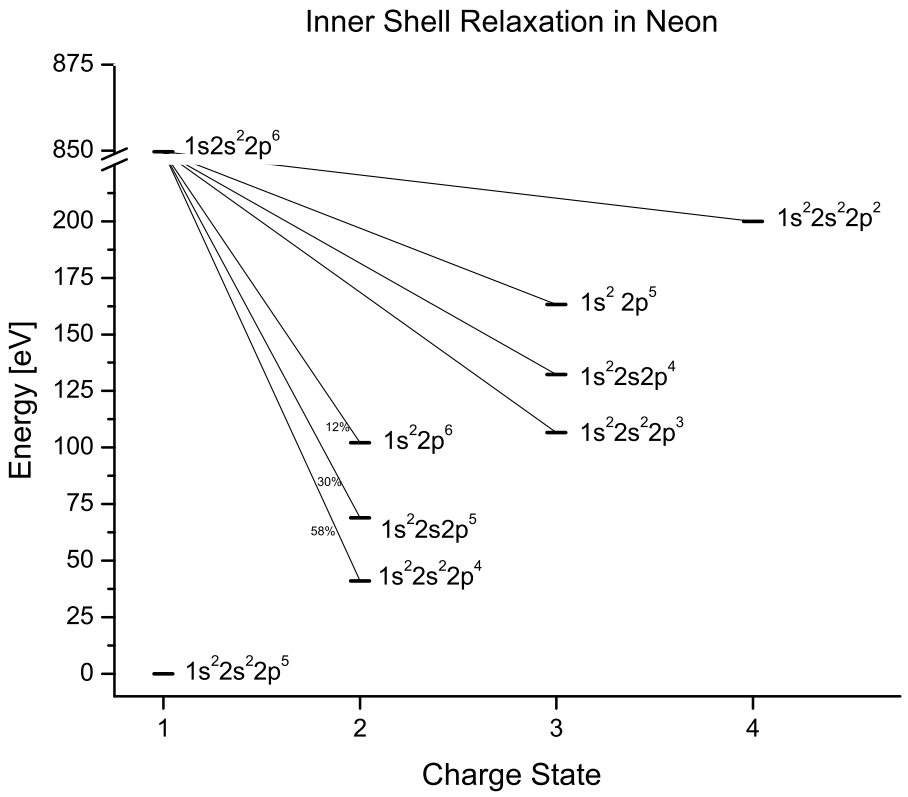

Figure 1.2: Theory predicts the following decay channels are possible with 1*s* core-ionized neon. Note, it is energetically forbidden to arrive at Ne^{3+} using Ne^{2+} as an intermediate step.

each decay channel makes to the charge state of interest. We will comment on this point once more in Chapter 6 when we look at the energy sharing characteristics of DA electrons.

1.3 Products of the Initial State

When we conducted our experiment at beamline 11.0.2, we observed five charge states associated with the decay of the intial state Eq.1.1. Additionally, three naturally occurring isotopes were revealed in their respective abundances (Fig.1.3). We briefly discuss these charge states below.

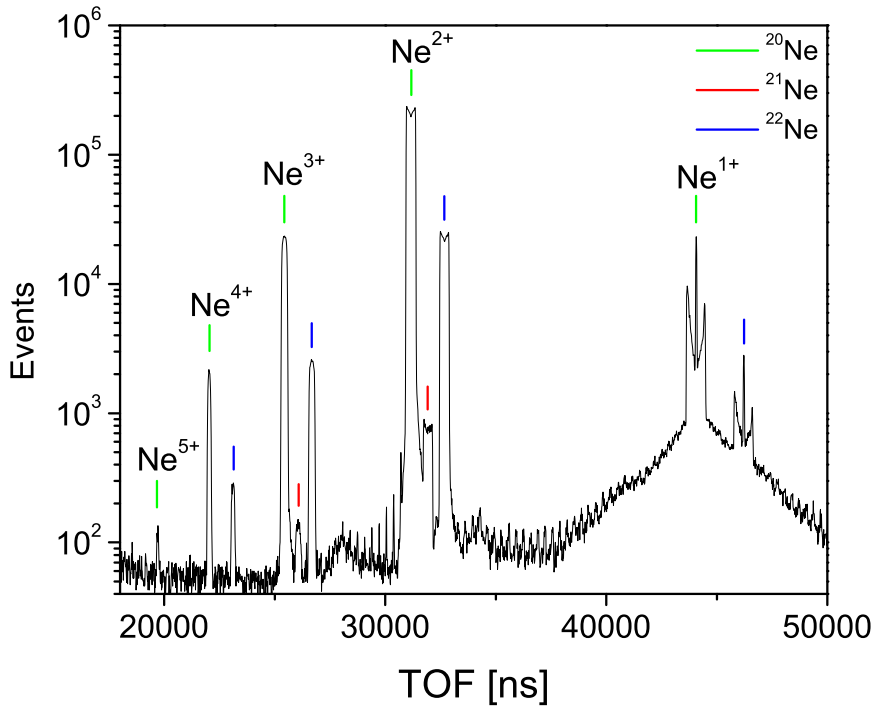

Figure 1.3: The charge states acquired during the experiment are shown. Note the dominant Ne^{2+} channel associated with single Auger decay. We also note smaller distributions of Ne^{3+} and Ne^{4+}. Each of the three naturally occurring isotopes is labeled, where applicable.

1.3.1 The Radiative Decay Channel

The 1^{st} decay channel of interest is the radiative decay channel. While the energy of the $2p \rightarrow 1s$ transition tends to transfer to one or more valence electrons, it is possible, albeit less likely, for this transition energy to manifest itself as a photon. The decay channels associated with Ne^{+} are shown in below,

$$\underbrace{Ne(1s^2 2s^2 2p^6) + h\nu(872.9eV)}_{\downarrow} \longrightarrow \overbrace{Ne^{+} + e^{-}_{fast}}^{\text{Direct Ionization/Recapture}}$$

$$Ne(1s^{-1})^{+} + e^{-}_{\gamma}(1.7eV) \rightarrow \underbrace{Ne(2p^{-1})^{+} + e^{-}_{\gamma} + \gamma}_{\text{Radiative Decay}}$$

We can use Figure 1.3 to identify the radiative decay channel. It is seen as a narrow central spike within the Ne^+ distribution (Fig.1.3). As will be discussed in Chapter 4, this narrow distribution reflects a minimum in momentum transfer to the recoil ion. This can only be reconciled if we consider that the low-momentum photo-electron is the only electronic emission to occur during the event. Given the required electronic relaxation that subsequently occurs, this transition energy must manifest itself as a photon (to minimize recoil momentum). By comparison, the structure that surrounds the central spike shows a much higher recoil momentum. We can attribute this to either the direct ionization of the valence shell or an Auger decay which occurs rapidly enough to allow the residual Ne^{2+} ion to recapture the photo-electron, a process to be explained in more detail later.

1.3.2 Angular Correlation of the Single Auger Decay Channel in Neon

The motivation to conduct research on the angular correlation between continuum electrons, emitted in the DA decay of neon roots in a discrepancy between experiment and theory. Until recently,[4] the model that was used to calculate the angular correlation between a fast Auger electron and a slow photo-electron predicted a greater interaction between particles than was observed.[40] Consider the most prominent decay channel that represents the single-Auger decay mechanism (Fig1.2):

$$Ne(1s2s^22p^6)^+ +^- e_\gamma \rightarrow Ne(1s^22s^22p^4)^{2+} + e_A + e_\gamma \tag{1.3}$$

We apply the "two-step" model to describe single Auger decay: 1) the beamline photon core-ionizes the target atom, placing a slow photo-electron into the continuum, 2) a subsequent electronic transition takes place within the recoil ion, launching the fast Auger electron into the continuum. If the Auger electron is fired in the same direction as the photo-electron, one would expect a Coulomb collision to occur (i.e, the photo-electron would simply be "pushed" out of the way). In this plot we take the Auger electron of each event and declare it to co-incide with the abscissa (this amounts

[4] At the time of writing this document, modifications were made to the theory which have resulted in agreement with experiment.

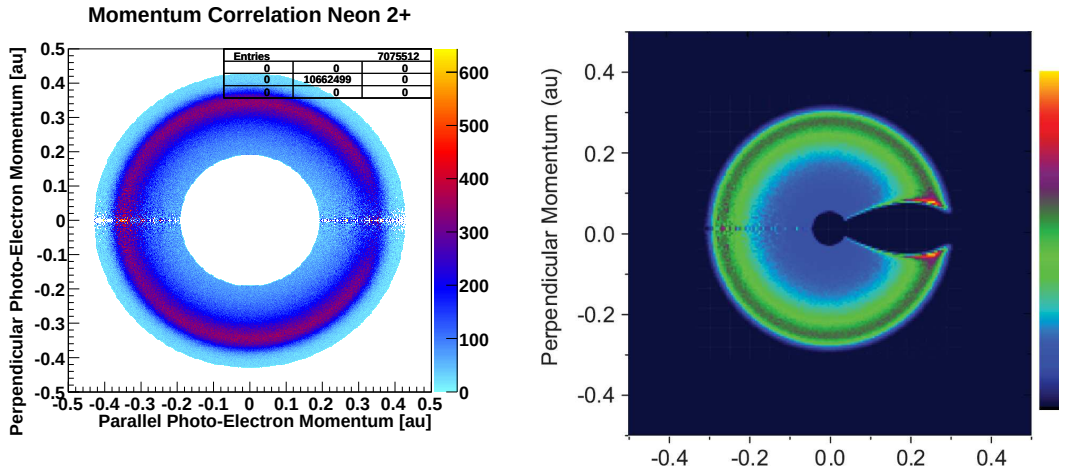

Figure 1.4: (a) The opening at 0^o indicates that the emitted Auger electron never takes the same trajectory as the photo-electron. The lack of intensity (or "pile-up") around the opening of the "C" implies that the classical notion of Coulomb scattering does not adequately explain the phenomenon. (b) A quantum mechanical Monte Carlo Simulation shows disagreement with experimental results. Here, a pile-up of event flux is present in the vicinity of the opening.

to a co-ordinate rotation of the axes). The perpendicular component of photo-electron momentum is plotted along the ordinate, the parallel component, along the abscissa. The isotropy shown throughout the majority of the plot is unsurprising; it simply corresponds to electrons which travel in differing directions. We also notice an opening along the abscissa of the plot that is also unsurprising; it corresponds to electrons traveling co-incidently. The discrepancy is found the region that borders the opening. While the theoretical calculation shows an increase of events (relative to the isotropic background), the experimental result shows no such pile-up of events[5]. The discovery challenged theorists to reconsider their models and motivated experimentalists to not only revisit the experiment, but to consider other experiments which could provide additional insight into the phenomenon (e.g., DA decay).

[5]In a later plot style the term "pile-up" will be replaced by the term, "splash."

1.3.3 Double Auger Decay

First observed nearly 50 years ago, the aptly named double-Auger decay process differs from single Auger decay in that *two* electrons are placed into the continuum subsequent to the photo-electron [3]. Figure 1.5 schematically illustrates DA decay as a two-step process. First, an incident photon core-ionizes the ground state neon atom; the low energy photo-electron is shown in red. A valance electron (shown in green) fills the $1s$ hole within its Auger lifetime ($\tau \approx 1$fs or $\Gamma = 270$meV). Two additional valance electrons (shown in blue) absorb the transition energy, leading to the triply charged ionic state.

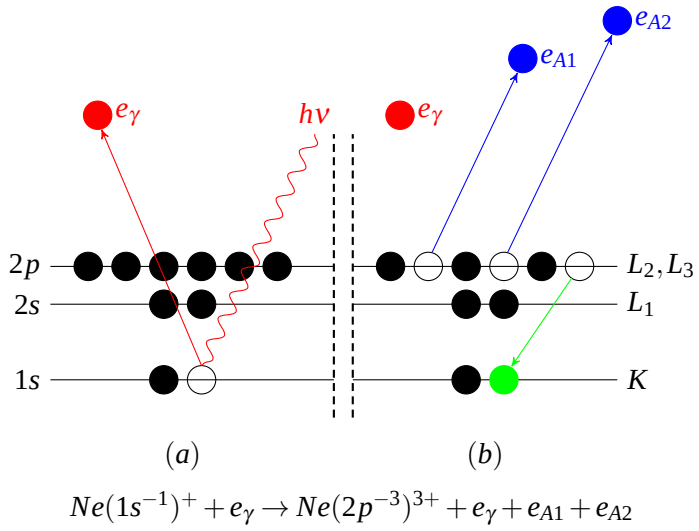

$$Ne(1s^{-1})^+ + e_\gamma \rightarrow Ne(2p^{-3})^{3+} + e_\gamma + e_{A1} + e_{A2}$$

Figure 1.5: We consider a two step representation for DA decay in Neon. Part (a) represents the initial K-ionized state of the target atom. Part (b) illustrates the exoergic transition (in green) that ultimately places two $2p$ electrons into the continuum.

1.3.4 Photo-Double Ionization of Helium

We compare the features of DA decay to those of Photo-Double Ionization (PDI) (of helium) since each represent a three-body process, whereby two electrons are placed into the continuum as a result of a single energy exchange.[23][33] A recent study by Knapp *et al.* furthered the understanding of the mechanisms that dominate the non-sequential process, specifically, the angular

correlation between emitted electrons. The referenced experiment, performed at the LBNL, utilized a COLTRIMS setup. Two photon energies were considered, $E_\gamma = 179$eV and $E_\gamma = 529$eV leading to energies in excess of the double ionization threshold of 100eV and 450eV, respectively. In addition to the experiment, Knapp *et al.* provided calculations of the final state of helium (with two electrons in the continuum).[33] In Chapter 6, we directly compare the angular correlation analyses of PDI of helium and DA decay of neon.

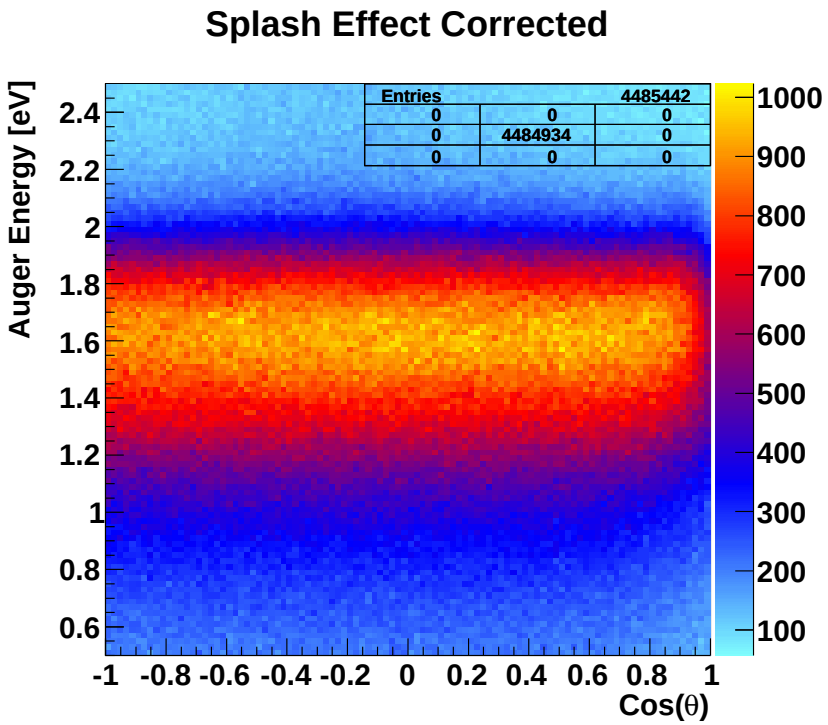

Figure 1.6: The lack of events surrounding $Cos(\theta) \approx 1$ illustrate the highlighted feature in the angular correlation between electrons in single Auger decay.

1.3.5 Higher Charge States

We also acknowledge the presence of higher charge states shown in Figure 1.3, namely Ne^{4+} and perhaps Ne^{5+}. It is suspected that the former is the result of triple-Auger decay. Noting the

possible decay channels available to the initial state (Fig.1.2), it is energetically forbidden to cascade to Ne^{4+}. Perhaps this will someday be a topic of interest, particularly, if the experiment is ever repeated (preferably with improved chamber pressure, to minimize the collection of random events not associated with the interaction region of the target).

1.4 Plot-Style and Statistics

It should be mentioned at this time that the analyses that make up the body of this dissertation are statistically limited relative to the Ne^{2+} decay channel (Table1.3).

Table 1.3: Relative Charge State Distribution

Charge State *	Relative Abundance (%)
Ne^{1+}	4.65
Ne^{2+}	89.47
Ne^{3+}	5.55
Ne^{4+}	0.31
Ne^{5+}	0.02

* Based on the ^{20}Ne isotope.

Further, the method of displaying the angular correlation as shown in Figure 1.4 is not optimum for showcasing the physics of these more statistically limited analyses. To establish an adequate basis of comparison between charge states, we introduce a few alternative plots styles.

The first plot-type considers the cosine between electrons as the abscissa and photo-electron energy as the ordinate (Fig.1.6). The second plot style takes events that correspond to a specified range of energy (from the 1^{st} plot and projects them onto the abscissa (Fig.1.7). This represents the distribution of Auger events as a function of the angle between the electrons. Note how this is nearly isotropic (flat) except in the region near 0^o (i.e., there is no pile-up, or "splash" of events). The third plot (Fig.1.8) is simply a convenient polar representation of the angular correlation between electrons (2^{nd} plot style); the opening at 0^o is shown as a "divot."

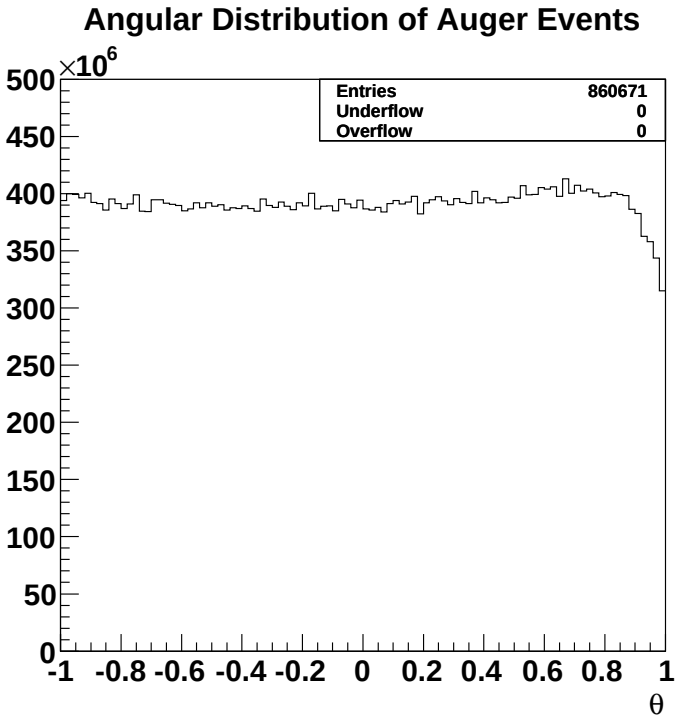

Figure 1.7: The trend of this histogram maintains isotropy except for the region around $Cos(\theta) \approx 1$. The "splash" predicted by theory is not present in these experimental results.

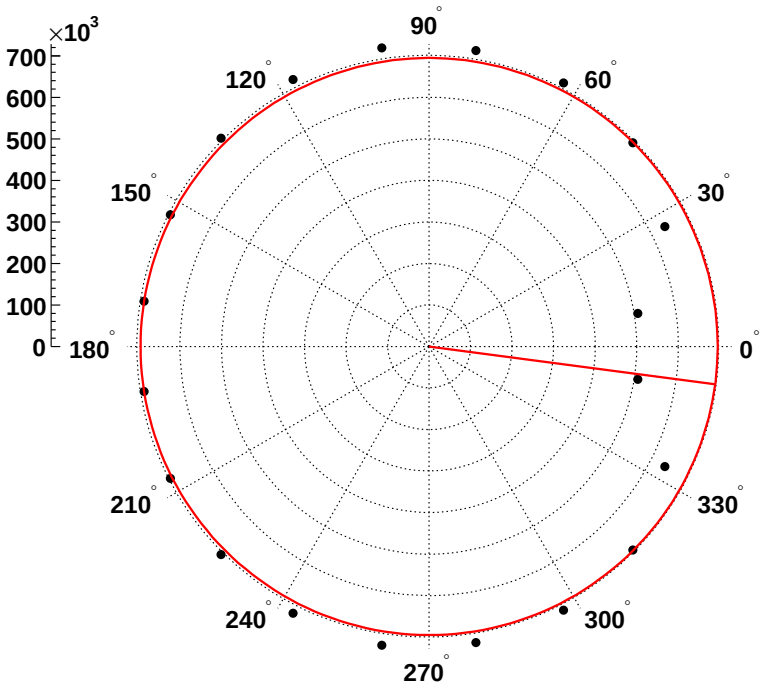

Figure 1.8: Once more, the trend of this histogram maintains isotropy except for the region surrounding $Cos(\theta) \approx 1$.

1.5 Neon Relaxation Dynamics

1.5.1 Accounting for Post-Collision-Interaction PCI

Having briefly explored the charge states that result from the relaxtion of the initial state (Eq.1.2), we describe the relaxation dynamics associated with these processes. For the purpose of this discussion, we shall consider the single-Auger decay channel.

As the highly energetic Auger electron is launched into the continuum, it can be thought to "suddenly" overtake the radial position of the photo-electron. As a result, the low-energy photo-electron experiences a shift of $1/r$ of its total energy due to this step-like change in potential. If the final energy of the photo-electron is negative, ($E_{e_\gamma} < 0$), the electron is recaptured into an excited/Rydberg state, $Ne(1s^2 2s^2 2p^4 nl)^+$. If the final electron energy is positive, ($E_{e_\gamma} > 0$) the electron simply escapes into the continuum with less energy, $Ne(1s^2 2s^2 2p^4)^{2+} + e_\gamma^- + e_A^-$. The probability that the photo-electron will escape into the continuum depends on the width of the 1*s* vacancy, $\Gamma = 270$meV.

The PCI between the photo-electron and recoil ion is most dramatically emphasized by plotting the photo-electron energy distribution for Ne^+, Ne^{2+} and Ne^{3+} (Fig. 1.9). These effects are particularly noticeable in the trailing edge of the photo-electron distribution (for the higher charge states).

1.5.2 Observation of Post Collision Effects

The photo-electron distribution in the Ne^{1+} radiative decay channel (Fig.1.9) is represented by a convolution of a Lorentzian and Gaussian function.[18] The former, which relates to the lifetime of the 1*s* hole ($\tau \approx 1$fs), affects the natural Gaussian-like distribution of photo-electron energy. This convolution function, formally termed "Voigt" overlays the measured photo-electron distribution in Figure 1.9. The theoretical curve shows excellent agreement with experiment. The parameters that dictate such a fit are as follows: $\Gamma = 270$meV, resolution$= 0.37$meV. The latter is related to the optical settings at the beamline. We relate Γ to τ below.

$$\tau = \frac{\hbar}{2\Gamma} \tag{1.4}$$

When one considers the Ne^{2+} decay channel, the photo-electron distribution not only broadens but shifts to a lower energy. This is a direct effect of Post Collision Interaction (PCI). After all, it is the departing Auger electron (due to the $2p \rightarrow 1s$ transition) that measurably affects the local (recoil) potential surface to which the photo-electron interacts. Due to the relative difference in electron velocity, the Auger electron has a minimal time in which it can influence the photo-electron. The change from Ne^{+} to Ne^{2+} requires the photo-electron transfer some of its kinetic energy to remain in the continuum. The quantity of energy exchanged is of course, dependent upon the time required for the recoil to undergo a $2p \rightarrow 1s$ transition since the potential energy is inversely proportional to the separation distance between charges. We observe that for the case where the target atom undergoes DA decay, the PCI effects are even *more* pronounced.

If the Auger decay takes place sufficiently fast, resulting in the recapture of the photo-electron, it becomes possible for the photo-electron to later be re-emitted. If the angular momentum of the Ne^{2+} core changes from a $Ne^{2+}(1s^2 2s^2 2p^4\ ^1D)$ to a $Ne^{2+}(1s^2 2s^2 2p^4\ ^3P)$ core, the recaptured Rydberg electron will be placed back into the continuum with approximately 0.3eV. We observe this feature in the Ne^{2+} distribution shown in Figure 1.9.

1.5.3 Photon Energy and Relaxation Dynamics

We specified the photon energy at the beamline to be 872.9eV, just 2.0eV above the K-ionization threshold. The selection of the photon energy near threshold was not an arbitrary decision. On the contrary, it was selected in an effort to maximize the correlation between the photo-electron and Auger electron(s) while simultaneously minimizing the chances of photo-electron recapture. Had we chosen a higher photon energy for the experiment, we would have diminished the probability of interaction between the emitted Auger electron(s) and the photo-electron.

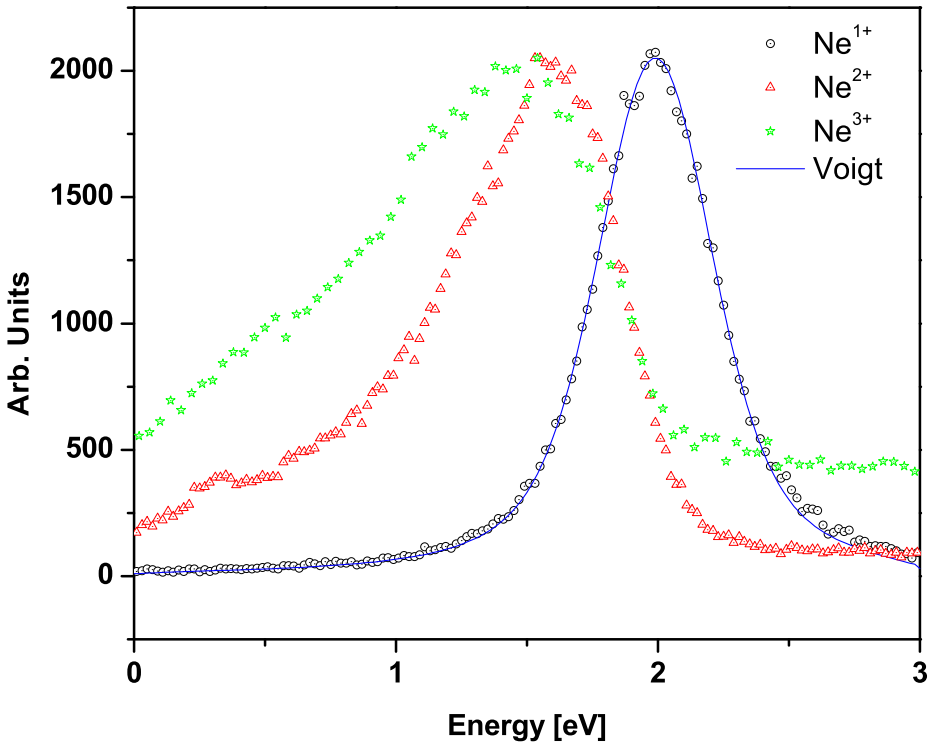

Figure 1.9: The photo-electron distributions representing Ne^{+}, Ne^{2+} and Ne^{3+} are shown from right to left. The increased potential subsequent to the electronic relaxation of the target atom results in a shift of the photo-electron energy. The small feature at 0.3eV in the Ne^{2+} data represents recaptured electrons that are re-emitted subsequent to a change in angular momentum.

1.5.4 The Lifetime of the 1*s* Vacancy

Consider a statistical ensemble of neon atoms, which upon core-absorption of a photon launch a photo-electron into the continuum with energy, E_{e_γ}. The subsequent Auger decay of the ensemble is given by the following exponential expression:

$$N = N_o e^{(-t/\tau)} \tag{1.5}$$

where, N_o is the initial population, N is the population of ions that Auger decays at time, t and τ represents the decay constant. Since the energy of the Auger electron far exceeds that of the photo-electron, ($E_A >> E_{e_\gamma}$), one may treat the Auger process as instantaneous. In other words, we shall use the sudden approximation to claim that the photo-electron "sees" the new potential energy associated with the Ne^{2+} at the instant the ion undergoes Auger decay. Ultimately, we seek to graphically represent the recapture/escape probability versus energy, relative to the 1s ionization of neon. The energy of the photo-electron is given in atomic units,

$$E_{e_\gamma} = \frac{v^2}{2} - \frac{1}{r} \tag{1.6}$$

To determine the distance between the photo-electron and the point-like ion, we integrate,

$$v = \frac{dr}{dt} \tag{1.7}$$

$$\frac{dr}{dt} = \sqrt{2\left(E_{e_\gamma} + \frac{1}{r}\right)} \tag{1.8}$$

$$\int_0^{t'} dt = \int_0^{r'} \frac{\mathrm{d}r}{\sqrt{2\left(E_{e_\gamma} + \frac{1}{r}\right)}} \tag{1.9}$$

$$t' = \frac{1}{\sqrt{2}}\left(\frac{1 + E_{e_\gamma} r'}{E_p \sqrt{E_{e_\gamma} + \frac{1}{r'}}}\right) \tag{1.10}$$

The above expression indicates the time, t' required for a photo-electron of given energy to travel a distance, r' from the point-like ion. It is at this time the electronic transition occurs, launching an Auger electron into the continuum. The energy of the photo-electron becomes,

$$E_{\gamma'} = \frac{v'^2}{2} - \frac{2}{r'} \tag{1.11}$$

Substituting the velocity of the particle (at the instant of Auger decay) we determine the new total energy of the photo-electron:

$$E_{\gamma'} = (E_{e_\gamma} + \frac{1}{r'}) - \frac{2}{r'} \tag{1.12}$$

$$E_{\gamma'} = E_{e_\gamma} - \frac{1}{r'} \tag{1.13}$$

Since the largest r' for recapture takes place when $E_{\gamma'} = 0$, the original photo-electron energy must be no greater than,

$$E_{e_\gamma} = \frac{1}{r'} \tag{1.14}$$

$$r' = \frac{1}{E_{e_\gamma}} \tag{1.15}$$

Substituting this into the previous expression for time yields,

$$t' = E_{e_\gamma}^{-(3/2)} \tag{1.16}$$

The calculated time serves as a marker to distinguish between a photo-electron that is captured and one that escapes into the continuum. To determine the curve that represents the probability of recapture for a given photo-electron energy, we begin by taking the area under the curve, $t \geq t'$ and normalize it as shown in Eq.1.17,

$$h[t] = \frac{\int_{t'}^{\infty} e^{(-t/\tau)}\,\mathrm{d}t}{\int_{0}^{\infty} e^{(-t/\tau)}\,\mathrm{d}t} \tag{1.17}$$

$$h[t] = e^{(-t/\tau)} \tag{1.18}$$

Noting that $t' = 4.166$ and using $\tau = 1.22$fs, we arrive at

$$g[E_{e_\gamma}] = e^{-\frac{E_{e_\gamma}^{-\frac{3}{2}}}{\tau}} \tag{1.19}$$

Equation 1.19 represents the probability of escape/recapture vs. photo-electron energy relative to the 1*s* threshold of neon and is illustrated graphically in Figure 1.10. The region under the curve represents the regime where photo-electrons will escape, while the area above the curve represents the electron recapture regime.

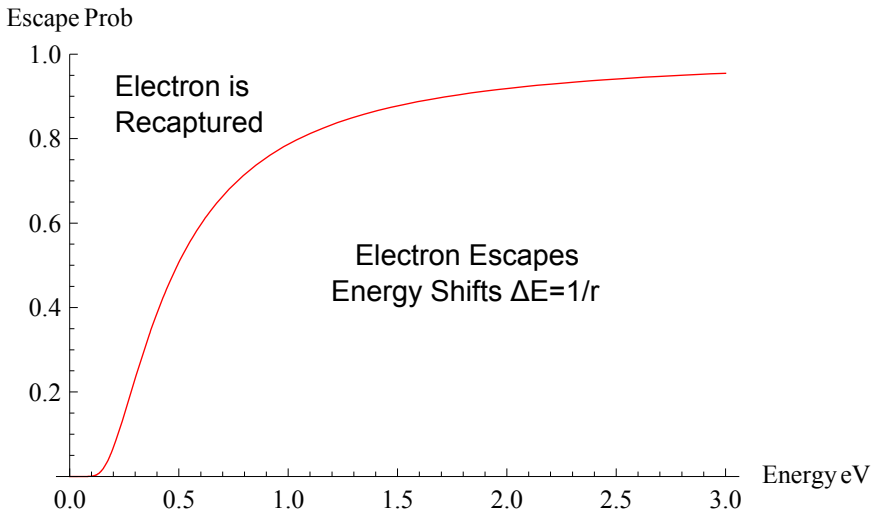

Figure 1.10: The curve represents the escape probability for the photo-electron, pending the occurrence of single-Auger decay.

1.5.5 Selection of Photon Energy for Double Auger Decay

Selection of the photon energy to optimize the statistics of DA decay is a bit more complicated. Let us once again consider the photo-ionization and subsequent DA decay of neon as a "two-step" process. Further, we consider such an event where the Auger electrons share the $2p \rightarrow 1s$ energy symmetrically. If we assume the sudden approximation is valid, despite having divided the transition energy in two, the photo-electron loses $2/r$ of its total energy. In this case, the photo-electron "sees" the residual Ne^{3+} ion and is more likely to be recaptured than in the case of single Auger decay (for a specified photon energy).

The situation changes entirely when we consider Auger electrons that share energy asymmetrically. In this case, the interaction between the fast-Auger electron and photo-electron closely resembles single Auger decay since the slow-Auger has not had sufficient time to distance itself from the residual ion. Classically, we can envision a Gaussian surface enclosing the recoil and slow Auger electron. Whether or not the slow-Auger ever overtakes the photo-electron depends on the energy sharing characteristics of the decay. Regardless, it is clear that the sudden approximation is no longer valid for this slower electron. Therefore, we select the photon energy according to whichever case is more prevalent: symmetric or asymmetric energy sharing between DA electrons. With *a priori* knowledge that DA electrons tend to share energy asymmetrically we select the photon energy based upon the results of single-Auger decay as it is our best approximation to the majority of DA events.

1.5.6 The Two-Step Model

Throughout Chapters (5&6), we use the two-step model to describe the Auger decay process in core-ionized neon. We have already briefly considered the model in a prior section; namely, we consider the 1^{st} step of this model to have taken place when a 1*s* electron absorbs a photon (sufficient to ionize). In the 2^{nd} step, a valence electron "falls" to fill this vacancy, transferring its energy to one or more valence electrons. Here, we consider two physics models used to describe specific cases within the two-step model, shake-off and knock-out. As an example, consider the core-ionization of a neon atom, $Ne(1s^{-})^{+}$. Let us assume the subsequent electronic relaxation results in a DA decay.

1.5.7 The Shake-Off Model

The shake-off model has been used with success to describe the physics of highly asymmetric energy sharing between electrons emitted in the PDI of helium.[23][33] Shake-off is a process whereby the electronic transition determines an initial state, which subsequently relaxes onto the

new eigenstates. We express electron shake-off in the context of the sudden approximation. Consider how an electron may be placed into the continuum by a "sudden" change in the central potential (e.g., an Auger decay resulting from a $2p \rightarrow 1s$ transition); accordingly, the Hamiltonian that describes the system changes "instantaneously" [5]. The probability that an electron with initial wave function, Ψ_i will be found in the final state, Ψ_f is given by the complex square of the overlap integral,

$$P_{i \rightarrow f} = \left| \int \Psi_f^* \Psi_i \mathrm{d}\tau \right| \tag{1.20}$$

1.5.8 The Knock-Out Model

Contrary to the shake-off model, the knock-out picture has been successful in describing the physics of highly symmetric energy sharing between electrons emitted in both the DA decay of atoms (e.g., neon and argon) as well as the PDI of helium.[23][24][25][33] is a classical model that can be used to describe the elastic-like collision between Auger electrons. This effect is particularly noticeable in the case where the electrons share the $2p \rightarrow 1s$ transition energy, symmetrically. This is not to say that the model does not apply to events of asymmetric energy sharing. Rather, it is the physics of shake-off that are improbable for symmetric energy sharing, ultimately giving us a clearer view of the physics in *this* regime.

To illustrate the knock-out model, we consider the billiard ball picture shown in Figure 1.11. Assuming the masses are equal, conservation of momentum dictates the outgoing trajectories of the masses be 90^o apart. As will be shown in Chapter 6, we observe an interior angle between particles that is greater than 90^o. These findings compliment previous research on DA decay [25].

If we return to the billiard ball model, we can begin to understand the mechanism that results in this opening of the interior angle. Consider an unlevel billiard ball table (i.e., where one end is elevated above the other). Given an elastic collision where the respective trajectory of each ball begins to ascend the incline, we expect the component of gravity, parallel to the surface, to act

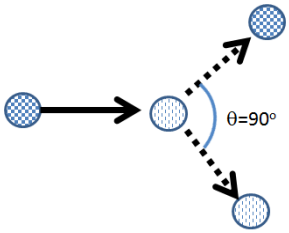

Figure 1.11: The knock-out picture can be used to model the interaction between Auger electrons as an elastic collision. We must also consider this interaction in the context of PCI with the residual ion, which effectively opens the expected 90^o angle between the outgoing trajectories.

on each ball, ultimately opening the 90^o angle that was initially between them. Hence, the Auger electrons are affected by PCI effects from the residual ion.

Chapter 2

THE EXPERIMENT

2.1 Introduction

Scientists the world over view the Lawrence Berkeley National Laboratory (LBNL) to be a hallowed ground of physics. Located near the harbor of the San Fransisco bay,[1] the laboratory claims 11 Nobel prize laureate, ranging from Ernest Orlando Lawrence for his invention of the cyclotron, to current U.S. Department of Energy Secretary, Steven Chu for his work on the laser cooling of atoms. At the heart of this facility is the Advanced Light Source (ALS), home of a third-generation synchrotron that is located upon the site of Lawrence's original 184 inch cyclotron.

Figure 2.1: The ALS (shown left) is located on the periphery of Berkeley, CA, overlooking the scenic San Francisco Bay.

The statistics boasted by the ALS are impressive indeed. Thanks to the integration of electron undulators, the beam line scientists can produce photons with brightness [2] at the ALS that is one billion times that of the sun. This brightness is utilized by researchers to probe statistically rare phenomenœ that otherwise, would not be possible. We had the priviledge of conducting research at this facility through a grant by the Department of Energy.[3].

[1] Image and beam line facts, compliments of http://www-als.lbl.gov/index.php/about-the-als/quick-facts.html

[2] Brightness is defined as the density of photons in 6D phase space, (photons/sec/mm^2/mrad^2/0.1%BW)

[3] Supported by Department of Energy, Basic Energy Sciences, AMOS program under grant DE-FG02-10ER16146

In the pages to follow, we describe some of the pertinent details regarding the beam line settings as well as the design of the COLd Target Recoil Ion Momentum Spectroscopy (COLTRIMS) experiment. It should be mentioned at this time, while the experimental details given here are sufficient to reproduce the conditions of the original experiment, they are not intended to serve as a comprehensive report on the COLTRIMS method.[4]

2.2 The Advanced Light Source

The ALS at LBNL has a number of beam lines, each of which provide to the user a specific set of optical features. Beam line 11.0.2 is configured to receive photons from an elliptically polarizing undulator with a 5cm period [31]. Given the operating energy of the ALS to be 1.9GeV, this provides us with a broad range (75 – 2150eV) of available photon energies [38]. The multi-chromatic beam is next focused onto a plane-grating monochromator (with two available gratings, 150 and 1200 lines per millimeter)[38]. Two toroidal focus mirrors are available to focus the light from the monochromator.[31] The focused light passes through the 4-jaw slits (Fig.2.2) and is further focused (for use in the experiment) by a pair of Kikpatrick-Baez (KB) mirrors[38].

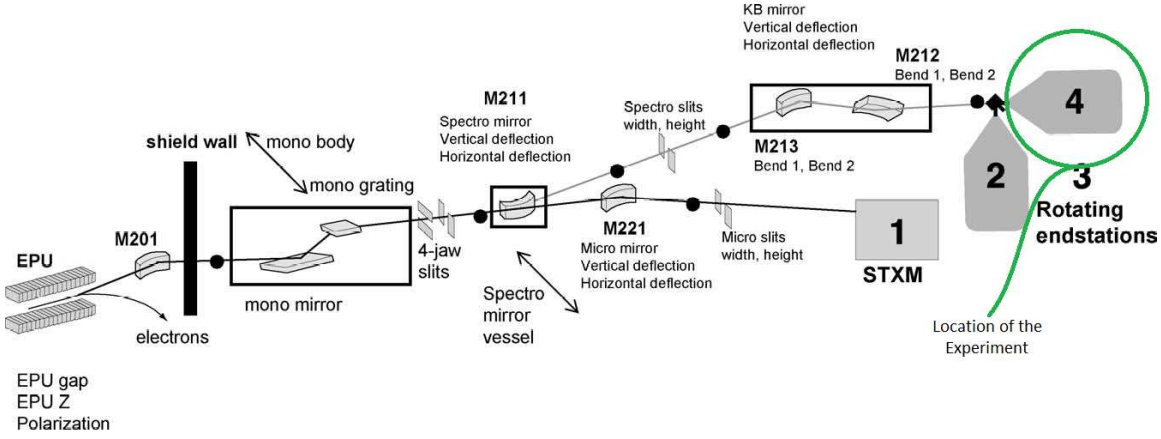

Figure 2.2: Schematic of the ALS beam line 11.0.2.

[4]For an exhaustive description of COLTRIMS, refer to www.atom.uni-frankfurt.de or www.roentek.de.

For the experiment considered here, we specified a source of monochromatic (872.9eV), circularly polarized light. This placed us within the 3^{rd} harmonic at a photon flux of $\sim 5 \cdot 10^{12} s^{-1}$ as shown in Figure 2.3.[5] However, this value of flux represents what is available in continuous beam mode. We configured the experiment to operate in "two-bunch" mode with "top-off." We briefly discuss each off these terms below.

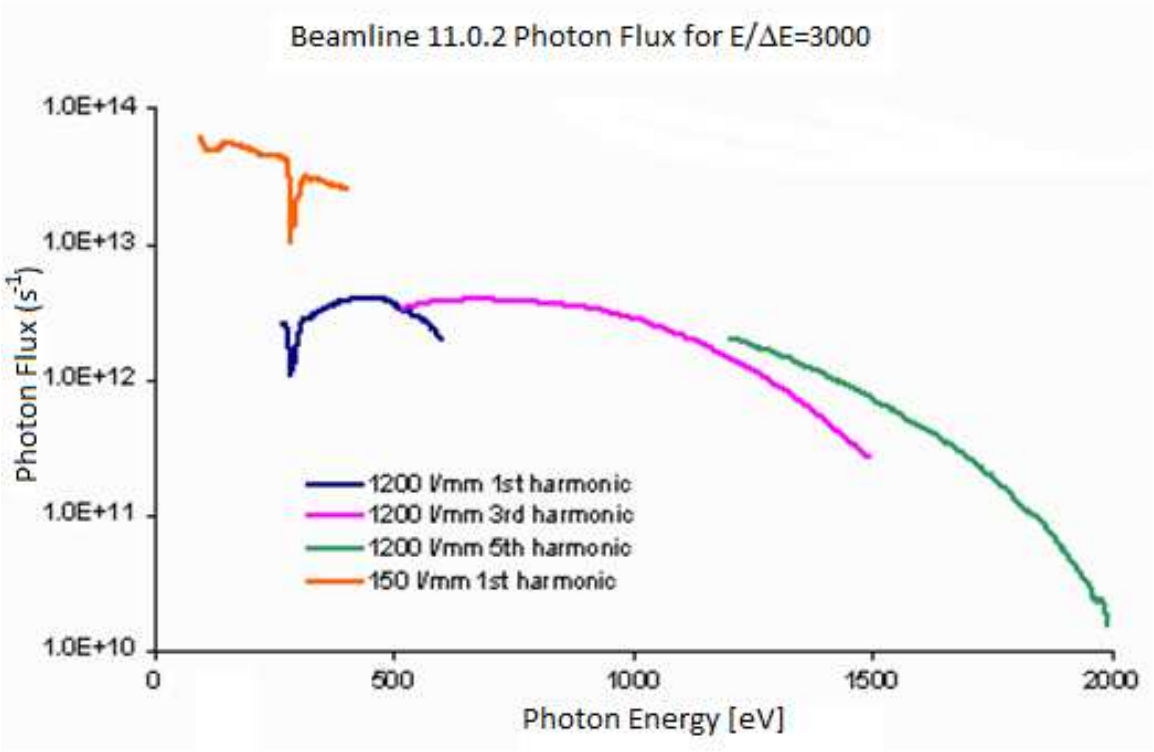

Figure 2.3: At 872.9eV, we are within the 3^{rd} harmonic of the beamline. The available flux is $\sim 5 \cdot 10^{12} s^{-1}$.

The ALS operates in continuous beam mode for approximately forty-eight weeks out of the year. In this mode, all electron buckets that are associated with the cyclotron are filled with electrons and accelerated to 99.999996% the speed of light. The result is a pulsed beam of photon flux (photons/sec) with a bunchspacing of a just 2ns. This setup is particularly advantageous to

[5] Image courtesy of http://beamline1102.als.lbl.gov/

researchers who perform experiments that require high flux and no time structure (e.g., X-ray crystalography). However, scientists who use COLTRIMS require a beam with greater bunchspacing in order to fully distiguish one physical event from another (i.e., a timing strategy). Beam scientists address this need, switching to "two-bunch" mode for the remaining four weeks of the year.

In two-bunch mode, only two buckets (one being the back azimuth of the other) are filled, which results is a substantially longer photon bunch spacing (328.228ns). Of course, running in two-bunch mode reduces the photon flux that is ordinarily available at the beamline. Also, regardless of mode, losses occur during the acceleration of the electrons through the undulators, which further diminish the flux over time. While we are forced to accept the former issue, beamline scientists have developed the "top off' mode to address the latter. As the electron buckets "revolve" about the cyclotron, additional electrons are, with great precision, deposited into the specified buckets, thus maintaining typical electron levels (~ 7.5 billion electrons/bunch).

2.3 An Overview of the COLTRIMS Apparatus

The COLTRIMS apparatus we assembled at the ALS (Fig.2.4)[6] was specifically designed to measure the constituents of core-ionized neon. A finely columnated jet of ground-state neon was introduced into a two-stage vacuum chamber, the latter of which was maintained at $\sim 1 \cdot 10^{-8}$ Torr (with the LN_2 trap filled). The jet intersected a pulsed beam of 872.9eV photons, forming an interaction region. The constituents of the core-ionized atom (born within the interaction region) were measured by two detectors (recoil & electron), located at the ends of the spectrometer as shown. The rate of data acquisition was approximately 1.0kHz for the recoils and 2.8kHz for the electrons. The detectors were each comprised of a stack of Micro-Channel Plates (MCP) that were coupled to a delay line anode. The detectors measured the 2D-position and time data associated with the constituents of the target atom. The corresponding signals were recorded by Time to Digital Converter (TDC) cards.[7]

[6] This image is a modified version of the one shown for PDI of helium.[33]

[7] TDC cards were provided by Cronologic.

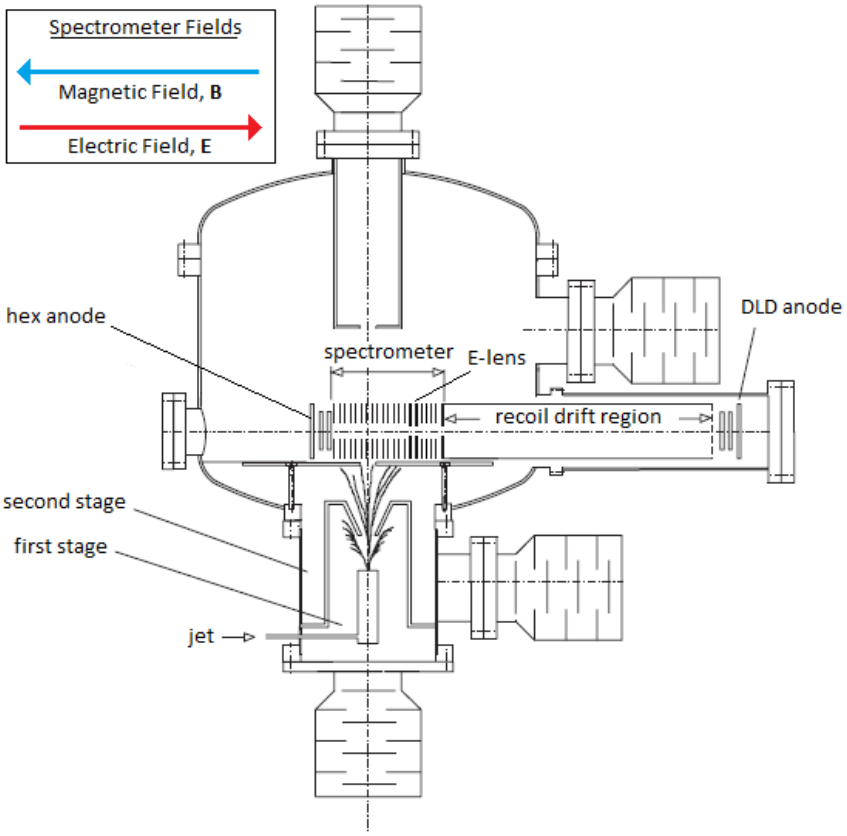

Figure 2.4: An overview of the COLTRIMS design. Shown is the point of entry of the neon (jet), its passage through two-stages of skimming and intersection with the longitudinal axis of the spectrometer, forming the interaction region. The constituents of the ionized target are directed to their respective detectors by way of an electric and magnetic field. Note also the electrostatic lens (E-lens) used in conjunction with a long drift tube, used to improve resolution on the recoil sider of the detector.

From the 2D position and time data, we were able to determine the respective particle's momentum. This can be achieved by two different methods. The first calculates the value directly from the particle's position and time data. The second indirectly calculates the value from the conservation of momentum. Of course, to perform the latter, we must measure all other particles within the event.

2.3.1 Spectrometer Details

A schematic of the spectrometer that was used throughout the experiment is shown in Figure 2.5. As previously mentioned, an external electric and magnetic field directed the constituents of the ionized target gas to their respective detectors – through data analysis, we precisely determined these values *a posteriori* to be, 2.24V/cm & 3.8G, respectively. The recoil detector was comprised of a delay-line-anode and an 80mm chevron-stacked MCP. The electron detector utilized a more sophisticated hex anode that was also coupled to an 80mm chevron stacked, MCP.[8] Additionally, we used a long drift tube ($\sim$ 1m) in conjunction with an electrostatic lens on the recoil side of the spectrometer to improve momentum resolution.

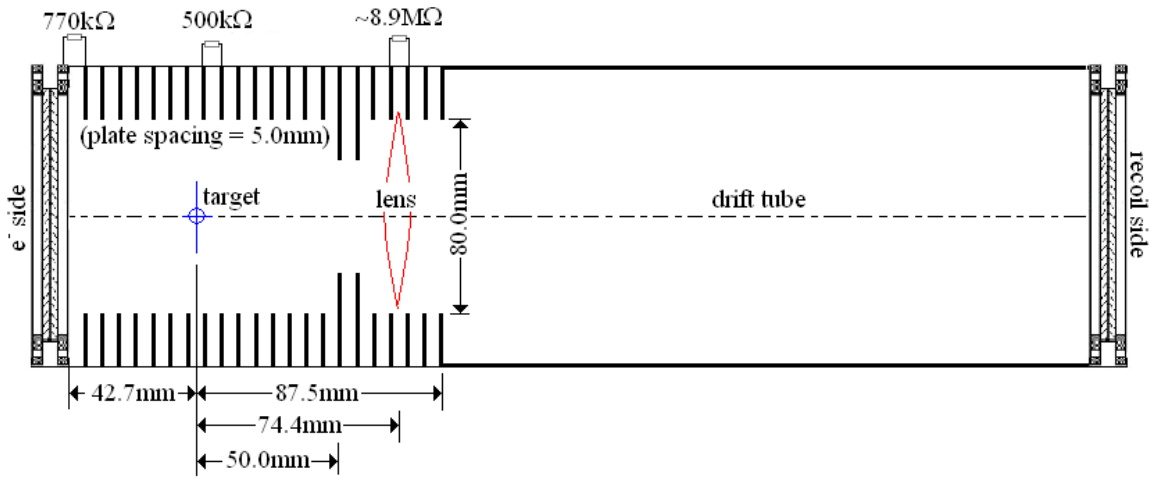

Figure 2.5: Schematic of a COLTRIM-Spectrometer). Shown are the dimensions, field strengths and resistor values used.

The Helmholtz Coils & Solid Angle Collection

In order to maximize the solid angle collection of the high-energy electrons without excessively compromising resolution, we designed the electron side of the spectrometer to have a rather short acceleration region (we precisely determined this value to be, $d = 42.7$ mm). While the design of the spectrometer ensured the collection of all recoil ions, the 4π solid angle collection for electrons

[8] The hex anode was selected in order to better distinguish multiple electron hits within a given event.

was limited to energies no greater than 5 eV. The solid angle collection is governed by the external magnetic field that is applied to the spectrometer by way of the Helmholtz coils. Helmholtz coils, such as the one shown in Figure 2.6 are designed to be separated a distance that is equal to their radius. If aligned properly, the region bounded by the coils (i.e., the region where we place the chamber with our spectrometer) produce a uniform magnetic field.

The applied uniform magnetic field (3.8G) was oriented anti-parallel to the electric field, $\vec{E}$ and was included for two reasons. First, the field served to shield the detectors from random electrons; these primarily resulted from the interaction between the pulsed photon beam and the residual background gas in the chamber ($\sim 1 \cdot 10^{-8}$ Torr). Second and more importantly, the magnetic field confined the electrons of interest by way of Larmor precession, keeping them within the bore of the spectrometer. As will be shown later in Chapter 6, in order to investigate the angular correlation between electrons emitted in DA decay, we must have some appreciation for the solid angle collection that is available to the spectrometer.

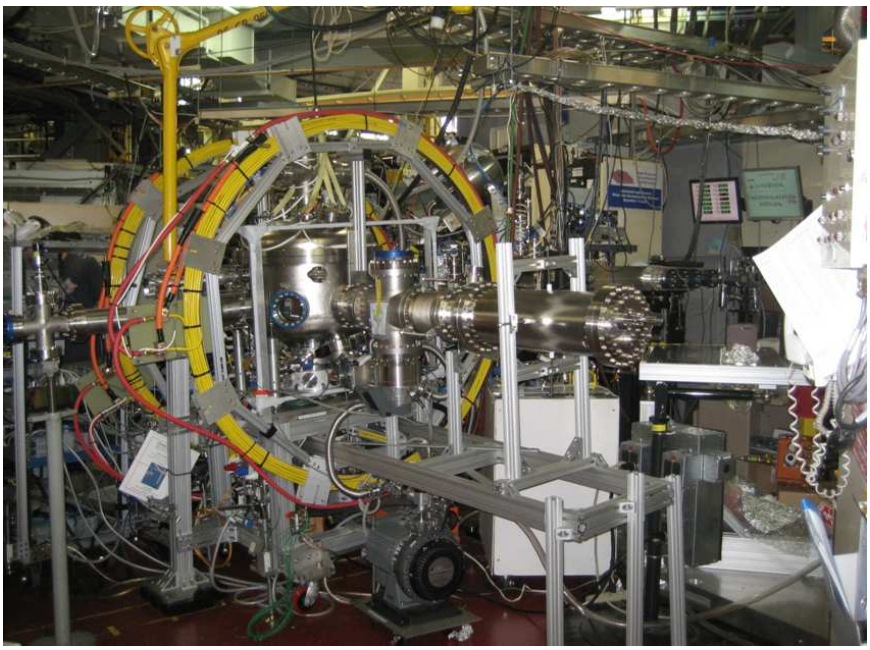

Figure 2.6: This shows the COLTRIMS setup including the Helmholtz coils (yellow) and the drift tube extending toward the viewer (along the longitudinal axis formed by the Helmholtz coils).

2.3.2 Calculating the Solid Angle Collection of Electrons

We begin by considering an electron that is launched into the continuum with energy, $\mathscr{E} = \frac{m_e v_\perp^2}{2}$, where $v_\perp$ is the electron velocity that is perpendicular to both the uniform external magnetic field, $\vec{B} \equiv B_o(\hat{i})$ and the uniform external electric field, $\vec{E} \equiv E_o(\hat{-i})$. Taking the interaction between the emitted electron and residual ion to be negligible, the equation of motion is elementary,

$$m\frac{v_\perp^2}{r_L} = q(v_\perp B_o) \tag{2.1}$$

Through algebraic manipulation, we arrive at the familiar cyclotron (Larmor radius) equation,

$$r_L = \frac{m_e v_\perp}{qB_o} \tag{2.2}$$

Taking the initial position of the electron to be at the interaction region (i.e, at a specific point along the longitudinal axis of the spectrometer), we note the maximum cyclotron radius that is allowed is, $20mm$.

$$p_\perp = qB_o r_L$$

Substituting appropriate values, we arrive at the maximum electron energy to which we can be assured 4π solid angle collection,

$$\begin{aligned}\mathscr{E} &= \frac{(qB_o r_L)^2}{2m_e} \\ &= \frac{\left(1.6\cdot 10^{-19}\text{C} * 3.75\cdot 10^{-4}\text{T} * 20\cdot 10^{-3}\text{m}\right)^2}{2 * 9.108\cdot 10^{-31}\text{kg}} / 1.6\cdot 10^{-19}\text{J/eV} \\ &\approx 5\text{eV} \end{aligned} \tag{2.3}$$

2.3.3 Drift Tube & Electrostatic Lens

A drift tube was used in conjunction with an electrostatic lens in order to improve the resolution on the recoil side of the detector. A brief look into the energetics of the recoil ion provides insight into why we incorporated this piece of apparatus into the COLTRIMS setup. Consider an event of direct ionization (i.e., a two-body breakup of the target atom),

$$Ne + \gamma(872.9)\text{eV} \rightarrow Ne(2p^{-1})^+ + e^- \tag{2.4}$$

Noting the 1^{st} ionization potential of neon is 21.6eV[7], the energy shared between the electron and recoil is, 851.3eV. The energy divides according to the mass ratios:

$$\begin{aligned}\mathscr{E}_{\text{electron}} &= \frac{(20*1834)+9}{(20*1834)+9+1} * 851.3\text{eV} \approx 851.27\text{eV} \\ \mathscr{E}_{\text{recoil}} &= \frac{1}{(20*1834)+9+1} * 851.3\text{eV} \approx 0.03\text{eV}\end{aligned}$$

The drift tube ($\sim$ 1m in length) ultimately increases the flight time of the recoil ions. This allows them to diverge, thus improving resolution (i.e., the ions spread across a greater area of the MCP). It will be shown in Chapter 3 that an imperfect control over the gradient of this electric lens results in a small degree of optical abberation.

2.4 The Detector

2.4.1 The MCP

Figure 2.7 represents a schematic of the MCP stack (in a chevron configuration). In this example, we apply a large negative voltage, V_{front} to the front side of the stack, and ground the back side. When an electron of sufficient energy, $\mathscr{E}_{elec}$ impacts the front side of the plate, it ricochets off the inner wall of a micro-channel. The collision liberates, N electrons from the wall in accordance with the work function, ϕ of the material (Eq.2.5).

$$K.E._{(avg)} = \frac{\mathscr{E}_{elec} - \phi}{N} \tag{2.5}$$

The electric field established by the applied voltage accelerates this group of, N electrons through the respective micro-channel. Each electron's successive impact with the channel wall, in turn, produces an additional group of electrons, provided the average kinetic energy, $K.E._{(avg)}$ of the electrons is sufficiently large. The rationale for arranging the plates in a chevron pattern is simply to increase the number of collisions within a channel wall. The charge cloud, now of detectable magnitude emerges from the back side of the plate and electrically interacts with the delay line anode.

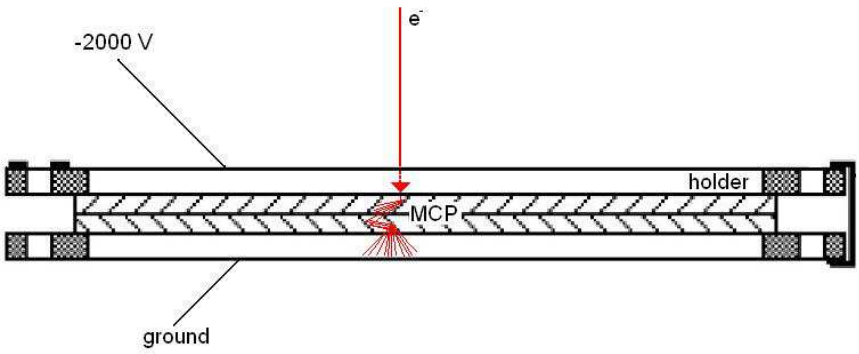

Figure 2.7: A side view schematic of a MCP stack in a chevron configuration. Note the applied voltage produces an acceleration region between the plates, enabling the stack to behave as an electron multiplier.

2.4.2 The Delay Line Anode

The charge cloud that emerges from the back side of the MCP stack induces a pulse (signal) on the wires that make up the delay line anode. In measuring the recoil ions, we used a two layer, square anode. Each anode layer is made up of a pair of closely spaced wires which are tightly wrapped about insulating spools (Fig.2.8); one wire is labeled "signal," the other is labeled "reference." The left panel shows the orthogonal orientation between layers (i.e., one layer has wires running vertically, the other, horizontally). The wire pairs are in fact, waveguides that propagate the electric pulse from the "hit" location at the MCP to the TDC card. With knowledge of the timing for photon pulses (i.e., the bunch marker), we are able to measure the propagation time along each wire pair. Moreover, we measure these values redundantly, noting that we measure the pulse (in nano-seconds) along each end of the wire pair. For example, u_1 & u_2 would represent the pulses measured from each end of the wire pair on the u layer. The sum of the measured pulse, $(u_1 + u_2)$ represents the time required to propagate the entire length of the anode wire. This turns out to be a useful fact when we set out to computationally sort the data in Chapter 3.

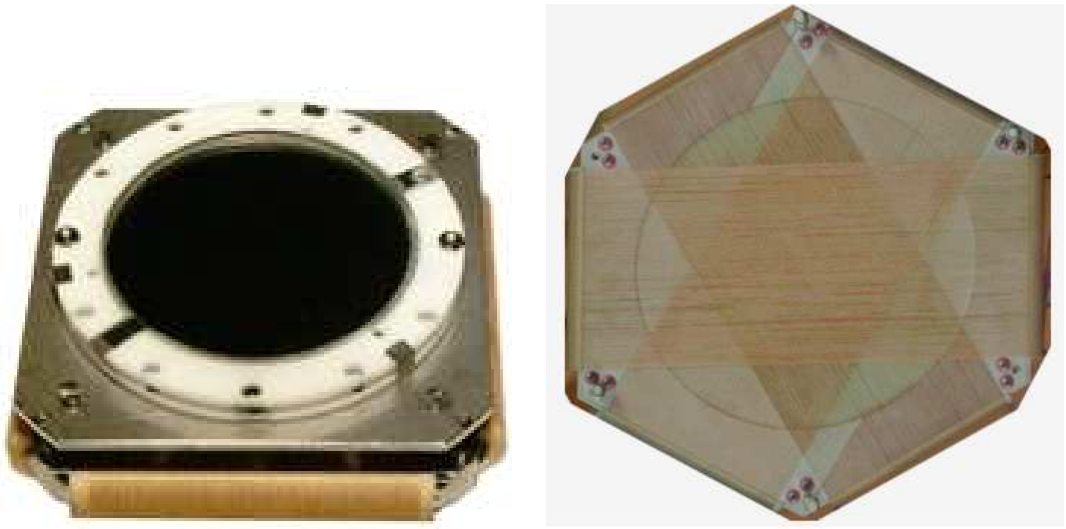

Figure 2.8: The left panel shows a two-layer, delay line anode used in the detection of recoil ions. An MCP stack is connected. The right panel shows a three-layer, hex anode that is used to detect electrons. Image courtesy of Roentdek: http://www.roentdek.com

A hex anode was used on the electron side of the detector (Fig.2.8) to improve the acquisition of events that had multiple electron hits. The anode is comprised of three layers, *u*,*v* and *w* oriented at 60^{o} intervals. The location of a particle can be determined using any combination of two layers. The built-in redundancy of having a 3^{rd} layer enables us to to sort out multiple hits that are closely separated by time. The details of interpreting hit data from the hex anode are provided in Chapter 3, specifically with regard to the "resort routine."

An array of plots is shown in Figure 2.9. In the proceeding chapters, these data will be refined to bring out specific details pertaining to the physics of K-ionized neon.

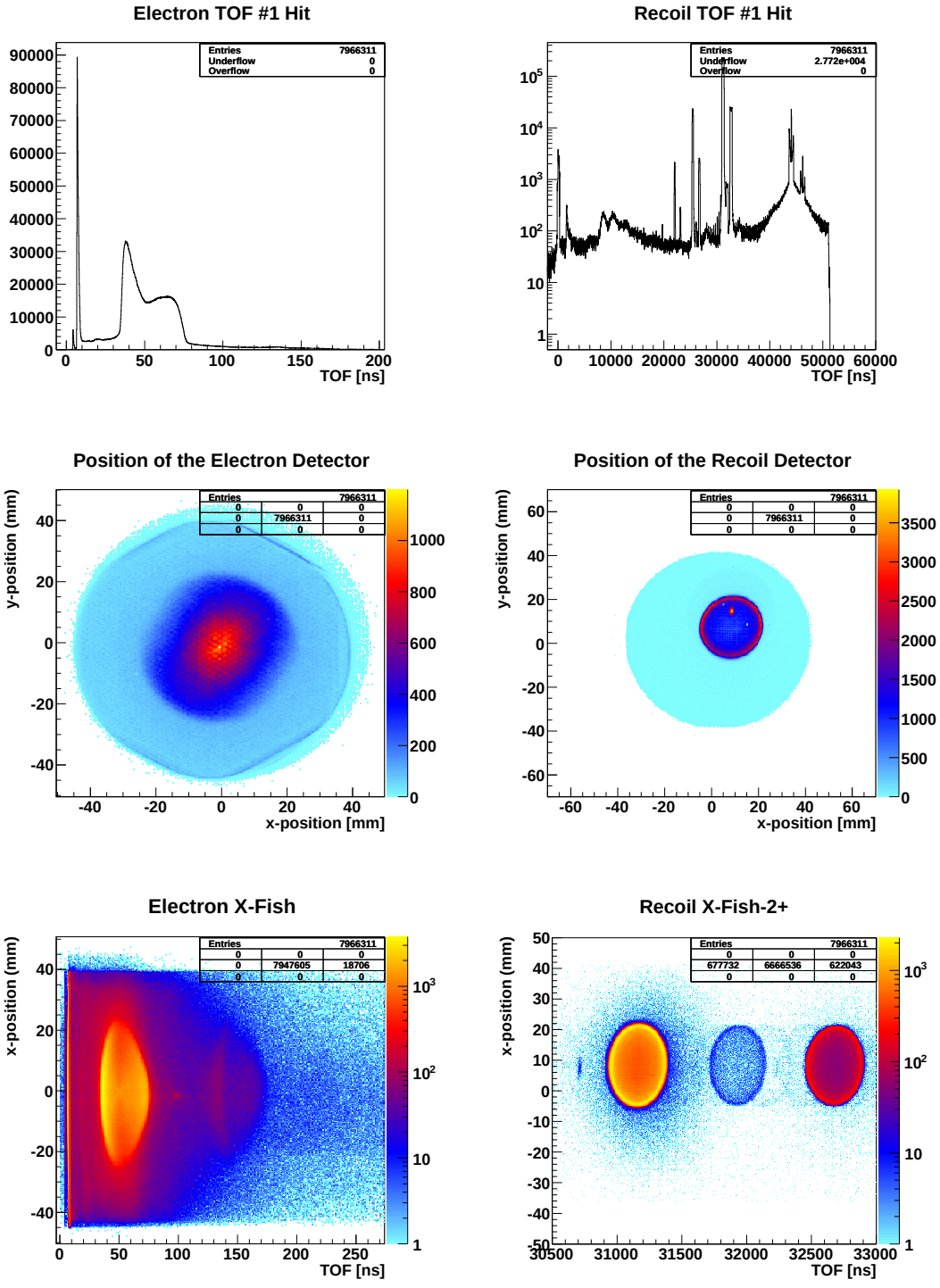

Figure 2.9: The top panels represent the measured TOF of the electrons and recoil ions, respectively. The middle panels show the raw position of the electron and recoil, respectively. The bottom panels show the position versus TOF for the electron and recoil, respectively (note, the recoil plot only considers the time range for Ne^{2+} events). The three distributions in the lower right are the isotopes of neon.

Chapter 3

COLTRIMS SPECTROMETER CALIBRATION

In this chapter we describe in detail a series of calibration techniques, used to "rough-in" the spectrometer.[1] At the conclusion of this procedure-like list we describe the process of aligning our line-energy spectrum with the published results of Yoshida [21][28]. This step leads to the accurate determination of both the spectrometer's electric field strength as well as the length of the acceleration region for electrons.

3.1 The Reconstruction Routine

Obstacles such as random hits on the detector, cross talk between anode signals, etc., adversely affect the data recording process. Some of these obstacles may be minimized or even overcome by way of increased control over the experiment (e.g., reducing background gas pressure, utilizing electronic decoupling devices, etc.). However, it is not possible to ensure a complete acquisition of hit data. For example, an unavoidable loss of hit data results from the the collection efficiency of the Micro-Channel Plate (MCP) - the ratio of open to closed area on the plates. When dealing with multi-electron co-incidence measurements, two additional limiting scenarios arise. The first relates to the "dead-time shadow" of the detector (i.e., the minimum recovery time required by the detector in order to measure a subsequent hit). The second relates to swapped hit data (i.e., data that has been incorrectly read-in by the Time to Digital Card or TDC).

[1] In an effort to facilitate the adoption of this calibration process by other members of the COLd Target Recoil Ion Momentum Spectroscopy (COLTRIMS) community, we have described these techniques in the order they are performed in the analysis.

The Dead-Time Shadow

While the detector is capable of collecting more than one electron hit (pulse) per event, if the time difference between two hits is sufficiently short, or if the respective position difference is sufficiently small, one of the two hits may go undetected. Whenever this occurs, the missed electron is said to be within the "dead-time shadow" of the detector (i.e., a period of time in which the system is electrically unable to process another hit). To properly illustrate this, we turn to the K-ionization data set (as it provides greater statistics) and computationally select (or "gate" on) events where three electrons are recorded in co-incidence with a Ne^{3+} recoil ion. Figure 3.1 plots the time and position difference associated with the second and third hit electrons. The plot reveals a triangular shaped feature between $(0-7)$ns and $(0-7)$mm, thus quantifying the dead time shadow for this particular detector.

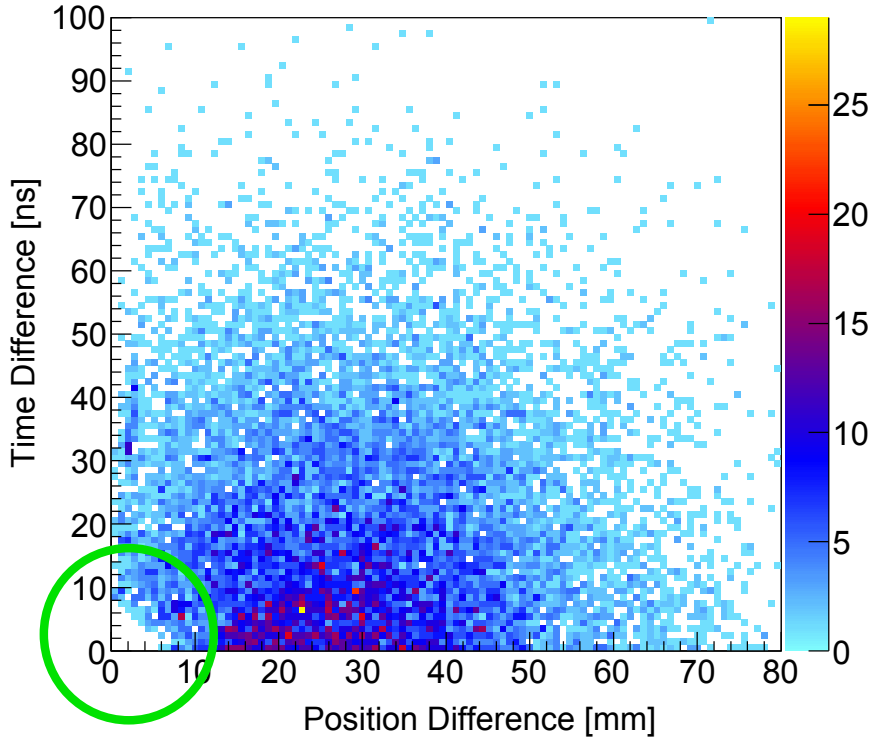

Figure 3.1: A small triangular void has been circled, highlighting the bound region, $(0-7)$ns and $(0-7)$mm. This represents the temporal and spatial limit to resolving successive hits on the detector.

Swapped Hit Data

Another scenario (outside of the dead time shadow of the detector) occurs when the TDC records a 2^{nd} hit in advance of the 1^{st} (i.e., the initial hit is headed off at the pass by the subsequent hit). To illustrate, let us consider an event where the 1^{st} hit corresponds to detector position (40mm,π) - in polar co-ordinates. The signal propagates along an anode wire pair (say, the *v* layer) in both directions. The TDC is configured to record the signals from each end of the anode wire as v_1 and v_2, respectively. Given the highly asymmetric position of the hit with respect to the anode wire length, the v_1 pulse will reach the TDC far sooner than the v_2 pulse. The longer travel time associated with the v_2 pulse results in an increased chance for a 2^{nd} hit, say at position (40mm,0), to reach the TDC in advance of the initial hit. In this case, a swap occurs between the two hit values on the "long" end of the wire, while the TDC correctly records the values on the "short" end.

If left as is, mishandled events (relating to legitimate target gas events) are no more useful to the analysis than the randoms. Furthermore, since this obstacle is directly related to the physics of ionization, it cannot be eliminated through improvements in experimental technique. Rather, it must be managed by computational means during the analysis process. These scenarios are particularly common in the case of K-ionized neon undergoing DA decay. Published results show a tendency toward asymmetric energy sharing between Auger electrons. Consequently, energy of the low-energy Auger electron is often on the order of the emitted photo-electron and hence, requires computational sorting. It should be noted that this particular issue is common to experiments that measure more than one electron in co-incidence.

Single electron experiments typically do not require such computational sorting. Consider the measurement of a recoil in co-incidence with just *one* electron. As there are fewer ways to interrupt an anode signal (there dœsn't exist a subsequent 2^{nd} hit to head off the 1^{st} hit), the number of mishandled events drops to an acceptably small percentage of the total (i.e., they are simply discarded along with the randoms). However, when measuring *more* than one electron hit per event (as is the situation in this experiment), the percentage of mishandled events increases to a level that makes it unacceptably wasteful to simply discard them.

A sorting algorithm was developed in proprietary fashion by Achim Czasch[3] to reconstruct populations of mishandled events. The "resort routine" as it has come to be known follows two prerequisite calibrations: the correction sum table, and the auto-calibration.[4] For the sake of clarity, we shall describe the "resort routine" in advance of our discussion on these prerequisite calibrations.

The Resort Routine

Execution of the resort routine must be preceded by two methods of calibration. However, before delving into the details of these methods, it is instructive to first present a subset of the techniques employed by the resort routine. The enumerated list shown below represents some of the primary features of this algorithm.

1. When a particle such as an electron encounters the MCP, it produces a signal that is closely followed by its respective anode signals. The resort routine looks for a correlation between these signals.

2. The algorithm calculates the position of a hit by measuring the anode signals with respect to the MCP signal. This position must verify the particle made contact with the surface of the MCP. If the combination of signals imply otherwise, it will be rejected by the algorithm.

3. The hex anode is made up of three layers: u, v & w. The routine needs only a single pair of anode layers to calculate the position of a hit: (u&v), (v&w) and (w&u). The algorithm uses this built-in redundancy to flag misplaced data within an event or in some cases, reconstruct a missing datum.

4. We measure the time required for a hit to propagate along a layer's anode wire (at both ends) with respect to the MCP signal (e.g., t_{u_1} & t_{u_2}). The sum of these time measurements is constant, reflecting the fixed length of the anode wire (e.g. $t_{u_1} + t_{u_2} \equiv t_{sum} \propto L$). The algorithm

[3]Special thanks to Achim Czasch for his development and subsequent explanation of his reconstruction algorithm – Institute for Nuclear Physics, University of Frankfurt, Germany. www.atom.uni-frankfurt.de

[4]The description of the resort routine is presented under the assumption the reader is familiar with the details of the detector; these details can be found in Chapter 2.

uses this systematic redundancy to reconstruct missing signals (i.e., we can infer t_{u_1}, by calculating $(t_{sum} - t_{u_2})$). As a result, the algorithm is able to reconstruct "missing" signals.

5. The algorithm will not reconstruct more than two signals that are outside the dead-time shadow of a real signal; a combination such as this will be rejected.

A Brief Example

Using figure 3.2 as a reference, we explore the methods used to reconstruct mishandled data within a given event. The rows enumerate the physical hits on the detector, while the columns correspond to the various signals. The routine begins by scanning each layer pair for agreement with its predetermined time sum - correct layer pairs are shown in boxes. Neighboring hits are also scanned in an effort to identify misplaced data within a given hit. The data points $[^{-e}hit_2{:}v_2]$ & $[^{-e}hit_3{:}v_2]$ are quickly identified as "swapped" via a comparison to the time sum. However, this step by itself is unable to identify the datum located at $[^{-e}hit_2{:}u_1]$ as misplaced. More information is required.

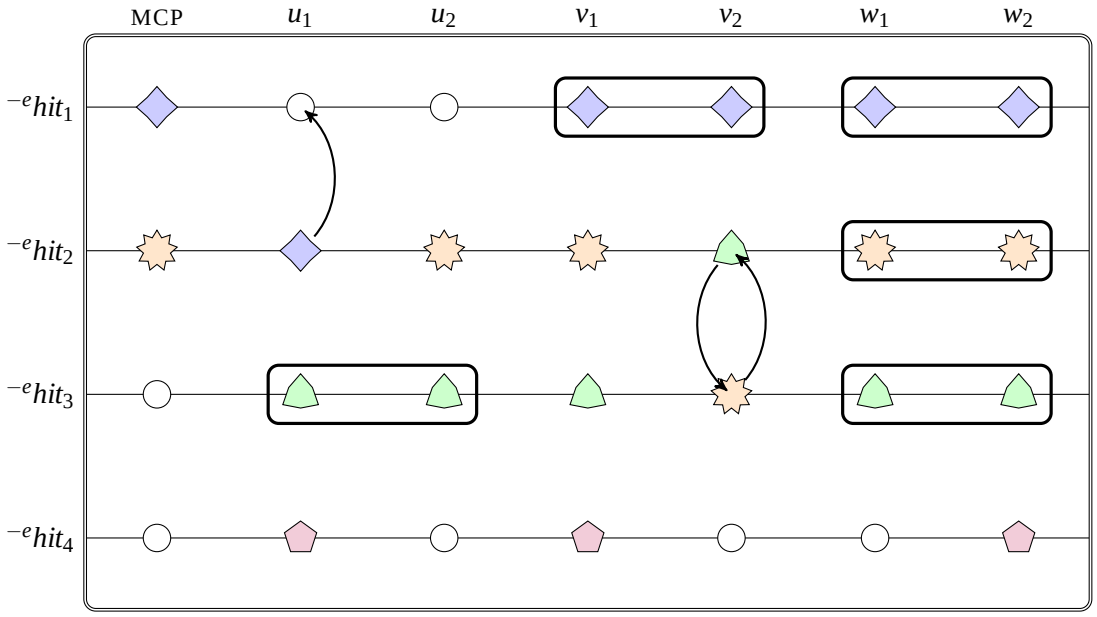

Figure 3.2: For a given event, data pertaining to a specific hit may be either lost or misassigned to a different event. It is the role of the resort routine to reallocate data or infer it altogether.

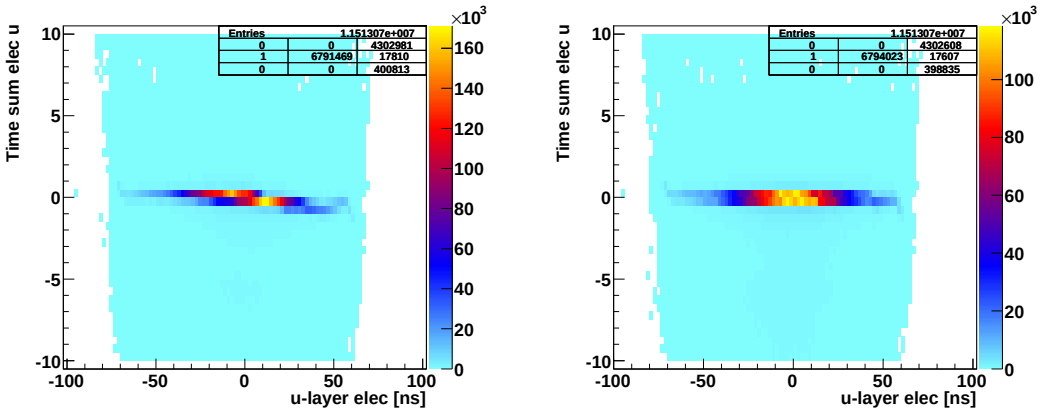

Figure 3.3: The left panel shows the time sum versus position plot before application of the correction table. The right panel show the corrected version.

The algorithm next calculates each hit position using the three combinations of layer pairs: *u*&*v*, *v*&*w* and *u*&*w*. The algorithm uses this redundancy in conjunction with the time sum scan to flag inappropriate data points. Layer pairs that have already been shown to agree with their respective time sums are used to infer information about mismatched layer pairs. It is in this way the routine identifies the data point, $[^{-e}hit_2{:}u_1]$ as misplaced, relocating it to the $[^{-e}hit_1{:}u_1]$ placeholder (shown by the arrow).

The Correction Table

The "correction table" is a built-in calibration technique used to improve both the accuracy of the reconstruction process as well as detector resolution. Its relevance to the resort routine is due to a non-linearity inherent to the anode signals. A plot of an anode layer time sum versus the respective position shown in Figure3.3 reveals a non-linearity (i.e., the time sum is not really a constant!) This is problematic since the algorithm uses the time sum to reconstruct missing MCP-signals. To correct this problem (i.e., to "straighten" out this non-linearity), we must generate a correction table.

The algorithm begins by building up three internal histograms corresponding to the time sum versus position data. After determining each respective maximum, the algorithm builds up a correction table for the position itself. Each delay line anode possesses a slight degree of non-linearity. For example, if one were to apply a fine wire mask to the front side of the MCP, one would expect these lines to appear in the position picture. Instead, upon closer inspection, one will see that these lines are not entirely straight. It should be noted that the non-linearity of one layer is independent of the others. Ergo, all that is necessary to correct for the non-linearity of the hex anode is three position correction tables (one for each layer).

In summary, we now have six correction tables: three time correction tables – one for each set of time sums (e.g. for $t_{u_1} + t_{u_2}$) and three position correction tables – one for each anode layer (e.g. $t_{u_1} - t_{u_2}$).[5] The algorithm transforms these six correction tables into six tables specific to the individual parameters: u_1, u_2, v_1, v_2, w_1, w_2. The result is a significant improvement on both position and timing resolution for all reconstructed hits.

The Automatic Calibration

The "automatic calibration" is the second built-in calibration feature of the reconstruction routine. The positions are first calculated using the time data from the u & v layers. The process is repeated for the v & w layers. The algorithm calculates the time-to-position coefficients such that they minimize the deviation between anode solutions. The free parameters are as follows: f_v, f_w & w_{offset}. We use parameter, w_{offset} to match the centers of the anode layers. Anode layer hit positions are calculated as follows:

[5] Note that these correction tables are orthogonal to one another.

$$u = (t_{u_1} - t_{u_2}) * f_u$$

$$v = (t_{v_1} - t_{v_2}) * f_v$$

$$w = (t_{w_1} - t_{w_2} + w_{offset}) * f_w$$

Anode Wire Discussion

As mentioned in Chapter 2, each anode layer is comprised of both a signal and reference wire, tightly wrapped around spools (Fig. 2.8). Together, they form a waveguide - when an electronic pulse interacts with an anode layer, the pulse begins to propagate along the waveguide. Since we directly infer the detector position from the anode timing signals, it is essential to accurately determine the time required for a pulse to travel one winding over. This is of course, dependent on the velocity of propagation, the spacing between windings and the length of the wire required to make a winding. While we shall assume for the time being that all the windings that comprise an anode layer are identical (i.e., the time to distance ratio is constant), the ratios generally differ between anode layers.

The resort routine uses an *a priori* estimate of the time to distance ratio for the *u* layer to generate the relative ratios for the *v*&*w* layers. After all, it has been mentioned that each pair of layers redundantly calculates the position on the detector. The routine minimizes the discrepancy between calculations by adjusting the time to distance ratios relative to the *u* layer. This can be verified by plotting the $x-y$ electron position for a specified slice of time, $e1\text{TOF}_{\text{min}} < t < e1\text{TOF}_{\text{max}}$ (Fig.3.4). If the routine is working properly, the distribution should be circular. Otherwise, we can modify the ratios we use to convert the acquired timing signals of the pulses to position data. Before moving on, we fist need to define what is meant by *x* position, *y* position and *z* position. Table 3.1 relates these axial directions to the laboratory frame.

Table 3.1: Spectrometer Axes Guide

Direction	Physical Assignment
x-dir	TOF-axis
y-dir	jet-axis
z-dir	beam-axis

It should be noted, the geometry of the u layer is taken to be known as is the active diameter of the MCP. Taking the propagation speed to be $\sim c$, the time to distance ratio can be calculated. If for example, the diameter is in reality 79mm, the error will be accounted for as we twiddle the values for the acceleration region of electrons and electric field. In essence, we produce a virtual experiment with MCP diameter 80mm that possesses the resolution inherent to the 79mm diameter experiment.

Up to this point, only the resort routine with its associated set of calibrations have been employed. While the effect of these calibrations has to a large extent improved the overall resolution of our data, the primary achievement was the salvaging of data to improve statistics. The next series of techniques will be discussed in an effort to further improve resolution and accuracy of the physical data. We begin by describing the process of presorting the reconstructed events; a process whereby data are grouped according to charge state as well as isotope.

3.2 Correction to The Power Supply Drift

Given the lengthy duration of the data acquisition process, it was deemed necessary that we evaluate the constancy of the power supply that produced the spectrometer's electric field. Using the statistically abundant Ne^{+2} charge state[6], we evaluated the dependence of the recoil TOF on the event counter[7]. The left panel shown in Figure 3.5 reveals the unsteady behavior of the recoil TOF and further, shows its functional dependence on real-time.

[6]It should be noted that this figure was generated using the "above K-ionization threshold" data set. The "3p-excitation" data set did not require this method of calibration since the overall recording time was comparably short (i.e. there was insufficient time to incur a noticeable power supply drift).

[7]The term "event counter" refers to the chronological enumeration of events collected in the laboratory.

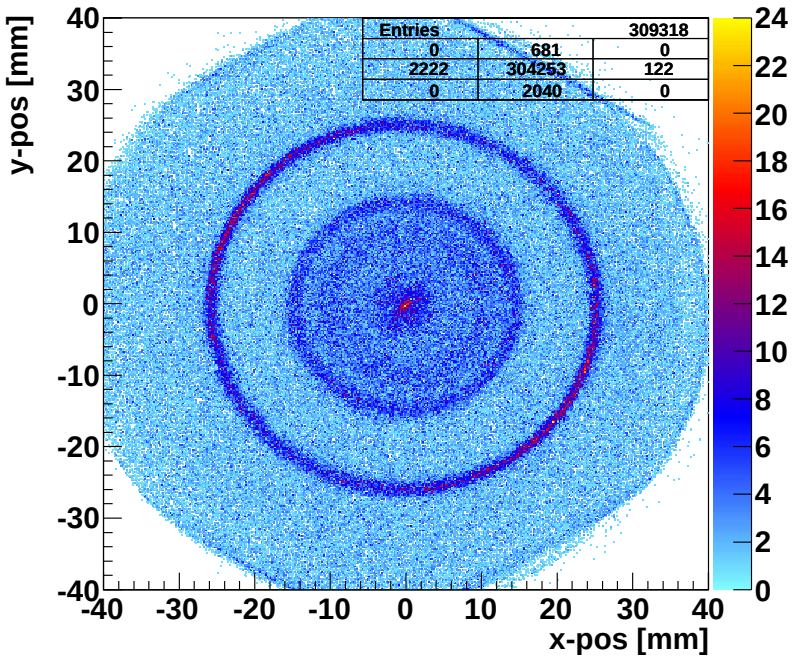

Figure 3.4: Shown is a plot of the electron position for a slice of the TOF data ($44 < e^{-}_{TOF} < 48$ns). A proper conversion of the signal-time data to position-data are confirmed by the presence of circular distributions.

We corrected for fluctuations in the recoil TOF by subdividing the distribution (Fig.3.5, left) into fifty columns. The TOF values along the top and bottom edge of each column were recorded. The average of these respective pairs was used to generate a 5^{th} order polynomial correction function. The correction was implemented by redefining the recoil TOF according to equation 3.1. The corresponding effect is shown in the right panel of Figure 3.5.

Our motivation for using the recoil TOF (Fig. 3.5) to correct the power supply drift was due to its direct relationship to the electric field. Consider two ions, each born with zero momentum – one at the start and one at the end of a data recording session. Assume the length of recording time is sufficiently long as to allow for the development of a small drift in the spectrometer power supply. We can write the kinematic equations that describe each respective particle as follows:

$$x = \frac{qE_1}{2m}t_1^2$$
$$x = \frac{qE_2}{2m}t_2^2$$

These equations reduce to,

$$\frac{E_2}{E_1} = \left(\frac{t_1}{t_2}\right)^2$$

The ratio of the electric field is shown to be proportional to the square of the inverse ratio of the recoil TOF. We plot the power supply fluctuation in the left panel of Figure 3.5. Next, we fit the data with a function, Γ. We use this function to calibrate the recoil TOF,

$$r_{1_{tof}} = r_{1_{tof}} * \left(\frac{r_{center}}{\Gamma}\right), \tag{3.1}$$

where r_{center} represents the average value determined from the first bin of data. The corrected plot is shown in the right hand panel of Figure 3.5.

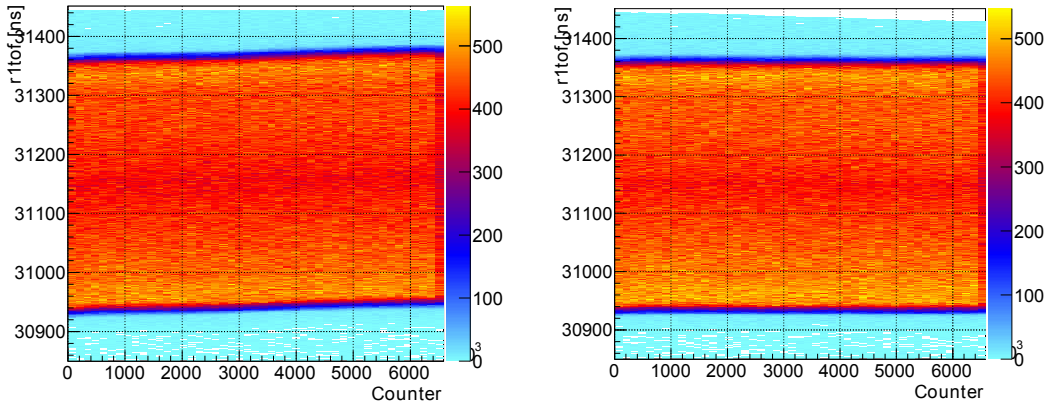

Figure 3.5: The left panel shows the drift of the power supply as a function of data acquisition. A function was fit to match the profile of the drift. The corrected data are shown in the panel, right.

3.3 Wiggles Spectrum

The previous section describes the first step toward the accurate determination of the spectrometer's electric field. We now turn our attention to the applied magnetic field in an effort to make a similar first step. While we can estimate the magnetic field strength by monitoring the amount of current we deliver to the Helmholtz coils, this is an inaccurate approach, akin to monitoring the level of voltage we apply to the spectrometer via the power supply. A far more accurate approach involves the analysis of what has come to be known as a "wiggles" spectrum. It should be noted that this technique requires a special data set that is typically generated in advance of a COLTRIMS experiment. For this special case, we lower the spectrometer voltage allowing the electrons sufficient time to execute numerous cyclotron gyrations before hitting the detector. This configuration allows us to generate a wiggles spectrum. In order to maximize the solid angle collection of the high-energy electrons without excessively compromising resolution, we designed the electron side of the spectrometer to have a rather short acceleration region ($d = 42.7$mm). While the design of the spectrometer ensured the collection of all recoil ions, the 4π solid angle collection for electrons was limited to energies no greater than 5 eV. The solid angle collection is governed by the external magnetic field that is applied to the spectrometer by way of the Helmholtz coils. A "wiggles" spectrum is a plot of the electron's radial position versus its corresponding TOF. Recently, this convention has evolved into a modified version where we plot either the x or y-direction with respect to the TOF. This "modern" form is depicted in the left panel of Figure 3.6. We identified the gyration nodes and plotted them in the right panel of Figure 3.6. The slope of the linear fit represents the gyration period, T for the electrons. The relationship between the gyration period and the magnetic field strength is derived below using Newton's 2^{nd} law and the Lorentz force equation,

$$\frac{mv_{\perp}^2}{r} = qv_{\perp}B_{\parallel}$$
$$\omega = \frac{qB_{\parallel}}{m} = \frac{2\pi}{T}$$
$$B_{\parallel} = \frac{2\pi m}{qT}$$
$$B_{\parallel} = 3.75G$$

where the empirically determined gyration period, $T = 95.406$ ns was used to determine $B_{\parallel}$. A comment should be made at this time – the calculation of the magnetic field strength is formulated on the assumption that $E_{\perp} = 0$. While great care is taken in the experimental setup to ensure that the $\vec{E}$ and $\vec{B}$ fields are anti-parallel to one another, perfect alignment is atypical, as will soon be evidenced in the next section. The question then becomes, is it the electric or magnetic field that is misaligned with respect to the spectrometer? The short answer is, it is the latter. The Helmholtz coils are much more prone to mis-alignment than the spectrometer, which is bolted down to a precisely machined platform. In summary, the electric field may be regarded as being correctly aligned with respect to the spectrometer (and the beamline for that matter); we are simply after its magnitude. The magnetic field on the other hand, will require a small correction.

3.4 Calibration of Electron Position Data

We designed the Helmholtz coils to produce a uniform magnetic field in the region of the spectrometer. An effort was made to ensure the field was oriented anti-parallel to the spectrometer's electric field (it is assumed that the electric field is already in alignment with the axis of the spectrometer). Despite these efforts however, the Helmholtz coils were found to be slightly askew during data acquisition as evidenced by way of a small $\vec{E} \times \vec{B}$ term for the electrons.[8] This section

[8]The effect this drift term has on the trajectory of the more massive recoil ions is negligible.

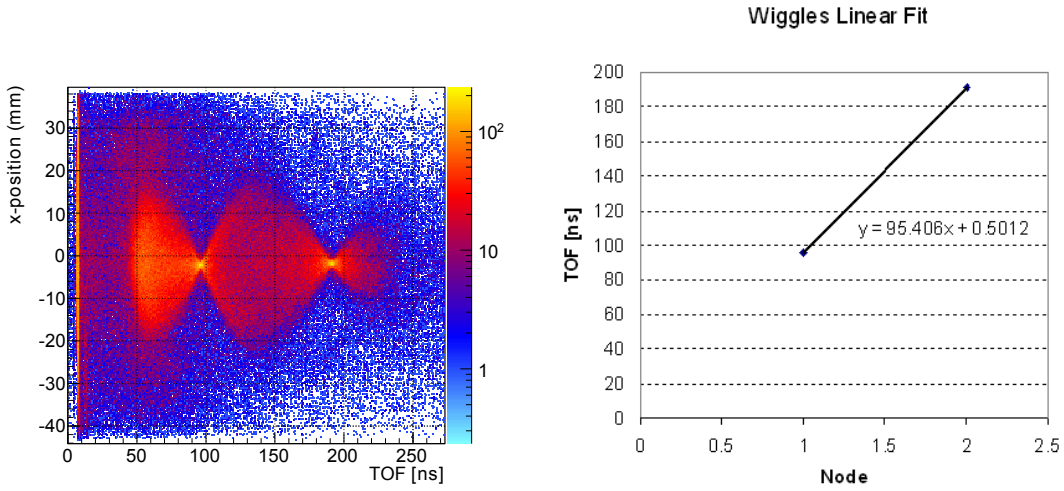

Figure 3.6: The nodes of the wiggles spectrum are identified in the left panel. The slope of the line that fits the nodes represents the gyration period [ns] of the electron and is directly related to the strength of the magnetic field.

begins by describing the method used to identify this drift. It concludes with details of the linear correction to offset the misalignment of the magnetic field.

The most effective method for checking the field alignment is by way of a "fish" plot.[10] Aptly named for its resemblance to the aquatic animal, this histogram shows the relationship between [electron] position and TOF (Fig.3.4). Since this plot is in actuality, a 3D surface that has been projected onto a 2D histogram, it is necessary to slice or "fillet" the plot in order to reveal the structure inside. Figure 3.8 shows such a fillet – the slice was taken such that $|ey_1| < 1.0$. The resulting plot contains events that take place within a 2 mm slice of the original 3D fish. Both a node and an anti-node are revealed in Figure 3.8 at $e1\text{TOF} = 93.6\text{ns}$ & 46.8ns, respectively. The node is produced by electrons that are "born" in the interaction region between the beam and the jet and have sufficient time to complete a full gyration. If the magnetic field was in line with the spectrometer, both the node and anti-node points would be found on the $x = 0$ line. Instead, we find these points to be off-axis, a result of the $\vec{E} \times \vec{B}$ drift. We correct for this drift by applying a linear correction to the electron position.

[10]The fish plot is equivalent to a wiggles plot, except the former is generated under conditions of a stronger applied electric field.

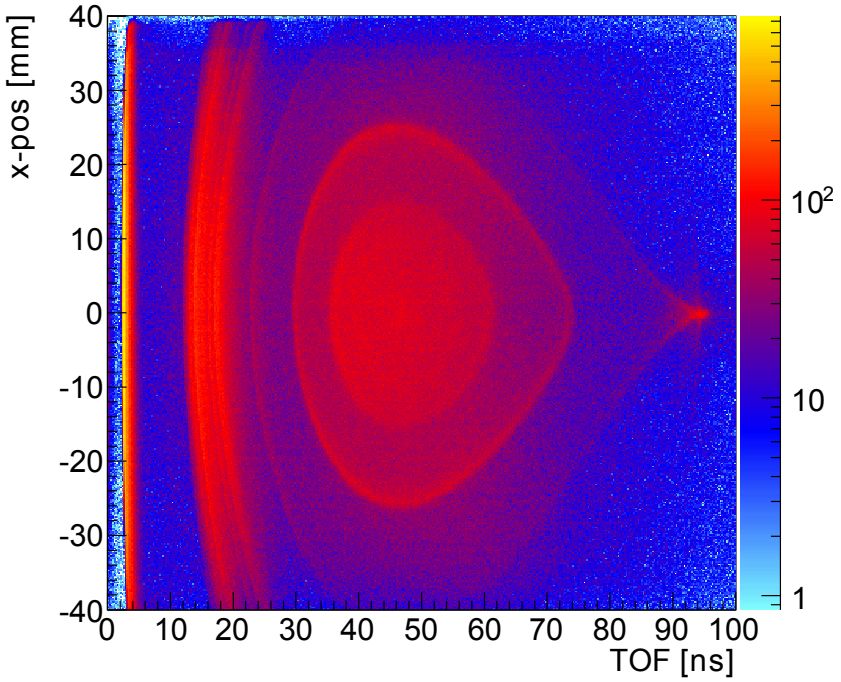

Figure 3.7: This plot shows the relationship between detector position and TOF for electrons associated with the $^{20}Ne^{2+}$ distribution. While a node is visible at ~ 95 ns, much of the structure of the plot is obscured as it is a 3D surface projected onto a 2D histogram.

While it is entirely possible for misaligned Helmholtz coils to produce curvilinear field lines in the spectrometer region, the radius of curvature of such a field is taken to be very large ($R \to \infty$), hence, justifying the use of a linear correction to offset the drift. Taking the equation of the line defined by these two points and subtracting it from each position datum point,

$$e_{x1} = e_{x1} - (mt_{\mathrm{TOF}} + b).$$

we correct for the misalignment of the magnetic field. The corrected x-fish plot is shown in Fig 3.8. We repeat the process for the y-fish plot.

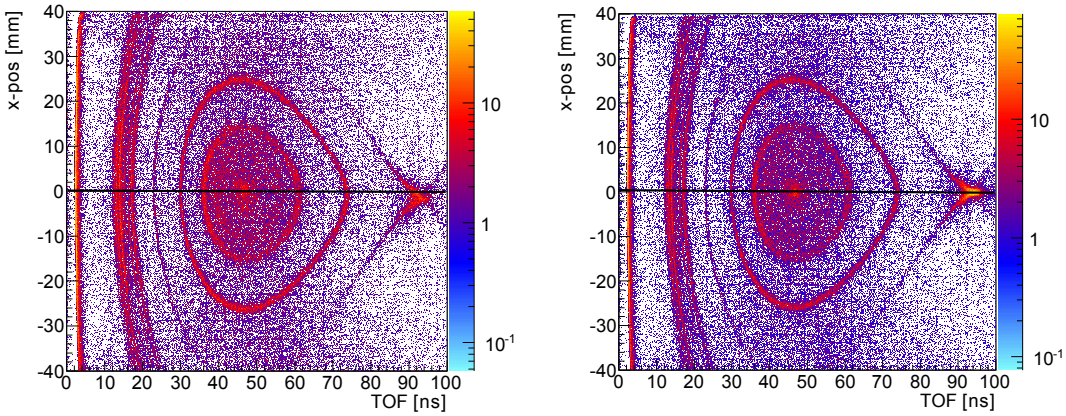

Figure 3.8: The left plot shows how slicing the 3D fish plot reveals the off-axis placement of an anti-node at ~ 46.8 ns and node at ~ 93.6 ns. We establish a linear correction to offset the $\vec{E} \times \vec{B}$ drift associated with the misalignment of the magnetic field. The right panel represents this correction.

3.5 Electron Momentum in the Time of Flight Direction

Taking the position data to be sufficiently calibrated, we next turn our attention to the momentum of the electrons. From kinematics, the component of momentum along the time of flight direction is as follows:

$$p_x = \frac{m_e d_e}{t_{\text{TOF}}} - \frac{qE}{2} t_{\text{TOF}} \tag{3.2}$$

This implies that energy ($\mathscr{E} = \frac{p^2}{2m_e}$) is dependent on two parameters: electron acceleration length, d_e and spectrometer field strength, E. Note, the former is inversely proportional to the time of flight; whereas, the latter is directly proportional. This is problematic if calibrating to a single line energy. For example, a line of high energy corresponds to electrons possessing a short time of flight. Consequently, the first term in equation 3.2 dominates the second. This uncertainty in the electric field, if carried throughout an analysis would lead to erroneous results indeed! Therefore, to ensure proper calibration of the spectrometer requires multiple line energies which span an acceptable range of energy. Before we proceed to the final stage of calibration, we first take note of the transverse components of electron momentum.

3.6 Electron Momentum in the Transverse Direction

In addition to determining the component of momentum in the TOF direction, we need to accurately measure the transverse components as well. Granted, this is not a specific method of calibration, but it is relevant to the energy calibration method discussed next. Calculating these components is a bit more complicated than finding the component of momentum in the time of flight direction. There is after all, a coaxial external magnetic field present (Fig.3.9)[32]).

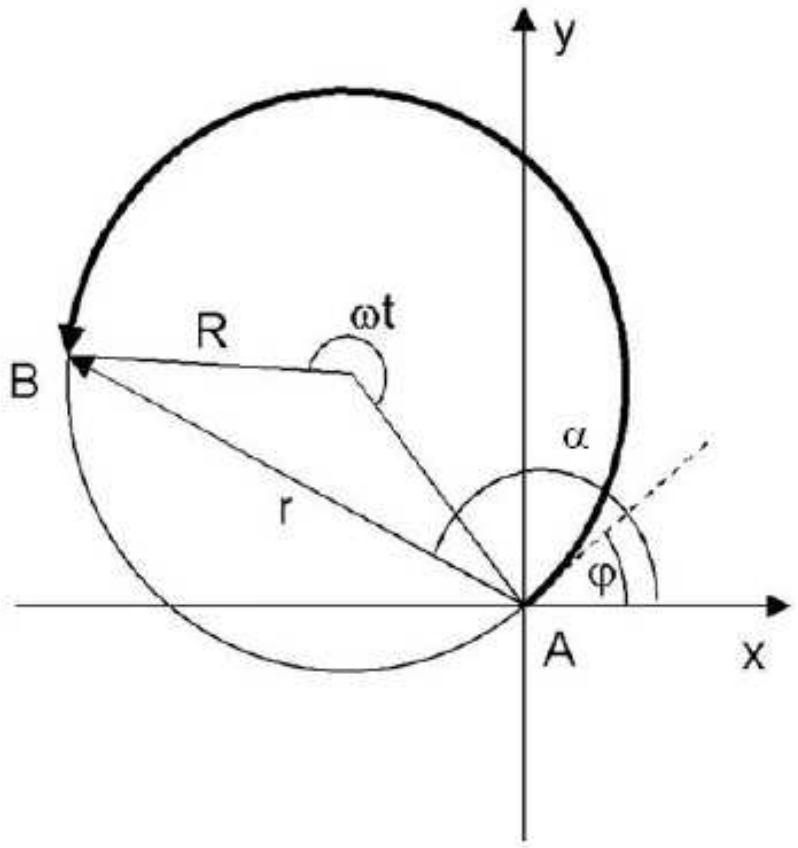

Figure 3.9: The electron momentum that is perpendicular to the magnetic field, $p_{\perp}$ will execute circular motion in this plane. We calculate the inital momentum components with respect to the lab axes analytically.

The electron's position on the detector depends on both the initial momentum of the particle as well as the time available for the particle to gyrate about a field line [32]. Using geometry and the Larmor radius equation (Eq.2.2), we can relate the parameters of Figure 3.9 as follows:

$$R = \frac{r}{2\,|Sin(\omega t/2)|} \tag{3.3}$$

$$\varphi = \alpha - \frac{\omega t}{2} \tag{3.4}$$

Knowledge of the perpendicular component of momentum (from the Larmor radius) and the emission angle, φ allows one to determine the transverse components of momentum relative to the cartesian axes.

3.7 A Comparison of Line Energies to Published Results

Our investigation into the core-excitation of neon has serendipitously revealed to us an excellent method of spectrometer calibration. A pulsed photon beam (867eV) was selected to promote core ($1s$) electrons to the $3p$ excited state (Eq.3.5). The subsequent electronic relaxation of this initial state produced among others, a population of Ne^{2+}. An analysis of this charge state revealed numerous channels that involve a two-step shake-off process.

$$Ne + \gamma \rightarrow Ne(1s2s^2 2p^6 3p) \tag{3.5}$$

The line energies of interest are shown in Figure 3.10. Table 3.3 provides identification of the enumerated lines in this plot and the respective energies.[21]. We use these energies as a benchmark, to calibrate the electron acceleration length and electric field of the spectrometer. Recalling, there are two terms in Equation 3.2 - a term that is proportional to time with the electric field strength

acting as a coefficient, the other term is inversely proportional to time with the acceleration length of the spectrometer acting as a coefficient. We used low-energy lines to calibrate the electric field coefficient and high-energy lines to calibrate the acceleration length parameter. We provide measured values of the line energies in the 4^{th} column of Table 3.3 as well as the percent difference with published values.[21]

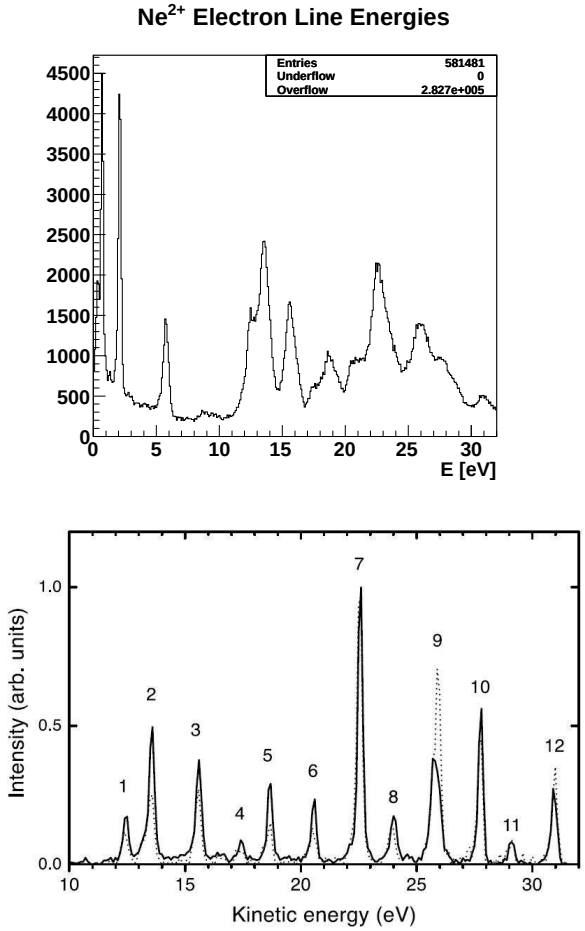

Figure 3.10: A part of the second-step auger spectrum resulting from the transition between the initial $Ne(1s^{-1}3p)$ and final Ne^{2+} states. The top panel represents our data, the lower panel represents published results [21]

Through a short iterative process, the line energies obtained through our experiment were aligned with published data (Fig. 3.10b). The parameters used to converge on these lines were

Table 3.2: A Comparison of Our Line Energies to Published Results

Line No.	Transition	$KE_{\text{published}}$ (eV)	KE_{measured} (eV)	% Difference
1	$2s^1 2p^5(^3P)3p \rightarrow 2s^2 2p^4(^1D_2)$	12.6	12.5	0.80
2	$2s^0 2p^6(^1S)3p \rightarrow 2s^1 2p^5(^1P_1)$	13.6	13.5	0.73
3	$2s^1 2p^5(^3P)3p \rightarrow 2s^2 2p^4(^3P)$	15.7	15.6	0.64
4	$2s^1 2p^5(^3P)4p \rightarrow 2s^2 2p^4(^1D_2)$	17.4	17.5	0.57
5	$2s^0 2p^6(^1S)4p \rightarrow 2s^1 2p^5(^1P_1)$	18.7	18.7	0.00
6	$2s^1 2p^5(^3P)4p \rightarrow 2s^2 2p^4(^3P)$	20.6	20.7	0.48
7	$2s^1 2p^5(^1P)3p \rightarrow 2s^2 2p^4(^1D_2)$	22.6	22.6	0.00
8	$2s^0 2p^6(^1S)3p \rightarrow 2s^1 2p^5(^3P)$	24.1	-	-
9	$2s^1 2p^5(^1P)3p \rightarrow 2s^2 2p^4(^3P)$	25.7	26.0	1.16
10	$2s^1 2p^5(^1P)4p \rightarrow 2s^2 2p^4(^1D_2)$	27.8	27.5	1.08
11	$2s^0 2p^6(^1S)4p \rightarrow 2s^1 2p^5(^3P)$	29.1	-	-
12	$2s^1 2p^5(^1P)4p \rightarrow 2s^2 2p^4(^3P)$	30.9	30.9	0.00

Table 3.3: The enumerated transition energies correspond to the peaks shown in bottom panel of Figure 3.10. We also provide published and measured values for the respective line energies. We include the percent difference to show the level of agreement between the two spectrum (Fig.3.10).

of course, the electric field, $|E|$ and the electron acceleration region, d_e. The values were found to be 2.24 V/m and 42.7 mm respectively.[10]

3.8 Recoil Momentum Calculation with Electrostatic Lens Calibration

Due to the mass of the recoil ion, we found it necessary to incorporate an electrostatic lens on the recoil side of the spectrometer to improve the resolution of the distribution. While the exact profile of the electric field in this region is unknown, it is only necessary for the profile to be axially symmetric in order to accurately calculate the recoil momentum along the TOF direction. From kinematics we find that two particles with equal and opposite momentum along the time of flight

[10]The acceleration length, d_e was recorded (as accurately as possible by hands-on means) in the laboratory book to be 41.5mm.

direction differ only by the turn around time of the particle whose momentum is initially anti-parallel to the $\vec{E}$-field of the spectrometer.

Aside

Consider two identical particles possessing momenta p_{oz} and $-p_{oz}$, respectively. From kinematics, the difference between the two TOF measurements is the turnaround time of the anti-parallel ion,

$$p_f = p_o - qEt$$

$$0 = p_{oz} - qEt$$

$$p_{oz} = \frac{qE}{2} t_{turn} \tag{3.6}$$

where $t_{turn} \equiv 2t$. From the recoil TOF histogram (Fig. 1.3 found on page 7), one can determine the maximum and minimum TOF for a given charge state. Then Eq. 3.6 becomes,

$$p_{oz} = \frac{qE}{2}(t_{max} - t_{min}). \tag{3.7}$$

Equation 3.7 is the maximum z-momentum for a given charge state. Next, we need to assign values to all events which occur for $(t_{min} \leq t \leq t_{max})$. Recognizing that momentum is a linear function of time, we first define t_o as the center of the TOF distribution. We then assign a momentum based on the time relative to this center, t_o,

$$p(t) = \frac{qE}{2}\left(\frac{t_{max} - t_{min}}{t_{max} - t_o}\right)(t - t_o) \tag{3.8}$$

By symmetry, the $\left(\frac{t_{max}-t_{min}}{t_{max}-t_o}\right)$ reduces to 2,

$$p(t) = qE(t - t_o) \tag{3.9}$$

When $t = t_{max}$, the equation for momentum becomes,

$$p(t) = qE(t_{max} - t_o) \tag{3.10}$$

which is equivalent to Eq. 3.7.

Using the Momentum Sum

If there exists a sufficient number of events that are "fully" measured (i.e., we directly measure the momentum of *all* constituents within an event), we can plot the corresponding momentum sum of these particles. Conservation of momentum requires that this total be zero; however, this does not happen due to resolution effects. While there will be some width to the distribution, it should be centered about zero. Adjustments to the offset parameters associated with the electrostatic lens can be made with a Gaussian fit on the sum-momentum distribution.

Chapter 4

DETECTOR RESOLUTION IN THE CONTEXT OF RADIATIVE DECAY

4.1 The Decay Channels of Ne^+

In this chapter, we identify and isolate events that correspond to the radiative decay channel of Ne^+. We shall see that the images associated with this channel press the limits of the detector resolution. Noting these limitations, we set out to quantify the detector resolution. Next, we calculate the momentum vector of the photon in order to investigate its correlation with the photo-electron. Additionally, we briefly investigate the non-radiative decay channel of Ne^+ in the context of the newly quantified detector resolution. As a final point of interest, we consider a novel concept of scattering between the emitted photon and photo-electron.

$$\underbrace{Ne(1s^2 2s^2 2p^6) + h\nu(872.9eV)}_{\downarrow} \longrightarrow \overbrace{Ne^+ + e^-_{fast}}^{\text{Direct Ionization/Recapture}}$$
$$Ne(1s^{-1})^+ + e^-_\gamma(1.7eV) \rightarrow \underbrace{Ne(2p^{-1})^+ + e^-_\gamma + \gamma}_{\text{Radiative Decay}}$$

4.1.1 Identifying the Radiative Decay Channel - Recoil Ion Distribution

As mentioned earlier in Chapter 1, we can identify the radiative decay channel from the recoil Time-Of-Flight (TOF) plot (Fig.1.3 found on page 7). The histogram serves as a concise record of the measured charge states as well as their respective ratios of abundance; each distribution has been identified accordingly. Focusing on the $^{20}Ne^+$ distribution, we observe a unique structure: two broad peaks that surround a narrow central spike.

The recoil ions within the central spike possess a minimum momentum relative to those of the surrounding peaks: $\left|\vec{k}_{\text{photon}}\right| \sim 0.23$ au (associated with the emitted photon). By comparison, the structure surrounding the central spike implies a much higher recoil momentum, due to either the direct ionization of the valance shell[1] or via Auger decay in conjunction with the recapture of the photo-electron.

To gain an appreciation for the rarity of the radiative decay channel, we calculate the relative charge state abundances (Table 4.1). This was accomplished by dividing the number of events for a given charge state by the respective total (Fig.1.3 found on page 7).[2] The charge state ratios depend upon the incident photon energy (which is assumed to be in excess of the K-ionization threshold value) and the lifetime of the 1*s* vacancy, ($\Gamma = 270$ meV) both of which affects these percentages.

Table 4.1: Relative Charge State Distribution

Charge State *	Relative Abundance (%)
Ne^{1+}	4.65
Ne^{2+}	89.47
Ne^{3+}	5.55
Ne^{4+}	0.31
Ne^{5+}	0.02

* Based on the ^{20}Ne isotope.

While the Ne^{+} distribution accounts for only 4.65% of the collected events and noting that the aforementioned central spike represents a subset of these events, the statistics available for such an analysis are small indeed.

4.1.2 Identifying the Radiative Decay Channel - Electron Distribution

Evidence of the radiative decay channel also appears in the electron TOF data (Fig.4.1.2). We observe a small distribution of hits at approximately 0.1ns, implying the Micro-Channel Plates

[1] The 1^{st} ionization potential of neon is 21.56 eV ([7]) which results in recoil momentum, $|\vec{p}_{recoil}| \sim 7.9$ au. We show in a later section that our detector cannot resolve this channel apart from the Auger/recapture channel.

[2] The ^{20}Ne isotope represents the only complete set of charge state distributions.

(MCP) are sufficiently sensitive to measure energetic photons. It should be mentioned that the statistics asssociated with measuring the photon are low; and the resolution that is associated with such low TOF values is poor. Yet, it is worthwhile to mention this interesting yet accidental discovery - the COLTRIMS system is capable of measuring *all* constituents of a radiative event (i.e., we can directly measure the momentum vector of an individual photon!).

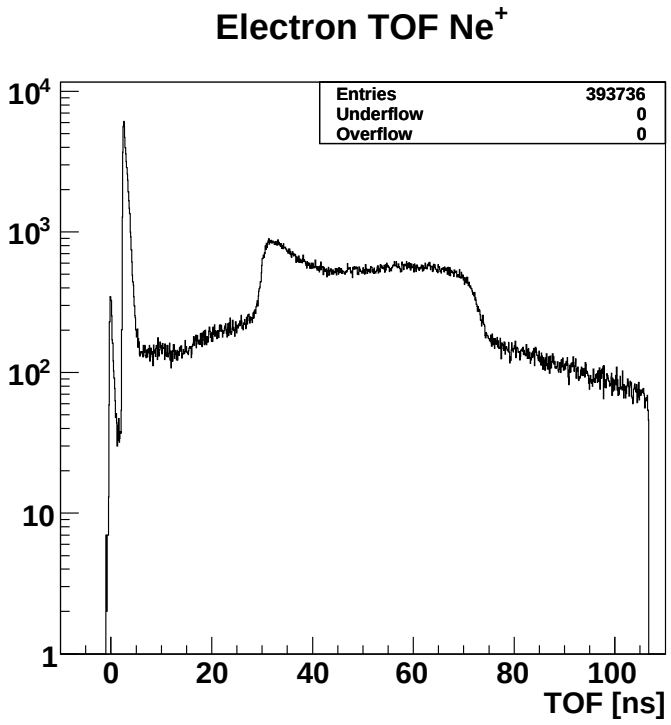

Figure 4.1: A small distribution of electron hits is apparent near 1ns. This corresponds to a direct measurement of photons, an interesting feature of the COLTRIMS system. Direct ionization/recapture is observed at approximately 3ns whereas the photo-electrons make up a much broader peak ($25-75$ns).

4.2 Quantifying Detector Resolution

To improve both statistics and overall resolution, we consider events where we measure the photo-electron (1^{st} hit) in co-incidence with the recoil ion. Next, we invoke the conservation of

momentum to infer the momentum vector of the photon. An array of momentum density plots is shown in Figure 4.2. The top row represents slices of the photo-electron momenutm sphere. The structure of the photo-electron distribution is observable with the detector resolution at this fixed energy. The middle row represents slices of the recoil ion momentum sphere. As will soon be shown, these slices should be nearly identical to that of the photo-electron. However, the inferior resolution at these energies made it clear that they are not. In fact, it was necessary to pan out to a wider range in order to observe all the recoil hits. Finally, the bottom row represents slices of the photon momentum sphere. The distribution is inferred via the conservation of momentum; therefore, it reflects the resolution of the other constituents of the event. After all, the photon distribution should be isotropic as it derives from the $2p \rightarrow 1s$ transition. Regardless, nearly 70k of radiative decay events have been successfully recorded with this COLTRIMS system.

4.2.1 Expected Values

At first glance, it appears that the TOF axis possesses superior resolution to the spatial dimensions (Fig.4.2). As a means of testing this claim, we turn to established values, using the well known L_1 ionization potential of neon and the calibrated beam-line energy (Chapter 3) to calculate the expected radii of the momentum distributions (in this temporal direction). Then the energy of the photo-electron is as follows:

$$\begin{aligned} E_{\text{synch}} &= 872.9\text{eV} \\ E_{L_1} &= 870.9\text{eV} \\ E_\gamma &= 2.0\text{eV} \\ k_\gamma &= 0.383\text{au} \end{aligned} \tag{4.1}$$

This value, which corresponds to a momentum of 0.38au agrees well with the data shown along the TOF axis in the top left panel of Figure 4.2. Consequently, we can take some confidence in the

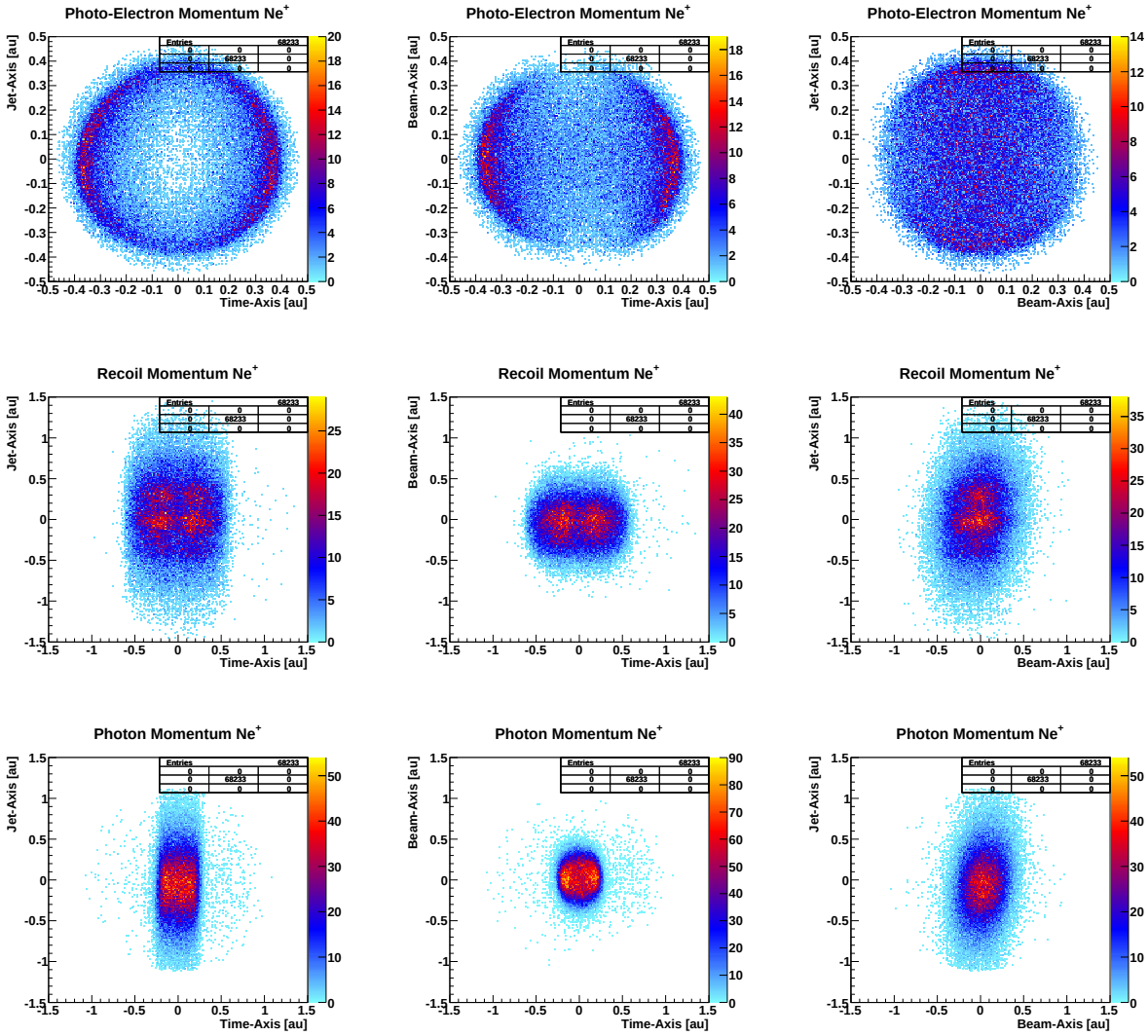

Figure 4.2: The width of each distribution along the time-axis agrees well with predicited values, showing superior resolution to that of the spatial dimensions. The slices of photon momentum in the bottom row confirm the successful measurement of the the radiative decay channel of Ne^{+}.

temporal resolution for electrons in this energy range. Of course, this is a rather specific statement on behalf of the electron detector. Later, we will quantify how the resolution behaves as a function of particle energy.

Upon core ionizing the target gas, a valence electron "falls" to fill the $1s$ vacancy. If the transition energy manifests itself as a photon, the recoil ion experiences a second smaller "kick" of momentum. Given the transition energy from the $2p$ valence shell to the $1s$ vacancy is 849.65eV (citePindzola), this value of photon momentum can be quantified as follows:

$$\begin{aligned} p_{h\nu} &= \frac{\mathscr{E}}{c} \\ &= \frac{849.65}{(27.212)(137.)} \\ &= 0.228\text{au} \end{aligned} \tag{4.2}$$

If we consider the case where the photon is emitted in the same direction as the photo-electron, then we can arrive at the total momentum that can be transferred to the recoil ion for this channel of decay.

$$\begin{aligned} p_{\text{recoil}} &= 0.383 + 0.228 \\ &= 0.611\text{au} \end{aligned} \tag{4.3}$$

We observe that this value is also in good agreement with Figure 4.3. Additionally, this comparison between calculated values and experiment serves to instill confidence in the accurate results that are associated with the recoil detector, at least for this value of momentum.

Up until now, we have compared the predicted momenta of the target gas constituents to the experimental results shown in the 1^{st} column of Figure 4.2, particularly along the time-axis. Having

concluded that the resolution is superior along this TOF axis, we note the lack of agreement between the values and the spatial dimensions (beam & jet axes).

Resolution Effects from Ne^{+}

Referring to Figure 4.2, we note how the resolution differs not only between electrons with differing flight times, but also with regard to whether the momentum derives from spatial or temporal coordinates. A more consice record of the behavior of temporal and spatial resolution can be viewed in Figure 4.3.

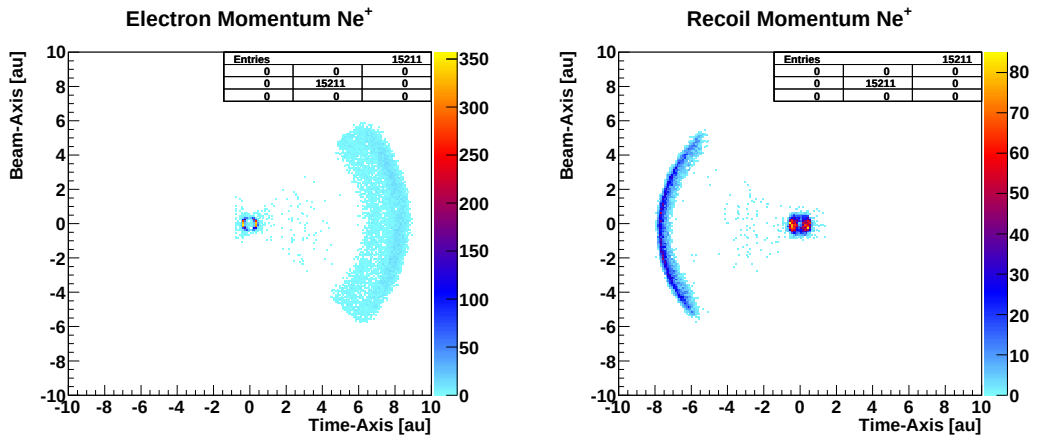

Figure 4.3: The left panel represents the direct measurement of the electrons associated with Ne^{+}. The right panel shows the direct measurement of the corresponding recoil ions. At this scale, these plots should be perfect mirrors of one another. However, the resolution changes as a function of particle energy and depends on what type of particle is being considered.

The left panel shows the resolution from the direct measurement of the 1^{st} hit electron. The low energy electrons can be associated with the radiative decay channel (Eq.4.1) while the high energy electrons represent the direct ionization (or Auger/recapture) channel. The right panel represents the measured recoil ions associated with each of these decay channels. Note, at this scale, these images should be perfect mirrors of one another (regardless of whether or not a photon was emitted). At lower momenta, the electron side of the spectrometer shows superior resolution. At higher momenta, the recoil side of the spectrometer shows superior resolution - attributed to the profile of

the electrostatic lens. It is appropriate at this time to quantify these transitions in resolution. For clarity throughout the subsequent calculations, we recall how the axes have been defined (Chapter 2),

Table 4.2: Spectometer Axes Guide

Direction	Physical Assignment
x-dir	TOF-axis
y-dir	jet-axis
z-dir	beam-axis

4.2.2 Quantifying the Electron Temporal Resolution

To quantify the resolution along the TOF axis, we take the partial derivative of the respective momentum equation (Eq.3.2) with respect to time.[3]

$$
\begin{aligned}
p_x &= \frac{m_e \Delta x}{t} - \frac{eE}{2} t \\
\Delta p_x &= \left| -\frac{m_e \Delta x}{t^2} - \frac{eE}{2} \right| \Delta t \\
\Delta p_x &= \left(\frac{9.108 \cdot 10^{-31} * 1 \cdot 10^{-3}}{(50 \cdot 10^{-9})^2} + \frac{1.6 \cdot 10^{-19} * 222}{2} \right) 5 \cdot 10^{-10} / 1.99 \cdot 10^{-24} \\
&\approx 0.01 au
\end{aligned}
$$

The equation above estimates the temporal resolution for photo-electrons, whereas, the equation below represents an estimate of the temporal resolution for Auger electrons.

$$
\begin{aligned}
\Delta p_x &= \left(\frac{9.108 \cdot 10^{-31} * 1 \cdot 10^{-3}}{(3 \cdot 10^{-9})^2} + \frac{1.6 \cdot 10^{-19} * 222}{2} \right) 5 \cdot 10^{-10} / 1.99 \cdot 10^{-24} \\
&\approx 0.034 au
\end{aligned}
$$

[3] In this rough estimate we neglect the contribution of other smaller order variants.

Regardless of energy, the resolution along the TOF axis is sufficient to analyze either channel that arises from Ne^+. However, the same cannot be said of the spatial dimensions, particularly the recoil ions.

4.2.3 Quantifying the Recoil Spatial Resolution

When considering the spatial resolution of the recoil ions, we cannot make the assumption that, $\Delta p_x \approx \Delta p_y$ as we did when calculating the resolution of the electrons. In fact, we can qualitatively observe a difference between the two spatial dimensions shown in Figure 4.4. Clearly the resolution along the beam-axis surpasses that of the jet-axis. This difference is the result of the way in which the target gas is introduced into the chamber. As the gas travels from the nozzle to the lower floor of the chamber, the spread of the thermal distribution causes the jet to diverge. This spread has been anticipated by the designers of the experiment and prior to entering the chamber the jet passes through a skimmer. Not only does the skimmer eliminate what would otherwise be an problematic background gas pressure in the chamber, but it also truncates the thermal distribution in the direction perpendicular to the jet velocity. Therefore, by the time the target gas reaches the interaction region with the beam, the thermal spread is narrower in the beam axis direction as compared to the jet velocity direction.

4.3 Analyzing the Non-Radiative Channel(s)

Here we apply the newfound knowledge regarding detector resolution to the non-radiative decay channel of Ne^+. Two channels are considered. The first occurs when the photon ionizes the valence shell of the target atom. The second can be represented using the two-step model. Subsequent to K-shell photo-ionization, an Auger decay occurs. The timescale of the second step must be sufficient to allow the ion to recapture the photo-electron.[4]. In this latter case, the recoil receives a momentum "kick" from the Auger that is considerably larger than that of the radiative

[4]In the sudden approximation, the photo-electron "sees" a potential change from $-1/r$ to $-2/r$

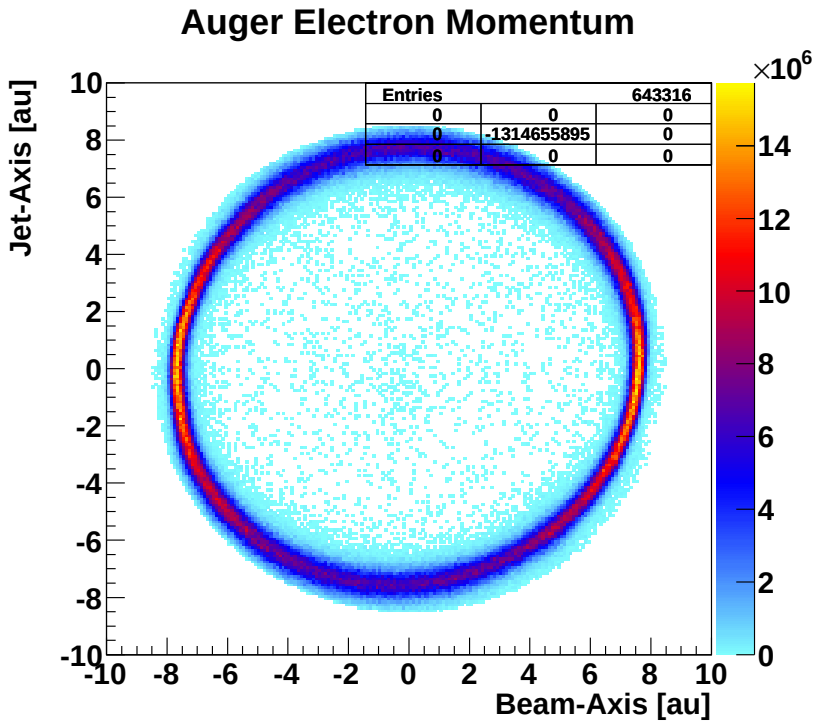

Figure 4.4: Shown is the calculated Auger momentum (which incorporates the spatial resolution differences of the recoil ion distribution). Note the spread in the jet direction is greater than that of the beam direction, the difference being attributed to the variation in thermal distributions.

decay channel. However, the energy difference between these two non-radiative decay channels is observed by comparing the respective final states,

$$Ne(1s^2 2s^2 2p^6)^+ + h\nu \rightarrow Ne(1s^2 2s^2 2p^5 np)^+ + e^-$$

$$Ne(1s^1 2s^2 2p^6)^+ + e^-_\gamma \rightarrow Ne(1s^2 2s^2 2p^5 np)^+ + e^-_A$$

The only means we have to resolve these two similarly energetic final states is to search within the recoil distribution. Figure 4.3 shows that we cannot resolve lines of such detail.

4.4 Scattering by way of the Radiative Decay Channel

A personal motivation for investigating the Ne^+ radiative decay channel is to observe the angular correlation between the emitted photo-electron and the photon. Specifically, an interest was taken in determining whether or not it was possible to observe this unique form of Compton scattering (i.e., the emitted photon scatters off the photo-electron, both of which are emitted from the same source). Depending on the time frame in which the photon is emitted, there may be interesting physics associated with such a scattering mechanism. If the photon were scattered by the photo-electron, this would potentially appear in the angular correlation between the constituents. In essence, the mechanism would be analogous to the angular correlation of K-shell ionized neon that results in Auger decay.

The primary motivation for the investigation of the aforementioned scattering is observed when comparing the photo-electron energy distribution for Ne^+ with the Voigt fit (Fig.4.5). It should be noted that we centered the Voigt curve (shown in red) at 1.99eV.[1] There exists very good agreement for all but the leading edge of the distribution. Here the deviation shows a greater number of hits than predicted by theory. At the time, it was considered plausible that a scattered photo-electron would end up in this region of the distribution. However, this notion was later dismissed; the "effect" observed is nothing more than an artifact of the resolution, which as described earlier, diminishes as energy increases.

Additionally, we plot the angular correlation between the photon and photo-electron (Fig.4.7). We observe isotropy across the angular range (Fig.4.6). Given this result, it is clear that no observed scattering occured between the photo-electron and the emitted photon.

There is still one feature/artifact that has gone unidentified. Referring to Figure 4.3, we observe what appears to be at least one line energy that cannot be attributed to a harmonic of the beam-line, a $2s$ ionization event, or any other electronic cascade that would produce a $Ne+$ ion. The feature is

[1] Note, from the calibration chapter, we determined the beam-line photon energy to be 872.9eV, resulting in an accurate measurement of the $1s$ ionization potential for neutral neon: 870.9eV.

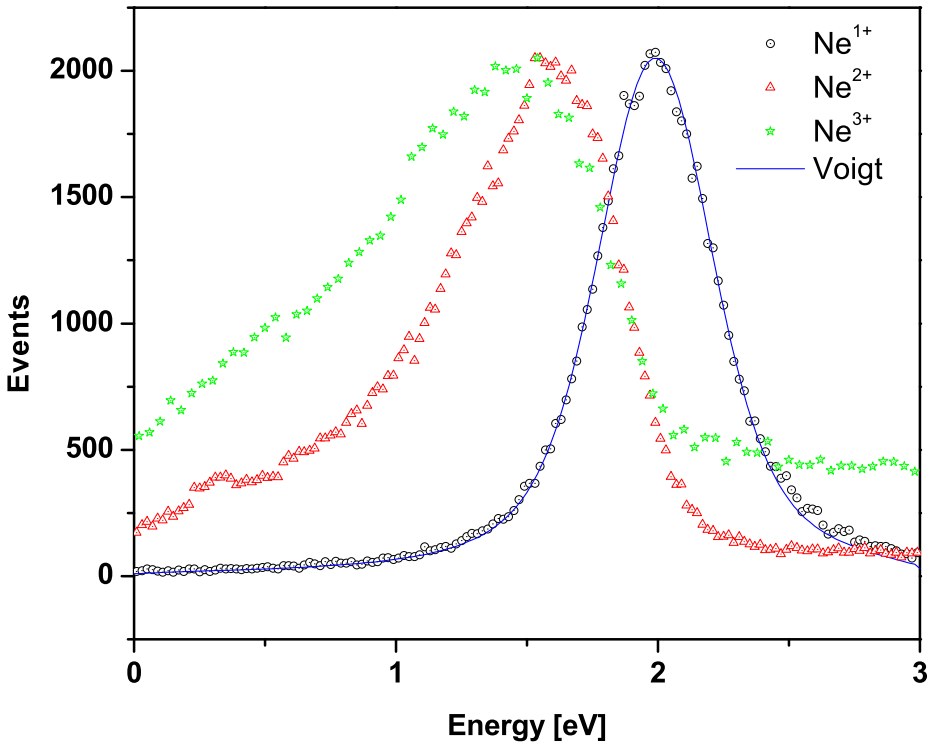

Figure 4.5: A Voigt fit is shown to fit well with the Ne^{1+} data. The slight deviation on the leading edge, initially thought to be electrons that had increased energy due to scattering with the photon, has been dismissed as nothing more than a diminishing resolution effect.

also present in Figure 4.7 which represents the energy of the electron associated with all events that measure a Ne^{+} recoil ion. It is an unanswered question as to what is causing this line-like feature.

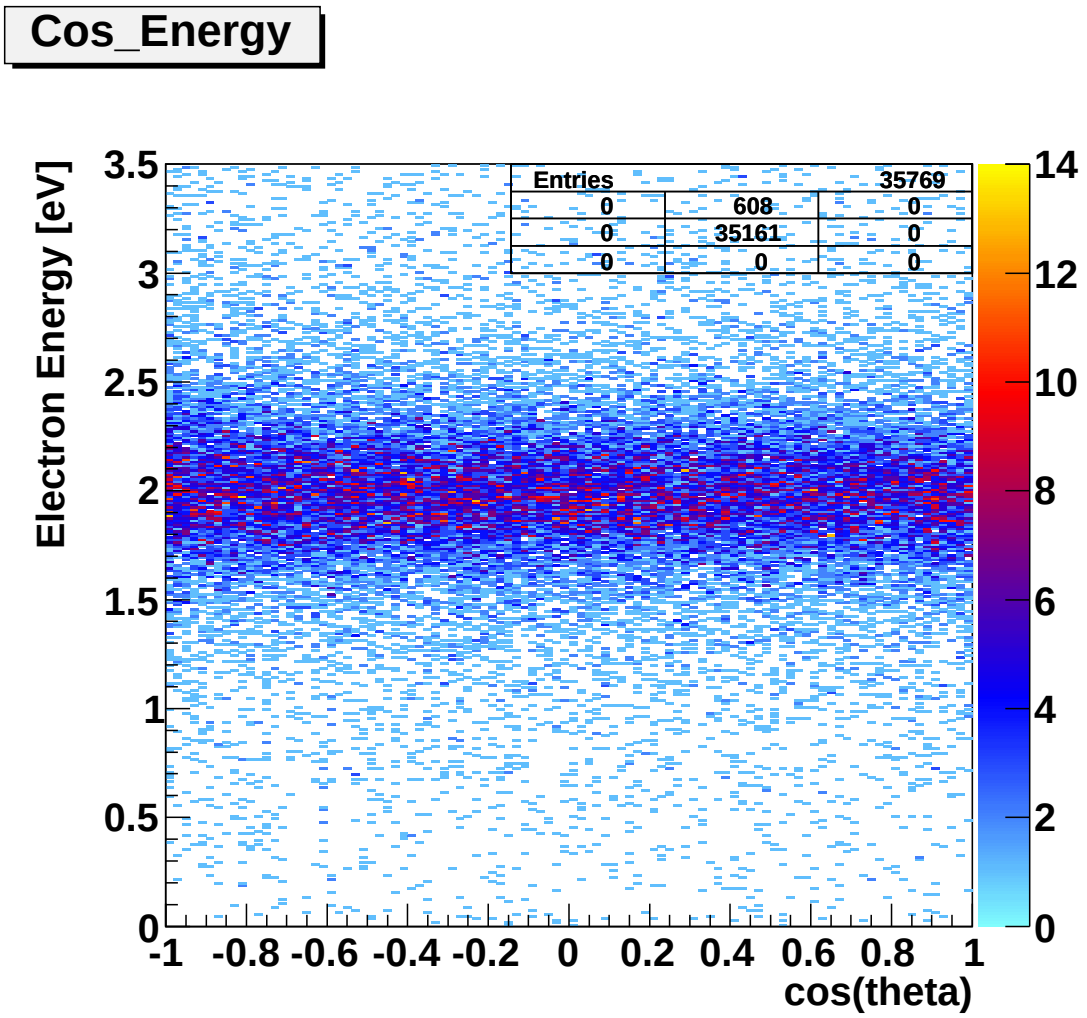

Figure 4.6: The angular correlation between the photo-electron and the photon shows isotropy. This is in agreement with the negligible cross section available, considering the lifetime of the 1*s* vacancy for radiative decay and the photo-electron energy.

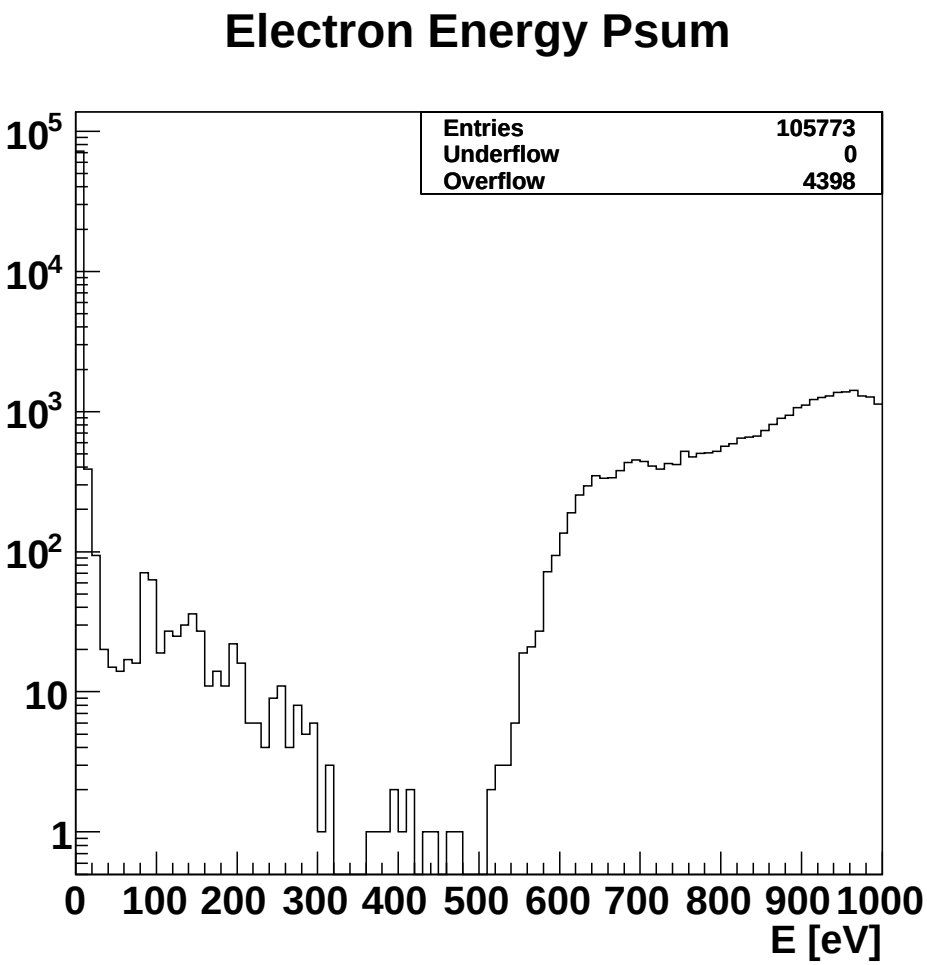

Figure 4.7: A low-energy photo-electron peak is prominant in the figure. A more broadly shaped high-energy peak is also observed, corresponding to the direct ionization/recapture channel. A third, unexplained feature is also present. Intermediate electron hits are visible in the plot and resemble low-energy lines.

Chapter 5

REVISITING THE PHYSICS OF SINGLE AUGER DECAY FROM K-SHELL IONIZED NEON

5.1 Introduction

In this chapter, we use the physics associated with the single-Auger decay of K-shell ionized neon to quantify the elliptical polarization of light used throughout the COLTRIMS experiment. From this determination, we describe a technique that computationally calibrates the polarization to suit a two-dimensional version of the experiment. Additionally, we discuss a similar computational technique that may be used to calibrate the respective Auger electron distribution. Next, we extrapolate elements of this calibration proceedure to develop a more statistically robust three-dimensional version. Finally, we present new angular correlation results that correspond to the following Ne^{2+} decay channels:

$$Ne(1s2s^22p^6)^+ + e_\gamma^- \Longrightarrow \begin{cases} Ne(1s^22s^22p^4)^{2+} + e_\gamma^- + e_{A_1}^- \\ Ne(1s^22s^12p^5)^{2+} + e_\gamma^- + e_{A_1}^- \\ Ne(1s^22s2p^5np)^{2+} + e_{A_1}^- + e_{A_2}^- \end{cases} \tag{5.1}$$

5.2 Quantifying the Ellipticity of Light

Recall that the primary motivation for conducting the COLTRIMS experiment was to measure the angular correlation of electrons associated with the double-Auger decay of K-shell ionized neon. To reach this end, we required that circularly polarized light be used to photo-ionize the target gas. However, we can show conclusively that the light from the beam-line was not circularly polarized, as previously thought. Rather, a non-negligible ellipticity is shown to have been present throughout the experiment - a fact that adds an angular bias to our results. In an effort to correct for the lack

of polarization control at the beam-line, we developed a computational method that corrects for the bias.

Physics dictates that the photo-electron distribution be symmetric about the beam-axis. While linearly polarized light gives way to a p-wave photo-electron momentum distribution, circularly polarized light essentially rotates this p-wave about the beam axis, producing a taurus-like distribution. Consequently, an elliptically polarized beam appears as an asymmetrically weighted taurus-like distribution (Fig.5.2).

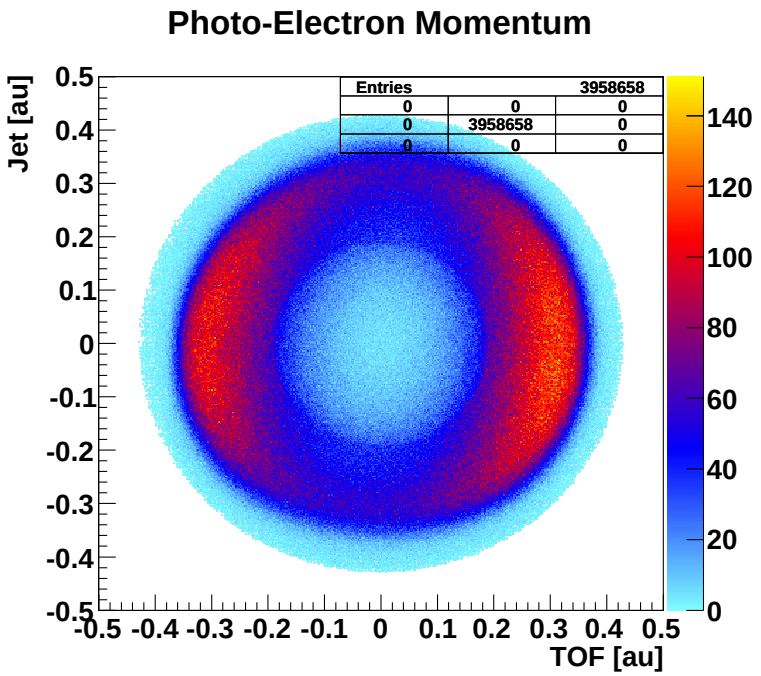

Figure 5.1: The photo-electron distribution ($0.5 < E_\gamma < 2.5$eV) shows uneven weighting suggesting elliptically polarized light was used at the beam-line. Note that the orientation of the major-axis of polarization is not orthogonal to the co-ordinate system.

Clearly, the density of events in this plot is not isotropic. Rather, we observe additional weighting along the TOF axis. Further, the axis of symmetry of this distribution is not orthogonal to the co-ordinate axes, rather it is offset by a few degrees. While the asymmetry was observed early in the analysis, it was disregarded pending the completion of the exhaustive list of calibrations described

in Chapter 3. Only after we applied this battery of calibration techniques were we able to deduce that the asymmetry was in fact, due to elliptically polarized light, and the offset is simply the major-axis of elliptical polarization relative to the lab frame. Accordingly, a point of interest among the group members was to quantify the polarization to prepare for future beam-times. The remainder of this section describes the process used to identify and quantify the elliptical nature of the light.

Selecting an Appropriate Subset of Data

In order to determine whether or not the angular distribution of photo-electrons is isotropic, we first take a planar slice of the data. However, we must exercise caution when selecting the subset of events to analyze. Consider the way in which the COLTRIMS system acquires data during the experiment. We recorded two varieties of events that corresponded to single-Auger decay, "complete" and "incomplete."

Table 5.1: Data Acquisition Chart

Type	Recoil	e^- Hit 1	e^- Hit 2	Calc.
Complete Event	X	X	X	X*
Incomplete Event	X	X	-	X
Incomplete Event	X	-	X	X

* Calculated for Improved Resolution

Referring to Table 5.1, a "complete" event occurs when we measure an Auger electron (1^{st} hit) and photo-electron (2^{nd} hit) in co-incidence with a recoil ion. An "incomplete" event occurs when we collect only a low-energy photo-electron (1^{st} or 2^{nd} hit) with a recoil ion (i.e., we regard the Auger electron "missed"). Given the limited solid angle collection of the high-energy Auger electrons, we find it statistically advantageous to focus on incomplete events, where we infer the "missed" Auger via conservation of momentum. Moreover, for the purposes of quantifying the ellipticity of the light, we do not fold in the "complete" events, since the detector collection efficiency changes when we require the co-incident measurement of *two* electrons.

Confining the Photo-Electron Momentum Distribution to 2D

To quantify the ellipticity of the light, we apply a wide-angle conical gate to the subset of events we regard as "incomplete" ($Cos(\theta_z) < 0.15$). This results in a planar slice of the photo-electron distribution, defined by the jet and TOF axes (Fig.5.2). The functional form of the angular distribution confirms the group's earlier suspicion that the polarization of the light at the beam-line was not circular but rather, it was elliptical.

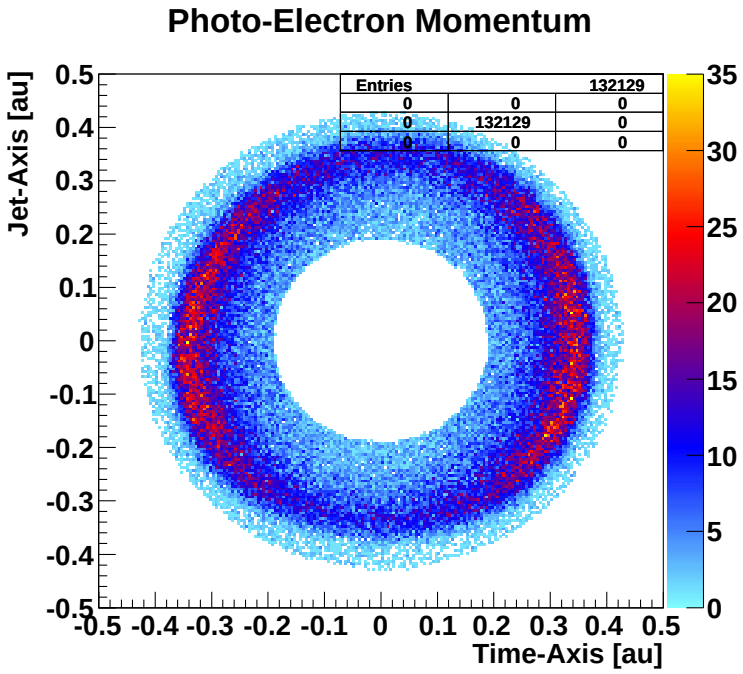

Figure 5.2: We restrict the subset of Ne^{2+} events to a plane. The resulting slice of the photo-electron momentum ($0.5 < E_\gamma < 2.5$eV) further reveals the anisotropic distribution we attribute to elliptically polarized light. The axis of symmetry is associated with the major-axis of polarization for the elliptical light.

We fit a function that quantifies the ellipticity in Figure 5.2. It should be noted that the curve does not match the data well at -180^o. Additionally, the troughs of the data are unequal. We do not attribute these lesser effects to the polarization; instead, they are associated with other artifacts of

the experiment. We address these effects in the next section when describing the two-dimensional method of analysis in greater detail.

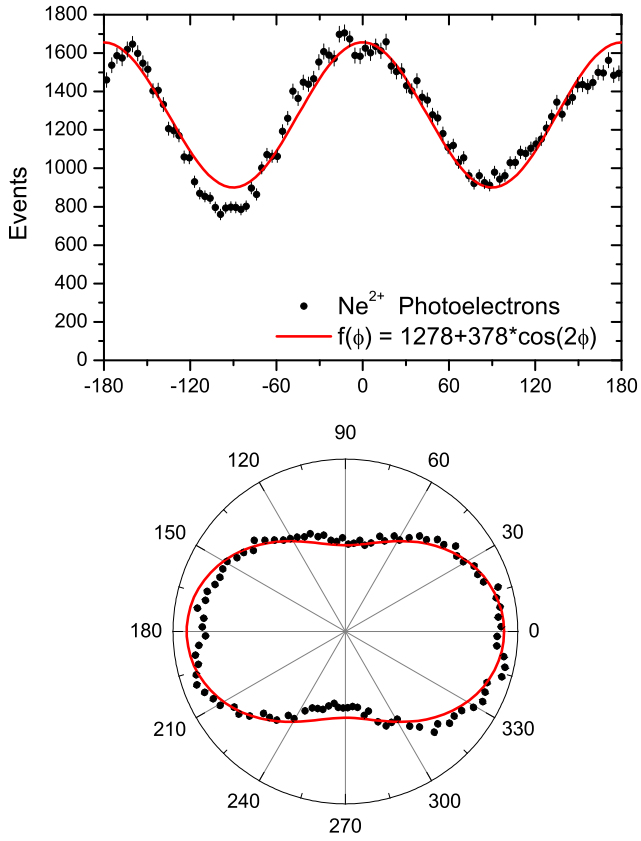

Figure 5.3: We use the angular distribution of the 2D subset of photo-electron events to quantify the ellipticity of the light at the beam-line. The top panel shows good agreement between the fitted function, $f(\phi)$ and the data. The lower panel represents the data in polar form.

To summarize, we have applied a wide-angle conical gate to the subset of events regarded as "incomplete" (Table 5.1). This results in a planar slice of the photo-electron distribution that can be used to reveal the elliptical nature of the light at the beam-line. The function, $f(\phi)$ (Fig.5.2) quantifies the deviation from circularly polarized light. Having concluded the aim of this section,

we turn to the next section, to consider what potential benefits may be gleaned from analyzing data with this two-dimensional method.

5.3 The 2D Experiment - A Novel Feature of COLTRIMS

Having quantified the ellipticity of the light (Fig.5.2), we next turn our attention to the two-dimensional method of COLTRIMS analysis that made it possible. Recall that in order to observe the anisotropy of the photo-electron distribution, we required the application of a wide-angle gate ($Cos(\theta_z) < 0.15$) to the events (i.e., we consider only those target gas constituents which are confined to a plane). This in essence, recasts the experiment in two-dimensions, making it possible to directly compare results to fixed-in-space spectrometry methods.

In the prior section, as we determined the function that best quantifies the elliptical nature of the light at the beam-line, we also noted regions where the two-termed function did not fit the data well. We attributed these unassigned mismatches to artifacts of the experimental process. Rather than calibrate the light using $f(\phi)$, we instead opt to calibrate the photo-electron distribution to isotropy using a Fourier weighting function. This approach removes any contribution by the aforementioned experimental artifacts.

Defining the statistical weighting function as the ratio of the isotropic average to the value of the Fourier function evaluated at the point of interest, we refill our histograms. The top row of Figure 5.4 shows the contrast between the uncalibrated and calibrated photo-electron angular distribution. The bottom row represents the respective photo-electron momentum density plots. We carry this weighting function throughout the subsequent 2D analysis to ensure that artifacts assoicated with the correction are not influencing the physics. Another interesting feature that arises from the statistical weighting of the histograms is that we are able to shape the photo-electron distribution to match any variety of polarization (e.g., linear).

5.3.1 Isotropy of the Auger Electron Distribution

In addition to calibrating the two-dimensional photo-electron distribution to isotropy, we can perform a similar proceedure with the Auger electron distribution. After all, we expect to observe an s-wave distribution of Auger electrons as a result of the filling of the 1*s* vacancy of the target atom. Using the same subset of 2D data, we can fit a many-termed Fourier function to the distribution, weighting the data in similar fashion to the photo-electron distribution. The top row of Figure 5.5 shows the contrast between the uncalibrated and calibrated Auger-electron angular distribution. The bottom row represents the respective Auger-electron momentum density plots. As in the case of the photo-electron calibration, we carry this weighting function throughout the subsequent 2D analysis to ensure that the artifacts assoicated with this correction do not influence the physics.

Planar Angular Correlation of Electrons

Having calibrated both the photo-electron and Auger electron distributions to isotropy, we analyze the data set. Of particular interest is the angular correlation between the emitted electrons of K-ionized neon (Eq.5.1). Taking the angle between the Auger momentum vector and the TOF axis as ϕ_1 and the angle of the photo-electron with the same axis as ϕ_2, we define $\phi_1 - \phi_2 > 0$ as belonging to the range: $(0 - 180^o)$ and $\phi_1 - \phi_2 < 0$ belonging to the range: $(180 - 360^o)$. We do this as a precaution (i.e., we may be able to better identify a systematic error, if present). The resulting polar plot is shown in Figure 5.3.1. The characteristic divot is clearly present whereas the remainder of the plot is isotropic.

Upon comparison with the (red) circle that overlays the data, one will notice a slight deviation from isotropy, broadly occuring at $(30^o < \theta < 90^o)$. With *a posteriori* knowledge, this splash is the result of physics and moreover, is in good agreement with theory. The details of this splash will be investigated in greater detail in the next section. However, it should be noted that at the time the results were first observed, the splash was flagged as being the result of an artifact associated with the two-dimensional experiment.

5.3.2 The Small Angle Approximation Applied to the 2D Method

While the calibration proceedures described above are useful for providing a basis of comparison to experiments which are conducted in a plane (or some arrangement of fixed-in-space spectrometers), there exists a *caveat* worthy of mention. The two-dimensional analysis is in actuality, only quasi-2D. In order to have sufficient statistics to perform an angular correlation, we have opened the angle of acceptance to approximately 8.5^o. While the momentum component of this 3^{rd} dimension is small, it is nevertheless, non-zero. As a result, the two-dimensional analysis becomes a bit of a balancing act between statistics and the error incurred by the acceptance angle.

Table 5.2: Relative Charge State Distribution

Charge State *	Relative Abundance (%)
Ne^{1+}	4.65
Ne^{2+}	89.47
Ne^{3+}	5.55
Ne^{4+}	0.31
Ne^{5+}	0.02

* Based on the ^{20}Ne isotope.

Given the relative rarity of the Ne^{3+} channel (Tab.5.2), we look for an alternative to calibrate the photo-electron distribution. We extrapolate the notion of statistically weighting the histograms in three-dimensions. The remaining section will describe the method employed that not only preserves statistics, but additionally yields new results that pertain to the single Auger decay of K-shell ionized neon.

5.4 Extrapolating the Polarization Calibration to 3D

Consider the torus-like distribution of the photo-electrons once more. In three-dimensions, two weighting functions may be considered. The first takes into account the angular distribution of events in the plane defined by the jet and TOF axes. The second considers the angular distribution of events in the plane defined by the jet and the beam axes. We shall designate ϕ and θ as the angles a photo-electron hit makes with respect to the TOF and beam axes, respectively. The top row of

Figure 5.7 shows the difference between the uncalibrated and calibrated photo-electron angular distributions for ϕ only. The bottom row represents the respective photo-electron momentum density plots.

Next, we can iteratively perform a similar calibration for the θ direction. Using the same Fourier series weighting function technique as described in the two-dimensional procedure, we can force the distribution shown in Figure 5.7 to be isotropic (i.e., we turn the torus-like distribution into a spherical distribution). By re-weighting the photo-electron distribution such that it is spherically symmetric, we can eliminate any angular bias originally present in the distribution. In the case of Ne^{2+} this is not a necessary correction as we infer the Auger electron with a virtual 4π solid angle of collection. However, when considering the case of DA decay, it will play a much larger role. Referring to the top row of Figure 5.7, we observe the difference between the uncalibrated and calibrated photo-electron angular distributions for θ only. The bottom row represents the photo-electron momentum density plots with only the ϕ correction applied.

Additionally, we consider the distribution of Auger electrons in three-dimensions as we did the photo-electrons. Applying a Fourier series to each of the two angular ranges, we can calibrate the Auger electrons. Referring to the top row of Figure 5.8, we observe the difference between the uncalibrated and calibrated Auger-electron angular distributions for ϕ only. The middle row represents the θ correction for the Auger electrons. The bottom row represents the photo-electron momentum density plots with both photo-electron and Auger electron corrections.

5.4.1 The Physics of Single Auger Decay

Having successfully calibrated both the photo-electron and Auger electron distributions to isotropy, we are assured there exist no angular biases in subsequent analysis. Accordingly, we consider the angular correlation between the emitted electrons in decay channels of Equation 5.1. Figure 5.10 represents the photo-electron energy plotted as a function of the angle between electrons. At first glance it appears the distribution is isotropic for all angles except in the vicinity of 0^o. Recall from the previous section that while the characteristic divot was present in (Fig.5.3.1), we

observed a broad splash. As it was unclear if this splash was physics or simply an artifact arising from an overreaching application of the small angle approximation, we turn to the three-dimensional analysis to probe the data further.

Taking thin slices of the photo-electron distribution (Fig.5.10), we produce polar plots that represent the angular correlation between these specific energy photo-electrons and their corresponding Auger electron. The ranges considered were as follows: $(1.0-1.4)$eV, $(1.4-1.8)$eV, $(1.8-2.2)$eV and are shown in Figure 5.10. In the lowest energy slice, we observe a blunt divot present without any noticeable splash. In the intermediate slice (where the bulk of events are present), the divot resembles published data (i.e., it is a more pronounced divot and lacking splash). The highest energy slice shows a broad splash effect at $30^o - 90^o$.

5.5 Final Remarks

After a thorough analysis of the data, we determined the light from the beam-line was not circularly polarized, but rather, it was elliptical. The preceding sections have served to describe an accurate means of quantifying the ellipticity as well as segue into a unique method of analysis. The procedure outlined above describes how to recast the COLTRIMS experiment in two dimensions and calibrate both the electron distributions to isotropy. Figure 5.3.1 represents the angular correlation between electrons in polar form. Of course, we require that sufficient statistics be present at the onset of such an analysis in order to consider physical trends that occur within the plane.

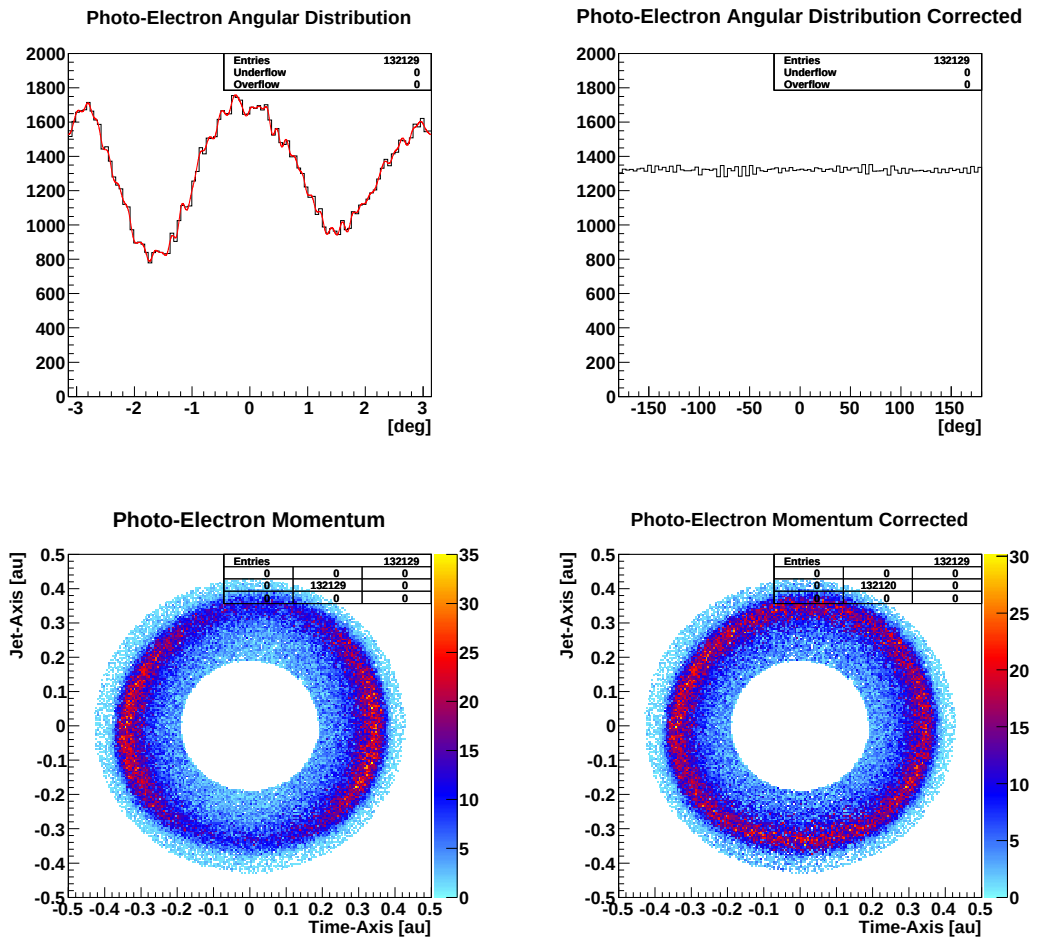

Figure 5.4: The top-left panel shows a lack of isotropy in the photo-electron distribution. A many-termed Fourier function calibrates the distribution to isotropy as shown in the top-right panel. The lower panels represent the photo-electron momentum density plots before and after calibration, respectively.

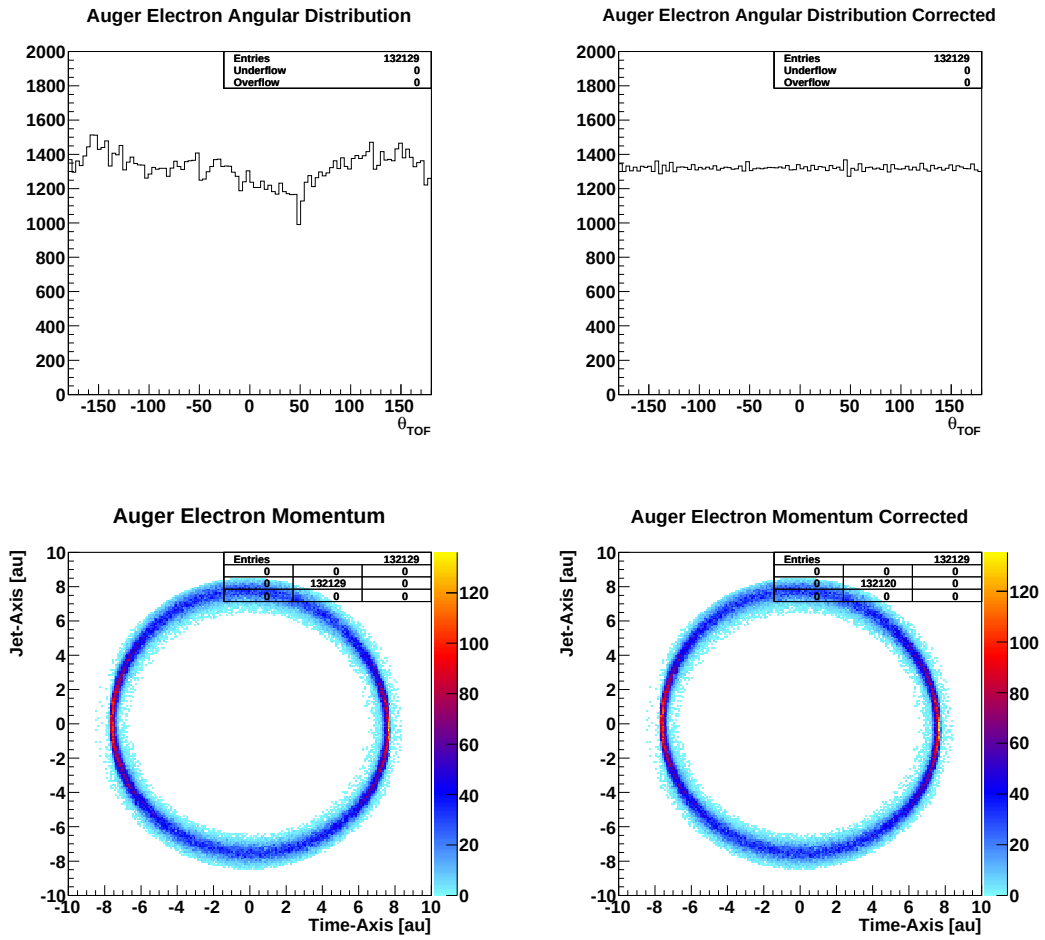

Figure 5.5: The top-left panel shows a lack of isotropy in the Auger-electron distribution. A many-termed Fourier function calibrates the distribution to isotropy as shown in the top-right panel. The lower panels represent the Auger-electron momentum density plots before and after calibration, respectively.

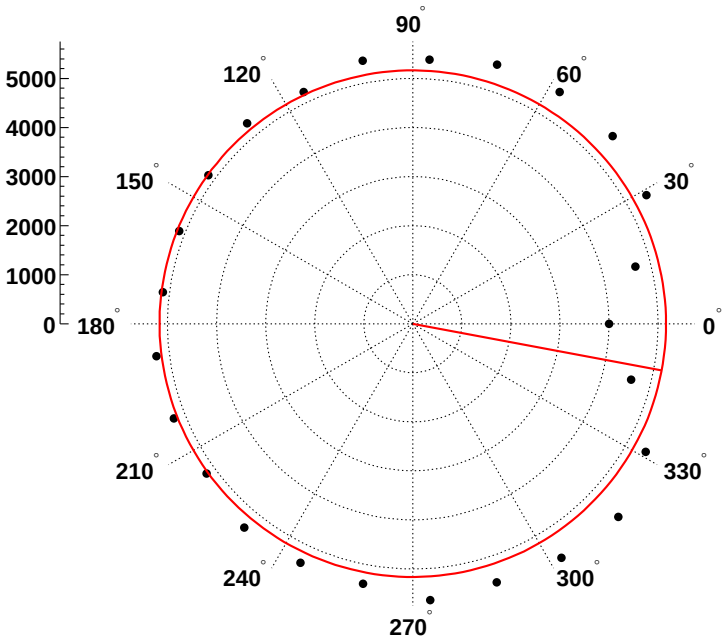

Figure 5.6: We use the calibrated data set to generate the angular correlation polar plot. The characteristic divot is present, as is a broad splash between ($30^o - 90^o$).

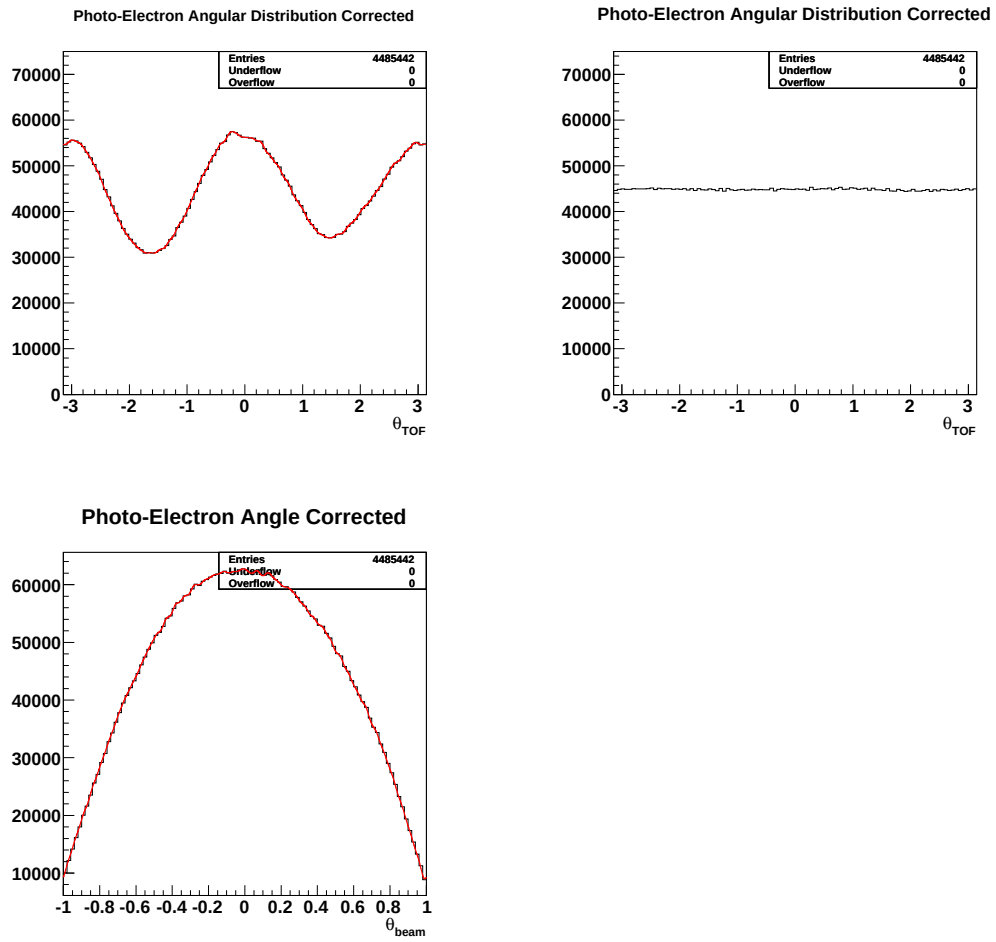

Figure 5.7: The top-row shows the photo-electron distribution before and after calibration. The lower panel reveals the profile of photo-electron distribution that corresponds to its torus-like shape. We choose not to calibrate this distribution to isotropy as it does not contribute to an angular bias among the decay channels of interest.

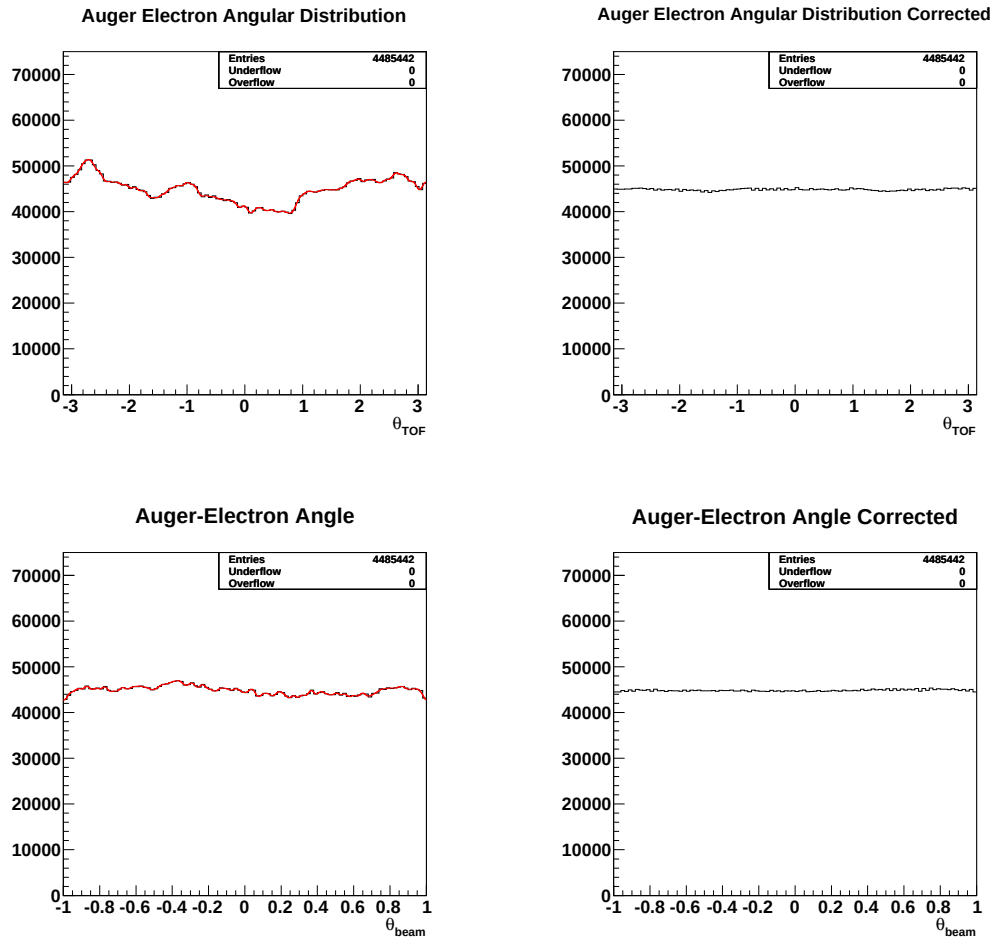

Figure 5.8: Top row: Auger electron distribution (ϕ-direction) before and after calibration. Bottom row: Auger electron distribution (θ-direction) before and after calibration.

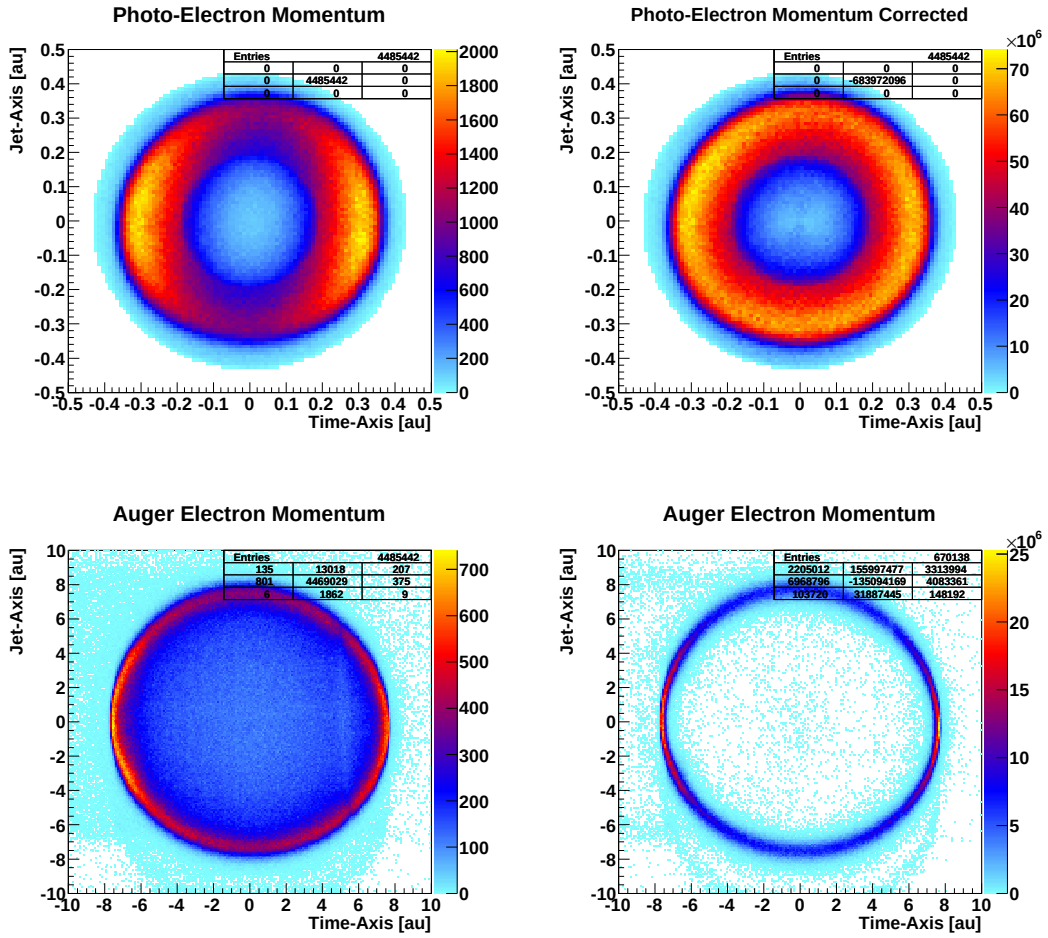

Figure 5.9: The panels in the top row represent the photo-electron momentum density plots before and after calibration, respectively. The panels in the bottom row represent the respective Auger electron momentum density plots. The calibrated Auger plot has been sliced to highlight the difference in spatial and temporal resolution present in the experiment.

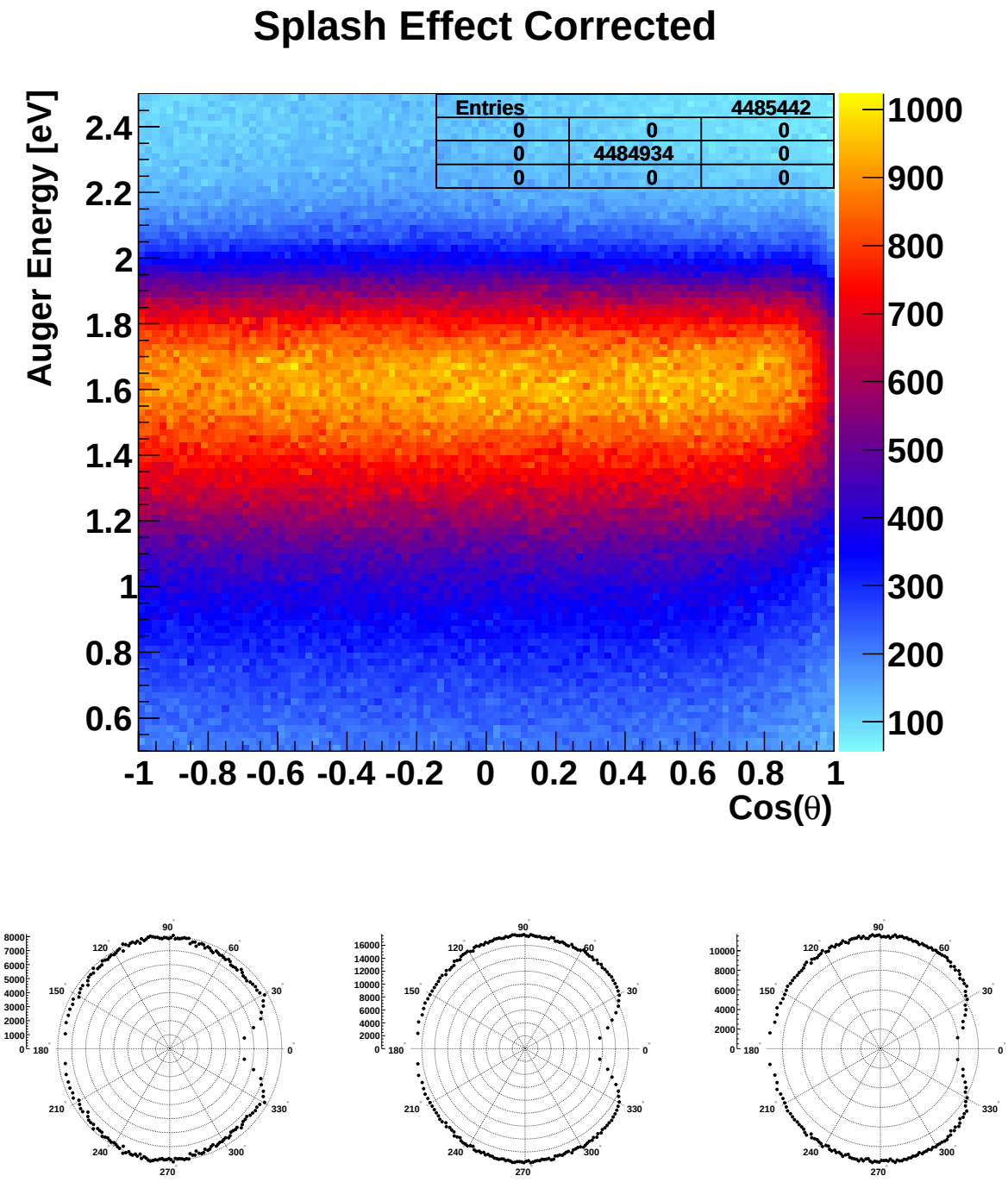

Figure 5.10: The top panel shows a lack of isotropy at small angles of correlation. The polar plots below represent the angular correlation in polar form for slices of the photo-electron energy. Note that a broad splash is visible for the range (1.8 – 2.2)eV.

Chapter 6

ANGULAR CORRELATION BETWEEN ELECTRONS IN CORE IONIZED NEON

The investigation into Ne^{2+} has brought forth many questions, a number of which cannot be answered by the experimental research that engendered them [40]. Of particular interest is the behavior of continuum electrons associated with single Auger decay, particularly when we vary the time difference between the ionization and subsequent Auger decay (Fig5.10 found on pg.90). Therefore, attention turns to the more complex, Double-Auger (DA) decay channel, in an effort to further investigate the Auger decay phenomenon. Specifically, we are interested in analyzing the following decay channels,

$$Ne(1s2s^2 2p^6)^+ + e_\gamma^- \Longrightarrow \begin{cases} Ne(1s^2 2p^5)^{3+} + e_\gamma^- + e_{A_1}^- + e_{A_2}^- \\ Ne(1s^2 2s^1 2p^4)^{3+} + e_\gamma^- + e_{A_1}^- + e_{A_2}^- \\ Ne(1s^2 2s^2 2p^3)^{3+} + e_\gamma^- + e_{A_1}^- + e_{A_2}^- \end{cases} \tag{6.1}$$

We begin the chapter with a look at the position data for the Ne^{3+} channel. Next, we consider the events of DA decay from the perspective of momentum space. It is here we identify the potential for angular bias. Accordingly, we discuss the strategy used to calibrate the photo-electron distribution to isotropy. Pending the implementation of the calibration process, we report on the results of the angular correlation analysis. Here, we catergorize the data according to the energy sharing characteristics of the DA electrons. Three specific ranges of Auger energy sharing are considered: "highly asymmetric," "intermediate" and "highly symmetric." We present these correlations in the context of the shake-off and knock-out models described in Chapter 1. We additionally consider (where applicable) similar features between DA decay and the Photo-Double-Ionization (PDI) of helium.

6.1 Identifying Sources of Angular Bias

Elliptically Polarized Light

When considering the angular correlation of electrons involved in the DA decay process, we must take caution to minimize the introduction of angular bias into the analysis. In the previous chapter, we showed evidence that the light used at the beam-line was elliptically polarized (rather than circularly polarized). We quantified the ellipticity by fitting the photo-electron data with a two-termed function (Fig.5.2) found on pg.78. Moreover, we determined that the observed anisotropy would ultimately superimpose an angular bias onto the subsequent correlation analysis. To prevent such an angular bias from obscuring these important results, we generated a weighting function to use in calibrating the data. We attributed the lack of agreement between the function (based upon Eq.6.2) and the data to additional experimental artifacts (e.g, inhomogeneities of the detector collection efficiency). Further, by calibrating the photo-electron data to this two-termed weighting function, we were only able to control the ellipticity of the light at the beamline; it did not enable for any control of the residual artifacts that were unrelated to the light.

$$f(\phi) = 1278 + 378 * cos(2\phi) \tag{6.2}$$

Experimental Artifacts

Consider the position of the recoil hit data associated with the Ne^{3+} channel (Figure 6.1). We observe a dead-spot on the detector at coordinate position, $(16, 8)$mm. While this particular defect is small and quite possibly, negligible with regard to its impact on data acquisition, it nevertheless is representative of a greater issue, the inhomogeneity of the detector.

Experimental artifacts which arise due to an inhomogeneous MCP, for example have the potential to further alter the representation of the physics (i.e., these effects can compound the angular bias that results from the use of elliptically polarized light). Fortunately, we can simultaneously correct

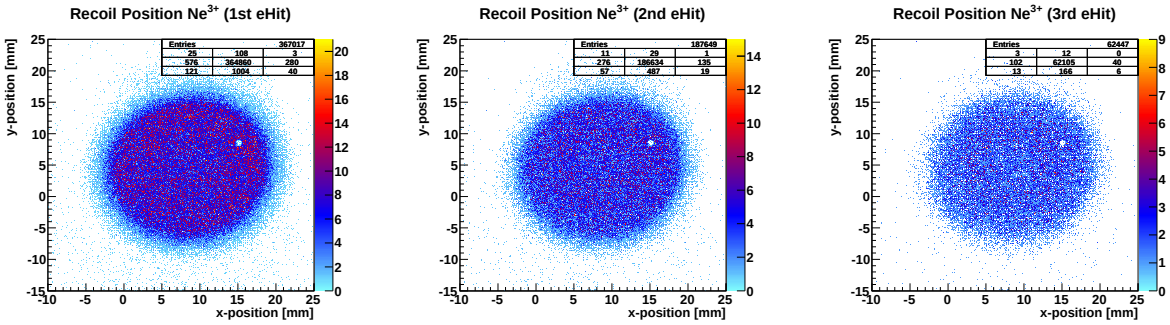

Figure 6.1: The density plots reveal dead-spots on the MCP (e.g., $(16, 8)$mm). These detector inhomogeneities adversely affect the physics of the experiment. Later in this chapter we correct for these anomolies with a many-termed Fourier weighting function.

all of these effects (identified or otherwise) by means of a many-termed Fourier weighting function, provided we have a clear undersanding of how these distribution ought to look (e.g. isotropic).

Angular Bias due to Solid Angle Collection

We can identify a third source of angular bias by considering the way in which the data streams into the TDC. This topic relates to the solid angle collection of the spectrometer. Since this effect is most easily observed in momentum space, the topic will be deferred until then.

6.2 Position Data

Given the relative rarity of directly measuring *all* the constituents of a DA event, we only consider "incomplete" events (Tab.6.1), where the fast-Auger and photo-electron have been measured directly, in co-incidence with the recoil ion. The remaining, "missed" Auger electron is inferred via the conservation of momentum.

We use the collection of plots shown in Figure 6.2,6.3&6.4 to illustrate some of the features of these "Incomplete" events. The first panel of Figure 6.2 shows a spike at about 5ns, which corresponds to high-energy Auger electrons. However, upon comparing the trailing edge of this distribution to the Ne^{2+} panel directly to the right of it, we catch a glimpse of how energy is shared

Table 6.1: Data Acquisition Chart

Type	Recoil	e^- Hit 1	e^- Hit 2	e^- Hit 3	Calc.
Complete Event	X	X	X	X	X*
Incomplete Event	X	X	X	-	X
Incomplete Event	-	X	X	X	X
Incomplete Event	X	-	X	X	X

* Calculated for Improved Resolution

between the two Auger electrons in DA decay. The broadening of the trailing edge implies that the fast-Auger electron can possess a value of energy that is less than the $(2p-1s)$ transition energy (shown as the Auger distribution in the lower panel). Of course, we attribute this energy difference to the second, slower Auger electron. Therefore, noting the shape of the Auger distribution, we can qualitatively determine that Auger electrons associated with DA decay tend to share energy asymmetrically.

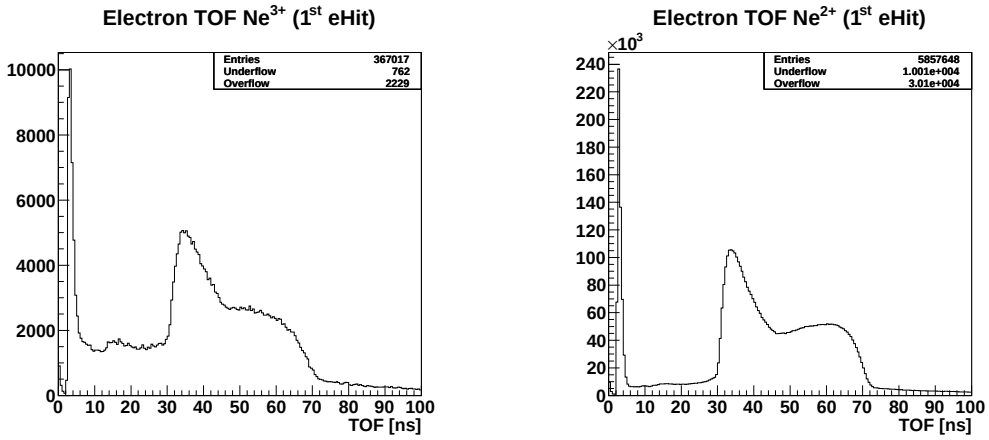

Figure 6.2: The left and right panels represents the 1^{st} electron hit data, for Ne^{3+} and Ne^{2+}, respectively. We note the spike at approx 5ns is broader at the trailing edge of Ne^{3+} as compared to Ne^{2+}. This broadening can be attributed to the energy sharing that occurs between the Auger electrons emitted in the DA process.

In Figure 6.3, we observe a prominent photo-electron peak between $(30-70)$ns. Upon comparison with the panel below (Ne^{2+}) the peak of the leading edge is shifted right (slightly), relative to

the corresponding Ne^{2+} peak. This is due to a greater PCI effect between the electron and the residual ion. These are unsurprising results having already observed how PCI effects the photo-electron energy distribution for various charge states (Fig.1.9 found on pg.17).

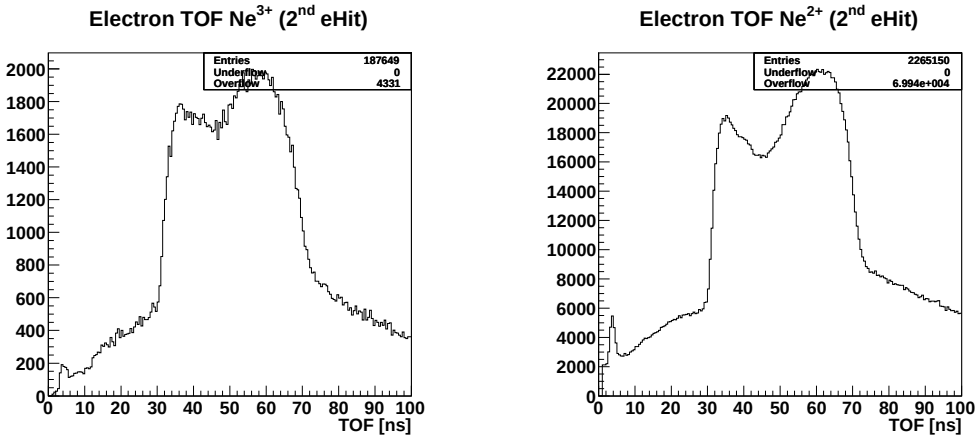

Figure 6.3: The left and right panels represents the 2^{nd} electron hit data, for Ne^{3+} and Ne^{2+}, respectively. The diminished spike at approx 5ns is the result of a random electron which triggers the MCP ahead of the Auger. We also note a slight shift in the leading edge of the Ne^{3+} photo-electron peak relative to $Ne2+$, attributing it to the greater PCI effects incurred by the Ne^{3+} recoil ion.

The left panel in the Figure 6.3 shows a much smaller fast-Auger peak. Its presence was initially attributed to two mechanisms: the direct measurement of photons in the 1^{st} hit (observed at approximately 1ns), and the measurement of random electrons (attributed to the background gas) in advance of the of Auger. However, this peak of Auger electrons is located within the dead-time shadow that was quantified (in Chapter 3) to be 7ns, rendering it impossible for the photon to be measured in co-incidence with such a high-energy electron. Therefore, we conclude that only the latter process is able to generate such a population of 2^{nd} hit *fast*-Auger electrons; the corresponding photo-electron is measured in the 3^{rd} hit as shown.

Another plausible scenerio of event acquisition is the measurement of a 1^{st} hit Auger electron in co-incidence with a 3^{rd} hit photo-electron (i.e., a random electron triggers the 2^{nd} hit on the detector). It is difficult to identify such a case from the individual plots (Figs.6.2&6.4); however if we plot the respective distributions, one versus the other, we can look at the correlation between

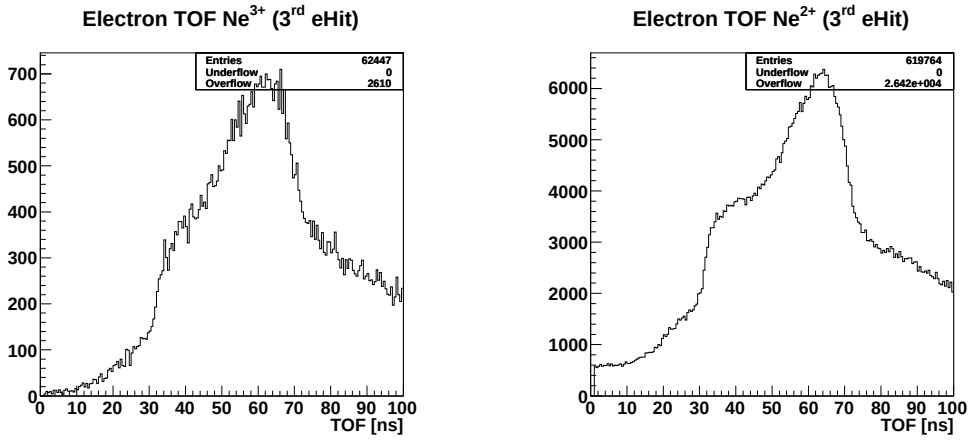

Figure 6.4: The left and right panels represents the 3^{rd} electron hit data, for Ne^{3+} and Ne^{2+}, respectively. The diminished photo-electron distribution results from a random electron triggering the MCP in either the 1^{st} or 2^{nd} hit.

these electron hits (Fig.6.5). Here, we can quickly assess the statistical influence of each of these types of "incomplete" events (Tab.6.1).

The first column of panels shows the correlation between electrons that correspond to the three different combinations of "incomplete" events, respectively. The second column of panels shows the correlations with a computational gate, restricting the energy of the presumed photo-electron to be, $E_\gamma < 2.5$eV. It should be noted that this range of energy was determined from the data shown in Figure 1.9 (found on pg.17).

Physics of the Fish Plot

As a final point of interest, we consider the position of the electrons with respect to their TOF, also known as the "fish" plot (Fig.6.6). Here, we can visually inspect the results of the ($\vec{E} \times \vec{B}$) correction, described in Chapter 3 by noting the alignment of the node and anti-node along the TOF axis. Turning to the physics of the fish plot, we observe a broadening of the Auger "line" (as compared with the Ne^{2+} fish plot below). Once again, this broadening effect is due to the energy sharing between the two Auger electrons. As a final point of interest, we note a halo that surrounds

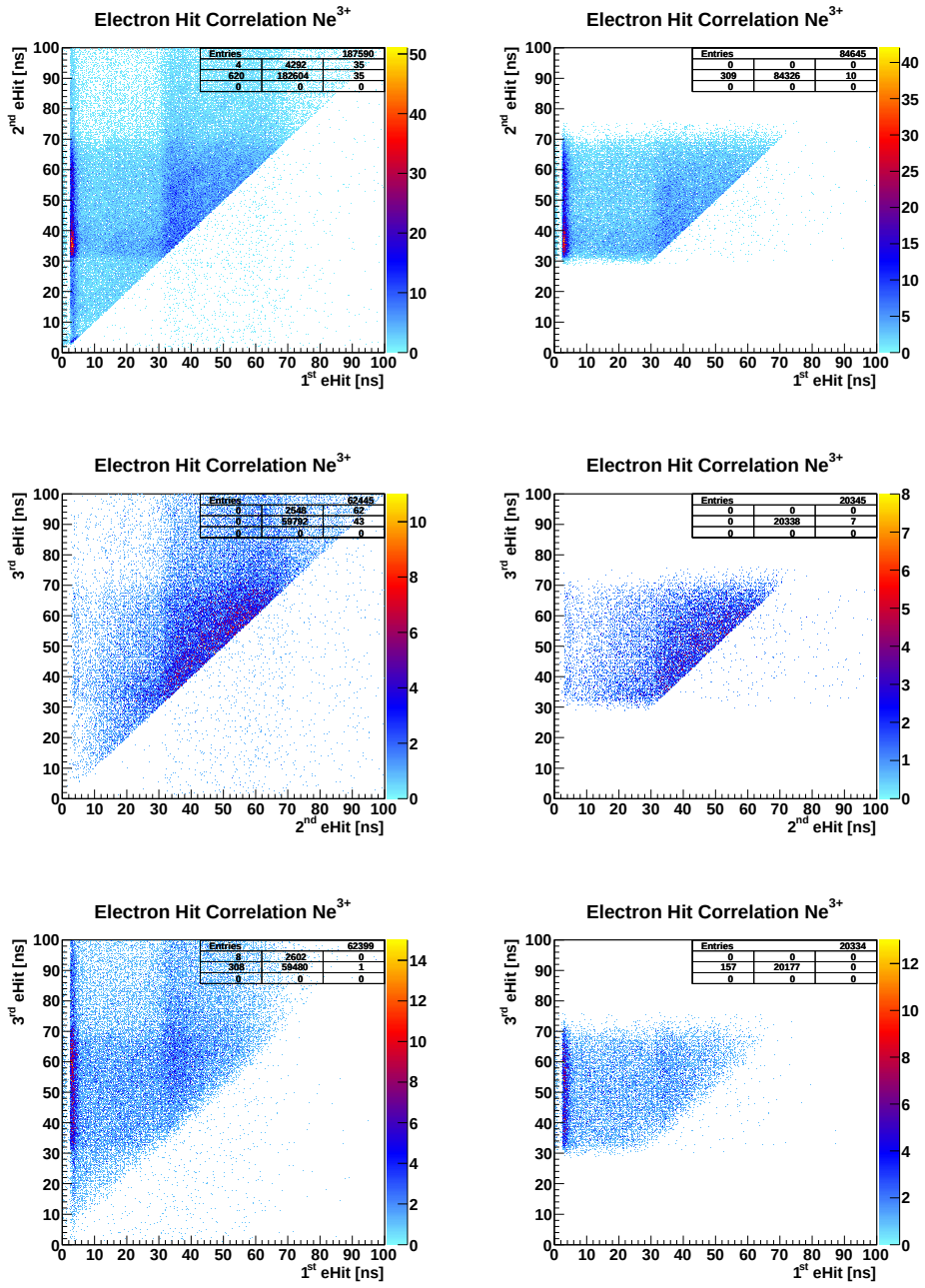

Figure 6.5: The correlation between the 1^{st} and 2^{nd} hits are shown in the first panel. Since a gate has been applied to the 2^{nd} hit which restricts its energy to less than 2.5eV, we are assured the prominent stripe in the first panel represents the correlation between the fast Auger and the photo-electron. The correlation between all combinations of electron hits is shown, accordingly.

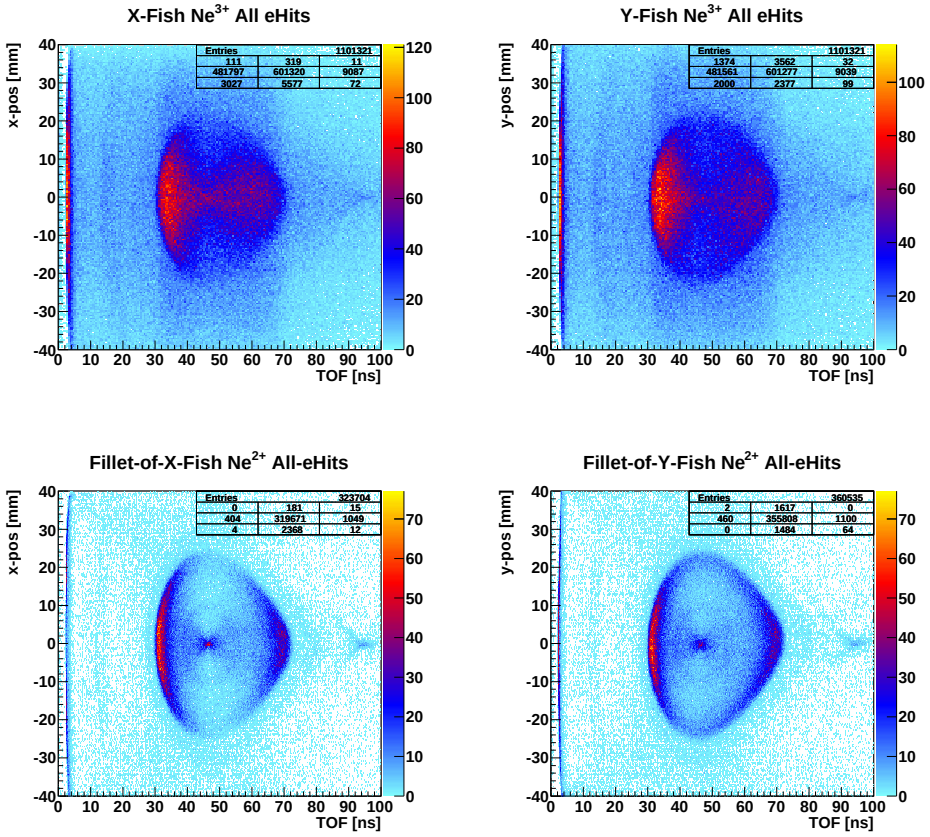

Figure 6.6: The node and anti-node of the Ne^{3+} fish plots (top row) align well with the TOF axis, an indication of a well calibrated spectrometer. The Ne^{2+} plots (bottom row) serve to contrast the physics of the plots above. Note, the broadening of the fast-Auger line as well as the slow-Auger halo that surrounds the photo-electron distribution.

the photo-electron distribution. This halo represents the slow-Auger electrons associated with DA decay, which have been directly measured by the detector.

6.3 A View of Momentum & Energy Space

In this section, we investigate the physics of DA decay by means of analyzing the constituent's respective momentum distributions. We also use this section to segue into a discussion regarding the calibration of the anisotropic photo-electron distribution.

Electron Momentum Analysis

We begin with a short analysis of the electron momentum slices shown in Figure 6.7 noting that all three types of "incomplete" events (Tab.6.1) are used to generate the momentum plots. The top row represents the measured Auger electron that is measured as either the 1^{st} or 2^{nd} hit on the detector. Regardless of event type, we computationally restrict the other measured hit (in the "incomplete" event) to be $E_\gamma < 2.5$eV (in accordance with the right column of plots shown in Figure 6.5). In this way, we ensure the plotted electron is indeed an Auger electron. In fact, upon closer inspection, we notice that the lowest-energy electrons do not possess a torus-like structure as would be expected from a photo-electron distribution (i.e., from elliptically polarized light).

Note also from this 1^{st} row of plots how the solid angle collection diminishes with increasing measured Auger momentum (Fig.6.7). In the most restrictive case, the open angle is approximately 45^o with respect to the TOF axis. Yet, at electron energies less than 5eV (or $|\vec{p}| < 0.61$ au), we maintain 4π solid angle collection. The mixing of solid angle collection within hit data can introduce an angular bias to subsequent results. To prevent this from occuring, we apply a conical gate to the distribution, ensuring that all measured Auger electrons used in the subsequent analysis have the same (limited) solid angle collection.

The 2^{nd} row of momentum slices (Fig.6.7) represents the photo-electron distribution. These plots have the familar dipole-like feature that results from the use of elliptically polarized light at the beamline (first described in Chapter 5). As noted earlier, this anisotropy will introduce an unacceptable bias unless corrective action is taken. We address this issue directly in the next section.

The 3^{rd} row represents the calculated electron momentum. Unsurprisingly, we observe a distribution that is dominated by low-momentum events, the profile of which alludes to the energy sharing characteristics of DA decay (i.e., Auger electrons tend to share energy asymmetrically in analogous fashion to the energy sharing between electrons that result from the PDI of helium).[23][30][33][22]

The reported angular correlation analyses between the two emitted electrons for 100eV and 450eV above double ionization threshold are shown in Figure (refpdi-1&**??**), respectively.

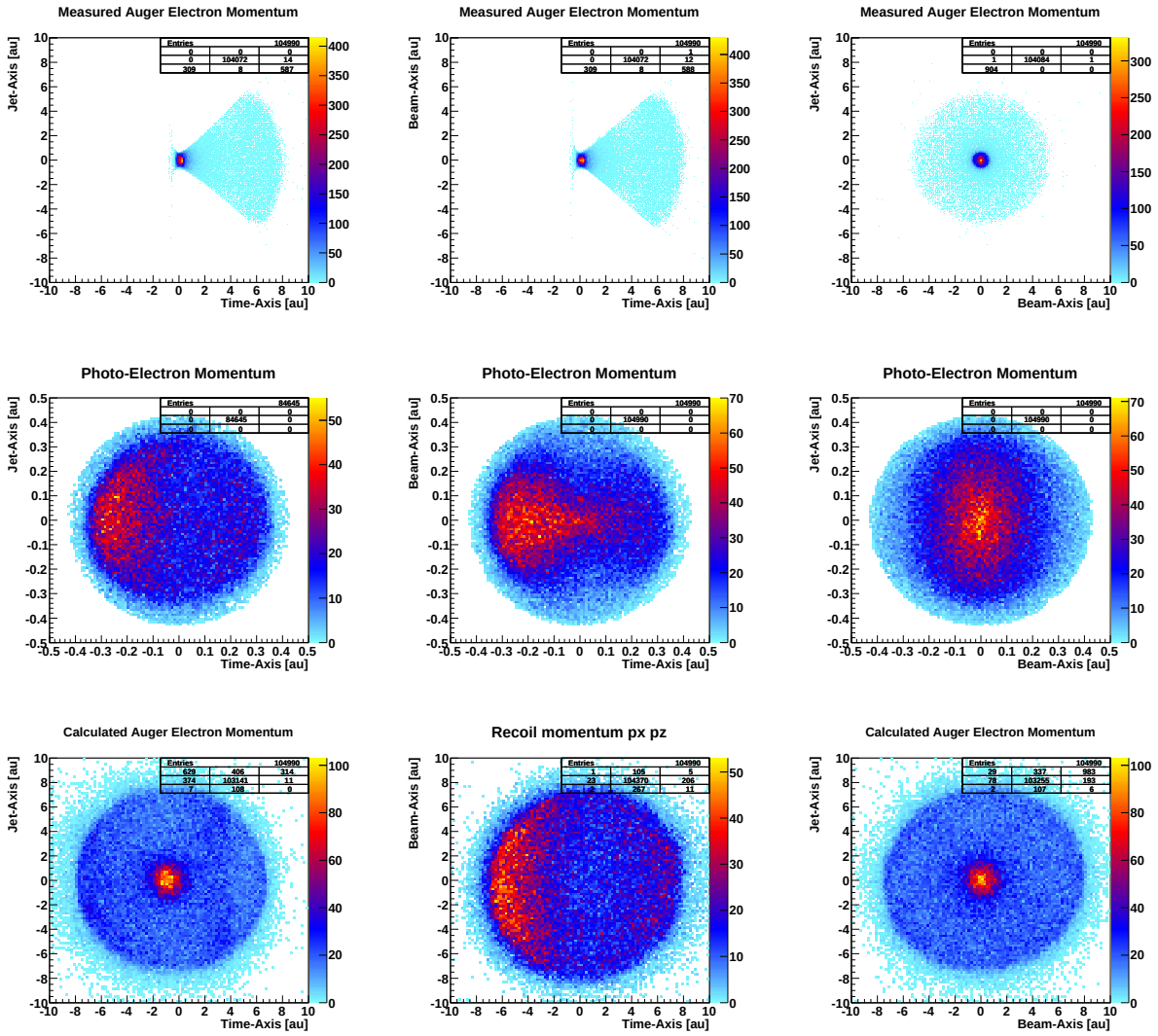

Figure 6.7: The 1^{st} row of plots represents the fast-Auger electron, the 2^{nd} row represents the photo-electron and the 3^{rd} row represents the calculated Auger electron. Given that solid angle efficiency is dependent on electron energy, we applied a conical gate to the 1^{st} row plots to prevent improper statistical weighting in the analysis.

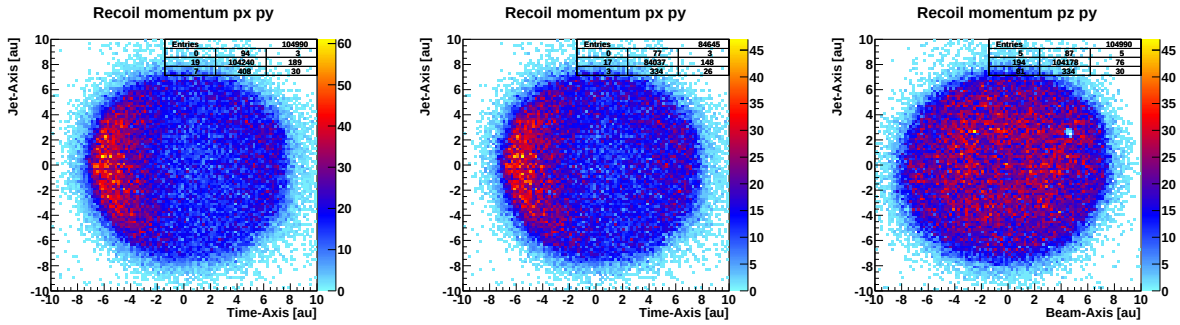

Figure 6.8: Slices of the recoil momentum associated with the DA of neon. Note the anisotropy of the distribution which is due to the angular bias imposed by the limited solid angle collection of the fast-Auger electron.

Aside - Resolution and Multi-Electron Co-Incidence Measurement

From a resolution stand-point, it would be ideal to consider the direct measurement of Auger electrons at energies near that of the subsequently measured photo-electron. However, due to the dead-time shadow of the detector, many of these photo-electrons could not be measured, thus introducing an angular bias to the results. Therefore, we must limit the slow-Auger threshold to a conservative 10eV or greater.

Recoil Momentum Analysis

The recoil momentum slices are shown in Figure 6.8. The lack of isotropy in these plots is an artifact of the solid angle limitations inherent to the measurement of an electron with energy, $E_A > 5$eV. Since the Auger must be launched in the direction of the detector in order to be directly measured, the conservation of momentum dictates that the recoil mirrir this bias.

Included in Figure 6.9 are the energy distributions for the respective electrons associated with DA decay. As can be observed in the measured Auger plot (left), there is a gradual transition between electrons of low and high energy. This is yet another glimpse into the energy sharing characteristics between the Auger electrons. The second plot (middle) resembles the profile of the photo-electron distribution previously shown in Figure 1.9 (found on page 17). The distribution of hits in the final

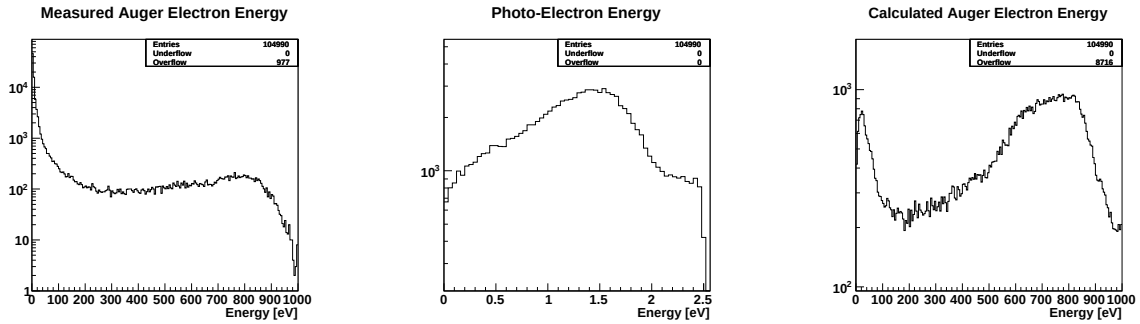

Figure 6.9: This array represents the energy plots for the three electrons that are associated with a DA event.

plot (right) provides additional evidence of asymmetric energy sharing between Auger electrons. Having exhausted the features of the momentum plots, we turn attention to the statistical weighting scheme used in calibrating the photo-electron momentum distribution (shown in Fig.6.7).

6.4 Statistically Weighting the Photo-Electron Distribution

In the previous section, we mentioned how the photo-electron momentum distribution is dipole-like due to the elliptically polarized light used at the beamline. We also recognized the presence of detector artifacts that result in a mismatch between the two-termed function Eq.6.2 and the photo-electron distribution. Consequently, we must be careful to minimize the introduction of angular bias into the subsequent DA angular correlation analysis. With this in mind, we consider the profile of the photo-electron distribution as well as an appropriate method to calibrate it.

Note that if circularly polarized light had been used at the beamline, the resulting photo-electron distribution would have resembled a torus; elliptically polarized light simply added statistical weight along an arbitrary axis of the distribution. Yet, a toroidal shape, while geometrically symmetric about a number of axes, is *not* spherical. Hence, even the use of a photo-electron distribution that has been produced with circularly polarized light requires statistical weighting in order to prevent the inclusion of an angular bias in the ensuing angular correlation analysis. We begin by

measuring the density of events across two angular ranges in order to fully describe the distribution of events. These angular directions are defined as follows:

$$\phi = atan\left(\frac{k_{\text{jet}}}{k_{\text{TOF}}}\right) \tag{6.3}$$

$$\theta = atan\left(\frac{k_{\text{beam}}}{k_{\text{magnitude}}}\right) \tag{6.4}$$

The primary objective is to calibrate the photo-electron distribution in two iterative steps, which accordingly yield a pair of independent weighting functions. In the first step, we calibrate the distribution in ϕ, establishing an isotropic torus-like shape. In the second step, we calibrate the distribution in θ. The subsequent application of these weighting functions has the effect of shaping the isotropic torus into an isotropic *sphere.*

In each step of the calibration, we used a many-termed Fourier series function to fit the corresponding angular distribution. We then applied a corresponding weighting function, as described in the previous chapter. The results of the first step in the calibration process are shown in the top right panel of Figure 6.10. Similarly, the results of the second step of the calibration process are shown in the bottom right panel.

The format of this section is of close resemblance to that of the previous chapter. However, we should point out that an important distinction arises between the two charge states when considering the Auger electrons. Since the Auger electrons associated with DA decay are correlated, we cannot statistically weight either distribution as we do not know *a priori* what these angular distributions ought to look like. Therefore, we are forced to accept any experimental artifact that may be present (e.g., an inhomogeneous detector collection efficiency). We apply the corrective weighting functions to the photo-electron data, and show the corresponding momentum plots in Figure 6.11.

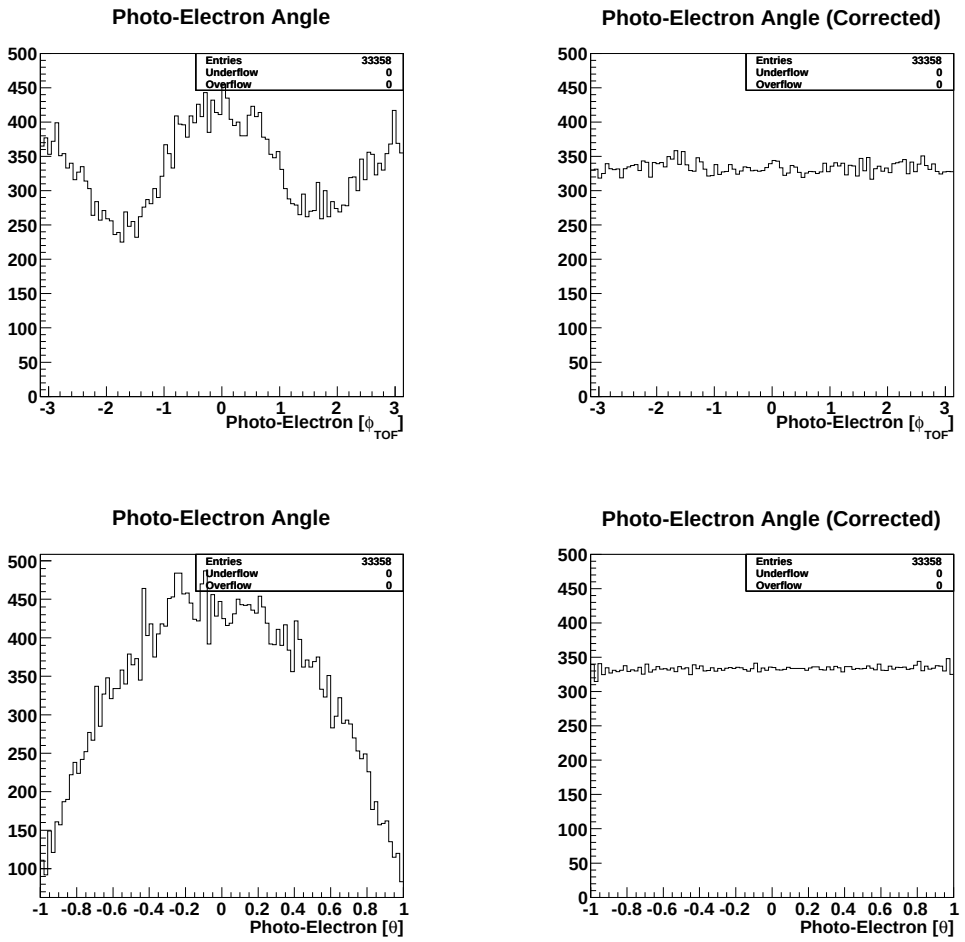

Figure 6.10: The top left panel represents the uncalibrated angular distribution of photo-electrons (*phi*-direction). The top-right panel represents the same distribution post-calibration. The bottom left panel shows the uncalibrated angular distribution of photo-electrons in the θ-direction. The lower right panel shows how the Fourier series weighting function brings the distribution to isotropy.

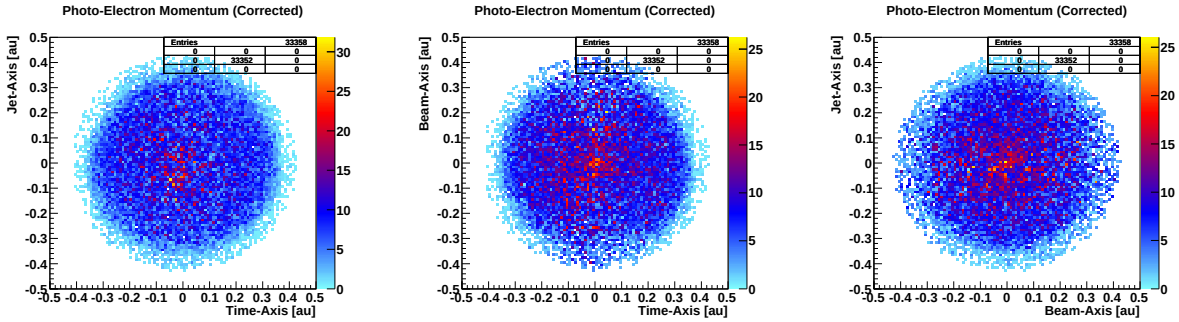

Figure 6.11: A two-step calibration of the photo-electron distribution shapes the anisotropic torus-like photo-electron distribution into an isotropic spherical distribution.

6.5 The Angular Correlation Analysis

Earlier, we noted how the fast-Auger distribution (Fig.6.2) was broader at the trailing edge in comparison to the Ne^{2+} case. While this provided a good qualitative impression of the energy sharing characteristics between DA Auger electrons (i.e., that the electrons tended to share energy asymmetrically), we can generate a much better picture of this relationship. We begin by identifying the signature of DA decay by plotting the energy of the calculated Auger electron versus the measured Auger electron energy.

6.6 Energy Sharing Between Auger Electrons

6.6.1 The Double-Auger Stripe

Figure 6.12 represents an electron-electron co-incidence map that corresponds to the Ne^{3+} charge state. The plot reveals a prominant diagonal band, which agrees with the three respective theoretical line energies (686.34, 717.44 and 743.04eV). While the spectrometer is unable to resolve these lines individually (for details about detector resolution, see Chapter 4), we are able to use computational gates to isolate events of Ne^{3+}. The result is a plot that is free of background contaminants such as water and serves as a compliment to the accurate work of Viefhaus [25].

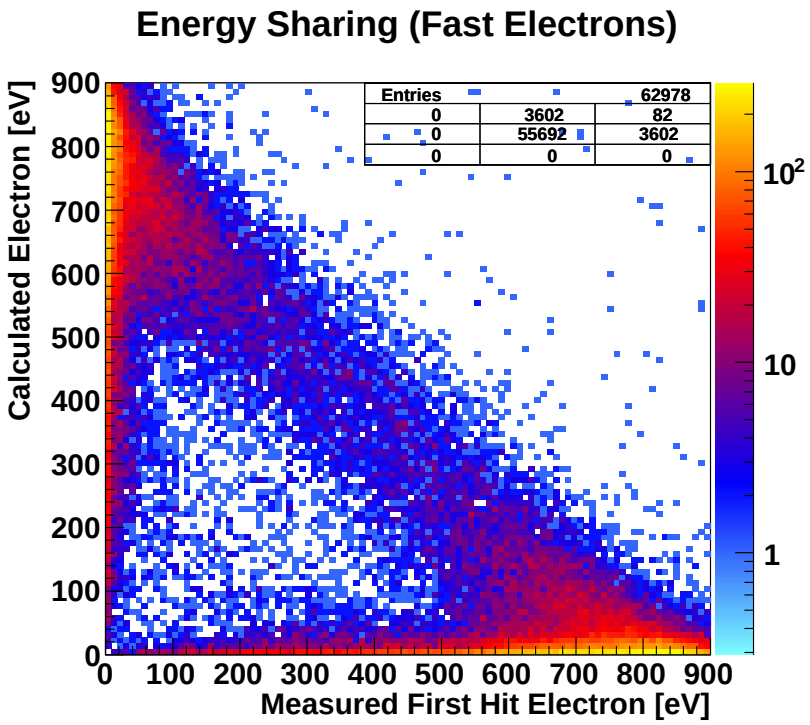

Figure 6.12: The diagonal stripe indicates the collection of DA events. The data shows agreement with the theoretical Auger line energies, (686.34, 717.44 and 743.04*eV*).

Events corresponding to DA decay were selected by placing a computational gate on the diagonal stripe shown in Figure 6.12; the energy sum was required to be within the range of 640 to 780 eV. These events were then projected onto the measured electron axis. Since the experiment was best suited to resolve low-energy electrons (Chapter 4) we generated this projection by mirroring the results that corresponded to "low" energy electrons: $0 - 370$ eV. Figure 6.13 is a plot of the energy sharing characteristics between the Auger electrons.

The plot clearly shows a tendency for Auger electrons to share energy asymmetrically. The plot agrees with previous experimental and theoretical work [15], [25] despite the latter being calculated

for the $Ne\,2s^{-2}2p^{-1}$ final states only. Additionally, the distribution bears resemblance to the published results from the PDI of helium; a result that further links two phenomena by which a single energy transition results in the emission of two electrons into the continuum.

6.6.2 The "Smile" Plot

Previous research on the PDI of helium shows the energy sharing characterisitcs between electrons to be preferably asymmetric [23][30][33][22] . This curve, which resembles a "smile" is a clear representation of the data and will be used as a basis of comparison to the energy sharing characteristics of DA decay. To produce the respective energy sharing plot for neon, we gate on the prominent DA stripe shown in Figure 6.12 and next, project the stripe onto the abscissa (i.e., we plot the measured electrons associated with the DA stripe). The results are shown in the left panel of Figure 6.13. We include the respective plot of helium for comparison. This similarity between the two seemingly different phenomenoa motivates a further investigation into the angular correlation between the respective electrons.

6.6.3 Angular Correlation Plots

Having determined that the Auger electrons that emmanate from the target tend to share the $(2p-1s)$ transition energy asymmetrically, we accordingly, partition the subsequent angular correlation analysis into the following catergories: The asymmetric case, the quasi-asymmetric case and the symmetric case. In this way, we are able to compare the results directly with published work pertaining not only to DA decay [25] but to the PDI of helium as well.[23][30][33][22]

Energy Sharing between Auger Electrons

While the Auger electrons emitted in the DA decay process tend to share the fixed electronic transition energy asymmetrically, they do so in arbitrary fashion (i.e., there are no discrete line energies present).

Photo-Double-Ionization of Helium

We have compared the features of DA decay to those of Photo Double Ionization (PDI).[23][30][33][22] In this analogous process, a single photon with energy above ionization threshold is incident on an atom (in the cited case, helium), resulting in the emission of two electrons. Research has shown that the electrons associated with PDI also tend to share energy asymmetrically and are modeled quite well by the shake-off process. Likewise, events of symmetric energy sharing behave according to the elastic-like knock-out process [23].

Angular Correlation Between Auger Electrons

We have conducted an angular correlation analysis for the emitted Auger electrons of DA decay. Figure 6.14 shows a density plot of the measured Auger electron versus the cosine of the angle between the electrons. At low energy, the angular correlation appears to be isotropic, as indicated by the uniform distribution of events along the horizontal axis. This isotropic behavor is in accordance with the shake-off model, where we collect only the low-energy electron of the asymmetric pair. At greater energies, a broad peak is realized at $\sim 120^o$. This represents an elastic-like knock-out model in conjunction with PCI effects from the residual ion.

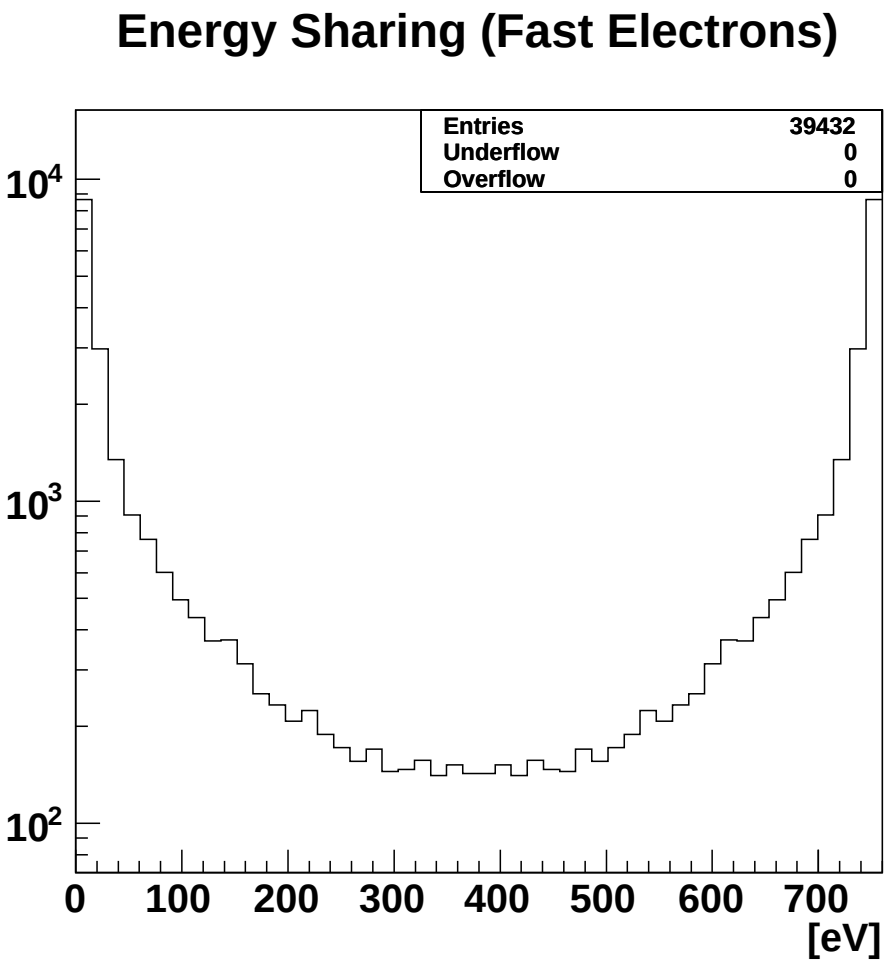

Figure 6.13: The number of events corresponding to a measured electron energy illustrate the transition from asymmetric to symmetric energy sharing between Auger electrons.

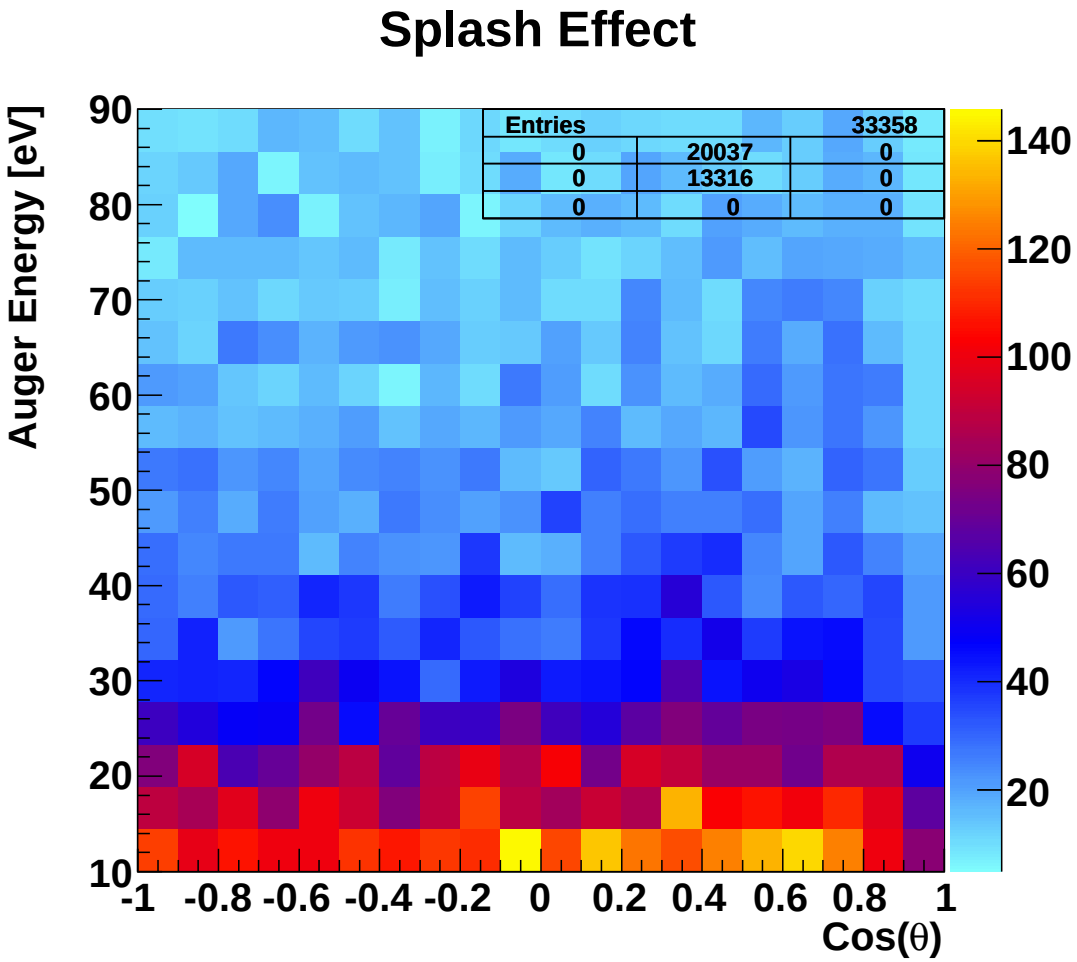

Figure 6.14: The energy of an Auger electron is plotted versus the cosine between the Augers.

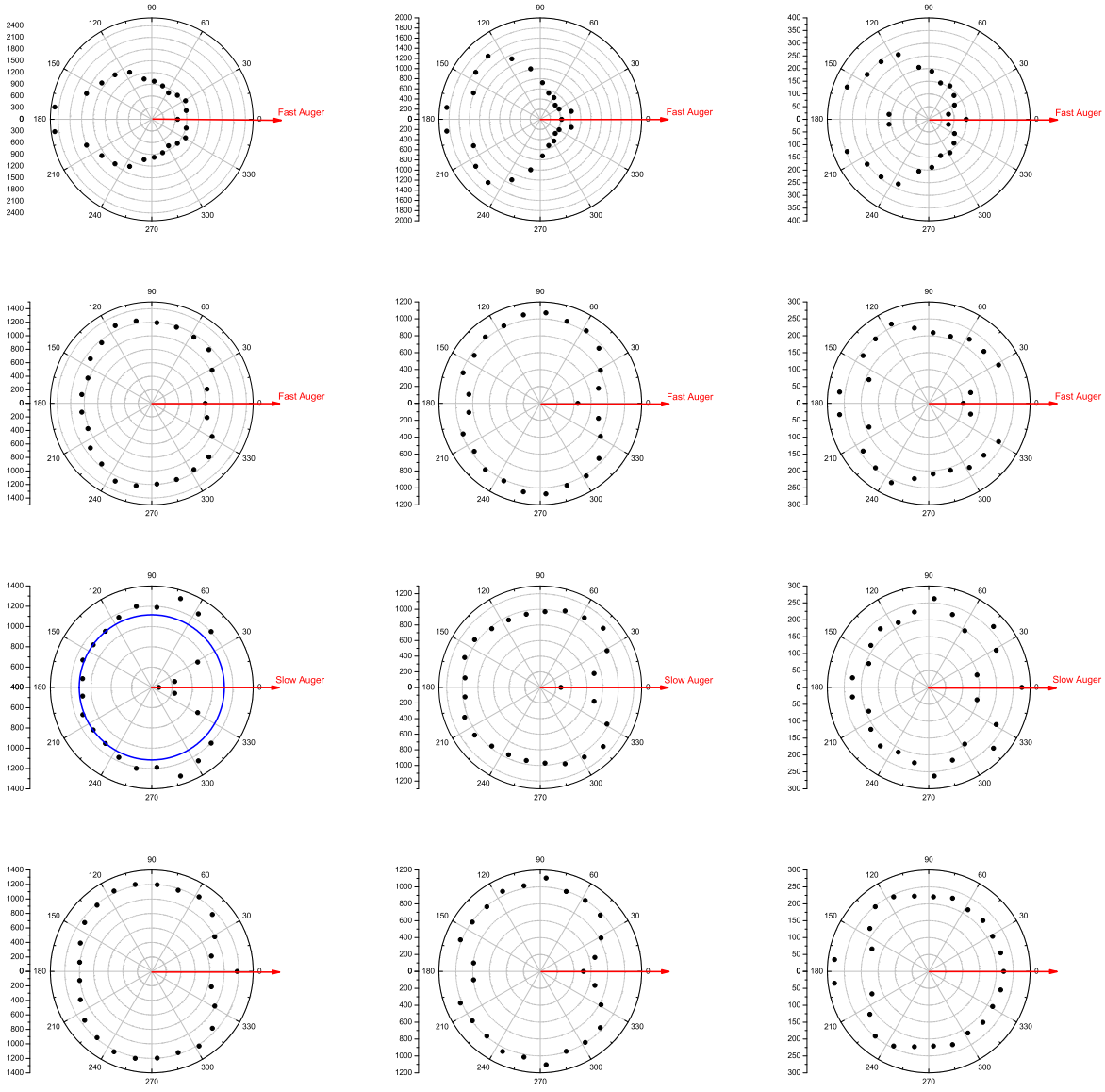

Figure 6.15: 1^{st} Row: Auger/Auger, 2^{nd} Row: fast-Auger/photo-electron, 3^{rd} Row: slow-Auger/photo-electron, 4^{th} Row: Auger-sum/photo-electron, Left Column: Asymmetric Energy Sharing, Middle Column: Intermediate Energy Sharing, Right Column: Symmetric Energy Sharing

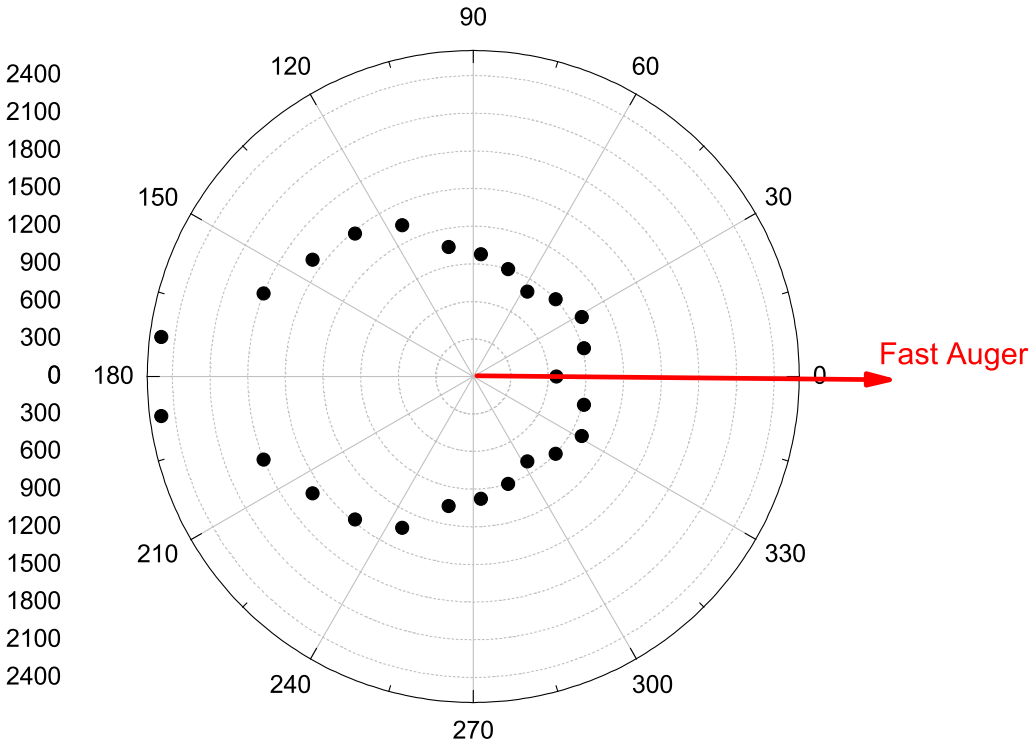

Figure 6.16: Asymmetric Auger / Auger Correlation

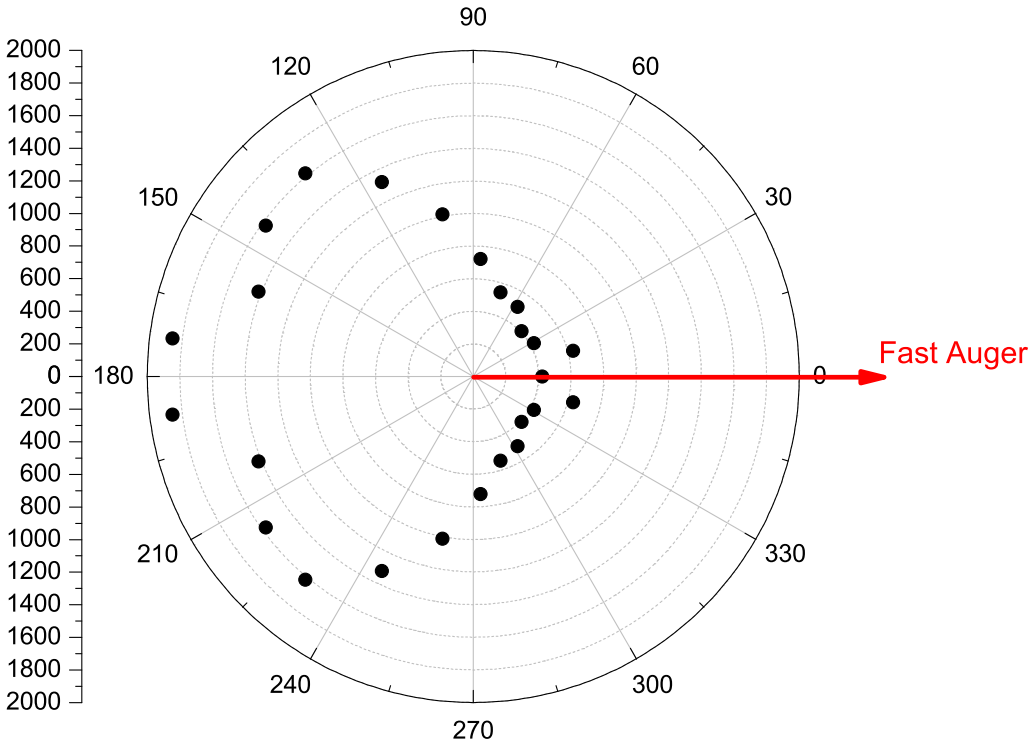

Figure 6.17: Intermediate Auger / Auger Correlation

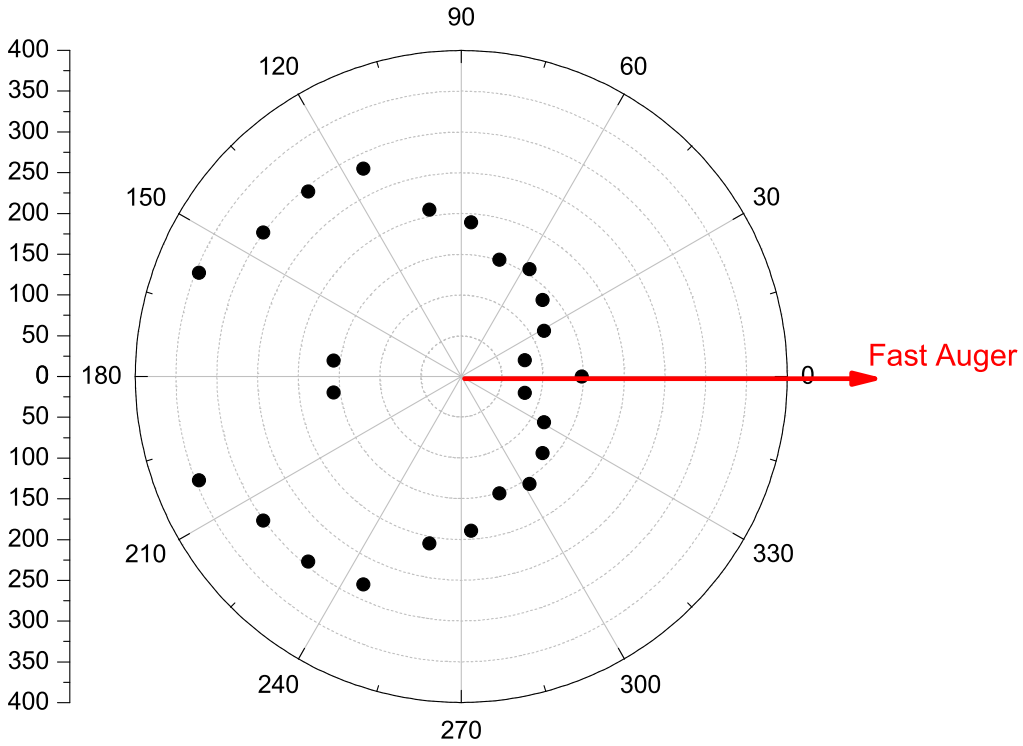

Figure 6.18: Symmetric Auger / Auger Correlation

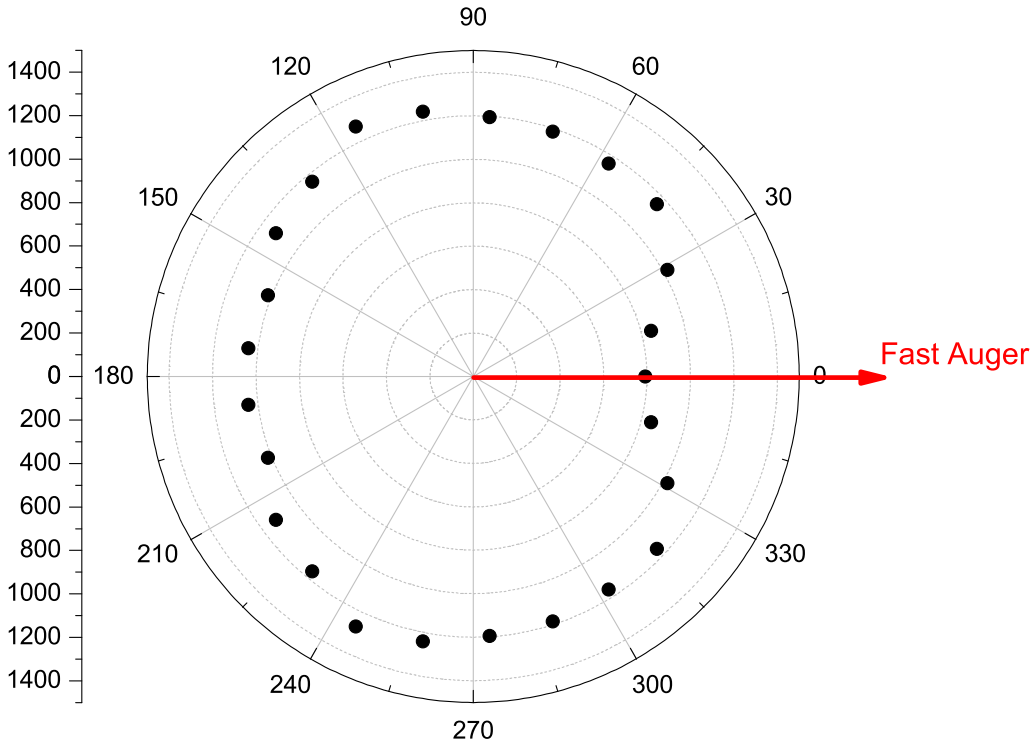

Figure 6.19: Asymmetric fast-Auger / Photo-Electron Correlation

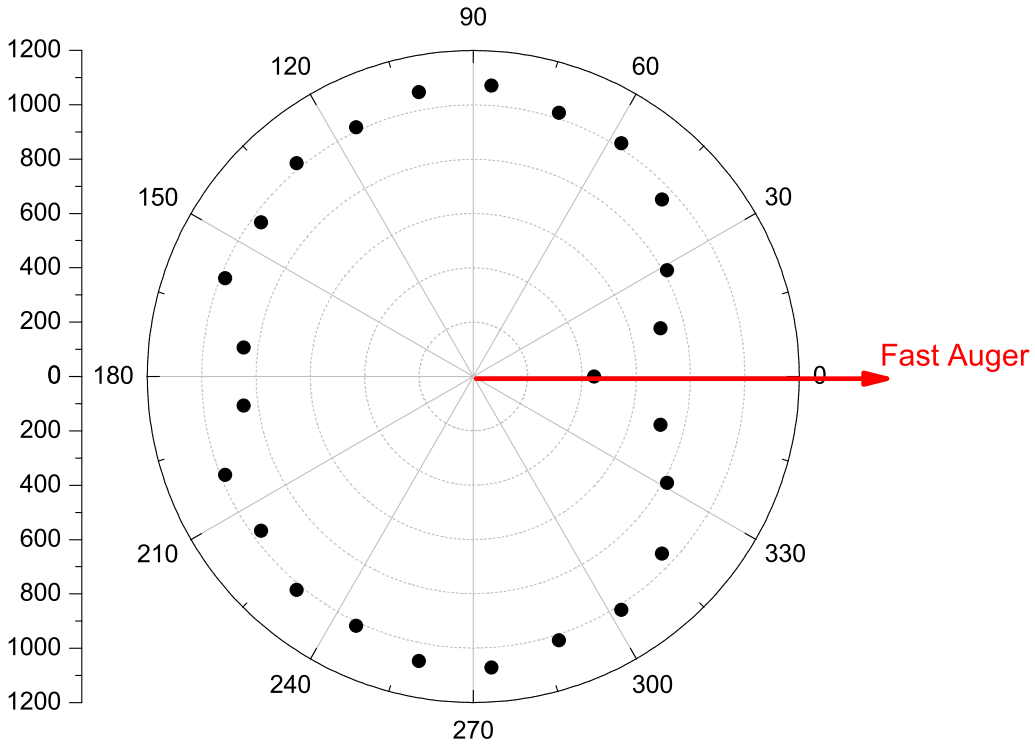

Figure 6.20: Intermediate fast-Auger / Photo-Electron Correlation

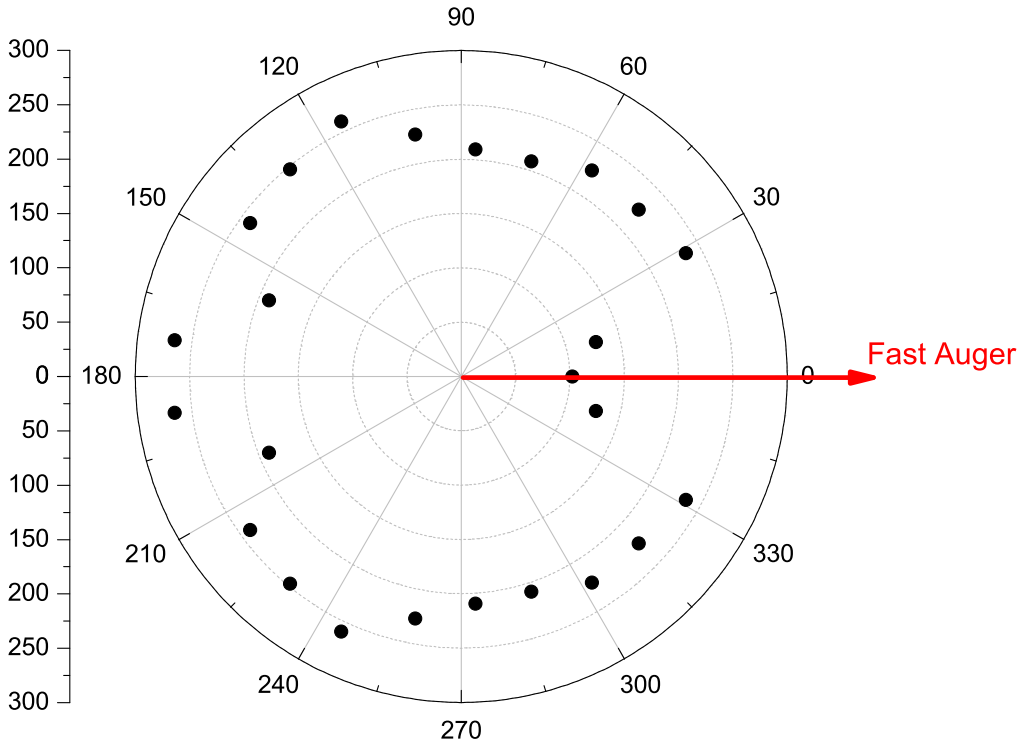

Figure 6.21: Symmetric fast-Auger / Photo-Electron Correlation

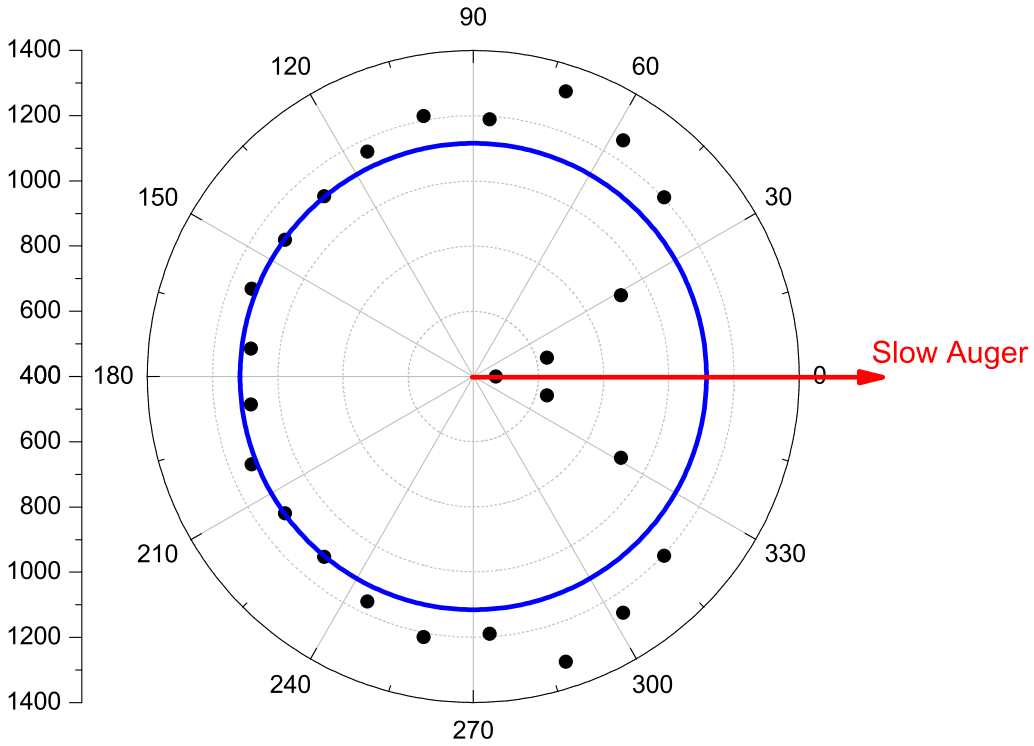

Figure 6.22: Asymmetric Slow-Auger / Photo-Electron Correlation

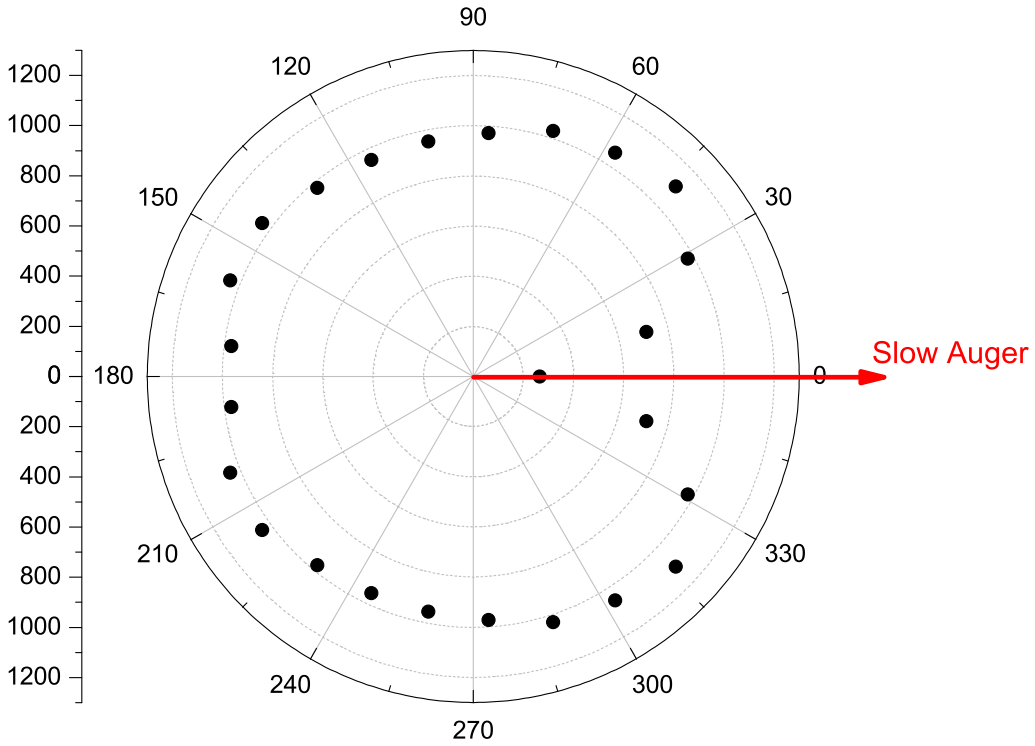

Figure 6.23: Intermediate Slow-Auger / Photo-Electron Correlation

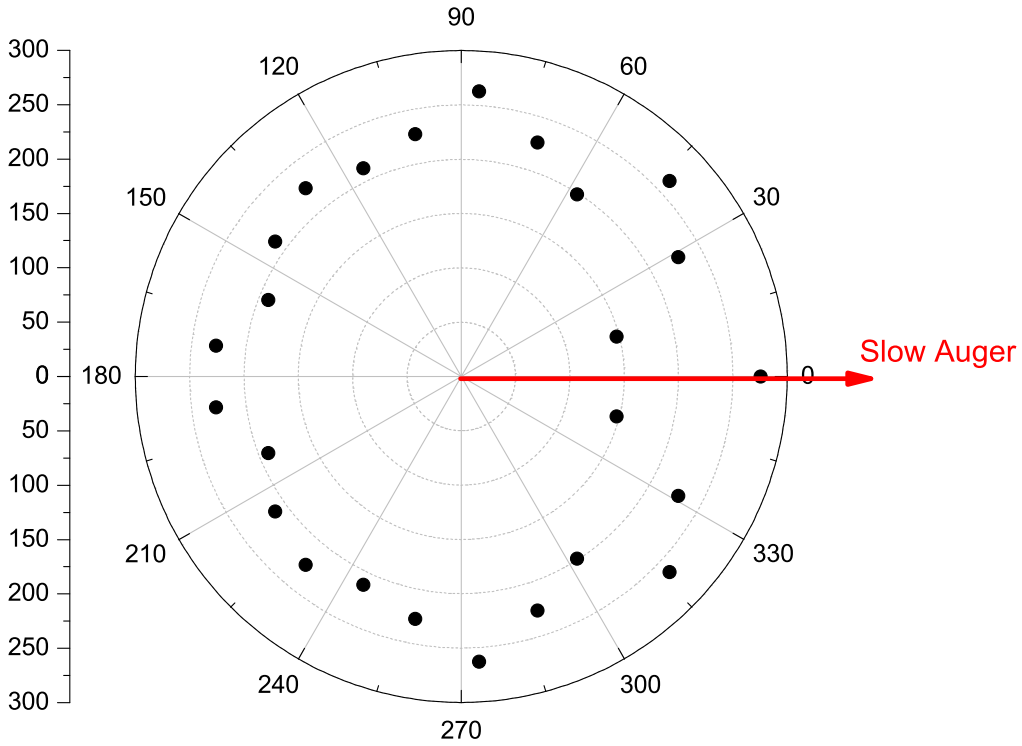

Figure 6.24: Symmetric Slow-Auger / Photo-Electron Correlation

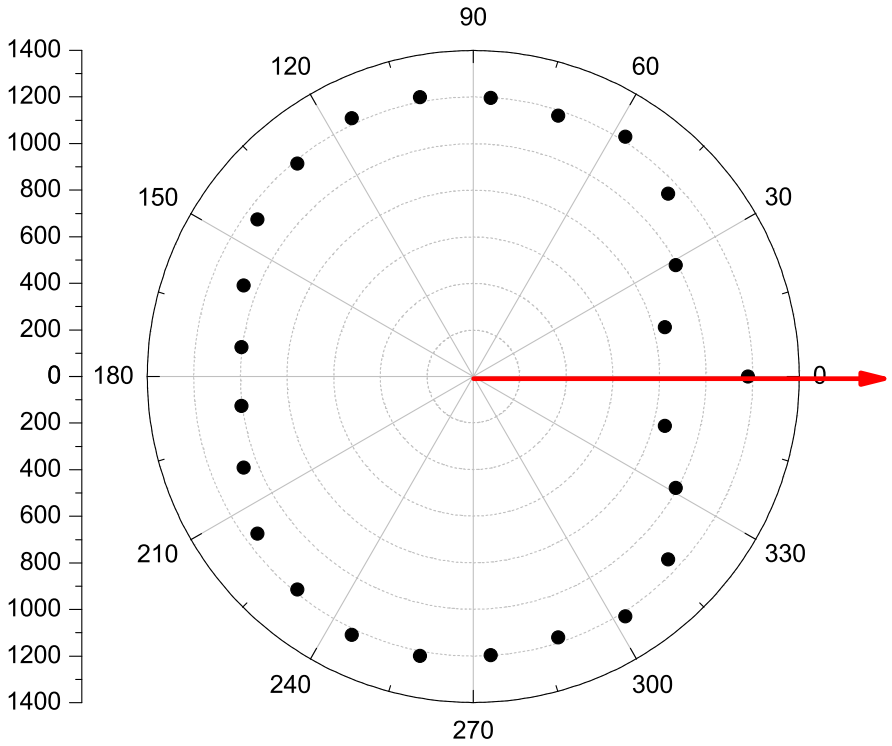

Figure 6.25: Asymmetric Auger-Sum / Photo-Electron Correlation

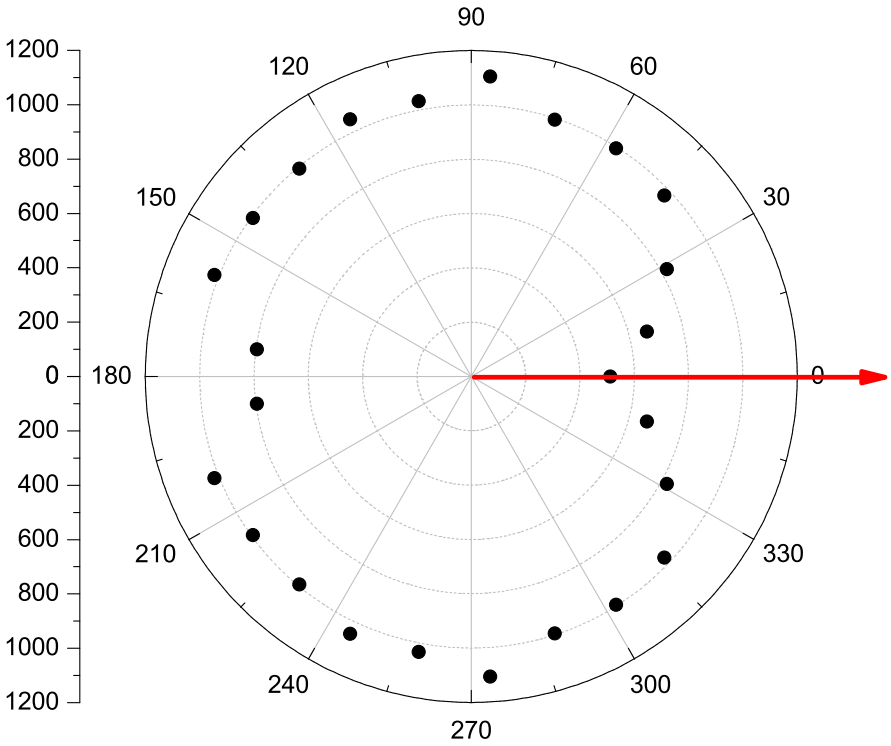

Figure 6.26: Intermediate Auger-Sum / Photo-Electron Correlation

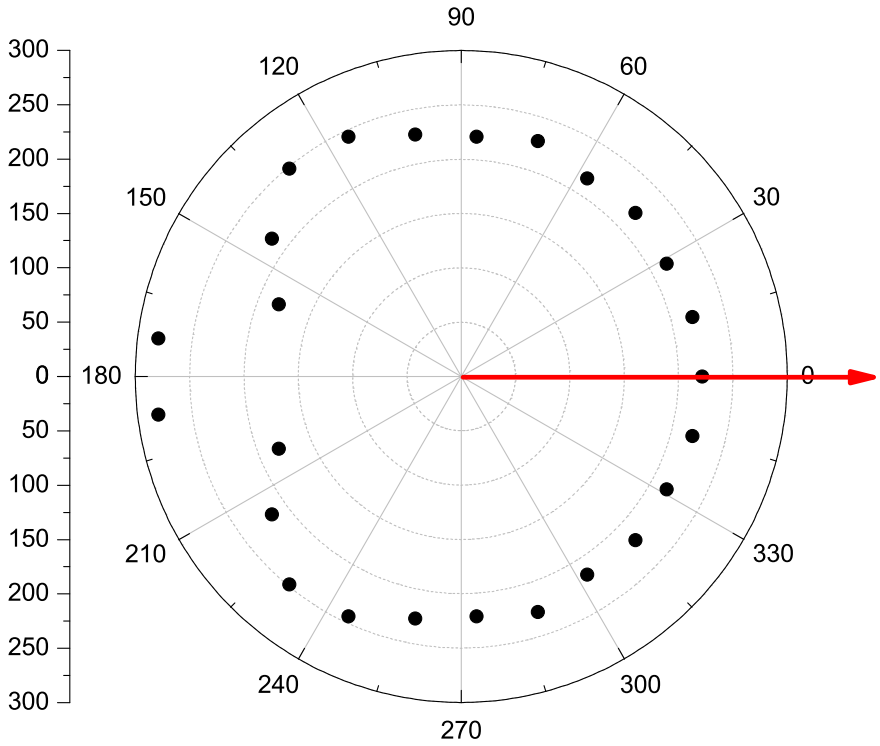

Figure 6.27: Symmetric Auger-Sum / Photo-Electron Correlation

Bibliography

[1] M. Pierre Auger, J. Phys. Radium **6**, 205-208 (1925).

[2] M.O. Krause, M.L. Vestal, W.H. Johnston and T.A. Carlson, Phys. Rev. 133 (1964), p. A385.

[3] T.A. Carlson and M.O. Krause, Phys. Rev. Lett. **14** (1965), p. 390.

[4] M.O. Krause and T.A. Carlson, Phys. Rev. 158 (1967), p. 18.

[5] T.A. Carlson and F.B. Malik, Phys. Rev. **169** (1968), p. 169.

[6] F.P. Larkins, J. Phys. B (1971), 4.

[7] V. Kaufman and L. Minnhagen, J. Opt. Soc. Am. 62, 92 (1972).

[8] T.A. Carlson, Photoelectron and Auger Spectroscopy, New York, Plenum Press, ISBN 0-306-33901-3.

[9] U. Becker, T. Prescher, E. Schmidt, B. Sonntag and H.-E. Wetzel, Phys. Rev. A 33 (1986), p. 3891.

[10] D.W. Lindle, L.J. Medhurst, T.A. Ferrett, P.A. Heimann, M.N. Piancastelli, S.H. Liu, D.A. Shirley, T.A. Carlson, P.C. Deshmukh, G. Nasreen and S.T. Manson, Phys. Rev. A 38 (1988), p. 2371.

[11] U. Becker, D. Szostak, M. Kupsch, H.G. Kerkhoff, B. Langer and R. Wehlitz, J. Phys. B 22 (1989), p. 749.

[12] U. Becker, D. Szostak, H.G. Kerkhoff, M. Kupsch, B. Langer, R. Wehlitz, A. Yagishita and T. Hayaishi, Phys. Rev. A 39 (1989), p. 3902.

[13] J.C. Levin, C. Biedermann, N. Keller, L. Liljeby, C.-S. O, R.T. Short, I.A. Sellin and D.W. Lindle, Phys. Rev. Lett. 65 (1990), p. 988.

[14] Y. Hikosaka, *et. al.*, Phys. Rev. A **80**, 031404 (1991).

[15] M.Ya. Amusia, I.S. Lee and V.A. Kilin, Phys. Rev. A 45 (1992), p. 4576.

[16] M.Ya. Amusia, V.A. Kilin, A. Ehresmann, H. Schmoranzer and K.-H. Schartner, J. Phys. B 26 (1993), p. 1281.

[17] M.M. Hindi, Z. Lin, A. Recep, P.M. Miocinovic, R.L. Kozub and G.J. Lapeyre, Phys. Rev. A 53 (1996), p. R3716.

[18] T.D. Thomas *et. al.*, J. Phys. B (1996), 29 3245-3256.

[19] V.A. Kilin, A. Ehresmann, F. Vollweiler, K.-H. Schartner and H. Schmoranzer, J. Phys. B 30 (1997), p. 5715.

[20] S. Sheinerman, J. Phys. B 31 (1998), p. L361.

[21] H. Yoshida, K. Ueda, N.M. Kabachnik, Y. Shimizu, Y. Senba, Y. Tamenori, H. Ohashi, I. Koyano, I.H. Suzuki, R. Hentges, J Viefhaus and U. Becker, J. Phys. B (2000), p. 4343-4352.

[22] S. Rioual and B. Rouvellou,L. Avaldi, G. Battera, and R. Camilloni,G. Stefani,G. Turri, PRL 86 (2001), 8.

[23] A. Knapp, *et. al.*, Phys. Rev. Lett. **89**, 033004 (2002).

[24] J. Viefhaus, A. Bianconi, A. Marcelli and N.L. Saini, X-Ray and Inner-Shell Processes, AIP Conference Proceedings 652, New York (2003), p. 307.

[25] J. Viefhaus, S. Cvejanovic, B. Langer, T. Lischke, G. Pr?mper, D. Rolles, A.V. Golovin, A.N. Grum-Grzhimailo, N.M. Kabachnik and U. Becker, Phys. Rev. Lett. 92 (2004), p. 083001.

[26] T. Jahnke, *et. al.*, Jour. Electron Spectroscopy **141**, 229 (2004).

[27] A.N. Grum-Grzhimailo and N.M. Kabachnik, J. Phys. B 37 (2004), p. 1879.

[28] R. Hentges *et. al.*, J. Phys. B (2004), 37 3245-3256.

[29] A.G. Kochur, V.L. Sukhorukov, V.F. Demekhin, J. Electron Spectrosc. Relat. Phenom. 137-140 (2004), p. 325-328.

[30] J Colgan and M S Pindzola, J. Phys. B (2004), 37 11531164.

[31] T. Warwick, *et. al.*, Synchrotron Radiation Instrumentation 2003 AIP Conference Proceedings, vol. 705, 2004, p. 458.

[32] T. Jahnke, *et. al.* J. Electron Spectrosc. Relat. Phenom. 141 (2004), p. 229-238.

[33] A. Knapp, *et. al.*, J. Phys. B **38**, 615-633 (2005).

[34] H. Yoshida *et. al.*, J. Phys. B (2005), 38 465-486.

[35] U. Hergenhahn *et. al.*, J. Phys. B (2006), 38 2843-2857.

[36] A. DeFanis *et. al.*, J. Phys. B (2006), 38 2229-2243.

[37] M. Kitajima *et. al.*, J. Phys. B (2006), 39 1299-1322.

[38] H. Bluhm, *et. al.*, Jour. Electron Spectroscopy **150**, 86-104 (2006).

[39] Y. Hikosaka, *et. al.*, Phys. Rev. A 158 (2009), 80 p. 031404.

[40] A.L. Landers *et. al.*, Phys. Rev. Lett. **102**, 223001 (2009).

footnotesize

```
1       1       file type to read (0 = read .lmf-File, 1 = read .root-file)

2       1       print .lmf-Headerinfo (0 = no, 1 = yes)

10      1       use all CPUs (enable multicore support) (0 = no, 1 = yes)
15      1       Anti-Moire    (0 = no, 1 = yes)

20      0       Calibration run - Wiggles (0 = no, 1 = yes)

49      0       write new listmode (.lmf) file including sorted TDC data (0 = no, 1 = yes)

50      0       demix channel (0 = no, 1 = yes)
51      0       channel to demix (channels are counted starting from "0")
52      0       number of channel to write the demixed to
53      0       number of channels (if 0 then number of channels in original LMF is used)
54      0       number of hits (if 0 then number of hits in original LMF is used)
55      1000.   demix region (times after this time belong to next channel)
56      5000000 number of events to write to new root file
```

57 0 start new file when number of events is (parameter[56]) (0 = no, 1 = yes)

90 7 channel number for bunchmarker / pulser / photodiode

91 15 channel number bunch cleaning

100 0 DLD/HEX (0=none; 1=DLD; 2=HEX) P R O J E C T I L E – detector

101 0 common mode (0=start, 1=stop) for PROJECTILE–detector

102 9 channel number for projectile u1

103 12 channel number for projectile u2

104 7 channel number for projectile v1

105 5 channel number for projectile v2

106 0 channel number for projectile w1

107 0 channel number for projectile w2

108 1 channel number for projectile MCP

109 1 use MCP–signal (0 = no, 1 = yes)

110 0.7 conversion factor for u–layer [mm/ns]

111 0.7 conversion factor for v–layer [mm/ns]

112 0.7 conversion factor for w–layer [mm/ns]

113 37.6 offset for timesum u [ns]

114 42.5 offset for timesum v [ns]

115 0. offset for timesum w [ns]

116 0. position offset w–layer [ns]

117 5. width of timesum u [ns] (half width at bottom)

118 5. width of timesum v [ns] (half width at bottom)

119 5. width of timesum w [ns] (half width at bottom)

120 20. deadtime anode [ns]

121 20. deadtime MCP [ns]

122 25. MCP–radius [mm] (choose always bigger than real radius)

123 43. runtime [ns] (max. runtime on largest layer)

126 0 auto calibration (0 = no, 1 = yes)

127 0 use resort routine (reconstruction) (0 = no, 1 = yes)

128 0 use sum correction (0 = no, 1 = yes)

200 1 DLD/HEX (0=none; 1=DLD; 2=HEX) R E C O I L – detector

201 0 common mode (0=start , 1=stop) for RECOIL–detector

202 4 channel number for Recoil u1

203 11 channel number for Recoil u2

204 2 channel number for Recoil v1

205 9 channel number for Recoil v2

206 0 channel number for Recoil w1

```
207     0       channel number for Recoil w2
208     0       channel number for Recoil MCP
209     1       Use MCP-Signal (0 = no, 1 = yes)
210     0.563   conversion factor for u-layer [mm/ns]   0.58
211     0.509   conversion factor for v-layer [mm/ns]   0.488
212     -1.0            conversion factor for w-layer [mm/ns]
213     -63.3   offset for timesum u [ns]
214     -68.3   offset for timesum v [ns]
215     0.      offset for timesum  w [ns]
216     0.      position offset w-layer [ns]
217     3.      width of timesum u [ns] (half width at bottom)
218     3.      width of timesum v [ns] (half width at bottom)
219     20.     width of timesum w [ns] (half width at bottom)
220     10.     deadtime anode [ns]
221     10.     deadtime MCP [ns]
222     45.     MCP-radius [mm] (choose always bigger than real
   radius)
223     85.     runtime [ns] (max. runtime on largest layer)
224     0.      shift detector to center x-direction
225     0.      shift detector to center y-direction
226     0       auto calibration (0 = no, 1 = yes)
227     1       use resort routine (reconstruction) (0 = no, 1 =
   yes)
228     1       use sum correction (0 = no, 1 = yes)
```

300 2 DLD/HEX (0=none; 1=DLD; 2=HEX) ELECTRON – detector

301 0 common mode (0=start, 1=stop) for ELECTRON–detector

302 10 channel number for Electron u1

303 13 channel number for Electron u2

304 12 channel number for Electron v1

305 5 channel number for Electron v2

306 14 channel number for Electron w1

307 6 channel number for Electron w2

308 1 channel number for Electron MCP

309 1 use MCP–Signal (0 = no, 1 = yes)

310 0.5807 conversion factor for u–layer [mm/ns] 0.537

311 0.5675 conversion factor for v–layer [mm/ns] 0.52475

312 0.5656 conversion factor for w–layer [mm/ns] 0.523

313 −66.9 offset for timesum u [ns]

314 −70.7 offset for timesum v [ns]

315 −72.7 offset for timesum w [ns]

316 −1.725 position offset w–layer [ns]

317 5. width of timesum u [ns] (half width at bottom)

318 5. width of timesum v [ns] (half width at bottom)

319 5. width of timesum w [ns] (half width at bottom)

320 10. deadtime anode [ns]

321 10. deadtime MCP [ns]

322 45. MCP–radius [mm] (choose always bigger than real radius)

323 85. runtime [ns] (max. runtime on largest layer)

324 0. shift detector to center x–direction

325 0. shift detector to center y–direction

326 0 auto calibration (0 = no, 1 = yes)

327 1 use resort routine (reconstruction) (0 = no, 1 = yes)

328 1 Use sum correction (0 = no, 1 = yes)

1100 44053 TOF for first Recoil [ns] (20 Neon 1+)

1101 625. half width TOF peak first Recoil [ns]

1105 31149. TOF for second Recoil [ns] (20 Neon 2+)

1106 400. half width TOF peak second Recoil [ns]

1110 25422. TOF for third Recoil [ns] (20 Neon 3+)

1111 300. half width TOF peak third Recoil [ns]

1115 22022. TOF for fourth Recoil [ns] (20 Neon 4+)

1116 150. half width TOF peak fourth Recoil [ns]

1150 55. TOF for electron [ns]

1151 56. half width TOF peak electron [ns]

1200 2.22 Electric Field electron side [V/cm]

1201 42.7 Acceleration Region electron side [mm]

1205 93.6 Gyration period [ns]

1206 1.99e–17 Momentum Conversion from [kg cm/ns] to [au]

1207 9.108e–31 Mass of electron [kg]

1208 5.e–3 Length of MCP acceleration region [m]

1210	−4.337	TOF offset electron side [ns]
1211	0.418	X–Offset [mm]
1212	−4.1865	Y–Offset [mm]
1213	−0.0179	X position shift with time (E–B–drift) [mm/ns]
1214	0.063	Y position shift with time (E–B–drift) [mm/ns]
1215	−60.	Rotation of detector (adjust accordingly) [deg]
1310	0.41	Ne 1+ stretch z [au/mm]
1311	0.40	Ne 1+ stretch y [au/mm]
1315	−3.58	Ne 1+ offset z [au]
1316	−5.8	Ne 1+ offset y [au]
1318	1.6e−19	Ne 1+ charge [C]
1320	0.584	Ne 2+ stretch z [au/mm]
1321	0.558	Ne 2+ stretch y [au/mm]
1325	−4.9	Ne 2+ offset z [au]
1326	−4.25	Ne 2+ offset y [au]
1328	3.2e−19	Ne 2+ charge [C]
1330	0.745	Ne 3+ stretch z [au/mm]
1331	0.68	Ne 3+ stretch y [au/mm]
1335	−6.65	Ne 3+ offset z [au]
1336	−3.2	Ne 3+ offset y [au]

1338	4.8e−19	Ne 3+ charge [C]
1340	0.826	Ne 4+ stretch z [au/mm]
1341	0.86	Ne 4+ stretch y [au/mm]
1345	−7.12	Ne 4+ offset z [au]
1346	−2.8	Ne 4+ offset y [au]
1348	6.4e−19	Ne 4+ charge [C]
1350	0.9235	Ne 5+ stretch z [au/mm] Not Calibrated
1351	0.9615	Ne 5+ stretch y [au/mm] Not Calibrated
1355	0.	Ne 5+ offset z [au] Not Calibrated
1356	0.	Ne 5+ offset y [au] Not Calibrated
1358	8.0e−19	Ne 5+ charge [C] Not Calibrated
1400	80.0	Actual size of electron detector
1401	80.0	Actual size of recoil detector
1500	0.1	Kslice I−VI
1501	110.2	Augslice I, II & III
1502	110.2	Aslice IV, V & VI
1503	110.2	Rslice I−VI
1601	200.0	Inverted sine function limit
1700	1321.29	Flatland−Ne2 Photo−electron (xy−plane)

```
1701    16.95           Flatland-Ne3 Photo-electron (xy-plane)

1710    11310.5         Isotropy Ne2 Auger x
1711    11310.5         Isotropy Ne2 Auger y
1712    11310.5         Isotropy Ne2 Auger z

1800    2000            photon Targe Value x
1801    2000            photon Targe Value x
1802    2000            photon Targe Value x

1850    44854.4         Ne2+ 3D correction photo
1851    12815.5         Ne2+ 3D correction Auger

1900    421.36          3D photo correction Ne3+
2000    312.2           Correction Allen
2001    333.58          pweightalt parameter

10000   0.      End_of_Parameter-list

0       Number_of_correction_points_layer_U on proj
0       Number_of_correction_points_layer_V on proj
0       Number_of_correction_points_layer_W on proj

49      Number_of_correction_points_layer_U on rec
-86.000000  0.000000
-82.416667  0.000000
-78.833333  0.000000
```

−75.250000 0.000000

−71.666667 0.000000

−68.083333 0.000000

−64.500000 0.188747

−60.916667 −0.234777

−57.333333 −0.355000

−53.750000 −0.276999

−50.166667 −0.330029

−46.583333 −0.285952

−43.000000 −0.385225

−39.416667 −0.371540

−35.833333 −0.396742

−32.250000 −0.412039

−28.666667 −0.421806

−25.083333 −0.424680

−21.500000 −0.184504

−17.916667 −0.407309

−14.333333 −0.468332

−10.750000 −0.473574

−7.166667 −0.488326

−3.583333 −0.508999

0.000000 −0.482357

3.583333 −0.523395

7.166667 −0.550112

10.750000 −0.537453

14.333333 −0.551077

17.916667 −0.565501

21.500000 −0.548726

25.083333 −0.555373

28.666667 −0.544827

32.250000 −0.535412

35.833333 −0.524436

39.416667 −0.505988

43.000000 −0.394978

46.583333 −0.288033

50.166667 −0.356207

53.750000 −0.387402

57.333333 −0.346250

60.916667 −0.405000

64.500000 0.046780

68.083333 −0.322316

71.666667 −0.599510

75.250000 −0.199208

78.833333 0.000000

82.416667 0.000000

86.000000 0.000000

49 Number_of_correction_points_layer_V on rec

−86.000000 0.000000

−82.416667 0.000000

−78.833333 0.000000

−75.250000 0.000000

−71.666667 −0.071858

−68.083333 0.000000

−64.500000 −0.377654

−60.916667 −0.492276

−57.333333 −0.724993

−53.750000 −0.777680

−50.166667 −0.819016

−46.583333 −0.904202

−43.000000 −0.927977

−39.416667 −0.963715

−35.833333 −1.052879

−32.250000 −1.061507

−28.666667 −1.004137

−25.083333 −1.056513

−21.500000 −1.136054

−17.916667 −1.027699

−14.333333 −1.007540

−10.750000 −1.047681

−7.166667 −1.074868

−3.583333 −1.014290

0.000000 −0.872650

3.583333 −0.787101

7.166667 −0.720500

10.750000 −0.696835

14.333333 −0.561116

17.916667 −0.455743

21.500000 −0.272314

25.083333 −0.150744

28.666667 0.033582

```
32.250000  0.169143
35.833333  0.276871
39.416667  0.352328
43.000000  0.402248
46.583333  0.518194
50.166667  0.423812
53.750000  0.395351
57.333333  0.286683
60.916667  0.193656
64.500000  0.105697
68.083333  -0.068587
71.666667  -0.042879
75.250000  -0.173446
78.833333  0.000000
82.416667  0.000000
86.000000  0.000000

0        Number_of_correction_points_layer_W on rec

49       Number_of_correction_points_layer_U on elec
-86.000000  0.000000
-82.416667  0.000000
-78.833333  6.202897
-75.250000  0.012791
-71.666667  0.000000
-68.083333  0.012692
-64.500000  0.000000
```

−60.916667 0.012829

−57.333333 0.117904

−53.750000 0.169613

−50.166667 0.168290

−46.583333 0.167141

−43.000000 0.182672

−39.416667 0.171865

−35.833333 0.149663

−32.250000 0.154224

−28.666667 0.132125

−25.083333 0.120293

−21.500000 0.125345

−17.916667 0.106971

−14.333333 0.075896

−10.750000 0.092161

−7.166667 0.077828

−3.583333 0.046141

0.000000 0.028098

3.583333 −0.001570

7.166667 −0.059828

10.750000 −0.152513

14.333333 −0.202574

17.916667 −0.239445

21.500000 −0.306548

25.083333 −0.372353

28.666667 −0.398875

32.250000 −0.431910

35.833333 −0.541047

39.416667 −0.600743

43.000000 −0.682319

46.583333 −0.4

50.166667 −0.4

53.750000 −0.2

57.333333 −0.2

60.916667 −0.200000

64.500000 0.0

68.083333 0.000000

71.666667 0.000000

75.250000 0.000000

78.833333 0.000000

82.416667 0.000000

86.000000 0.000000

49 Number_of_correction_points_layer_V on elec

−86.000000 0.000000

−82.416667 0.000000

−78.833333 0.000000

−75.250000 2.052897

−71.666667 −0.823750

−68.083333 −0.593520

−64.500000 −0.589489

−60.916667 −0.774071

−57.333333 −0.857069

−53.750000 −0.908023

−50.166667 −0.957812

−46.583333 −0.980213

−43.000000 −0.969901

−39.416667 −0.938994

−35.833333 −0.907156

−32.250000 −0.889880

−28.666667 −0.845304

−25.083333 −0.801016

−21.500000 −0.726426

−17.916667 −0.643592

−14.333333 −0.559422

−10.750000 −0.431799

−7.166667 −0.342607

−3.583333 −0.198731

0.000000 −0.056163

3.583333 0.019399

7.166667 0.118002

10.750000 0.226812

14.333333 0.315267

17.916667 0.385726

21.500000 0.444863

25.083333 0.475918

28.666667 0.530699

32.250000 0.568945

35.833333 0.572452

39.416667 0.598802

43.000000 0.580508

46.583333 0.589724

50.166667 0.574297

53.750000 0.546745

57.333333 0.583300

60.916667 0.500630

64.500000 0.672850

68.083333 0.974768

71.666667 0.013036

75.250000 0.013392

78.833333 0.000000

82.416667 0.000000

86.000000 0.000000

49 Number_of_correction_points_layer_W on elec

−86.000000 0.000000

−82.416667 4.853323

−78.833333 0.395393

−75.250000 0.451647

−71.666667 0.553766

−68.083333 0.357297

−64.500000 0.405882

−60.916667 0.441907

−57.333333 0.469281

−53.750000 0.460319

−50.166667 0.449475

−46.583333 0.424904

−43.000000 0.412802

−39.416667 0.406881

−35.833333 0.391470

−32.250000 0.362464

−28.666667 0.334760

−25.083333 0.287657

−21.500000 0.251015

−17.916667 0.219105

−14.333333 0.178532

−10.750000 0.098633

−7.166667 0.037846

−3.583333 −0.005279

0.000000 −0.074243

3.583333 −0.226551

7.166667 −0.394598

10.750000 −0.533549

14.333333 −0.685846

17.916667 −0.883491

21.500000 −1.099899

25.083333 −1.284736

28.666667 −1.464083

32.250000 −1.606950

35.833333 −1.722440

39.416667 −1.828752

43.000000 −1.882496

46.583333 −1.904131

50.166667 −1.887992

53.750000 −1.849591

```
57.333333  -1.755475
60.916667  -1.919790
64.500000  -2.479800
68.083333  0.012348
71.666667  2.152584
75.250000  0.000000
78.833333  0.000000
82.416667  0.000000
86.000000  0.000000

Ne_872_1_analysis
Ne_872_1_process.root
ende

Ne_872_1_process
C:\ALS_Data_March_2009\080309\Ne_RC_872.1eV_.lmf00000
C:\ALS_Data_March_2009\080309\Ne_RC_872.1eV_.lmf00001
C:\ALS_Data_March_2009\080309\Ne_RC_872.1eV_.lmf00002
C:\ALS_Data_March_2009\080309\Ne_RC_872.1eV_.lmf00003
C:\ALS_Data_March_2009\080309\Ne_RC_872.1eV_.lmf00004
C:\ALS_Data_March_2009\080309\Ne_RC_872.1eV_.lmf00005
C:\ALS_Data_March_2009\080309\Ne_RC_872.1eV_.lmf00006
C:\ALS_Data_March_2009\080309\Ne_RC_872.1eV_.lmf00007
C:\ALS_Data_March_2009\080309\Ne_RC_872.1eV_.lmf00008
C:\ALS_Data_March_2009\080309\Ne_RC_872.1eV_.lmf00009
C:\ALS_Data_March_2009\080309\Ne_RC_872.1eV_.lmf00010
C:\ALS_Data_March_2009\080309\Ne_RC_872.1eV_.lmf00011
```

C:\ALS_Data_March_2009\080309\Ne_RC_872.1eV_.lmf00012

C:\ALS_Data_March_2009\080309\Ne_RC_872.1eV_.lmf00013

C:\ALS_Data_March_2009\080309\Ne_RC_872.1eV_.lmf00014

C:\ALS_Data_March_2009\080309\Ne_RC_872.1eV_.lmf00015

C:\ALS_Data_March_2009\080309\Ne_RC_872.1eV_.lmf00016

C:\ALS_Data_March_2009\080309\Ne_RC_872.1eV_.lmf00017

C:\ALS_Data_March_2009\080309\Ne_RC_872.1eV_.lmf00018

C:\ALS_Data_March_2009\080309\Ne_RC_872.1eV_.lmf00019

C:\ALS_Data_March_2009\080309\Ne_RC_872.1eV_.lmf00020

C:\ALS_Data_March_2009\080309\Ne_RC_872.1eV_.lmf00021

C:\ALS_Data_March_2009\080309\Ne_RC_872.1eV_.lmf00022

C:\ALS_Data_March_2009\080309\Ne_RC_872.1eV_.lmf00023

C:\ALS_Data_March_2009\080309\Ne_RC_872.1eV_.lmf00024

C:\ALS_Data_March_2009\080309\Ne_RC_872.1eV_.lmf00025

C:\ALS_Data_March_2009\080309\Ne_RC_872.1eV_.lmf00026

C:\ALS_Data_March_2009\080309\Ne_RC_872.1eV_.lmf00027

C:\ALS_Data_March_2009\080309\Ne_RC_872.1eV_.lmf00028

C:\ALS_Data_March_2009\080309\Ne_RC_872.1eV_.lmf00029

C:\ALS_Data_March_2009\080309\Ne_RC_872.1eV_.lmf00030

C:\ALS_Data_March_2009\080309\Ne_RC_872.1eV_.lmf00031

C:\ALS_Data_March_2009\080309\Ne_RC_872.1eV_.lmf00032

C:\ALS_Data_March_2009\080309\Ne_RC_872.1eV_.lmf00033

C:\ALS_Data_March_2009\080309\Ne_RC_872.1eV_.lmf00034

C:\ALS_Data_March_2009\080309\Ne_RC_872.1eV_.lmf00035

C:\ALS_Data_March_2009\080309\Ne_RC_872.1eV_.lmf00036

C:\ALS_Data_March_2009\080309\Ne_RC_872.1eV_.lmf00037

C:\ALS_Data_March_2009\080309\Ne_RC_872.1eV_.lmf00038

```
C:\ALS_Data_March_2009\080309\Ne_RC_872.1eV_.lmf00039
C:\ALS_Data_March_2009\080309\Ne_RC_872.1eV_.lmf00040
C:\ALS_Data_March_2009\080309\Ne_RC_872.1eV_.lmf00041
C:\ALS_Data_March_2009\080309\Ne_RC_872.1eV_.lmf00042
C:\ALS_Data_March_2009\080309\Ne_RC_872.1eV_.lmf00043
C:\ALS_Data_March_2009\080309\Ne_RC_872.1eV_.lmf00044
C:\ALS_Data_March_2009\080309\Ne_RC_872.1eV_.lmf00045
C:\ALS_Data_March_2009\080309\Ne_RC_872.1eV_.lmf00046
C:\ALS_Data_March_2009\080309\Ne_RC_872.1eV_.lmf00047
C:\ALS_Data_March_2009\080309\Ne_RC_872.1eV_.lmf00048
C:\ALS_Data_March_2009\080309\Ne_RC_872.1eV_.lmf00049
C:\ALS_Data_March_2009\080309\Ne_RC_872.1eV_.lmf00050
C:\ALS_Data_March_2009\080309\Ne_RC_872.1eV_.lmf00051
C:\ALS_Data_March_2009\080309\Ne_RC_872.1eV_.lmf00052
C:\ALS_Data_March_2009\080309\Ne_RC_872.1eV_.lmf00053
C:\ALS_Data_March_2009\080309\Ne_RC_872.1eV_.lmf00054
C:\ALS_Data_March_2009\080309\Ne_RC_872.1eV_.lmf00055
C:\ALS_Data_March_2009\080309\Ne_RC_872.1eV_.lmf00056
C:\ALS_Data_March_2009\080309\Ne_RC_872.1eV_.lmf00057
ende
```

footnotesize

```
#pragma warning(disable : 4800)
#include "RootVersion.h"
#include "TCanvas.h"
#include "TH1D.h"
#include "TH2D.h"
```

```
#include "TFile.h"
#include "TTree.h"
#include "TNtupleD.h"
#include <math.h>
#include "rootstuff.h"
#include "histo.h"
#include "TF1.h"
#include "TMinuit.h"

#include "functions.h"
#include "weights.h"
#include "Ueberstruct.h"

#include "linear.h"             // all these four to make linear
   fits
#include "iostream"
#include "iomanip"
#include "TApplication.h"
using namespace std;

//#include "resort64c.h"

////////////////////////////////////////////////////////////////////////

int analysis(unsigned __int64 eventcounter, double  parameter[],
   rootstuff * rt, TTree * Data, Ueberstruct * Ueber)
```

```
//////////////////////////////////////////////////////////////////////////////

{
// read root data file in here (adjust variables and array size)

Histo * Hist = Ueber->Hist;

double r1x=-111111.,r1y=-1111111.,r1tof=-11111111.,r1flag
   =-111111111.;
double e1x=-222222.,e1y=-2222222.,e1tof=-22222222.,e1flag
   =-222222222.;
double e2x=-333333.,e2y=-3333333.,e2tof=-33333333.,e2flag
   =-333333333.;
double e3x=-444444.,e3y=-4444444.,e3tof=-44444444.,e3flag
   =-444444444.;
double bunch_cleaning=0.0; double pi = 3.14159265359;

double NTupleData[17];

// BOOLEAN Initialization Section
bool WriteNTuple = false;

bool Neon1 = false;  //condition on recoil charge state
bool Neon2 = false;
bool Neon3 = false;
bool Neon4 = false;
```

```
bool Elec1 = false; //condition on electron hit number
bool Elec2 = false;
bool Elec3 = false;

bool Psum1 = false; //condition on momenutm sum
bool Psum2 = false;
bool Psum3 = false;

bool Cone1 = false; //condition on solid angle
bool Cone2 = false;
bool Cone3 = false;

// END BOOLEAN Initialization Section

if(eventcounter == 0) {
Ueber->EntriesInFile = 0;
Ueber->eventswritten = 0;
}

if(Ueber->EntriesInFile == 0) {
Data->SetBranchAddress("r1x",&r1x);
Data->SetBranchAddress("r1y",&r1y);
Data->SetBranchAddress("r1tof",&r1tof);
Data->SetBranchAddress("r1flag",&r1flag);
Data->SetBranchAddress("e1x",&e1x);
Data->SetBranchAddress("e1y",&e1y);
Data->SetBranchAddress("e1tof",&e1tof);
```

```
Data->SetBranchAddress("e1flag",&e1flag);
Data->SetBranchAddress("e2x",&e2x);
Data->SetBranchAddress("e2y",&e2y);
Data->SetBranchAddress("e2tof",&e2tof);
Data->SetBranchAddress("e2flag",&e2flag);
Data->SetBranchAddress("e3x",&e3x);
Data->SetBranchAddress("e3y",&e3y);
Data->SetBranchAddress("e3tof",&e3tof);
Data->SetBranchAddress("e3flag",&e3flag);
Data->SetBranchAddress("bunch_cleaning",&bunch_cleaning);
            // 0=inactive; 1=active
}

Data->GetEntry(Ueber->EntriesInFile);
if(Ueber->EntriesInFile < Data->GetEntries()-1) {
Ueber->EntriesInFile++;
} else {
Ueber->EntriesInFile = 0;
}

// Recoil TOF Plot
Hist->fill1(99,"Recoil_TOF",r1tof,1.,"Recoil TOF
   ",2000,-10.,47000.,"TOF [ns]");

// BooLeaN SeCTioN
if (( r1tof  < ( parameter[1100]+parameter[1101] )) && ( r1tof  >
    ( parameter[1100]-parameter[1101] ))) Neon1 = true;
```

```
if (( r1tof  < ( parameter[1105]+parameter[1106] )) && ( r1tof  >
    ( parameter[1105]-parameter[1106] ))) Neon2 = true;
if (( r1tof  < ( parameter[1110]+parameter[1111] )) && ( r1tof  >
    ( parameter[1110]-parameter[1111] ))) Neon3 = true;
if (( r1tof  < ( parameter[1115]+parameter[1116] )) && ( r1tof  >
    ( parameter[1115]-parameter[1116] ))) Neon4 = true;

if (e1tof > -1.) Elec1 = true;
if (e2tof > 1.) Elec2 = true;
if (e3tof > 1.) Elec3 = true;

double x=eventcounter;

//////////////////////////////////////////////////////////////////////////

/////
          DRiFTiNG PoWeR SuPPLY CoRReCTioN SeCTioN

             /////
//////////////////////////////////////////////////////////////////////////


//Data points were taken from the plot below - used to generate a
    5th order polynomial correction function for all r1tof
```

```
if (Neon2)      Hist->fill2(100,"
   Counter_r1tof_Neon2_large_bins_uncorrected",eventcounter,r1tof
   ,1.,"Counter_vs_rtof",50,0.,7000000.,"Counter
   ",400,30850.,31451.,"r1tof [ns]","power_supply");
r1tof = r1tof * 31148.1598/(31148.1598 + (2.74446e-6)*x -
   (2.15274e-12)*x*x + (1.06409e-18)*x*x*x - (1.74009e-25)*x*x*x*
   x + (9.12425e-33)*x*x*x*x*x*x);
if (Neon2)      Hist->fill2(101,"Counter_r1tof_Neon2",
   eventcounter,r1tof,1.,"Counter_vs_rtof",400,0.,7000000.,"
   Counter",400,30850.,31451.,"r1tof [ns]","power_supply");

////////////////////////////////////////////////////////////////////////////

/////
          aNaLYSiS oF NeoN iN CoNFiGuRaTioN SPaCe

             /////
////////////////////////////////////////////////////////////////////////////


//Recoil Fish Plots
Hist->fill2(102,"rec_xfish1",r1x,r1tof,1.,"Recoil x-fish1
   ",400,-20.,30.,"x-pos [mm]",400,43450.,44650.,"TOF [ns]");
Hist->fill2(103,"rec_xfish2",r1x,r1tof,1.,"Recoil x-fish2
   ",400,-20.,30.,"x-pos [mm]",400,30850.,31450.,"TOF [ns]");
Hist->fill2(104,"rec_xfish3",r1x,r1tof,1.,"Recoil x-fish3
   ",400,-20.,30.,"x-pos [mm]",400,25200.,25660.,"TOF [ns]");
```

```
Hist->fill2(105,"rec_xfish4",r1x,r1tof,1.,"Recoil x-fish4
   ",400,-20.,30.,"x-pos [mm]",400,21800.,22300.,"TOF [ns]");
Hist->fill2(106,"rec_xfish5",r1x,r1tof,1.,"Recoil x-fish5
   ",400,-20.,30.,"x-pos [mm]",400,19400.,20000.,"TOF [ns]");

//////////////////////////////////////////////////////////////////////////

/////
            eLeCTRoN FiSH CaLiBRaTioN SeCTioN

                        /////
//////////////////////////////////////////////////////////////////////////

// Histogram used to identify the node and anti-node.
if (Neon2 && fabs(e1y)<1.0) Hist->fill2(107,"filet_o_xfish_Neon2-
   uncorrected",e1tof,e1x,1.,"Uncorrected Fillet O' X-Fish Ne2+
   ",400,0.,100.,"TOF [ns]",400,-40.,40.,"x-pos [mm]");

// Calculate TOF Information (offset, gyration periode, magnetic
   field and shifts)
// This corrects for the small (ExB) drift present in the
   experiment.
e1x = e1x - e1tof*parameter[1213] - parameter[1211];
e2x = e2x - e2tof*parameter[1213] - parameter[1211];
e3x = e3x - e3tof*parameter[1213] - parameter[1211];

e1y = e1y - e1tof*parameter[1214] - parameter[1212];
```

```
e2y = e2y - e2tof*parameter[1214] - parameter[1212];
e3y = e3y - e3tof*parameter[1214] - parameter[1212];

////////////////////////////////////////////////////////////////////////////

/////
            MoMeNTuM SPaCe                    x=time dir., y=jet dir
   ., z=prop. dir.                                 /////
////////////////////////////////////////////////////////////////////////////


// DeCLaRaTioN SeCTioN
// Measured electron momentum components are catergorized by hit
   number (i.e. epx1)
// Calculated electron momentum components are catergorized first
    by the ehit number(s) used in the calculation (i.e. kpx12 =
   -(epx1 + epx2 + r1px)).
// Calculated momentum sum components indicate the electron(s)
   used to infer the quantity (i.e. kpx1 = -(epx1 + r3px)).
double epx1=-55555555.0, epy1=-66666666.0, epz1=-77777777.0, epr1
   =-88888888.0, eE1=-99999999.0;
double epx2=-55555555.0, epy2=-66666666.0, epz2=-77777777.0, epr2
   =-88888888.0, eE2=-99999999.0;
double epx3=-55555555.0, epy3=-66666666.0, epz3=-77777777.0, epr3
   =-88888888.0, eE3=-99999999.0;
```

```
double r1px=-55555555.0, r1py=-66666666.0, r1pz=-77777777.0, r1pr
   =-88888888.0, r1E=-99999999.0;
double r2px=-55555555.0, r2py=-66666666.0, r2pz=-77777777.0, r2pr
   =-88888888.0, r2E=-99999999.0;
double r3px=-55555555.0, r3py=-66666666.0, r3pz=-77777777.0, r3pr
   =-88888888.0, r3E=-99999999.0;
double r4px=-55555555.0, r4py=-66666666.0, r4pz=-77777777.0, r4pr
   =-88888888.0, r4E=-99999999.0;

double kpx1=-55555555.0, kpy1=-66666666.0, kpz1=-77777777.0, kpr1
   =-88888888.0, kE1=-99999999.0;
double kpx2=-55555555.0, kpy2=-66666666.0, kpz2=-77777777.0, kpr2
   =-88888888.0, kE2=-99999999.0;
double kpx3=-55555555.0, kpy3=-66666666.0, kpz3=-77777777.0, kpr3
   =-88888888.0, kE3=-99999999.0;

double kpx12=-55555555.0, kpy12=-66666666.0, kpz12=-77777777.0,
   kpr12=-88888888.0, kE12=-99999999.0;
double kpx23=-55555555.0, kpy23=-66666666.0, kpz23=-77777777.0,
   kpr23=-88888888.0, kE23=-99999999.0;
double kpx13=-55555555.0, kpy13=-66666666.0, kpz13=-77777777.0,
   kpr13=-88888888.0, kE13=-99999999.0;

double kpx123=-55555555.0, kpy123=-66666666.0, kpz123
   =-77777777.0, kpr123=-88888888.0, kE123=-99999999.0; //Used
   exclusively for Neon 4+
```

```
double ppx1=-55555555.0, ppy1=-55555555.0, ppz1=-55555555.0, ppr1
   =-55555555.0, pE1=-55555555.0; // photon in Neon 1+ radiative
   channel

double spx=-55555555.0, spy=-66666666.0, spz=-77777777.0, spr
   =-888888888.0;

double costhetx1=0.0, costhety1=0.0, costhetz1=0.0;
double costhetx2=0.0, costhety2=0.0, costhetz2=0.0;
double costhetx3=0.0, costhety3=0.0, costhetz3=0.0;

if (Elec1){// Measured electron momenta for 1st hit
epz1 = elec2momx(e1x, e1y, e1tof, parameter[1205], parameter
   [1215]);
epy1 = elec2momy(e1x, e1y, e1tof, parameter[1205], parameter
   [1215]);
epx1 = tof2mom(e1tof, parameter[1201], parameter[1200], 1.0);
epr1 = sqrt(epx1*epx1 + epy1*epy1 + epz1*epz1);
eE1  = (epr1*epr1) /2. * 27.212;
}

if (Elec2){// Measured electron momenta for 2nd hit
epz2 = elec2momx(e2x, e2y, e2tof, parameter[1205], parameter
   [1215]);
epy2 = elec2momy(e2x, e2y, e2tof, parameter[1205], parameter
   [1215]);
epx2 = tof2mom(e2tof, parameter[1201], parameter[1200], 1.0);
```

```
epr2 = sqrt(epx2*epx2 + epy2*epy2 + epz2*epz2);
eE2  = (epr2*epr2) /2. * 27.212;
}

if (Elec3){// Measured electron momenta for 3rd hit
epz3 = elec2momx(e3x, e3y, e3tof, parameter[1205], parameter
   [1215]);
epy3 = elec2momy(e3x, e3y, e3tof, parameter[1205], parameter
   [1215]);
epx3 = tof2mom(e3tof, parameter[1201], parameter[1200], 1.0);
epr3 = sqrt(epx3*epx3 + epy3*epy3+ epz3*epz3);
eE3  = (epr3*epr3) /2. * 27.212;
}

// Recoil Momentum Neon 1+
if (Neon1) {// Recoil Momentum Neon 1+
r1pz = r1x * parameter[1310] * parameter[1100]/r1tof + parameter
   [1315];
r1py = r1y * parameter[1311] * parameter[1100]/r1tof + parameter
   [1316];
r1px = (parameter[1318]*parameter[1200]/parameter[1206])*(r1tof-
   parameter[1100]); //charge state, E-field, converstion factor,
    center of tof dist.
r1pr = sqrt(r1px*r1px + r1py*r1py + r1pz*r1pz);
r1E = (r1pr*r1pr)/(2.0*20.0*1836.0) * 27.212;
}
```

```
// Recoil Momentum Neon 2+
if (Neon2) {// Recoil Momentum Neon 2+
r2pz = r1x * parameter[1320] * parameter[1105]/r1tof + parameter
   [1325];
r2py = r1y * parameter[1321] * parameter[1105]/r1tof + parameter
   [1326];
r2px = (parameter[1328]*parameter[1200]/parameter[1206])*(r1tof-
   parameter[1105]); //charge state, E-field, converstion factor,
    center of tof dist.
r2pr = sqrt(r2px*r2px + r2py*r2py + r2pz*r2pz);
r2E = (r2pr*r2pr)/(2.0*20.0*1836.0) * 27.212;
}

// Recoil Momentum Neon 3+
if (Neon3) {// Recoil Momentum Neon 3+
r3pz = r1x * parameter[1330] * parameter[1110]/r1tof + parameter
   [1335];
r3py = r1y * parameter[1331] * parameter[1110]/r1tof + parameter
   [1336];
r3px = (parameter[1338]*parameter[1200]/parameter[1206])*(r1tof-
   parameter[1110]); //charge state, E-field, converstion factor,
    center of tof dist.
r3pr = sqrt(r3px*r3px + r3py*r3py + r3pz*r3pz);
r3E = (r3pr*r3pr)/(2.0*20.0*1836.0) * 27.212;
}

// Recoil Momentum Neon 4+
```

```
if (Neon4) {// Recoil Momentum Neon 4+
r4pz = r1x * parameter[1340] * parameter[1115]/r1tof + parameter
   [1345];
r4py = r1y * parameter[1341] * parameter[1115]/r1tof + parameter
   [1346];
r4px = (parameter[1348]*parameter[1200]/parameter[1206])*(r1tof-
   parameter[1115]); //charge state, E-field, converstion factor,
    center of tof dist.
r4pr = sqrt(r4px*r4px + r4py*r4py + r4pz*r4pz);
r4E = (r4pr*r4pr)/(2.0*20.0*1836.0) * 27.212;
}

////////////////////////////////////////////////////////////////////////////

/////
          CaLCuLaTeD eLeCTRoN MoMeNTuM SeCTioN

             /////
////////////////////////////////////////////////////////////////////////////


//*************************
// oNe eLeCTRon CalCuLaTioNS
//*************************

// Ne1+ Recapture/Direct Ionization Channel
```

```
if (Neon1) {//The recoil detector has better resolution than fast
    electrons
kpx1 = -(r1px);
kpy1 = -(r1py);
kpz1 = -(r1pz);
kpr1 = sqrt(kpx1*kpx1 + kpy1*kpy1 + kpz1*kpz1);
kE1 = (kpr1*kpr1) / 2. * 27.212;
}

// Ne1+ Radiative Decay Photons
if (Neon1 && Elec1) {//calculated Photon
ppx1 = -(r1px+epx1);
ppy1 = -(r1py+epy1);
ppz1 = -(r1pz+epz1);
ppr1 = sqrt(ppx1*ppx1 + ppy1*ppy1 + ppz1*ppz1);
pE1 = ppr1 /2.7e-4;
}

// Ne2+ Calculated Auger Electron
if (Neon2 && Elec1) {//1st Hit Electron
kpx1 = -(epx1 + r2px);
kpy1 = -(epy1 + r2py);
kpz1 = -(epz1 + r2pz);
kpr1 = sqrt(kpx1*kpx1 + kpy1*kpy1 + kpz1*kpz1);
kE1 = (kpr1*kpr1) / 2. * 27.212;
}
```

```
// Ne2+ Calculated Auger Electron
if (Neon2 && Elec2) {//2nd Hit Electron
kpx2 = -(epx2 + r2px);
kpy2 = -(epy2 + r2py);
kpz2 = -(epz2 + r2pz);
kpr2 = sqrt(kpx2*kpx2 + kpy2*kpy2 + kpz2*kpz2);
kE2 = (kpr2*kpr2) / 2. * 27.212;
}

// Ne2+ Calculated Auger Electron - (negligible contribution)
if (Neon2 && Elec3) {//3rd Hit Electron
kpx3 = -(epx3 + r2px);
kpy3 = -(epy3 + r2py);
kpz3 = -(epz3 + r2pz);
kpr3 = sqrt(kpx3*kpx3 + kpy3*kpy3 + kpz3*kpz3);
kE3 = (kpr3*kpr3) / 2. * 27.212;
}

// Ne3+ Calculated Auger Sum
if (Neon3 && Elec1) {// 1st hit is assumed to be a photoelectron.
kpx1 = -(epx1 + r3px);
kpy1 = -(epy1 + r3py);
kpz1 = -(epz1 + r3pz);
kpr1 = sqrt(kpx1*kpx1 + kpy1*kpy1 + kpz1*kpz1);
kE1 = (kpr1*kpr1) / 2. * 27.212;
}
```

```
// Ne3+ Calculated Auger Sum
if (Neon3 && Elec2) {// 2nd hit is assumed to be a photoelectron.
kpx2 = -(epx2 + r3px);
kpy2 = -(epy2 + r3py);
kpz2 = -(epz2 + r3pz);
kpr2 = sqrt(kpx2*kpx2 + kpy2*kpy2 + kpz2*kpz2);
kE2 = (kpr2*kpr2) / 2. * 27.212;
}

// Ne3+ Calculated Auger Electron
if (Neon3 && Elec3) {//3rd Hit Photo-Electron
kpx3 = -(epx3 + r3px);
kpy3 = -(epy3 + r3py);
kpz3 = -(epz3 + r3pz);
kpr3 = sqrt(kpx3*kpx3 + kpy3*kpy3 + kpz3*kpz3);
kE3 = (kpr3*kpr3) / 2. * 27.212;
}

// Ne4+ Calculated Auger Sum
if (Neon4 && Elec1) {// 1st hit is assumed to be a photoelectron.
kpx1 = -(epx1 + r3px);
kpy1 = -(epy1 + r3py);
kpz1 = -(epz1 + r3pz);
kpr1 = sqrt(kpx1*kpx1 + kpy1*kpy1 + kpz1*kpz1);
kE1 = (kpr1*kpr1) / 2. * 27.212;
}
```

```
// Ne4+ Calculated Auger Sum
if (Neon4 && Elec2) {// 1st hit is assumed to be a photoelectron.
kpx2 = -(epx2 + r3px);
kpy2 = -(epy2 + r3py);
kpz2 = -(epz2 + r3pz);
kpr2 = sqrt(kpx2*kpx2 + kpy2*kpy2 + kpz2*kpz2);
kE2 = (kpr2*kpr2) / 2. * 27.212;
}

//**************************
// TWo eLeCTRon CalCuLaTioNS
//**************************

// Ne3+ Calculated Auger
if (Neon3 && Elec1 && Elec2) {//1st hit = photoelectron, 2nd hit
   = slow Auger
kpx12 = -(epx1 + epx2 + r3px);
kpy12 = -(epy1 + epy2 + r3py);
kpz12 = -(epz1 + epz2 + r3pz);
kpr12 = sqrt(kpx12*kpx12 + kpy12*kpy12 + kpz12*kpz12);
kE12 = (kpr12*kpr12) / 2. * 27.212;
}

// Using Neon3 and 2nd hit electron
if (Neon3 && Elec2 && Elec3) {//2nd hit = photoelectron, 3rd hit
   = slow Auger
kpx23 = -(epx2 + epx3 + r3px);
```

```
kpy23 = –(epy2 + epy3 + r3py);
kpz23 = –(epz2 + epz3 + r3pz);
kpr23 = sqrt(kpx23*kpx23 + kpy23*kpy23 + kpz23*kpz23);
kE23 = (kpr23*kpr23) / 2. * 27.212;
}

// Using Neon3 and 2nd hit electron
if (Neon3 && Elec1 && Elec3) {//3rd hit = photoelectron, 1st hit
   = Auger
kpx13 = –(epx1 + epx3 + r3px);
kpy13 = –(epy1 + epy3 + r3py);
kpz13 = –(epz1 + epz3 + r3pz);
kpr13 = sqrt(kpx13*kpx13 + kpy13*kpy13 + kpz13*kpz13);
kE13 = (kpr13*kpr13) / 2. * 27.212;
}

//****************************
// THRee eLeCTRon CalCuLaTioNS
//****************************

// Ne4+ Calculated Auger
if (Neon4 && Elec1 && Elec2 & Elec3) {
kpx123 = –(epx1 + epx2 + epx3 + r4px);
kpy123 = –(epy1 + epy2 + epy3 + r4py);
kpz123 = –(epz1 + epz2 + epz3 + r4pz);
kpr123 = sqrt(kpx123*kpx123 + kpy123*kpy123 + kpz123*kpz123);
kE123 = (kpr123*kpr123) / 2. * 27.212;
```

```
}

//**************
//CoNiCaL GaTeS
//**************
if (epx1/epr1>0.707) Cone1=true; //These gates restrict a single
   hit to a fixed solid angle collection
if (epx2/epr2>0.707) Cone2=true;
if (epx3/epr3>0.707) Cone3=true;

////////////////////////////////////////////////////////////////////////////////

/////
            MoMeNTuM SuM SeCTioN

                                  /////
////////////////////////////////////////////////////////////////////////////////


// Sum Neon 1+
if (Neon1 && Elec1) {
spx = (r1px + epx1);
spy = (r1py + epy1);
spz = (r1pz + epz1);
spr = (spz*spz + spy*spy + spx*spx);
```

```
Hist->fill2(127,"01_spx_spy_Neon1",spx,spy,1.,"Electron momentum
    spx spy Neon1",400,-10.,10.,"spx [au]",400,-10.,10.,"spy [au
    ]","Psum1");
Hist->fill2(128,"03_spz_spx_Neon1",spz,spx,1.,"Electron momentum
    spz spx Neon1",400,-10.,10.,"spz [au]",400,-10.,10.,"spx [au
    ]","Psum1");
Hist->fill2(129,"05_spz_spy_Neon1",spz,spy,1.,"Electron momentum
    spz spy Neon1",400,-10.,10.,"spz [au]",400,-10.,10.,"spy [au
    ]","Psum1");

if (spr<1.25) Psum1=true;

if (Psum1){
Hist->fill2(130,"02_spx_spy_Neon1",spx,spy,1.,"Electron momentum
    spx spy Neon1",400,-10.,10.,"spx [au]",400,-10.,10.,"spy [au
    ]","Psum1");
Hist->fill2(131,"04_spz_spx_Neon1",spz,spx,1.,"Electron momentum
    spz spx Neon1",400,-10.,10.,"spz [au]",400,-10.,10.,"spx [au
    ]","Psum1");
Hist->fill2(132,"06_spz_spy_Neon1",spz,spy,1.,"Electron momentum
    spz spy Neon1",400,-10.,10.,"spz [au]",400,-10.,10.,"spy [au
    ]","Psum1");
}
}

// Sum Neon 2+
if (Neon2 && Elec1 && Elec2) {
```

```
spx = (r2px + epx1 + epx2);
spy = (r2py + epy1 + epy2);
spz = (r2pz + epz1 + epz2);
spr = (spz*spz + spy*spy + spx*spx);

Hist->fill2(227,"01_spx_spy_Neon2",spx,spy,1.,"Electron momentum
    spx spy Neon2",400,-10.,10.,"spx [au]",400,-10.,10.,"spy [au
    ]","Psum2");
Hist->fill2(228,"03_spz_spx_Neon2",spz,spx,1.,"Electron momentum
    spz spx Neon2",400,-10.,10.,"spz [au]",400,-10.,10.,"spx [au
    ]","Psum2");
Hist->fill2(229,"05_spz_spy_Neon2",spz,spy,1.,"Electron momentum
    spz spy Neon2",400,-10.,10.,"spz [au]",400,-10.,10.,"spy [au
    ]","Psum2");

if (spr<3.0) Psum2=true;

if (Psum2){
Hist->fill2(230,"02_spx_spy_Psum2_Neon2",spx,spy,1.,"Electron
    momentum spx spy Neon2",400,-10.,10.,"spx [au]",400,-10.,10.,"
    spy [au]","Psum2");
Hist->fill2(231,"04_spz_spx_Psum2_Neon2",spz,spx,1.,"Electron
    momentum spz spx Neon2",400,-10.,10.,"spz [au]",400,-10.,10.,"
    spx [au]","Psum2");
Hist->fill2(232,"06_spz_spy_Psum2_Neon2",spz,spy,1.,"Electron
    momentum spz spy Neon2",400,-10.,10.,"spz [au]",400,-10.,10.,"
    spy [au]","Psum2");
```

```
}
}

// Sum Neon 3+
if (Neon3 && Elec1 && Elec2 && Elec3) {
spx = (r3px + epx1 + epx2 + epx3);
spy = (r3py + epy1 + epy2 + epy3);
spz = (r3pz + epz1 + epz2 + epz3);
spr = (spz*spz + spy*spy + spx*spx);

Hist->fill2(327,"01_spx_spy_Psum3_Neon3",spx,spy,1.,"Electron
   momentum spx spy Neon3",400,-10.,10.,"spx [au]",400,-10.,10.,"
   spy [au]","Psum3");
Hist->fill2(328,"03_spz_spx_Psum3_Neon3",spz,spx,1.,"Electron
   momentum spz spx Neon3",400,-10.,10.,"spz [au]",400,-10.,10.,"
   spx [au]","Psum3");
Hist->fill2(329,"05_spz_spy_Psum3_Neon3",spz,spy,1.,"Electron
   momentum spz spy Neon3",400,-10.,10.,"spz [au]",400,-10.,10.,"
   spy [au]","Psum3");

if (spr <3.0) Psum3=true;

if (Psum3){
Hist->fill2(330,"02_spx_spy_Psum3_Neon3",spx,spy,1.,"Electron
   momentum spx spy Neon3",400,-10.,10.,"spx [au]",400,-10.,10.,"
   spy [au]","Psum3");
```

```
Hist->fill2(331,"04_spz_spx_Psum3_Neon3",spz,spx,1.,"Electron
    momentum spz spx Neon3",400,-10.,10.,"spz [au]",400,-10.,10.,"
    spx [au]","Psum3");
Hist->fill2(332,"06_spz_spy_Psum3_Neon3",spz,spy,1.,"Electron
    momentum spz spy Neon3",400,-10.,10.,"spz [au]",400,-10.,10.,"
    spy [au]","Psum3");
}
}

////////////////////////////////////////////////////////////////////////////

/////
            aNGuLaR CoRReLaTioN DeFiNiTioN SeCTioN

                /////
////////////////////////////////////////////////////////////////////////////

double par1=-123456., par1r=-123456., par1a=-123456., par1b
    =-123456., par1c=-123456.,par2=-123456., par3=-12345., par3a
    =-123456., par3b=-123456., par3c=-123456., par4=-123456.,
    par4a=-123456., par5=-123456., par6=-123456.;
double perp1=-123456., perp1r=-123456., perp1a=-123456., perp1b
    =-123456., perp1c=-123456.,perp2=-123456., perp3=-12345.,
    perp3a=-123456., perp3b=-123456., perp3c=-123456., perp4
    =-123456., perp4a=-123456., perp5=-123456., perp6=-123456.;
```

```
double sin_inv1=-2., sin_inv1r=-2., sin_inv1a=-2., sin_inv1b=-2.,
    sin_inv1c=-2., sin_inv2=-2., sin_inv3=-2., sin_inv3a=-2.,
   sin_inv3b=-2., sin_inv3c=-2., sin_inv4=-2., sin_inv4a=-2.,
   sin_inv5=-2., sin_inv6=-2.;

//Used in Ne1+ Radiative Decay Analysis
par1r=(ppx1*epx1 + ppy1*epy1 + ppz1*epz1)/ppr1;
perp1r=sqrt((ppy1*epz1-ppz1*epy1)*(ppy1*epz1-ppz1*epy1) + (ppz1*
   epx1-ppx1*epz1)*(ppz1*epx1-ppx1*epz1) + (ppx1*epy1-ppy1*epx1)
   *(ppx1*epy1-ppy1*epx1))/ppr1;
sin_inv1r=epr1/perp1r;

//Used in Ne2+ "C-Plot" (1st Hit=Photo-Electron)
par1=(kpx1*epx1 + kpy1*epy1 + kpz1*epz1)/kpr1;
perp1=sqrt((kpy1*epz1-kpz1*epy1)*(kpy1*epz1-kpz1*epy1) + (kpz1*
   epx1-kpx1*epz1)*(kpz1*epx1-kpx1*epz1) + (kpx1*epy1-kpy1*epx1)
   *(kpx1*epy1-kpy1*epx1))/kpr1;
sin_inv1=epr1/perp1;

//Used in Ne2+ PSUM analysis (both electrons are measured) & Used
    in Ne3+ (measured Auger) analyses
par1a=(epx2*epx1 + epy2*epy1 + epz2*epz1)/epr1;
perp1a=sqrt((epy1*epz2-epz1*epy2)*(epy1*epz2-epz1*epy2) + (epz1*
   epx2-epx1*epz2)*(epz1*epx2-epx1*epz2) + (epx1*epy2-epy1*epx2)
   *(epx1*epy2-epy1*epx2))/epr1;
sin_inv1a=epr2/perp1a;
```

```
//Used in Ne2+ PSUM analysis (both electrons are measured) & Used
    in Ne3+ (measured Auger) analyses
par1b=(epx3*epx2 + epy3*epy2 + epz3*epz2)/epr2;
perp1b=sqrt((epy2*epz3-epz2*epy3)*(epy2*epz3-epz2*epy3) + (epz2*
   epx3-epx2*epz3)*(epz2*epx3-epx2*epz3) + (epx2*epy3-epy2*epx3)
   *(epx2*epy3-epy2*epx3))/epr2;
sin_inv1b=epr3/perp1b;

//Used in Ne2+ PSUM analysis (both electrons are measured) & Used
    in Ne3+ (measured Auger) analyses
par1c=(epx3*epx1 + epy3*epy1 + epz3*epz1)/epr1;
perp1c=sqrt((epy1*epz3-epz1*epy3)*(epy1*epz3-epz1*epy3) + (epz1*
   epx3-epx1*epz3)*(epz1*epx3-epx1*epz3) + (epx1*epy3-epy1*epx3)
   *(epx1*epy3-epy1*epx3))/epr1;
sin_inv1c=epr3/perp1c;

//Used in Ne2+ "C-Plot" (2nd Hit=Photo-Electron) & Used in Ne3+
   kSum Analysis
par2=(kpx2*epx2 + kpy2*epy2 + kpz2*epz2)/kpr2;
perp2=sqrt((kpy2*epz2-kpz2*epy2)*(kpy2*epz2-kpz2*epy2) + (kpz2*
   epx2-kpx2*epz2)*(kpz2*epx2-kpx2*epz2) + (kpx2*epy2-kpy2*epx2)
   *(kpx2*epy2-kpy2*epx2))/kpr2;
sin_inv2=epr2/perp2;

//Used in Ne2+ "C-Plot" (3rd Hit=Photo-Electron) & Used in Ne3+
   kSum Analysis - (negligible contribution)
par3=(epx3*kpx3 + epy3*kpy3 + epz3*kpz3)/kpr3;
```

```
perp3=sqrt((kpy3*epz3-kpz3*epy3)*(kpy3*epz3-kpz3*epy3) + (kpz3*
    epx3-kpx3*epz3)*(kpz3*epx3-kpx3*epz3) + (kpx3*epy3-kpy3*epx3)
    *(kpx3*epy3-kpy3*epx3))/kpr3;
sin_inv3=epr3/perp3;

//Used in Ne3+ Auger-Auger analysis
par3a=(kpx12*epx1 + kpy12*epy1 + kpz12*epz1)/kpr12; //Assumes
    ke12 is fast
perp3a=sqrt((kpy12*epz1-kpz12*epy1)*(kpy12*epz1-kpz12*epy1) + (
    kpz12*epx1-kpx12*epz1)*(kpz12*epx1-kpx12*epz1) + (kpx12*epy1-
    kpy12*epx1)*(kpx12*epy1-kpy12*epx1))/kpr12;
sin_inv3a=epr1/perp3a;

//Used in Ne3+ Auger-Auger analysis
par3b=(kpx12*epx1 + kpy12*epy1 + kpz12*epz1)/epr1; //Assumes e1
    is fast
perp3b=sqrt((kpy12*epz1-kpz12*epy1)*(kpy12*epz1-kpz12*epy1) + (
    kpz12*epx1-kpx12*epz1)*(kpz12*epx1-kpx12*epz1) + (kpx12*epy1-
    kpy12*epx1)*(kpx12*epy1-kpy12*epx1))/epr1;
sin_inv3b=kpr12/perp3b;

//Used in Ne3+ Auger-Auger analysis
par3c=(kpx13*epx1 + kpy13*epy1 + kpz13*epz1)/epr1; //Assumes e1
    is fast
perp3c=sqrt((kpy13*epz1-kpz13*epy1)*(kpy13*epz1-kpz13*epy1) + (
    kpz13*epx1-kpx13*epz1)*(kpz13*epx1-kpx13*epz1) + (kpx13*epy1-
    kpy13*epx1)*(kpx13*epy1-kpy13*epx1))/epr1;
```

```
sin_inv3c=kpr13/perp3c;

//Used in Ne3+ Auger-Photo Analysis
par4=(kpx12*epx2 + kpy12*epy2 + kpz12*epz2)/kpr12; //Assumes k12
   is fast
perp4=sqrt((kpy12*epz2-kpz12*epy2)*(kpy12*epz2-kpz12*epy2) + (
   kpz12*epx2-kpx12*epz2)*(kpz12*epx2-kpx12*epz2) + (kpx12*epy2-
   kpy12*epx2)*(kpx12*epy2-kpy12*epx2))/kpr12;
sin_inv4=epr2/perp4;

//Used in Ne3+ Auger-Photo Analysis
par4a=(kpx13*epx3 + kpy13*epy3 + kpz13*epz3)/kpr13; //Assumes k12
    is fast
perp4a=sqrt((kpy13*epz3-kpz13*epy3)*(kpy13*epz3-kpz13*epy3) + (
   kpz13*epx3-kpx13*epz3)*(kpz13*epx3-kpx13*epz3) + (kpx13*epy3-
   kpy13*epx3)*(kpx13*epy3-kpy13*epx3))/kpr13;
sin_inv4a=epr3/perp4a;

//Used in Ne3+ Correlation Analysis
par5=(kpx23*epx2 + kpy23*epy2 + kpz23*epz2)/epz2;
perp5=sqrt((kpy23*epz2-kpz23*epy2)*(kpy23*epz2-kpz23*epy2) + (
   kpz23*epx2-kpx23*epz2)*(kpz23*epx2-kpx23*epz2) + (kpx23*epy2-
   kpy23*epx2)*(kpx23*epy2-kpy23*epx2))/epz2;
sin_inv5=kpr23/perp5;

//Used in Ne3+ and Ne4+ Auger-Photo Analysis
par6=(kpx23*epx3 + kpy23*epy3 + kpz23*epz3)/kpr23;
```

```
perp6=sqrt((kpy23*epz3-kpz23*epy3)*(kpy23*epz3-kpz23*epy3) + (
   kpz23*epx3-kpx23*epz3)*(kpz23*epx3-kpx23*epz3) + (kpx23*epy3-
   kpy23*epx3)*(kpx23*epy3-kpy23*epx3))/kpr23;
sin_inv6=epr3/perp6;

////////////////////////////////////////////////////////////////////////////

/////
```

ADDITIONAL DECLARATIONS

```
/////
////////////////////////////////////////////////////////////////////////////

double g1=10.0, g2=110., g3=280., g4=380.;
int bin1=25, bin2=25, bin3=25;

//double g1=7.5, g2=175., g3=290., g4=380.;
//int bin1=30, bin2=50, bin3=30;

double cosAx1=1234., funcAx1=-12345., cosAx2=1234., funcAx2
   =-12345.;
double cosAy1=1234., funcAy1=-12345., cosAy2=1234., funcAy2
   =-12345.;
double cosAz1=1234., funcAz1=-12345., cosAz2=1234., funcAz2
   =-12345.;
cosAx1=kpx1/kpr1;
cosAx2=kpx2/kpr2;
```

```
cosAy1=kpy1/kpr1;
cosAy2=kpy2/kpr2;
cosAz1=kpz1/kpr1;
cosAz2=kpz2/kpr2;

// Neon 1+
if (Neon1){
if (Elec1) Hist->fill1(111,"01_etof_Neon1",e1tof,1.,"Electron TOF
    Ne^{+}",1200,-10.,110.,"TOF [ns]","Neon1_raw");
if (Elec2) Hist->fill1(111,"01_etof_Neon1",e2tof,1.,"Electron TOF
    Ne^{+}",1200,-10.,110.,"TOF [ns]","Neon1_raw");
if (Elec3) Hist->fill1(113,"03_e3tof_Elec3_Neon1",e3tof,1.,"
   Electron TOF Neon 1+ (3rd eHit)",2000,0.,100.,"TOF [ns]","
   Neon1_raw");

if (Elec1) Hist->fill2(114,"04_rxy_Elec1_Neon1",r1x,r1y,1.,"
   Recoil Position Neon 1+ (1st eHit)",400,-50.,50.,"x-position [
   mm]",400,-50.,50.,"y-position [mm]","Neon1_raw");
if (Elec2) Hist->fill2(115,"05_rxy_Elec2_Neon1",r1x,r1y,1.,"
   Recoil Position Neon 1+ (2nd eHit)",400,-50.,50.,"x-position [
   mm]",400,-50.,50.,"y-position [mm]","Neon1_raw");
if (Elec3) Hist->fill2(116,"06_rxy_Elec3_Neon1",r1x,r1y,1.,"
   Recoil Position Neon 1+ (3rd eHit)",400,-50.,50.,"x-position [
   mm]",400,-50.,50.,"y-position [mm]","Neon1_raw");

// 2D TOF Histograms
```

```
if (Elec1 && Elec2) Hist->fill2(117,"07
   _e1tof_e2tof_Elec1_Elec2_Neon1",e1tof,e2tof,1.,"Neon 1+ e1tof
   vs e2tof",400,0.,100.,"e1TOF [ns]",400,0.,100.,"e2TOF [ns]","
   Neon1_raw");
if (Elec1 && Elec3) Hist->fill2(118,"08
   _e1tof_e3tof_Elec1_Elec3_Neon1",e1tof,e3tof,1.,"Neon 1+ e1tof
   vs e3tof",400,0.,100.,"e1TOF [ns]",400,0.,100.,"e3TOF [ns]","
   Neon1_raw");
if (Elec2 && Elec3) Hist->fill2(119,"09
   _e2tof_e3tof_Elec2_Elec3_Neon1",e2tof,e3tof,1.,"Neon 1+ e2tof
   vs e3tof",400,0.,100.,"e2TOF [ns]",400,0.,100.,"e3TOF [ns]","
   Neon1_raw");

// Recoil Fish
if (Elec1) Hist->fill2(120,"10_r1x_r1tof_Elec1",r1tof,r1x,1.,"
   Recoil x-fish Neon 1+",400,43400.,44700.,"r1tof [ns
   ]",400,-50.,50.,"x-position [mm]","Neon1_raw");
if (Elec1) Hist->fill2(121,"11_r1y_r1tof_Elec1",r1tof,r1y,1.,"
   Recoil y-fish Neon 1+",400,43400.,44700.,"r1tof [ns
   ]",400,-50.,50.,"y-position [mm]","Neon1_raw");

// Filet O' Fish
if (fabs(e1y)<1.0) Hist->fill2(122,"12_elec_filet_o_xfish",e1tof,
   e1x,1.,"x-fish Hit ALL corrected offsets TOF, position and EB-
   drift",400,0.,100.,"TOF [ns]",400,-50.,50.,"x-pos [mm]","
   Neon1_raw");
```

```
if (fabs(e1x)<1.0) Hist->fill2(123,"13_elec_filet_o_yfish",e1tof,
   e1y,1.,"y-fish Hit ALL corrected offsets TOF, position and EB-
   drift",400,0.,100.,"TOF [ns]",400,-50.,50.,"y-pos [mm]","
   Neon1_raw");

// Corrected Elec Position
if (Elec1) Hist->fill2(124,"14_xy_Elec1_Neon1",e1x,e1y,1.,"xy
   Neon 1+ position (1st eHit)",200,-50.,50.,"x-pos [mm
   ]",200,-50.,50.,"y-pos [mm]","Neon1_raw");
if (Elec2) Hist->fill2(125,"15_xy_Elec2_Neon1",e2x,e2y,1.,"xy
   Neon 1+ position (2nd eHit)",200,-50.,50.,"x-pos [mm
   ]",200,-50.,50.,"y-pos [mm]","Neon1_raw");
if (Elec3) Hist->fill2(126,"16_xy_Elec3_Neon1",e3x,e3y,1.,"xy
   Neon 1+ position (3rd eHit)",200,-50.,50.,"x-pos [mm
   ]",200,-50.,50.,"y-pos [mm]","Neon1_raw");
}

// Neon 2+
if (Neon2){
if (Elec1) Hist->fill1(211,"01_e1tof_Elec1_Neon2",e1tof,1.,"
   Electron TOF Ne^{2+} (1^{st} eHit)",200,0.,100.,"TOF [ns]","
   Neon2_raw");
if (Elec2) Hist->fill1(212,"02_e2tof_Elec2_Neon2",e2tof,1.,"
   Electron TOF Ne^{2+} (2^{nd} eHit)",200,0.,100.,"TOF [ns]","
   Neon2_raw");
```

```
if (Elec3) Hist->fill1(213,"03_e3tof_Elec3_Neon2",e3tof,1.,"
    Electron TOF Ne^{2+} (3^{rd} eHit)",200,0.,100.,"TOF [ns]","
    Neon2_raw");

if (Elec1) Hist->fill2(214,"04_rxy_Elec1_Neon2",r1x,r1y,1.,"
    Recoil Position Neon 2+ (1st eHit)",400,-10.,25.,"x-position [
    mm]",400,-15.,25.,"y-position [mm]","Neon2_raw");
if (Elec2) Hist->fill2(215,"05_rxy_Elec2_Neon2",r1x,r1y,1.,"
    Recoil Position Neon 2+ (2nd eHit)",400,-10.,25.,"x-position [
    mm]",400,-15.,25.,"y-position [mm]","Neon2_raw");
if (Elec3) Hist->fill2(216,"06_rxy_Elec3_Neon2",r1x,r1y,1.,"
    Recoil Position Neon 2+ (3rd eHit)",400,-10.,25.,"x-position [
    mm]",400,-15.,25.,"y-position [mm]","Neon2_raw");

// 2D TOF Histograms
if (Elec1 && Elec2) Hist->fill2(217,"07
    _e1tof_e2tof_Elec1_Elec2_Neon2",e1tof,e2tof,1.,"Neon 2+ e1tof
    vs e2tof",400,0.,100.,"e1TOF [ns]",400,0.,100.,"e2TOF [ns]","
    Neon2_raw");
if (Elec1 && Elec3) Hist->fill2(218,"08
    _e1tof_e3tof_Elec1_Elec3_Neon2",e1tof,e3tof,1.,"Neon 2+ e1tof
    vs e3tof",400,0.,100.,"e1TOF [ns]",400,0.,100.,"e3TOF [ns]","
    Neon2_raw");
if (Elec2 && Elec3) Hist->fill2(219,"09
    _e2tof_e3tof_Elec2_Elec3_Neon2",e2tof,e3tof,1.,"Neon 2+ e2tof
    vs e3tof",400,0.,100.,"e2TOF [ns]",400,0.,100.,"e3TOF [ns]","
    Neon2_raw");
```

```
// Recoil Fish
if (Elec1) Hist->fill2(220,"10_r1x_r1tof_Elec1",r1tof,r1x,1.,"
   Recoil x-fish Neon 2+",400,30850.,31450.,"r1tof [ns
   ]",400,-50.,50.,"x-position [mm]","Neon2_raw");
if (Elec1) Hist->fill2(221,"11_r1y_r1tof_Elec1",r1tof,r1y,1.,"
   Recoil y-fish Neon 2+",400,30850.,31450.,"r1tof [ns
   ]",400,-50.,50.,"y-position [mm]","Neon2_raw");

// Filet O' Fish
if (fabs(e1y)<1.0) Hist->fill2(222,"12_elec_filet_o_xfish",e1tof,
   e1x,1.,"Fillet-of-X-Fish Ne^{2+} All-eHits",400,0.,100.,"TOF [
   ns]",400,-50.,50.,"x-pos [mm]","Neon2_raw");
if (fabs(e1x)<1.0) Hist->fill2(223,"13_elec_filet_o_yfish",e1tof,
   e1y,1.,"Fillet-of-Y-Fish Ne^{2+} All-eHits",400,0.,100.,"TOF [
   ns]",400,-50.,50.,"y-pos [mm]","Neon2_raw");

// Corrected Elec Position //if (e1tof>45.8 && e1tof<47.8)
if (Elec1) Hist->fill2(224,"14_xy_Elec1_Neon2",e1x,e1y,1.,"xy
   Neon 2+ corrected offsets, position and EB-drift (1st eHit)
   ",200,-50.,50.,"x-pos [mm]",200,-50.,50.,"y-pos [mm]","
   Neon2_raw");
if (Elec2) Hist->fill2(225,"15_xy_Elec2_Neon2",e2x,e2y,1.,"xy
   Neon 2+ corrected offsets, position and EB-drift (2nd eHit)
   ",200,-50.,50.,"x-pos [mm]",200,-50.,50.,"y-pos [mm]","
   Neon2_raw");
```

```
if (Elec3) Hist->fill2(226,"16_xy_Elec3_Neon2",e3x,e3y,1.,"xy
    Neon 2+ corrected offsets, position and EB-drift (3rd eHit)
    ",200,-50.,50.,"x-pos [mm]",200,-50.,50.,"y-pos [mm]","
    Neon2_raw");
}

// Neon 3+
if (Neon3){
if (Elec1) Hist->fill1(311,"01_e1tof_Elec1_Neon3",e1tof,1.,"
    Electron TOF Ne^{3+} (1^{st} eHit)",200,0.,100.,"TOF [ns]","
    Neon3_raw");
if (Elec2) Hist->fill1(312,"02_e2tof_Elec2_Neon3",e2tof,1.,"
    Electron TOF Ne^{3+} (2^{nd} eHit)",200,0.,100.,"TOF [ns]","
    Neon3_raw");
if (Elec3) Hist->fill1(313,"03_e3tof_Elec3_Neon3",e3tof,1.,"
    Electron TOF Ne^{3+} (3^{rd} eHit)",200,0.,100.,"TOF [ns]","
    Neon3_raw");

if (Elec1) Hist->fill2(314,"04_rxy_Elec1_Neon3",r1x,r1y,1.,"
    Recoil Position Ne^{3+} (1st eHit)",400,-10.,25.,"x-position [
    mm]",400,-15.,25.,"y-position [mm]","Neon3_raw");
if (Elec2) Hist->fill2(315,"05_rxy_Elec2_Neon3",r1x,r1y,1.,"
    Recoil Position Ne^{3+} (2nd eHit)",400,-10.,25.,"x-position [
    mm]",400,-15.,25.,"y-position [mm]","Neon3_raw");
if (Elec3) Hist->fill2(316,"06_rxy_Elec3_Neon3",r1x,r1y,1.,"
    Recoil Position Ne^{3+} (3rd eHit)",400,-10.,25.,"x-position [
    mm]",400,-15.,25.,"y-position [mm]","Neon3_raw");
```

```
// 2D TOF Histograms
if (Elec1 && Elec2 && eE2<2.5) Hist->fill2(317,"07
    _e1tof_e2tof_Elec2_Neon3",e1tof,e2tof,1.,"Electron Hit
    Correlation Ne^{3+}",400,0.,100.,"1^{st} eHit [ns
    ]",400,0.,100.,"2^{nd} eHit [ns]","Neon3_raw");
if (Elec1 && Elec3 && eE3<2.5) Hist->fill2(318,"08
    _e1tof_e3tof_Elec3_Neon3",e1tof,e3tof,1.,"Electron Hit
    Correlation Ne^{3+}",400,0.,100.,"1^{st} eHit [ns
    ]",400,0.,100.,"3^{rd} eHit [ns]","Neon3_raw");
if (Elec2 && Elec3 && eE3<2.5) Hist->fill2(319,"09
    _e2tof_e3tof_Elec3_Neon3",e2tof,e3tof,1.,"Electron Hit
    Correlation Ne^{3+}",400,0.,100.,"2^{nd} eHit [ns
    ]",400,0.,100.,"3^{rd} eHit [ns]","Neon3_raw");

// Recoil Fish
if (Elec1) Hist->fill2(320,"10_r1x_r1tof_Elec1",r1tof,r1x,1.,"
    Recoil x-fish Ne^{3+}",400,25105.,25655.,"r1tof [ns
    ]",400,-50.,50.,"x-position [mm]","Neon3_raw");
if (Elec1) Hist->fill2(321,"11_r1y_r1tof_Elec1",r1tof,r1y,1.,"
    Recoil y-fish Ne^{3+}",400,25105.,25655.,"r1tof [ns
    ]",400,-50.,50.,"y-position [mm]","Neon3_raw");

// Filet O' Fish
Hist->fill2(322,"12_elec_filet_o_xfish",e1tof,e1x,1.,"X-Fish Ne
    ^{3+} All eHits",200,0.,100.,"TOF [ns]",200,-40.,40.,"x-pos [
    mm]","Neon3_raw");
```

```
Hist->fill2(323,"13_elec_filet_o_yfish",e1tof,e1y,1.,"Y-Fish Ne
    ^{3+} All eHits",200,0.,100.,"TOF [ns]",200,-40.,40.,"y-pos [
    mm]","Neon3_raw");
Hist->fill2(322,"12_elec_filet_o_xfish",e2tof,e1x,1.,"X-Fish Ne
    ^{3+} All eHits",200,0.,100.,"TOF [ns]",200,-40.,40.,"x-pos [
    mm]","Neon3_raw");
Hist->fill2(323,"13_elec_filet_o_yfish",e2tof,e1y,1.,"Y-Fish Ne
    ^{3+} All eHits",200,0.,100.,"TOF [ns]",200,-40.,40.,"y-pos [
    mm]","Neon3_raw");
Hist->fill2(322,"12_elec_filet_o_xfish",e3tof,e1x,1.,"X-Fish Ne
    ^{3+} All eHits",200,0.,100.,"TOF [ns]",200,-40.,40.,"x-pos [
    mm]","Neon3_raw");
Hist->fill2(323,"13_elec_filet_o_yfish",e3tof,e1y,1.,"Y-Fish Ne
    ^{3+} All eHits",200,0.,100.,"TOF [ns]",200,-40.,40.,"y-pos [
    mm]","Neon3_raw");

// Corrected Elec Position
if (Elec1) Hist->fill2(324,"14_xy_Elec1_Neon3",e1x,e1y,1.,"
    Electron Position Ne^{3+} (1st eHit)",200,-50.,50.,"x-pos [mm
    ]",200,-50.,50.,"y-pos [mm]","Neon3_raw");
if (Elec2) Hist->fill2(325,"15_xy_Elec2_Neon3",e2x,e2y,1.,"
    Electron Position Ne^{3+} (2nd eHit)",200,-50.,50.,"x-pos [mm
    ]",200,-50.,50.,"y-pos [mm]","Neon3_raw");
if (Elec3) Hist->fill2(326,"16_xy_Elec3_Neon3",e3x,e3y,1.,"
    Electron Position Ne^{3+} (3rd eHit)",200,-50.,50.,"x-pos [mm
    ]",200,-50.,50.,"y-pos [mm]","Neon3_raw");
}
```

```
// Neon 4+
if (Neon4){
if (Elec1) Hist->fill1(411,"01_e1tof_Elec1_Neon4",e1tof,1.,"
   Electron TOF Neon 4+ (1st eHit)",100,0.,100.,"TOF [ns]","
   Neon4_raw");
if (Elec2) Hist->fill1(412,"02_e2tof_Elec2_Neon4",e2tof,1.,"
   Electron TOF Neon 4+ (2nd eHit)",100,0.,100.,"TOF [ns]","
   Neon4_raw");
if (Elec3) Hist->fill1(413,"03_e3tof_Elec3_Neon4",e3tof,1.,"
   Electron TOF Neon 4+ (3rd eHit)",100,0.,100.,"TOF [ns]","
   Neon4_raw");

if (Elec1) Hist->fill2(414,"04_rxy_Elec1_Neon4",r1x,r1y,1.,"
   Recoil Position Neon 4+ (1st eHit)",400,-10.,25.,"x-position [
   mm]",400,-15.,25.,"y-position [mm]","Neon4_raw");
if (Elec2) Hist->fill2(415,"05_rxy_Elec2_Neon4",r1x,r1y,1.,"
   Recoil Position Neon 4+ (2nd eHit)",400,-10.,25.,"x-position [
   mm]",400,-15.,25.,"y-position [mm]","Neon4_raw");
if (Elec3) Hist->fill2(416,"06_rxy_Elec3_Neon4",r1x,r1y,1.,"
   Recoil Position Neon 4+ (3rd eHit)",400,-10.,25.,"x-position [
   mm]",400,-15.,25.,"y-position [mm]","Neon4_raw");

// 2D TOF Histograms
if (Elec1 && Elec2) Hist->fill2(417,"07_e1tof_e2tof_Elec2_Neon4",
   e1tof,e2tof,1.,"Neon 4+ e1tof vs e2tof",400,0.,100.,"e1TOF [ns
   ]",400,0.,100.,"e2TOF [ns]","Neon4_raw");
```

```
if (Elec1 && Elec3) Hist->fill2(418,"08_e1tof_e3tof_Elec3_Neon4",
    e1tof,e3tof,1.,"Neon 4+ e1tof vs e3tof",400,0.,100.,"e1TOF [ns
    ]",400,0.,100.,"e3TOF [ns]","Neon4_raw");
if (Elec2 && Elec3) Hist->fill2(419,"09_e2tof_e3tof_Elec3_Neon4",
    e2tof,e3tof,1.,"Neon 4+ e2tof vs e3tof",400,0.,100.,"e2TOF [ns
    ]",400,0.,100.,"e3TOF [ns]","Neon4_raw");

// Recoil Fish
if (Elec1) Hist->fill2(420,"10_r1x_r1tof_Elec1",r1tof,r1x,1.,"
    Recoil x-fish Neon 4+",400,21800.,22300.,"r1tof [ns
    ]",400,-50.,50.,"x-position [mm]","Neon4_raw");
if (Elec1) Hist->fill2(421,"11_r1y_r1tof_Elec1",r1tof,r1y,1.,"
    Recoil y-fish Neon 4+",400,21800.,22300.,"r1tof [ns
    ]",400,-50.,50.,"y-position [mm]","Neon4_raw");

// Electron Fish
Hist->fill2(422,"12_elec_xfish",e1tof,e1x,1.,"x-fish Hit ALL
    corrected offsets TOF, position and EB-drift",400,0.,100.,"TOF
     [ns]",400,-50.,50.,"x-pos [mm]","Neon4_raw");
Hist->fill2(423,"13_elec_yfish",e1tof,e1y,1.,"y-fish Hit ALL
    corrected offsets TOF, position and EB-drift",400,0.,100.,"TOF
     [ns]",400,-50.,50.,"y-pos [mm]","Neon4_raw");

// Corrected Elec Position
```

```
if (Elec1) Hist->fill2(424,"14_xy_Elec1_Neon4",e1x,e1y,1.,"xy
   Neon 4+ corrected offsets, position and EB-drift (1st eHit)
   ",200,-50.,50.,"x-pos [mm]",200,-50.,50.,"y-pos [mm]","
   Neon4_raw");
if (Elec2) Hist->fill2(425,"15_xy_Elec2_Neon4",e2x,e2y,1.,"xy
   Neon 4+ corrected offsets, position and EB-drift (2nd eHit)
   ",200,-50.,50.,"x-pos [mm]",200,-50.,50.,"y-pos [mm]","
   Neon4_raw");
if (Elec3) Hist->fill2(426,"16_xy_Elec3_Neon4",e3x,e3y,1.,"xy
   Neon 4+ corrected offsets, position and EB-drift (3rd eHit)
   ",200,-50.,50.,"x-pos [mm]",200,-50.,50.,"y-pos [mm]","
   Neon4_raw");
}

//////////////////////////////////////////////////////////////////////////

/////
                              PSUM NeoN 1+

                                        /////
//////////////////////////////////////////////////////////////////////////

//PSuM PLoTS
if (Neon1 && Psum1){
Hist->fill2(1001,"01_epx1_epz1_Neon1_Psum1",epx1,epz1,1.,"
   Electron momentum px pz Psum",400,-10.,10.,"px [au
   ]",400,-10.,10.,"pz [au]","Psum1-Analysis");
```

```
Hist->fill2(1002,"02_r1px_r1pz_Neon1_Psum1",r1px,r1pz,1.,"Recoil
    momentum px pz Psum",400,-10.,10.,"px [au]",400,-10.,10.,"pz [
    au]","Psum1-Analysis");
Hist->fill2(1003,"03_kpx1_kpz1_Neon1",kpx1,kpz1,1.,"Calculated
    electron momentum kx1 kz1",300,-10.,10.,"kx [au
    ]",300,-10.,10.,"kz [au]","Psum1-Analysis");
if (kpx1>1.5 && kpx1<3.) Hist->fill2(1004,"04_kpz1_kpy1_Neon1",
    kpz1,kpy1,1.,"Calculated electron momentum kz1 ky1
    ",100,-10.,10.,"kz [au]",100,-10.,10.,"ky [au]","Psum1-
    Analysis");
Hist->fill1(1005,"04_E1_Neon1_Psum1",eE1,1.,"Electron Energy Hit
    1 Psum",150,0.,3.,"E [eV]","Psum1-Analysis");
}

//RaDiaTiVe aNaLYSiS
double funcPx=-12345.0, funcPy=-12345.0, funcPz=-12345.0;
double electron1=-12345., photon1=-12345., relative1=-12345.;

if (Neon1 && Psum1 && fabs(epy1/epr1)<0.4 && fabs(ppy1/ppr1)<0.4
   && fabs(r1py/r1pr)<0.4){//uSeS PSuM since photon momentum
    contribution is small
electron1=atan2(epz1,epx1);
photon1=atan2(ppz1,ppx1);
Hist->fill2(1101,"01_epx1_epy1_Neon1_Psum1",epx1,epy1,1.,"Photo-
    Electron Momentum Ne^{+}",200,-0.5,0.5,"Time-Axis [au
    ]",200,-0.5,0.5,"Jet-Axis [au]","Radiative");
```

```
Hist->fill2(1102,"02_epx1_epz1_Neon1_Psum1",epx1,epz1,1.,"
    Electron Momentum Ne^{+}",200,-10.,10.,"Time-Axis [au
    ]",200,-10.,10.,"Beam-Axis [au]","Radiative");
Hist->fill2(1103,"03_epz1_epy1_Neon1 Psum1",epz1,epy1,1.,"Photo-
    Electron Momentum Ne^{+}",200,-0.5,0.5,"Beam-Axis [au
    ]",200,-0.5,0.5,"Jet-Axis [au]","Radiative");

Hist->fill2(1104,"04_r1px_r1py_Neon1_Psum1",r1px,r1py,1.,"Recoil
    Momentum Ne^{+}",200,-0.5,0.5,"Time-Axis [au]",200,-0.5,0.5,"
    Jet-Axis [au]","Radiative");
Hist->fill2(1105,"05_r1px_r1pz_Neon1_Psum1",r1px,r1pz,1.,"Recoil
    Momentum Ne^{+}",200,-10.,10.,"Time-Axis [au]",200,-10.,10.,"
    Beam-Axis [au]","Radiative");
Hist->fill2(1106,"06_r1pz_r1py_Neon1_Psum1",r1pz,r1py,1.,"Recoil
    Momentum Ne^{+}",200,-0.5,0.5,"Beam-Axis [au]",200,-0.5,0.5,"
    Jet-Axis [au]","Radiative");

Hist->fill2(1107,"07_ppx1_ppy1_Neon1",ppx1,ppy1,1.,"Photon
    Momentum Ne^{+}",200,-1.5,1.5,"Time-Axis [au]",200,-1.5,1.5,"
    Jet-Axis [au]","Radiative");
Hist->fill2(1108,"08_ppx1_ppz1_Neon1",ppx1,ppz1,1.,"Photon
    Momentum Ne^{+}",200,-1.5,1.5,"Time-Axis [au]",200,-1.5,1.5,"
    Beam-Axis [au]","Radiative");
Hist->fill2(1109,"09_ppz1_ppy1_Neon1",ppz1,ppy1,1.,"Photon
    Momentum Ne^{+}",200,-1.5,1.5,"Beam-Axis [au]",200,-1.5,1.5,"
    Jet-Axis [au]","Radiative");
```

```
Hist->fill1(1110,"10_eE1_Neon1_Psum1",eE1,1.,"Electron Energy
    Psum",100,0.,1000,"E [eV]","Radiative");
Hist->fill1(1111,"11_rE1_Neon1_Psum1",r1E,1.,"Electron Energy
    Psum",300,0.,5.e-4,"E [eV]","Radiative");
Hist->fill1(1112,"12_pE1_Neon1_Psum1",pE1,1.,"Calculated Photon
    Energy",300,0.,2000.,"E [eV]","Radiative");

Hist->fill1(1113,"13_photon_Cosx-hit",ppx1/ppr1,1,"Auger Cosx
    ",50,-1.,1.,"Cos[x]","Radiative");
Hist->fill1(1114,"14_photon_Cosy-hit",ppy1/ppr1,1,"Auger Cosy
    ",50,-1.,1.,"Cos[y]","Radiative");
Hist->fill1(1115,"15_photon_Cosz-hit",ppz1/ppr1,1,"Auger Cosz
    ",50,-1.,1.,"Cos[z]","Radiative");

//aNGuLaR CoRReLaTioN
if(electron1<0.) electron1=electron1+(2.*pi); //normalizes the
    angular range, (0:2pi)
if(photon1<0.) photon1=photon1+(2.*pi);
relative1=(electron1-photon1); //relative angle (in x-y plane) of
     Ne2+ electrons
if(relative1>pi) relative1=relative1-(2.*pi);//recasts angular
    range, (-pi:pi)
if(relative1<-pi) relative1=relative1-(2.*pi);

Hist->fill1(1120,"18_Cos_Energy",relative1*180./pi,1,"CosNe2sum
    ",25,-180.,180.,"cos(#theta)","Radiative");//Calculated Auger
    and Photo-Electron
```

```
Hist->fill1(1120,"18_Cos_Energy",-relative1*180./pi,1,"CosNe2sum
    ",25,-180.,180.,"cos(#theta)","Radiative");// Calculated Auger
    and Photo-Electron

//Hist->fill2(1116,"16_par_perp",par1r,perp1r,sin_inv1r,"
    Radiative Correlation Neon 1+",400,-0.5,0.5,"Parallel Photo-
    Electron Momentum [au]",400,-0.5,0.5,"Perpendicular Photo-
    Electron Momentum [au]","Radiative");
//Hist->fill2(1116,"16_par_perp",par1r,-perp1r,sin_inv1r,"
    Radiative Correlation Neon 1+",400,-0.5,0.5,"Parallel Photo-
    Electron Momentum [au]",400,-0.5,0.5,"Perpendicular Photo-
    Electron Momentum [au]","Radiative");
//if(eE1<3.5 && eE1>0.0) Hist->fill2(1117,"17_Cos_Energy",par1r/
    epr1,eE1,1,"Cos_Energy",100,-1.,1.,"cos(theta)",350,0.0,3.5,"
    Electron Energy [eV]","Radiative");
//if(eE1<3.5 && eE1>0.0) Hist->fill1(1118,"Photon-prox",par1r/
    epr1,1,"Neon1 Theta",50,-1.,1.,"cos(theta)","Radiative");
//if(eE1<3.5 && eE1>0.0) Hist->fill1(1119,"Photo-electron",eE1
    ,1,"Electron Energy",150,0.,3.5,"E [eV]","Radiative");
}

////////////////////////////////////////////////////////////////////////////

/////
```

PSUM NeoN 2+

```
/////
```

```
//////////////////////////////////////////////////////////////////////////////

//PSum aNaLYSiS
if (Neon2 && Psum2 && eE2>0.0 && eE2<5.0 && fabs(epz2/epr2)<0.35)
   {//poor res. on 1st hit, use 2nd hit to calc 1st.
//Hist->fill2(2001,"01_epx1_epy1_Neon2_Psum2",epx1,epy1,1.,"
   Electron momentum epx epy Hit 1 Psum",400,-10.,10.,"epx [au
   ]",400,-10.,10.,"epy [au]","Psum2-Analysis");
//Hist->fill2(2002,"02_epx1_epz1_Neon2_Psum2",epx1,epz1,1.,"
   Electron momentum epx epz Hit 1 Psum",400,-10.,10.,"epx [au
   ]",400,-10.,10.,"epz [au]","Psum2-Analysis");
//Hist->fill2(2003,"03_epz1_epy1_Neon2_Psum2",epz1,epy1,1.,"
   Electron momentum epz epy Hit 1 Psum",400,-10.,10.,"epz [au
   ]",400,-10.,10.,"epy [au]","Psum2-Analysis");

Hist->fill2(2004,"04_epx2_epy2_Neon2_Psum2",epx2,epy2,1.,"
   Electron momentum epx epy Hit 2 Psum",400,-1.,1.,"epx [au
   ]",400,-1.,1.,"epy [au]","Psum2-Analysis");
Hist->fill2(2005,"05_epx2_epz2_Neon2_Psum2",epx2,epz2,1.,"
   Electron momentum epx epz Hit 2 Psum",400,-1.,1.,"epx [au
   ]",400,-1.,1.,"epz [au]","Psum2-Analysis");
Hist->fill2(2006,"06_epz2_epy2_Neon2_Psum2",epz2,epy2,1.,"
   Electron momentum epz epy Hit 2 Psum",400,-1.,1.,"epz [au
   ]",400,-1.,1.,"epy [au]","Psum2-Analysis");
```

```
Hist->fill2(2007,"07_r2px_r2py_Neon2_Psum2",r2px,r2py,1.,"Recoil
    momentum px py Psum",400,-10.,10.,"px [au]",400,-10.,10.,"py [
    au]","Psum2-Analysis");
Hist->fill2(2008,"08_r2px_r2pz_Neon2_Psum2",r2px,r2pz,1.,"Recoil
    momentum px pz Psum",400,-10.,10.,"px [au]",400,-10.,10.,"pz [
    au]","Psum2-Analysis");
Hist->fill2(2009,"09_r2pz_r2py_Neon2_Psum2",r2pz,r2py,1.,"Recoil
    momentum pz py Psum",400,-10.,10.,"pz [au]",400,-10.,10.,"py [
    au]","Psum2-Analysis");

//Hist->fill2(2010,"10_kpx1_kpy1_Neon2_Psum2",kpx1,kpy1,1.,"
    Calculated electron momentum kx1 ky1 Psum",400,-10.,10.,"kx [
    au]",400,-10.,10.,"ky [au]","Psum2-Analysis");
//Hist->fill2(2011,"11_kpx1_kpz1_Neon2_Psum2",kpx1,kpz1,1.,"
    Calculated electron momentum kx1 kz1 Psum",400,-10.,10.,"kx [
    au]",400,-10.,10.,"kz [au]","Psum2-Analysis");
//Hist->fill2(2012,"12_kpz1_kpy1_Neon2_Psum2",kpz1,kpy1,1.,"
    Calculated electron momentum kz1 ky1 Psum",400,-10.,10.,"kz [
    au]",400,-10.,10.,"ky [au]","Psum2-Analysis");

Hist->fill2(2013,"13_kpx2_kpy2_Neon2_Psum2",kpx2,kpy2,1.,"
    Calculated electron momentum kx2 ky2 Psum",400,-10.,10.,"kx [
    au]",400,-10.,10.,"ky [au]","Psum2-Analysis");
Hist->fill2(2014,"14_kpx2_kpz2_Neon2_Psum2",kpx2,kpz2,1.,"
    Calculated electron momentum kx2 kz2 Psum",400,-10.,10.,"kx [
    au]",400,-10.,10.,"kz [au]","Psum2-Analysis");
```

```
Hist->fill2(2015,"15_kpz2_kpy2_Neon2_Psum2",kpz2,kpy2,1.,"
    Calculated electron momentum kz2 ky2 Psum",400,-10.,10.,"kz [
    au]",400,-10.,10.,"ky [au]","Psum2-Analysis");

Hist->fill1(2016,"16_Photo-Electron-Energy_Neon2-Psum2",eE1,1.,"
    Photo Electron Energy Neon2-Psum",300,0.,3.5,"E [eV]","Psum2-
    Analysis");
Hist->fill1(2017,"17_E1_Neon2_Psum2-large",eE1,1.,"Electron
    Energy Hit 1 Psum",300,0.,1200.,"E [eV]","Psum2-Analysis");
Hist->fill1(2016,"16_Photo-Electron-Energy_Neon2-Psum2",eE2,1.,"
    Photo Electron Energy Neon2-Psum",300,0.,3.5,"E [eV]","Psum2-
    Analysis");
Hist->fill1(2019,"19_E2_Neon2_Psum2-large",eE2,1.,"Electron
    Energy Hit 2 Psum",300,0.,1200.,"E [eV]","Psum2-Analysis");
Hist->fill1(2021,"20_kE2_Neon2_Psum2-large",kE2,1.,"Calculated
    Electron Energy Hit 2 Psum",300,0.,1200.,"E [eV]","Psum2-
    Analysis");

Hist->fill2(2022,"21_par_perp-Psum",par1a,perp1a,sin_inv1a,"
    Momentum Correlation Neon 2+",400,-0.5,0.5,"Parallel Photo-
    Electron Momentum [au]",400,-0.5,0.5,"Perpendicular Photo-
    Electron Momentum [au]","Psum2-Analysis");
Hist->fill2(2022,"21_par_perp-Psum",par1a,-perp1a,sin_inv1a,"
    Momentum Correlation Neon 2+",400,-0.5,0.5,"Parallel Photo-
    Electron Momentum [au]",400,-0.5,0.5,"Perpendicular Photo-
    Electron Momentum [au]","Psum2-Analysis");
```

```
Hist->fill2(2023,"22_Cos_Energy-Psum",par1a/epr2,eE2,1,"
    Cos_Energy",100,-1.,1.,"cos(theta)",350,0.0,3.5,"Electron
    Energy [eV]","Psum2-Analysis");
if (eE2>1.0 && eE2<2.0) Hist->fill1(2024,"23_Cos-Prox",par1a/epr2
    ,1,"Projection of Cos_Energy",100,-1.,1.,"cos(theta)","Psum2-
    Analysis");

Hist->fill1(2025,"24_E2_Neon2_Psum2",eE2,1.,"Electron Energy Hit
    2 Psum",150,0.,3.,"E [eV]","Psum2-Analysis");

if (eE2>1.0 && eE2<2.0) Hist->fill1(2026,"Theta_Neon2",acos(par1a
    /epr2)*180./pi,sin_inv1a,"Neon2 Theta",40,-180.,180.,"cos(
    theta)","Psum2-Analysis");
if (eE2>1.0 && eE2<2.0) Hist->fill1(2026,"Theta_Neon2",-acos(
    par1a/epr2)*180./pi,sin_inv1a,"Neon2 Theta",40,-180.,180.,"cos
    (theta)","Psum2-Analysis");
}

//////////////////////////////////////////////////////////////////////////

/////

                    PSUM NeoN 3+

                              /////

//////////////////////////////////////////////////////////////////////////
```

```
if (Neon3 && Elec1 && Elec2 && Elec3 && Psum3){
//DeaD TiMe SHaDoW
double dr=-12345.0, dt=-12345.0; // Used to quantify the "dead-
    time shadow" of the MCP
dr=sqrt((e2x-e3x)*(e2x-e3x) + (e2y-e3y)*(e2y-e3y)); // Position
    and time difference between 2nd & 3rd ehits in Ne3+
dt=(e3tof-e2tof);

//Hist->fill2(3001,"01_epx1_epy1_Neon3_Psum3",epx1,epy1,1.,"
    Electron momentum epx epy Hit 1 Psum",400,-10.,10.,"epx [au
    ]",400,-10.,10.,"epy [au]","Psum3-Analysis");
//Hist->fill2(3002,"02_epx1_epz1_Neon3_Psum3",epx1,epz1,1.,"
    Electron momentum epx epz Hit 1 Psum",400,-10.,10.,"epx [au
    ]",400,-10.,10.,"epz [au]","Psum3-Analysis");
//Hist->fill2(3003,"03_epz1_epy1_Neon3_Psum3",epz1,epy1,1.,"
    Electron momentum epz epy Hit 1 Psum",400,-10.,10.,"epz [au
    ]",400,-10.,10.,"epy [au]","Psum3-Analysis");

//Hist->fill2(3004,"04_epx2_epy2_Neon3_Psum3",epx2,epy2,1.,"
    Electron momentum epx epy Hit 2 Psum",400,-6.,6.,"epx [au
    ]",400,-6.,6.,"epy [au]","Psum3-Analysis");
//Hist->fill2(3005,"05_epx2_epz2_Neon3_Psum3",epx2,epz2,1.,"
    Electron momentum epx epz Hit 2 Psum",400,-6.,6.,"epx [au
    ]",400,-6.,6.,"epz [au]","Psum3-Analysis");
//Hist->fill2(3006,"06_epz2_epy2_Neon3_Psum3",epz2,epy2,1.,"
    Electron momentum epz epy Hit 2 Psum",400,-6.,6.,"epz [au
    ]",400,-6.,6.,"epy [au]","Psum3-Analysis");
```

```
//Hist->fill2(3007,"07_epx3_epy3_Neon3_Psum3",epx3,epy3,1.,"
    Electron momentum epx epy Hit 3 Psum",400,-6.,6.,"epx [au
    ]",400,-6.,6.,"epy [au]","Psum3-Analysis");
//Hist->fill2(3008,"08_epx3_epz3_Neon3_Psum3",epx3,epz3,1.,"
    Electron momentum epx epz Hit 3 Psum",400,-6.,6.,"epx [au
    ]",400,-6.,6.,"epz [au]","Psum3-Analysis");
//Hist->fill2(3009,"09_epz3_epy3_Neon3_Psum3",epz3,epy3,1.,"
    Electron momentum epz epy Hit 3 Psum",400,-6.,6.,"epz [au
    ]",400,-6.,6.,"epy [au]","Psum3-Analysis");

Hist->fill2(3010,"10_r3px_r3py_Neon3_Psum3",r3px,r3py,1.,"Recoil
    momentum px py Psum",400,-10.,10.,"px [au]",400,-10.,10.,"py [
    au]","Psum3-Analysis");
Hist->fill2(3011,"11_r3px_r3pz_Neon3_Psum3",r3px,r3pz,1.,"Recoil
    momentum px pz Psum",400,-10.,10.,"px [au]",400,-10.,10.,"pz [
    au]","Psum3-Analysis");
Hist->fill2(3012,"12_r3pz_r3py_Neon3_Psum3",r3pz,r3py,1.,"Recoil
    momentum pz py Psum",400,-10.,10.,"pz [au]",400,-10.,10.,"py [
    au]","Psum3-Analysis");

//Hist->fill2(3013,"13_kpx23_kpy23_Neon3_Psum3",kpx23,kpy23,1.,"
    Calculated electron momentum kx23 ky23 Psum",400,-10.,10.,"kx
    [au]",400,-10.,10.,"ky [au]","Psum3-Analysis");
//Hist->fill2(3014,"14_kpx23_kpz23_Neon3_Psum3",kpx23,kpz23,1.,"
    Calculated electron momentum kx23 kz23 Psum",400,-10.,10.,"kx
    [au]",400,-10.,10.,"kz [au]","Psum3-Analysis");
```

```
//Hist->fill2(3015,"15_kpz23_kpy23_Neon3_Psum3",kpz23,kpy23,1.,"
    Calculated electron momentum kz23 ky23 Psum",400,-10.,10.,"kz
    [au]",400,-10.,10.,"ky [au]","Psum3-Analysis");

//Hist->fill1(3016,"16_E1_Neon3_Psum3-small",eE1,1.,"Electron
    Energy Hit 1 Psum",300,0.,3.5,"E [eV]","Psum3-Analysis");
Hist->fill1(3017,"17_E1_Neon3_Psum3-large",eE1,1.,"Electron
    Energy Hit 1 Psum",300,0.,1200.,"E [eV]","Psum3-Analysis");
Hist->fill1(3018,"18_E2_Neon3_Psum3-small",eE2,1.,"Electron
    Energy Hit 2 Psum",150,0.,3.,"E [eV]","Psum3-Analysis");
Hist->fill1(3019,"19_E2_Neon3_Psum3-large",eE2,1.,"Electron
    Energy Hit 2 Psum",300,0.,1200.,"E [eV]","Psum3-Analysis");
Hist->fill1(3020,"20_E3_Neon3_Psum3-small",eE3,1.,"Calculated
    Electron Energy Hit 3 Psum",150,0.,3.,"E [eV]","Psum3-Analysis
    ");
Hist->fill1(3021,"21_E3_Neon3_Psum3-large",eE3,1.,"Calculated
    Electron Energy Hit 3 Psum",300,0.,1200.,"E [eV]","Psum3-
    Analysis");
Hist->fill1(3022,"22_kE23_Neon3_Psum3-large",kE23,1.,"Calculated
    Electron Energy Psum",300,0.,1200.,"E [eV]","Psum3-Analysis");

Hist->fill1(3023,"23_r1tof_Psum3_Neon3",r1tof,1.,"Recoil TOF Neon
     3+ (3-ehit)",200,25000.,25750.,"TOF [ns]","Psum3-Analysis");
Hist->fill2(3024,"24_r1x_r1tof_Psum3_Neon3",r1tof,r1x,1.,"Recoil
    x-fish Neon 3+ (3-ehit)",400,25200,25750.,"r1tof [ns
    ]",200,-5.,20.,"x-position [mm]","Psum3-Analysis");
```

```
Hist->fill1(3025,"25_e1tof_Psum3_Neon3",e1tof,1.,"e1tof Neon 3+
   (3-ehit)",200,0.,120.,"e1tof [ns]","Psum3-Analysis");
Hist->fill1(3026,"26_e2tof_Psum3_Neon3",e2tof,1.,"e2tof Neon 3+
   (3-ehit)",200,0.,120.,"e2tof [ns]","Psum3-Analysis");
Hist->fill1(3027,"27_e3tof_Psum3_Neon3",e3tof,1.,"e3tof Neon 3+
   (3-ehit)",200,0.,120.,"e3tof [ns]","Psum3-Analysis");

Hist->fill2(3028,"28_e1tof_e2tof_Psum3_Neon3",e1tof,e2tof,1.,"
   e2tof vs e1tof Neon 3+ (3-ehit)",400,0.,120.,"e1tof [ns
   ]",400,0.,120.,"e2tof [ns]","Psum3-Analysis");
Hist->fill2(3029,"29_e2tof_e3tof_Psum3_Neon3",e2tof,e3tof,1.,"
   e3tof vs e2tof Neon 3+ (3-ehit)",200,0.,120.,"e2tof [ns
   ]",400,0.,120.,"e3tof [ns]","Psum3-Analysis");
Hist->fill2(3030,"30_e3tof_e1tof_Psum3_Neon3",e1tof,e3tof,1.,"
   e3tof vs e1tof Neon 3+ (3-ehit)",400,0.,120.,"e1tof [ns
   ]",400,0.,120.,"e3tof [ns]","Psum3-Analysis");
Hist->fill2(3031,"31_dr_dt_Psum3_Neon3",dr,dt,1.,"dr vs dt Neon
   3+ (3-ehit)",200,0.,80.,"dr [mm]",200,0.,100.,"dt [ns]","Psum3
   -Analysis");
}

//*************************************************************

// NE2+ ANGULAR CORRELATION ANALYSES
//*************************************************************

// STD. ANALYSIS
```

```
//aNGuLaR CoRReLaTioN
if (Neon2) {
if (Elec1 && eE1>0.5 && eE1<2.5 && kpr1>6.5 && kpr1<8.5){// "C"
    plot
Hist->fill2(2101,"01_par_perp",par1,perp1,sin_inv1,"Momentum
    Correlation Neon 2+",400,-0.5,0.5,"Parallel Photo-Electron
    Momentum [au]",400,-0.5,0.5,"Perpendicular Photo-Electron
    Momentum [au]","Momentum2");
Hist->fill2(2101,"01_par_perp",par1,-perp1,sin_inv1,"Momentum
    Correlation Neon 2+",400,-0.5,0.5,"Parallel Photo-Electron
    Momentum [au]",400,-0.5,0.5,"Perpendicular Photo-Electron
    Momentum [au]","Momentum2");
Hist->fill1(2102,"02_photoE",eE1,1.,"Electron Energy
    ",300,0.,3.5,"Energy [eV]","Momentum2");
if(fabs(epz1/epr1)<0.15) Hist->fill2(2103,"03_epx_epy_Neon2",epx1
    ,epy1,1,"Electron momentum epx epy",400,-0.5,0.5,"Time-Axis [
    au]",400,-0.5,0.5,"Jet-Axis [au]","Momentum2");
Hist->fill1(2104,"04_polar",acos(par1/epr1)*180./pi,sin_inv1,"
    Angular Correlation",20,-180.,180.,"Cos(#theta)","Momentum2");
Hist->fill1(2104,"04_polar",-acos(par1/epr1)*180./pi,sin_inv1,"
    Angular Correlation",20,-180.,180.,"Cos(#theta)","Momentum2");
}

if (Elec2 && epr1>6.5 && eE1>0.5 && eE1<2.5 && kpr1>6.5 && kpr1
    <8.5){//Adding in 2nd hit results and throwing out nonsense 1
    st hit events
```

```
Hist->fill2(2101,"01_par_perp",par2,perp2,sin_inv2,"Momentum
    Correlation Neon 2+",400,-0.5,0.5,"Parallel Photo-Electron
    Momentum [au]",400,-0.5,0.5,"Perpendicular Photo-Electron
    Momentum [au]","Momentum2");
Hist->fill2(2101,"01_par_perp",par2,-perp2,sin_inv2,"Momentum
    Correlation Neon 2+",400,-0.5,0.5,"Parallel Photo-Electron
    Momentum [au]",400,-0.5,0.5,"Perpendicular Photo-Electron
    Momentum [au]","Momentum2");
Hist->fill1(2102,"02_photoE",eE2,1.,"Electron Energy
    ",300,0.,3.5,"Energy [eV]","Momentum2");
if(fabs(epz2/epr2)<0.15) Hist->fill2(2103,"03_epx_epy_Neon2",epx2
    ,epy2,1,"Electron momentum epx epy",400,-0.5,0.5,"Time-Axis [
    au]",400,-0.5,0.5,"Jet-Axis [au]","Momentum2");
Hist->fill1(2104,"04_polar",acos(par2/epr2)*180./pi,sin_inv2,"
    Angular Correlation",20,-180.,180.,"Cos(#theta)","Momentum2");
Hist->fill1(2104,"04_polar",-acos(par2/epr2)*180./pi,sin_inv2,"
    Angular Correlation",20,-180.,180.,"Cos(#theta)","Momentum2");
}
}

// FLATLAND NE2+ (AUGMENTATION METHOD)
//In this section, only Ne2+ events that are confined to a plane
    will be considered. In order to properly consider this flat-
    land scenario, the ellipticity of the light
//must be addressed. The photo-electron distribution will be
    plotted as a function of angle. A fourier series function
    will be fit to this distribution to be used as a
```

```
//weighting function. weightp1(epx1/epr1,parameter[1700])
double phi=-12345.0;
double aug=-12345.0;
double rel2=-12345.0;

if (Neon2 && fabs(r2pz/r2pr)<0.15){
if (Elec1 && eE1>0.5 && eE1<2.5 && kpr1>6.5 && kpr1<8.5 && fabs(
    epz1/epr1)<0.15){
phi=atan2(epy1,epx1);
aug=atan2(kpy1,kpx1);

Hist->fill2(2201,"01_epx_epy_Neon2",epx1,epy1,weightp(phi,
    parameter[1700])*weightA(aug,parameter[1700]),"Photo-Electron
    Momentum Corrected",200,-0.5,0.5,"Time-Axis [au
    ]",200,-0.5,0.5,"Jet-Axis [au]","Flatland2");
Hist->fill2(2202,"02_epx_epz_Neon2",epx1,epz1,weightp(phi,
    parameter[1700])*weightA(aug,parameter[1700]),"Electron
    momentum epx epz",400,-1.,1.,"epx [au]",400,-1.,1.,"epz [au
    ]","Flatland2");
Hist->fill2(2203,"03_epz_epy_Neon2",epz1,epy1,weightp(phi,
    parameter[1700])*weightA(aug,parameter[1700]),"Electron
    momentum epz epy",400,-1.,1.,"epz [au]",400,-1.,1.,"epy [au
    ]","Flatland2");
```

```
Hist->fill2(2204,"04_r2px_r2py_Neon2",r2px,r2py,weightp(phi,
    parameter[1700])*weightA(aug,parameter[1700]),"Recoil momentum
     px py",400,-10.,10.,"px [au]",400,-10.,10.,"py [au]","
    Flatland2");
Hist->fill2(2205,"05_r2px_r2pz_Neon2",r2px,r2pz,weightp(phi,
    parameter[1700])*weightA(aug,parameter[1700]),"Recoil momentum
     px pz",400,-10.,10.,"px [au]",400,-10.,10.,"pz [au]","
    Flatland2");
Hist->fill2(2206,"06_r2pz_r2py_Neon2",r2pz,r2py,weightp(phi,
    parameter[1700])*weightA(aug,parameter[1700]),"Recoil momentum
     pz py",400,-10.,10.,"pz [au]",400,-10.,10.,"py [au]","
    Flatland2");

Hist->fill2(2207,"07_kpx_kpy_Neon2",kpx1,kpy1,1.,"Auger Electron
    Momentum",200,-10.,10.,"Time-Axis [au]",200,-10.,10.,"Jet-Axis
     [au]","Flatland2");
Hist->fill2(2208,"08_kpx_kpz_Neon2",kpx1,kpz1,weightp(phi,
    parameter[1700])*weightA(aug,parameter[1700]),"Calculated
    electron momentum kx kz",400,-10.,10.,"kx [au]",400,-10.,10.,"
    kz [au]","Flatland2");
Hist->fill2(2209,"09_kpz_kpy_Neon2",kpz1,kpy1,weightp(phi,
    parameter[1700])*weightA(aug,parameter[1700]),"Calculated
    electron momentum kz ky",400,-10.,10.,"kz [au]",400,-10.,10.,"
    ky [au]","Flatland2");

Hist->fill1(2210,"10_Photo_Ne2",phi,1,"Photo-Electron Angular
    Distribution",100,-pi,pi,"[deg]","Flatland2");
```

```
Hist->fill1(2211,"11_Photo_Ne2-corrected",phi*180./pi,weightp(phi
    ,parameter[1700])*weightA(aug,parameter[1700]),"Photo-Electron
     Angular Distribution Corrected",100,-180.,180.,"[deg]","
    Flatland2");
Hist->fill1(2212,"12_Auger_Ne2",aug*180./pi,1,"Auger Electron
    Angular Distribution",100,-180.,180.,"#theta_{TOF}","Flatland2
    ");
Hist->fill1(2213,"13_Auger_Ne2-corrected",aug*180/pi,weightp(phi,
    parameter[1700])*weightA(aug,parameter[1700]),"Auger Electron
    Angular Distribution Corrected",100,-180,180,"#theta_{TOF}","
    Flatland2");
Hist->fill1(2214,"14_Photo-Electron-Energy-Neon2",eE1,weightp(phi
    ,parameter[1700])*weightA(aug,parameter[1700]),"Photo-Electron
     Energy",350,0.5,2.5,"E [eV]","Flatland2");

if(phi<0.) phi=phi+(2.*pi); //normalizes the angular range, (0:2
    pi)
if(aug<0.) aug=aug+(2.*pi);

rel2=(phi-aug); //relative angle (in x-y plane) of Ne2+ electrons
if(rel2>pi) rel2=rel2-(2.*pi);//recasts angular range, (-pi:pi)
if(rel2<-pi) rel2=rel2+(2.*pi);

Hist->fill1(2215,"15_Cos_Energy",rel2*180./pi,weightp(phi,
    parameter[1700])*weightA(aug,parameter[1700]),"CosNe2sum
    ",25,-180.,180.,"cos(theta)","Flatland2");//Calculated Auger
    and Photo-Electron
```

```
}
if (Elec2 && eE2>0.5 && eE2<2.5 && kpr2>6.5 && kpr2<8.5 && fabs(
    epz2/epr2)<0.15){//This adds back in the events that
    correspond to 2nd hit photo-electrons
phi=atan2(epy2,epx2);
aug=atan2(kpy2,kpx2);

Hist->fill2(2201,"01_epx_epy_Neon2",epx2,epy2,weightp(phi,
    parameter[1700])*weightA(aug,parameter[1700]),"Photo-Electron
    Momentum Corrected",200,-0.5,0.5,"Time-Axis [au
    ]",200,-0.5,0.5,"Jet-Axis [au]","Flatland2");
Hist->fill2(2202,"02_epx_epz_Neon2",epx2,epz2,weightp(phi,
    parameter[1700])*weightA(aug,parameter[1700]),"Electron
    momentum epx epz",400,-1.,1.,"epx [au]",400,-1.,1.,"epz [au
    ]","Flatland2");
Hist->fill2(2203,"03_epz_epy_Neon2",epz2,epy2,weightp(phi,
    parameter[1700])*weightA(aug,parameter[1700]),"Electron
    momentum epz epy",400,-1.,1.,"epz [au]",400,-1.,1.,"epy [au
    ]","Flatland2");

Hist->fill2(2204,"04_r2px_r2py_Neon2",r2px,r2py,weightp(phi,
    parameter[1700])*weightA(aug,parameter[1700]),"Recoil momentum
     px py",400,-10.,10.,"px [au]",400,-10.,10.,"py [au]","
    Flatland2");
```

```
Hist->fill2(2205,"05_r2px_r2pz_Neon2",r2px,r2pz,weightp(phi,
    parameter[1700])*weightA(aug,parameter[1700]),"Recoil momentum
     px pz",400,-10.,10.,"px [au]",400,-10.,10.,"pz [au]","
    Flatland2");
Hist->fill2(2206,"06_r2pz_r2py_Neon2",r2pz,r2py,weightp(phi,
    parameter[1700])*weightA(aug,parameter[1700]),"Recoil momentum
     pz py",400,-10.,10.,"pz [au]",400,-10.,10.,"py [au]","
    Flatland2");

Hist->fill2(2207,"07_kpx_kpy_Neon2",kpx2,kpy2,1.,"Auger Electron
    Momentum",200,-10.,10.,"Time-Axis [au]",200,-10.,10.,"Jet-Axis
     [au]","Flatland2");
Hist->fill2(2208,"08_kpx_kpz_Neon2",kpx2,kpz2,weightp(phi,
    parameter[1700])*weightA(aug,parameter[1700]),"Calculated
    electron momentum kx kz",400,-10.,10.,"kx [au]",400,-10.,10.,"
    kz [au]","Flatland2");
Hist->fill2(2209,"09_kpz_kpy_Neon2",kpz2,kpy2,weightp(phi,
    parameter[1700])*weightA(aug,parameter[1700]),"Calculated
    electron momentum kz ky",400,-10.,10.,"kz [au]",400,-10.,10.,"
    ky [au]","Flatland2");

Hist->fill1(2210,"10_Photo_Ne2",phi,1,"Photo-Electron Angular
    Distribution",100,-pi,pi,"[deg]","Flatland2");
Hist->fill1(2211,"11_Photo_Ne2-corrected",phi*180./pi,weightp(phi
    ,parameter[1700])*weightA(aug,parameter[1700]),"Photo-Electron
     Angular Distribution Corrected",100,-180.,180.,"[deg]","
    Flatland2");
```

```
Hist->fill1(2212,"12_Auger_Ne2",aug*180./pi,1,"Auger Electron
    Angular Distribution",100,-180.,180.,"#theta_{TOF}","Flatland2
    ");
Hist->fill1(2213,"13_Auger_Ne2-corrected",aug*180/pi,weightp(phi,
    parameter[1700])*weightA(aug,parameter[1700]),"Auger Electron
    Angular Distribution Corrected",100,-180,180,"#theta_{TOF}","
    Flatland2");
Hist->fill1(2214,"14_Photo-Electron-Energy-Neon2",eE2,weightp(phi
    ,parameter[1700])*weightA(aug,parameter[1700]),"Photo-Electron
     Energy",350,0.5,2.5,"E [eV]","Flatland2");

if(phi<0.) phi=phi+(2.*pi); //normalizes the angular range, (0:2
    pi)
if(aug<0.) aug=aug+(2.*pi);

rel2=(phi-aug); //relative angle (in x-y plane) of Ne2+ electrons
if(rel2>pi) rel2=rel2-(2.*pi);//recasts angular range, (-pi:pi)
if(rel2<-pi) rel2=rel2+(2.*pi);

Hist->fill1(2215,"15_Cos_Energy",rel2*180./pi,weightp(phi,
    parameter[1700])*weightA(aug,parameter[1700]),"CosNe2sum
    ",25,-180.,180.,"cos(theta)","Flatland2");//Calculated Auger
    and Photo-Electron
}
}
```

```
// AUGER ISOTROPY METHOD NE2+
// In this section, the Auger electron is measured with respect
   to the lab frame axes.  Fitting a Fourier series to each
   function, a weighted polar
// plot is generated weightAx(kpx1/kpr1,parameter[1710])

if (Neon2){
if (Elec1 && eE1>0.5 && eE1<2.5 && kpr1>6.5 && kpr1<8.5){
Hist->fill2(2301,"01_epx_epy_Neon2",epx1,epy1,1,"Photo-Electron
   Momentum",400,-0.5,0.5,"Time-Axis [au]",400,-0.5,0.5,"Jet-Axis
    [au]","Isotropy2");
Hist->fill2(2302,"02_epx_epz_Neon2",epx1,epz1,1.,"Photo-Electron
   Momentum",400,-0.5,0.5,"Time-Axis [au]",400,-0.5,0.5,"Beam-
   Axis [au]","Isotropy2");
Hist->fill2(2303,"03_epz_epy_Neon2",epz1,epy1,1.,"Photo-Electron
   Momentum",400,-0.5,0.5,"Beam-Axis [au]",400,-0.5,0.5,"Jet-Axis
    [au]","Isotropy2");

Hist->fill2(2304,"04_r2px_r2py_Neon2",r2px,r2py,1,"Recoil
   momentum px py",400,-10.,10.,"px [au]",400,-10.,10.,"py [au
   ]","Isotropy2");
Hist->fill2(2305,"05_r2px_r2pz_Neon2",r2px,r2pz,1.,"Recoil
   momentum px pz",400,-10.,10.,"px [au]",400,-10.,10.,"pz [au
   ]","Isotropy2");
Hist->fill2(2306,"06_r2pz_r2py_Neon2",r2pz,r2py,1.,"Recoil
   momentum pz py",400,-10.,10.,"pz [au]",400,-10.,10.,"py [au
   ]","Isotropy2");
```

```
Hist->fill2(2307,"07_kpx_kpy_Neon2",kpx1,kpy1,1,"Calculated
    electron momentum kx ky",400,-10.,10.,"kx [au]",400,-10.,10.,"
    ky [au]","Isotropy2");
Hist->fill2(2308,"08_kpx_kpz_Neon2",kpx1,kpz1,1.,"Calculated
    electron momentum kx kz",400,-10.,10.,"kx [au]",400,-10.,10.,"
    kz [au]","Isotropy2");
Hist->fill2(2309,"09_kpz_kpy_Neon2",kpz1,kpy1,1.,"Calculated
    electron momentum kz ky",400,-10.,10.,"kz [au]",400,-10.,10.,"
    ky [au]","Isotropy2");

Hist->fill1(2310,"10_Flat-photo_Cosx-hit",epx1/epr1,1.,"Photo-
    Electron Angular Distribution",50,-1.,1.,"Cos(#theta)","
    Isotropy2");
Hist->fill1(2312,"12_Flat-photo_Cosx-corrected",epx1/epr1,1,"
    Photo-Electron-Angular-Distribution",400,-1.,1.,"Cosx","
    Isotropy2");

Hist->fill1(2313,"13_Photo-Electron-Energy_Neon2",eE1,1,"Photo-
    Electron Energy",350,0.5,2.5,"E [eV]","Isotropy2");
Hist->fill2(2314,"14_Cos_Energy",par1/epr1,eE1,1,"Cos_Energy
    ",100,-1.,1.,"cos(theta)",350,0.5,2.5,"Electron Energy [eV]","
    Isotropy2");
Hist->fill1(2315,"15_Energy-Photo-Proy",eE1,1,"Energy
    ",350,0.5,2.5,"Electron Energy [eV]","Isotropy2");
```

```
Hist->fill1(2316,"16_Auger_Cosx_Neon2",kpx1/kpr1,1,"Auger Cosx
    ",350,-1.,1.,"Cos(#theta_{x})","Isotropy2");
Hist->fill1(2317,"17_Auger_Cosy_Neon2",kpy1/kpr1,1,"Auger Cosy
    ",350,-1.,1.,"cosy","Isotropy2");
Hist->fill1(2318,"18_Auger_Cosz_Neon2",kpz1/kpr1,1,"Auger Cosz
    ",350,-1.,1.,"cosz","Isotropy2");

Hist->fill1(2319,"19_Auger_Cosx_Neon2-corrected",kpx1/kpr1,
    weightAx(kpx1/kpr1,parameter[1710]),"Auger Cosx",350,-1.,1.,"
    Cos(#theta_{x})","Isotropy2");
Hist->fill1(2320,"20_Auger_Cosy_Neon2-corrected",kpy1/kpr1,
    weightAy(kpy1/kpr1,parameter[1711]),"Auger Cosy",350,-1.,1.,"
    cosy","Isotropy2");
Hist->fill1(2321,"21_Auger_Cosz_Neon2-corrected",kpz1/kpr1,
    weightAz(kpz1/kpr1,parameter[1712]),"Auger Cosz",350,-1.,1.,"
    cosz","Isotropy2");

Hist->fill2(2322,"22_Cos_Energy",par1/epr1,eE1,weightAx(kpx1/kpr1
    ,parameter[1710])*weightAy(kpy1/kpr1,parameter[1711])*weightAz
    (kpz1/kpr1,parameter[1712]),"Cos_Energy",100,-1.,1.,"Cos(#
    theta)",100,0.5,2.5,"Photo Electron [eV]","Isotropy2");
if (eE1>1.8 && eE1<2.2) Hist->fill1(2323,"23_prox1",par1/epr1,
    weightAx(kpx1/kpr1,parameter[1710])*weightAy(kpy1/kpr1,
    parameter[1711])*weightAz(kpz1/kpr1,parameter[1712]),"Cos(#
    theta)",50,-1.,1.,"Cos(#theta)","Isotropy2");
```

```
if (eE1>1.4 && eE1<1.8) Hist->fill1(2324,"24_prox2",par1/epr1,
    weightAx(kpx1/kpr1,parameter[1710])*weightAy(kpy1/kpr1,
    parameter[1711])*weightAz(kpz1/kpr1,parameter[1712]),"Cos(#
    theta)",50,-1.,1.,"Cos(#theta)","Isotropy2");
if (eE1>1.0 && eE1<1.4) Hist->fill1(2325,"25_prox3",par1/epr1,
    weightAx(kpx1/kpr1,parameter[1710])*weightAy(kpy1/kpr1,
    parameter[1711])*weightAz(kpz1/kpr1,parameter[1712]),"Cos(#
    theta)",50,-1.,1.,"Cos(#theta)","Isotropy2");
}
if (Elec2 && eE2>0.5 && eE2<2.5 && kpr2>6.5 && kpr2<8.5 && eE1
    >6.5){//This adds back in the events that correspond to 2nd
    hit photo-electrons
Hist->fill2(2301,"01_epx_epy_Neon2",epx2,epy2,1,"Photo-Electron
    Momentum",400,-0.5,0.5,"Time-Axis [au]",400,-0.5,0.5,"Jet-Axis
     [au]","Isotropy2");
Hist->fill2(2302,"02_epx_epz_Neon2",epx2,epz2,1.,"Photo-Electron
    Momentum",400,-0.5,0.5,"Time-Axis [au]",400,-0.5,0.5,"Beam-
    Axis [au]","Isotropy2");
Hist->fill2(2303,"03_epz_epy_Neon2",epz2,epy2,1.,"Photo-Electron
    Momentum",400,-0.5,0.5,"Beam-Axis [au]",400,-0.5,0.5,"Jet-Axis
     [au]","Isotropy2");

Hist->fill2(2304,"04_r2px_r2py_Neon2",r2px,r2py,1,"Recoil
    momentum px py",400,-10.,10.,"px [au]",400,-10.,10.,"py [au
    ]","Isotropy2");
```

```
Hist->fill2(2305,"05_r2px_r2pz_Neon2",r2px,r2pz,1.,"Recoil
    momentum px pz",400,-10.,10.,"px [au]",400,-10.,10.,"pz [au
    ]","Isotropy2");
Hist->fill2(2306,"06_r2pz_r2py_Neon2",r2pz,r2py,1.,"Recoil
    momentum pz py",400,-10.,10.,"pz [au]",400,-10.,10.,"py [au
    ]","Isotropy2");

Hist->fill2(2307,"07_kpx_kpy_Neon2",kpx2,kpy2,1,"Calculated
    electron momentum kx ky",400,-10.,10.,"kx [au]",400,-10.,10.,"
    ky [au]","Isotropy2");
Hist->fill2(2308,"08_kpx_kpz_Neon2",kpx2,kpz2,1.,"Calculated
    electron momentum kx kz",400,-10.,10.,"kx [au]",400,-10.,10.,"
    kz [au]","Isotropy2");
Hist->fill2(2309,"09_kpz_kpy_Neon2",kpz2,kpy2,1.,"Calculated
    electron momentum kz ky",400,-10.,10.,"kz [au]",400,-10.,10.,"
    ky [au]","Isotropy2");

Hist->fill1(2310,"10_Flat-photo_Cosx-hit",epx2/epr2,1.,"Photo-
    Electron Angular Distribution",50,-1.,1.,"Cos(#theta)","
    Isotropy2");
Hist->fill1(2312,"12_Flat-photo_Cosx-corrected",epx2/epr2,1,"
    Photo-Electron-Angular-Distribution",400,-1.,1.,"Cosx","
    Isotropy2");
Hist->fill1(2313,"13_Photo-Electron-Energy_Neon2",eE2,1,"Photo-
    Electron Energy",350,0.5,2.5,"E [eV]","Isotropy2");
```

```
Hist->fill2(2314,"14_Cos_Energy",par2/epr2,eE2,1,"Cos_Energy
    ",100,-1.,1.,"cos(theta)",350,0.5,2.5,"Electron Energy [eV]","
    Isotropy2");
Hist->fill1(2315,"15_Energy-Photo-Proy",eE2,1,"Energy
    ",350,0.5,2.5,"Electron Energy [eV]","Isotropy2");

Hist->fill1(2316,"16_Auger_Cosx_Neon2",kpx2/kpr2,1,"Auger Cosx
    ",350,-1.,1.,"Cos(#theta_{x})","Isotropy2");
Hist->fill1(2317,"17_Auger_Cosy_Neon2",kpy2/kpr2,1,"Auger Cosy
    ",350,-1.,1.,"cosy","Isotropy2");
Hist->fill1(2318,"18_Auger_Cosz_Neon2",kpz2/kpr2,1,"Auger Cosz
    ",350,-1.,1.,"cosz","Isotropy2");

Hist->fill1(2319,"19_Auger_Cosx_Neon2-corrected",kpx2/kpr2,
    weightAx(kpx2/kpr2,parameter[1710]),"Auger Cosx",350,-1.,1.,"
    Cos(#theta_{x})","Isotropy2");
Hist->fill1(2320,"20_Auger_Cosy_Neon2-corrected",kpy2/kpr2,
    weightAy(kpy2/kpr2,parameter[1711]),"Auger Cosy",350,-1.,1.,"
    cosy","Isotropy2");
Hist->fill1(2321,"21_Auger_Cosz_Neon2-corrected",kpz2/kpr2,
    weightAz(kpz2/kpr2,parameter[1712]),"Auger Cosz",350,-1.,1.,"
    cosz","Isotropy2");

Hist->fill2(2322,"22_Cos_Energy",par2/epr2,eE2,weightAx(kpx2/kpr2
    ,parameter[1710])*weightAy(kpy2/kpr2,parameter[1711])*weightAz
    (kpz2/kpr2,parameter[1712]),"Cos_Energy",100,-1.,1.,"Cos(#
    theta)",100,0.5,2.5,"Photo Electron [eV]","Isotropy2");
```

```
if (eE2>1.8 && eE2<2.2) Hist->fill1(2323,"23_prox1",par2/epr2,
    weightAx(kpx2/kpr2,parameter[1710])*weightAy(kpy2/kpr2,
    parameter[1711])*weightAz(kpz2/kpr2,parameter[1712]),"Cos(#
    theta)",50,-1.,1.,"Cos(#theta)","Isotropy2");
if (eE2>1.8 && eE2<2.2) Hist->fill1(2323,"23_prox1",par2/epr2,
    weightAx(kpx2/kpr2,parameter[1710])*weightAy(kpy2/kpr2,
    parameter[1711])*weightAz(kpz2/kpr2,parameter[1712]),"Cos(#
    theta)",50,-1.,1.,"Cos(#theta)","Isotropy2");
if (eE2>1.4 && eE2<1.8) Hist->fill1(2324,"24_prox2",par2/epr2,
    weightAx(kpx2/kpr2,parameter[1710])*weightAy(kpy2/kpr2,
    parameter[1711])*weightAz(kpz2/kpr2,parameter[1712]),"Cos(#
    theta)",50,-1.,1.,"Cos(#theta)","Isotropy2");
if (eE2>1.0 && eE2<1.4) Hist->fill1(2325,"25_prox3",par2/epr2,
    weightAx(kpx2/kpr2,parameter[1710])*weightAy(kpy2/kpr2,
    parameter[1711])*weightAz(kpz2/kpr2,parameter[1712]),"Cos(#
    theta)",50,-1.,1.,"Cos(#theta)","Isotropy2");
}
}

double phi1=-12345.0, phi2=-12345.0, phi2a=-12345.0, phi3
    =-12345.0, phi4=-12345.0, phi5=-12345.0, phi6=-12345.0;
double relativeAA=-12345.0, relativeAP=-12345.0, relativeKP
    =-12345.0, relativekSum=-12345.0, relative2=-12345.0,
    relativepho=-12345.0;

phi1=atan2(epy1,epx1);
phi2=atan2(epy2,epx2);
```

```
phi2a=atan2(epy3,epx3);
phi3=atan2(kpy12,kpx12);
phi4=atan2(kpy1,kpx1);
phi5=atan2(kpy2,kpx2);
double weight=-12345.;

//Pweight Section Ne2+
if (Neon2 && Elec1 && eE1>0.5 && eE1<2.5){//Assumes 1st hit is
    photo-electron
weight = pweightNe2a(phi1,parameter[1850])*Apweight(epz1/epr1,
    parameter[1850])*Apweight2(kpz1/kpr1,parameter[1850]);//*
    pweightNe2b(epz1/epr1,parameter[1850]);

Hist->fill2(2401,"01_epx_epy_Neon2",epx1,epy1,weight,"Photo-
    Electron Momentum Corrected",100,-0.5,0.5,"Time-Axis [au
    ]",100,-0.5,0.5,"Jet-Axis [au]","Pweight2");
if(fabs(kpx1/kpr1)<0.15 && kpr1<8.5) Hist->fill2(2402,"02
    _kpz_kpy_Neon2",kpz1,kpy1,weight,"Auger Electron Momentum
    ",200,-10.,10.,"Beam-Axis [au]",200,-10.,10.,"Jet-Axis [au]","
    Pweight2");
Hist->fill2(2403,"03_epx_epz_Neon2",epx1,epz1,weight,"Measured
    electron momentum kx kz",100,-0.5,0.5,"ex [au]",100,-0.5,0.5,"
    ez [au]","Pweight2");

Hist->fill1(2404,"04_Photo_Ellipticity_Ne2",phi1,weight,"Photo-
    Electron Angular Distribution Corrected",100,-pi,pi,"#theta_{
    TOF}","Pweight2");
```

```
Hist->fill2(2405,"05_donut_cross_Neon2_unweighted",sqrt(epx1*epx1
    + epy1*epy1),epz1,(epr1/sqrt(epx1*epx1 + epy1*epy1)),"Cross
    Section of Photo-Electron Distribution",400,-1.,1.,"e#_{perp}
    [au]",400,-1.,1.,"ez [au]","Pweight2");
Hist->fill2(2406,"06_donut_cross_Neon2",sqrt(epx1*epx1 + epy1*
    epy1),epz1,weight*(epr1/sqrt(epx1*epx1 + epy1*epy1)),"Cross
    Section of Photo-Electron Distribution",400,-1.,1.,"e#_{perp}
    [au]",400,-1.,1.,"ez [au]","Pweight2");
Hist->fill1(2407,"07_counts_cosz",epz1/epr1,weight,"Photo-
    Electron Angle Corrected",100,-1,1,"#theta_{beam}","Pweight2")
    ;
Hist->fill1(2408,"photo_all_unweighted",eE1,1.,"Photo Electron
    Energy",60,0,180,"Energy [eV]","Pweight2");
Hist->fill1(2409,"photo_all",eE1,weight,"Photo Electron Energy
    ",60,0,180,"Energy [eV]","Pweight2");
Hist->fill1(2410,"photo_zoom_unweighted",eE1,1.,"Photo Electron
    Energy",60,0,90,"Energy [eV]","Pweight2");
Hist->fill1(2411,"photo_zoom",eE1,weight,"Photo Electron Energy
    ",60,0,90,"Energy [eV]","Pweight2");
Hist->fill2(2412,"splish-splash_unweighted",par1/epr1,eE1,1.,"
    Splash Effect",100,-1.,1.,"Cos(#theta)",100,0.5,2.5,"Auger
    Energy [eV]","Pweight2");
Hist->fill2(2413,"splish-splash",par1/epr1,eE1,weight,"Splash
    Effect Corrected",100,-1.,1.,"Cos(#theta)",100,0.5,2.5,"Auger
    Energy [eV]","Pweight2");
```

```
Hist->fill1(2414,"08_Auger_Ne2",phi4,weight,"Auger Electron
    Angular Distribution Corrected",100,-pi,pi,"#theta_{TOF}","
    Pweight2");
Hist->fill1(2415,"09_Acounts_cosz",kpz1/kpr1,weight,"Auger-
    Electron Angle Corrected",100,-1,1,"#theta_{beam}","Pweight2")
    ;

if (eE1>0.5 && eE1<2.5){//Correlation between Auger and Photo-
    Electron
Hist->fill1(2416,"angular_photo",acos(par1/epr1)*180./pi,sin_inv1
    *weight,"CosNe2sum",20,-180.,180.,"cos(#theta)","Pweight2");
Hist->fill1(2417,"angular_photo",-acos(par1/epr1)*180./pi,
    sin_inv1*weight,"CosNe2sum",20,-180.,180.,"cos(#theta)","
    Pweight2");
}
}

if (Neon2 && Elec2 && eE2>0.5 && eE2<2.5){//Assumes 2nd hit is
    photo-electron
weight = pweightNe2a(phi2,parameter[1850])*Apweight(epz2/epr2,
    parameter[1850])*Apweight2(kpz2/kpr2,parameter[1850]);//*
    pweightNe2b(epz2/epr2,parameter[1850]);//

Hist->fill2(2401,"01_epx_epy_Neon2",epx2,epy2,weight,"Photo-
    Electron Momentum Corrected",100,-0.5,0.5,"Time-Axis [au
    ]",100,-0.5,0.5,"Jet-Axis [au]","Pweight2");
```

```
if(fabs(kpx2/kpr2)<0.15 && kpr2<8.5) Hist->fill2(2402,"02
    _kpz_kpy_Neon2",kpz2,kpy2,weight,"Auger Electron Momentum
    ",200,-10.,10.,"Beam-Axis [au]",200,-10.,10.,"Jet-Axis [au]","
    Pweight2");
Hist->fill2(2403,"03_epx_epz_Neon2",epx2,epz2,weight,"Measured
    electron momentum kx kz",100,-0.5,0.5,"ex [au]",100,-0.5,0.5,"
    ez [au]","Pweight2");

Hist->fill1(2404,"04_Photo_Ellipticity_Ne2",phi2,weight,"Photo-
    Electron Angular Distribution Corrected",100,-pi,pi,"#theta_{
    TOF}","Pweight2");
Hist->fill2(2405,"05_donut_cross_Neon2_unweighted",sqrt(epx2*epx2
     + epy2*epy2),epz2,(epr2/sqrt(epx2*epx2 + epy2*epy2)),"Cross
    Section of Photo-Electron Distribution",400,-1.,1.,"e#_{perp}
    [au]",400,-1.,1.,"ez [au]","Pweight2");
Hist->fill2(2406,"06_donut_cross_Neon2",sqrt(epx2*epx2 + epy2*
    epy2),epz2,weight*(epr2/sqrt(epx2*epx2 + epy2*epy2)),"Cross
    Section of Photo-Electron Distribution",400,-1.,1.,"e#_{perp}
    [au]",400,-1.,1.,"ez [au]","Pweight2");
Hist->fill1(2407,"07_counts_cosz",epz2/epr2,weight,"Photo-
    Electron Angle Corrected",100,-1,1,"#theta_{beam}","Pweight2")
    ;
Hist->fill1(2408,"photo_all_unweighted",eE2,1.,"Photo Electron
    Energy",60,0,180,"Energy [eV]","Pweight2");
Hist->fill1(2409,"photo_all",eE2,weight,"Photo Electron Energy
    ",60,0,180,"Energy [eV]","Pweight2");
```

```
Hist->fill1(2410,"photo_zoom_unweighted",eE2,1.,"Photo Electron
    Energy",60,0,90,"Energy [eV]","Pweight2");
Hist->fill1(2411,"photo_zoom",eE2,weight,"Photo Electron Energy
    ",60,0,90,"Energy [eV]","Pweight2");
Hist->fill2(2412,"splish-splash_unweighted",par2/epr2,eE2,1.,"
    Splash Effect",100,-1.,1.,"Cos(#theta)",100,0.5,2.5,"Auger
    Energy [eV]","Pweight2");
Hist->fill2(2413,"splish-splash",par2/epr2,eE2,weight,"Splash
    Effect Corrected",100,-1.,1.,"Cos(#theta)",100,0.5,2.5,"Auger
    Energy [eV]","Pweight2");

Hist->fill1(2414,"08_Auger_Ne2",phi5,weight,"Auger Electron
    Angular Distribution Corrected",100,-pi,pi,"#theta_{TOF}","
    Pweight2");
Hist->fill1(2415,"09_Acounts_cosz",kpz2/kpr2,weight,"Auger-
    Electron Angle Corrected",100,-1,1,"#theta_{beam}","Pweight2")
    ;

if (eE2>0.5 && eE2<2.5){
Hist->fill1(2416,"angular_photo",acos(par2/epr2)*180./pi,sin_inv2
    *weight,"CosNe2sum",20,-180.,180.,"cos(#theta)","Pweight2");
Hist->fill1(2417,"angular_photo",-acos(par2/epr2)*180./pi,
    sin_inv2*weight,"CosNe2sum",20,-180.,180.,"cos(#theta)","
    Pweight2");
Hist->fill1(2418,"Prox-1D",par2/epr2,weight,"Angular Distribution
     of Auger Events",100,-1.,1.,"#theta","Pweight2");
}
```

```
}

//Ne3+
//4Pi CoLLeCTioN SeCTioN
//if (Neon3 && Elec1 && Elec2 && Cone1 && eE2<2.5){
if (Neon3 && Elec1 && Elec2 && eE2<2.5){
Hist->fill2(3101,"01_epx1_epy1_Neon3",epx1,epy1,1.,"Measured
    Auger Electron Momentum",400,-10.,10.,"Time-Axis [au
    ]",400,-10.,10.,"Jet-Axis [au]","Momentum3");
Hist->fill2(3102,"02_epx1_epz1_Neon3",epx1,epz1,1.,"Measured
    Auger Electron Momentum",400,-10.,10.,"Time-Axis [au
    ]",400,-10.,10.,"Beam-Axis [au]","Momentum3");
Hist->fill2(3103,"03_epz1_epy1_Neon3",epz1,epy1,1.,"Measured
    Auger Electron Momentum",400,-10.,10.,"Beam-Axis [au
    ]",400,-10.,10.,"Jet-Axis [au]","Momentum3");

Hist->fill2(3104,"04_epx2_epy2_Neon3",epx2,epy2,1.,"Photo-
    Electron Momentum",400,-0.5,0.5,"Time-Axis [au
    ]",400,-0.5,0.5,"Jet-Axis [au]","Momentum3");
Hist->fill2(3105,"05_epx2_epz2_Neon3",epx2,epz2,1.,"Photo-
    Electron Momentum",400,-0.5,0.5,"Time-Axis [au
    ]",400,-0.5,0.5,"Beam-Axis [au]","Momentum3");
Hist->fill2(3106,"06_epz2_epy2_Neon3",epz2,epy2,1.,"Photo-
    Electron Momentum",400,-0.5,0.5,"Beam-Axis [au
    ]",400,-0.5,0.5,"Jet-Axis [au]","Momentum3");
```

```
//Hist->fill2(3107,"07_epx3_epy3_Neon3",epx3,epy3,1.,"Electron
    momentum epx epy Hit 3",400,-10.,10.,"Time-Axis [au
    ]",400,-10.,10.,"Jet-Axis [au]","Momentum3");
//Hist->fill2(3108,"08_epx3_epz3_Neon3",epx3,epz3,1.,"Electron
    momentum epx epz Hit 3",400,-10.,10.,"Time-Axis [au
    ]",400,-10.,10.,"Beam-Axis [au]","Momentum3");
//Hist->fill2(3109,"09_epz3_epy3_Neon3",epz3,epy3,1.,"Electron
    momentum epz epy Hit 3",400,-10.,10.,"Beam-Axis [au
    ]",400,-10.,10.,"Jet-Axis [au]","Momentum3");

Hist->fill2(3110,"10_r3px_r3py_Neon3",r3px,r3py,1.,"Recoil
    momentum px py",400,-10.,10.,"Time-Axis [au]",400,-10.,10.,"
    Jet-Axis [au]","Momentum3");
Hist->fill2(3111,"11_r3px_r3pz_Neon3",r3px,r3pz,1.,"Recoil
    momentum px pz",400,-10.,10.,"Time-Axis [au]",400,-10.,10.,"
    Beam-Axis [au]","Momentum3");
Hist->fill2(3112,"12_r3pz_r3py_Neon3",r3pz,r3py,1.,"Recoil
    momentum pz py",400,-10.,10.,"Beam-Axis [au]",400,-10.,10.,"
    Jet-Axis [au]","Momentum3");

Hist->fill2(3113,"13_kpx12_kpy12_Neon3",kpx12,kpy12,1.,"
    Calculated Auger Electron Momentum",400,-10.,10.,"Time-Axis [
    au]",400,-10.,10.,"Jet-Axis [au]","Momentum3");
Hist->fill2(3114,"14_kpx12_kpz12_Neon3",kpx12,kpz12,1.,"
    Calculated Auger Electron Momentum",400,-10.,10.,"Time-Axis [
    au]",400,-10.,10.,"Beam-Axis [au]","Momentum3");
```

```
Hist->fill2(3115,"15_kpz12_kpy12_Neon3",kpz12,kpy12,1.,"
    Calculated Auger Electron Momentum",400,-10.,10.,"Beam-Axis [
    au]",400,-10.,10.,"Jet-Axis [au]","Momentum3");

Hist->fill2(3116,"16_kpx23_kpy23_Neon3",kpx23,kpy23,1.,"
    Calculated Auger Electron Momentum",400,-10.,10.,"Time-Axis [
    au]",400,-10.,10.,"Jet-Axis [au]","Momentum3");
Hist->fill2(3117,"17_kpx23_kpz23_Neon3",kpx23,kpz23,1.,"
    Calculated Auger Electron Momentum",400,-10.,10.,"Time-Axis [
    au]",400,-10.,10.,"Beam-Axis [au]","Momentum3");
Hist->fill2(3118,"18_kpz23_kpy23_Neon3",kpz23,kpy23,1.,"
    Calculated Auger Electron Momentum",400,-10.,10.,"Beam-Axis [
    au]",400,-10.,10.,"Jet-Axis [au]","Momentum3");

Hist->fill1(3119,"19_E1_Neon3-small",eE1,1.,"Measured Auger
    Electron Energy",200,0.,1000,"Energy [eV]","Momentum3");
//Hist->fill1(3120,"20_E1_Neon3-large",eE1,1.,"Electron Energy
    Hit 1",300,0.,1250.,"Energy [eV]","Momentum3");
Hist->fill1(3121,"21_E2_Neon3-small",eE2,1.,"Photo-Electron
    Energy",75,0.,3.,"Energy [eV]","Momentum3");
//Hist->fill1(3122,"22_E2_Neon3-large",eE2,1.,"Electron Energy
    Hit 2",300,0.,1250.,"Energy [eV]","Momentum3");
Hist->fill1(3123,"23_kE12_Neon3-large",kE12,1.,"Calculated Auger
    Electron Energy",200,0.,1000.,"Energy [eV]","Momentum3");
Hist->fill1(3124,"24_kE23_Neon3-large",kE23,1.,"Calculated Auger
    Electron Energy",200,0.,1000.,"Energy [eV]","Momentum3");
```

```
Hist->fill2(3125,"25_Double_Auger",eE1,kE12,1.,"Double Auger
    Events",200,0.,1250.,"Measured [eV]",200,0.,1250.,"Calculated
    [eV]","Momentum3");
}

if (Neon3 && Elec2 && Elec3 && eE3<2.5){
Hist->fill2(3101,"01_epx1_epy1_Neon3",epx2,epy2,1.,"Measured
    Auger Electron Momentum",400,-10.,10.,"Time-Axis [au
    ]",400,-10.,10.,"Jet-Axis [au]","Momentum3");
Hist->fill2(3102,"02_epx1_epz1_Neon3",epx2,epz2,1.,"Measured
    Auger Electron Momentum",400,-10.,10.,"Time-Axis [au
    ]",400,-10.,10.,"Beam-Axis [au]","Momentum3");
Hist->fill2(3103,"03_epz1_epy1_Neon3",epz2,epy2,1.,"Measured
    Auger Electron Momentum",400,-10.,10.,"Beam-Axis [au
    ]",400,-10.,10.,"Jet-Axis [au]","Momentum3");

Hist->fill2(3104,"04_epx2_epy2_Neon3",epx3,epy3,1.,"Photo-
    Electron Momentum",400,-0.5,0.5,"Time-Axis [au
    ]",400,-0.5,0.5,"Jet-Axis [au]","Momentum3");
Hist->fill2(3105,"05_epx2_epz2_Neon3",epx3,epz3,1.,"Photo-
    Electron Momentum",400,-0.5,0.5,"Time-Axis [au
    ]",400,-0.5,0.5,"Beam-Axis [au]","Momentum3");
Hist->fill2(3106,"06_epz2_epy2_Neon3",epz3,epy3,1.,"Photo-
    Electron Momentum",400,-0.5,0.5,"Beam-Axis [au
    ]",400,-0.5,0.5,"Jet-Axis [au]","Momentum3");
```

```
//Hist->fill2(3107,"07_epx3_epy3_Neon3",epx3,epy3,1.,"Electron
    momentum epx epy Hit 3",400,-10.,10.,"Time-Axis [au
    ]",400,-10.,10.,"Jet-Axis [au]","Momentum3");
//Hist->fill2(3108,"08_epx3_epz3_Neon3",epx3,epz3,1.,"Electron
    momentum epx epz Hit 3",400,-10.,10.,"Time-Axis [au
    ]",400,-10.,10.,"Beam-Axis [au]","Momentum3");
//Hist->fill2(3109,"09_epz3_epy3_Neon3",epz3,epy3,1.,"Electron
    momentum epz epy Hit 3",400,-10.,10.,"Beam-Axis [au
    ]",400,-10.,10.,"Jet-Axis [au]","Momentum3");

Hist->fill2(3110,"10_r3px_r3py_Neon3",r3px,r3py,1.,"Recoil
    momentum px py",400,-10.,10.,"Time-Axis [au]",400,-10.,10.,"
    Jet-Axis [au]","Momentum3");
Hist->fill2(3111,"11_r3px_r3pz_Neon3",r3px,r3pz,1.,"Recoil
    momentum px pz",400,-10.,10.,"Time-Axis [au]",400,-10.,10.,"
    Beam-Axis [au]","Momentum3");
Hist->fill2(3112,"12_r3pz_r3py_Neon3",r3pz,r3py,1.,"Recoil
    momentum pz py",400,-10.,10.,"Beam-Axis [au]",400,-10.,10.,"
    Jet-Axis [au]","Momentum3");

Hist->fill2(3113,"13_kpx12_kpy12_Neon3",kpx23,kpy23,1.,"
    Calculated Auger Electron Momentum",400,-10.,10.,"Time-Axis [
    au]",400,-10.,10.,"Jet-Axis [au]","Momentum3");
Hist->fill2(3114,"14_kpx12_kpz12_Neon3",kpx23,kpz23,1.,"
    Calculated Auger Electron Momentum",400,-10.,10.,"Time-Axis [
    au]",400,-10.,10.,"Beam-Axis [au]","Momentum3");
```

```
Hist->fill2(3115,"15_kpz12_kpy12_Neon3",kpz23,kpy23,1.,"
    Calculated Auger Electron Momentum",400,-10.,10.,"Beam-Axis [
    au]",400,-10.,10.,"Jet-Axis [au]","Momentum3");

Hist->fill2(3116,"16_kpx23_kpy23_Neon3",kpx23,kpy23,1.,"
    Calculated Auger Electron Momentum",400,-10.,10.,"Time-Axis [
    au]",400,-10.,10.,"Jet-Axis [au]","Momentum3");
Hist->fill2(3117,"17_kpx23_kpz23_Neon3",kpx23,kpz23,1.,"
    Calculated Auger Electron Momentum",400,-10.,10.,"Time-Axis [
    au]",400,-10.,10.,"Beam-Axis [au]","Momentum3");
Hist->fill2(3118,"18_kpz23_kpy23_Neon3",kpz23,kpy23,1.,"
    Calculated Auger Electron Momentum",400,-10.,10.,"Beam-Axis [
    au]",400,-10.,10.,"Jet-Axis [au]","Momentum3");

Hist->fill1(3119,"19_E1_Neon3-small",eE2,1.,"Measured Auger
    Electron Energy",200,0.,1000,"Energy [eV]","Momentum3");
//Hist->fill1(3120,"20_E1_Neon3-large",eE1,1.,"Electron Energy
    Hit 1",300,0.,1250.,"Energy [eV]","Momentum3");
Hist->fill1(3121,"21_E2_Neon3-small",eE3,1.,"Photo-Electron
    Energy",75,0.,3.,"Energy [eV]","Momentum3");
//Hist->fill1(3122,"22_E2_Neon3-large",eE2,1.,"Electron Energy
    Hit 2",300,0.,1250.,"Energy [eV]","Momentum3");
Hist->fill1(3123,"23_kE12_Neon3-large",kE23,1.,"Calculated Auger
    Electron Energy",200,0.,1000.,"Energy [eV]","Momentum3");
Hist->fill1(3124,"24_kE23_Neon3-large",kE23,1.,"Calculated Auger
    Electron Energy",200,0.,1000.,"Energy [eV]","Momentum3");
```

```
Hist->fill2(3125,"25_Double_Auger",eE2,kE23,1.,"Double Auger
    Events",200,0.,1250.,"Measured [eV]",200,0.,1250.,"Calculated
    [eV]","Momentum3");
}

if (Neon3 && Elec1 && Elec3 && eE3<2.5){//consider throwing out
Hist->fill2(3101,"01_epx1_epy1_Neon3",epx1,epy1,1.,"Measured
    Auger Electron Momentum",400,-10.,10.,"Time-Axis [au
    ]",400,-10.,10.,"Jet-Axis [au]","Momentum3");
Hist->fill2(3102,"02_epx1_epz1_Neon3",epx1,epz1,1.,"Measured
    Auger Electron Momentum",400,-10.,10.,"Time-Axis [au
    ]",400,-10.,10.,"Beam-Axis [au]","Momentum3");
Hist->fill2(3103,"03_epz1_epy1_Neon3",epz1,epy1,1.,"Measured
    Auger Electron Momentum",400,-10.,10.,"Beam-Axis [au
    ]",400,-10.,10.,"Jet-Axis [au]","Momentum3");

Hist->fill2(3104,"04_epx2_epy2_Neon3",epx3,epy3,1.,"Photo-
    Electron Momentum",400,-0.5,0.5,"Time-Axis [au
    ]",400,-0.5,0.5,"Jet-Axis [au]","Momentum3");
Hist->fill2(3105,"05_epx2_epz2_Neon3",epx3,epz3,1.,"Photo-
    Electron Momentum",400,-0.5,0.5,"Time-Axis [au
    ]",400,-0.5,0.5,"Beam-Axis [au]","Momentum3");
Hist->fill2(3106,"06_epz2_epy2_Neon3",epz3,epy3,1.,"Photo-
    Electron Momentum",400,-0.5,0.5,"Beam-Axis [au
    ]",400,-0.5,0.5,"Jet-Axis [au]","Momentum3");
```

```
//Hist->fill2(3107,"07_epx3_epy3_Neon3",epx3,epy3,1.,"Electron
    momentum epx epy Hit 3",400,-10.,10.,"Time-Axis [au
    ]",400,-10.,10.,"Jet-Axis [au]","Momentum3");
//Hist->fill2(3108,"08_epx3_epz3_Neon3",epx3,epz3,1.,"Electron
    momentum epx epz Hit 3",400,-10.,10.,"Time-Axis [au
    ]",400,-10.,10.,"Beam-Axis [au]","Momentum3");
//Hist->fill2(3109,"09_epz3_epy3_Neon3",epz3,epy3,1.,"Electron
    momentum epz epy Hit 3",400,-10.,10.,"Beam-Axis [au
    ]",400,-10.,10.,"Jet-Axis [au]","Momentum3");

Hist->fill2(3110,"10_r3px_r3py_Neon3",r3px,r3py,1.,"Recoil
    momentum px py",400,-10.,10.,"Time-Axis [au]",400,-10.,10.,"
    Jet-Axis [au]","Momentum3");
Hist->fill2(3111,"11_r3px_r3pz_Neon3",r3px,r3pz,1.,"Recoil
    momentum px pz",400,-10.,10.,"Time-Axis [au]",400,-10.,10.,"
    Beam-Axis [au]","Momentum3");
Hist->fill2(3112,"12_r3pz_r3py_Neon3",r3pz,r3py,1.,"Recoil
    momentum pz py",400,-10.,10.,"Beam-Axis [au]",400,-10.,10.,"
    Jet-Axis [au]","Momentum3");

Hist->fill2(3113,"13_kpx12_kpy12_Neon3",kpx13,kpy13,1.,"
    Calculated Auger Electron Momentum",400,-10.,10.,"Time-Axis [
    au]",400,-10.,10.,"Jet-Axis [au]","Momentum3");
Hist->fill2(3114,"14_kpx12_kpz12_Neon3",kpx13,kpz13,1.,"
    Calculated Auger Electron Momentum",400,-10.,10.,"Time-Axis [
    au]",400,-10.,10.,"Beam-Axis [au]","Momentum3");
```

```
Hist->fill2(3115,"15_kpz12_kpy12_Neon3",kpz13,kpy13,1.,"
    Calculated Auger Electron Momentum",400,-10.,10.,"Beam-Axis [
    au]",400,-10.,10.,"Jet-Axis [au]","Momentum3");

Hist->fill2(3116,"16_kpx23_kpy23_Neon3",kpx13,kpy13,1.,"
    Calculated Auger Electron Momentum",400,-10.,10.,"Time-Axis [
    au]",400,-10.,10.,"Jet-Axis [au]","Momentum3");
Hist->fill2(3117,"17_kpx23_kpz23_Neon3",kpx13,kpz13,1.,"
    Calculated Auger Electron Momentum",400,-10.,10.,"Time-Axis [
    au]",400,-10.,10.,"Beam-Axis [au]","Momentum3");
Hist->fill2(3118,"18_kpz23_kpy23_Neon3",kpz13,kpy13,1.,"
    Calculated Auger Electron Momentum",400,-10.,10.,"Beam-Axis [
    au]",400,-10.,10.,"Jet-Axis [au]","Momentum3");

Hist->fill1(3119,"19_E1_Neon3-small",eE1,1.,"Measured Auger
    Electron Energy",200,0.,1000,"Energy [eV]","Momentum3");
//Hist->fill1(3120,"20_E1_Neon3-large",eE1,1.,"Electron Energy
    Hit 1",300,0.,1250.,"Energy [eV]","Momentum3");
Hist->fill1(3121,"21_E2_Neon3-small",eE3,1.,"Photo-Electron
    Energy",75,0.,3.,"Energy [eV]","Momentum3");
//Hist->fill1(3122,"22_E2_Neon3-large",eE2,1.,"Electron Energy
    Hit 2",300,0.,1250.,"Energy [eV]","Momentum3");
Hist->fill1(3123,"23_kE12_Neon3-large",kE13,1.,"Calculated Auger
    Electron Energy",200,0.,1000.,"Energy [eV]","Momentum3");
Hist->fill1(3124,"24_kE23_Neon3-large",kE13,1.,"Calculated Auger
    Electron Energy",200,0.,1000.,"Energy [eV]","Momentum3");
```

```
Hist->fill2(3125,"25_Double_Auger",eE1,kE13,1.,"Double Auger
    Events",200,0.,1250.,"Measured [eV]",200,0.,1250.,"Calculated
    [eV]","Momentum3");
}

//*****************************************************************

// NE3+ ANGULAR CORRELATION ANALYSES
//*****************************************************************

// AUGER ISOTROPY METHOD NE3+
// In this section, the photo-electron is measured with respect
    to the lab frame axes.  Fitting a Fourier series to the
    function, a weighted polar
// plot is generated

if (Neon3 && Elec1 && Elec2 && eE2<2.5 && Cone1){//Assumes 2nd
    hit is photo-electron
double phi = atan2(epy2,epx2);
Hist->fill2(3201,"01_epx_epy_Neon3",epx2,epy2,weight3D(phi,
    parameter[1900]),"Photo Electron momentum epx epy
    ",400,-1.,1.,"epx [au]",400,-1.,1.,"epy [au]","Isotropy3");
Hist->fill2(3202,"02_epx_epz_Neon3",epx2,epz2,weight3D(phi,
    parameter[1900]),"Photo Electron momentum epx epz
    ",400,-1.,1.,"epx [au]",400,-1.,1.,"epz [au]","Isotropy3");
```

```
Hist->fill2(3203,"03_epz_epy_Neon3",epz2,epy2,weight3D(phi,
    parameter[1900]),"Photo Electron momentum epz epy
    ",400,-1.,1.,"epz [au]",400,-1.,1.,"epy [au]","Isotropy3");

Hist->fill2(3204,"04_r2px_r2py_Neon3",r3px,r3py,1.,"Recoil
    momentum px py",400,-10.,10.,"px [au]",400,-10.,10.,"py [au
    ]","Isotropy3");
Hist->fill2(3205,"05_r2px_r2pz_Neon3",r3px,r3pz,1.,"Recoil
    momentum px pz",400,-10.,10.,"px [au]",400,-10.,10.,"pz [au
    ]","Isotropy3");
Hist->fill2(3206,"06_r2pz_r2py_Neon3",r3pz,r3py,1.,"Recoil
    momentum pz py",400,-10.,10.,"pz [au]",400,-10.,10.,"py [au
    ]","Isotropy3");

Hist->fill2(3207,"07_kpx_kpy_Neon3",epx1,epy1,1.,"Measured
    electron momentum kx ky",400,-10.,10.,"kx [au]",400,-10.,10.,"
    ky [au]","Isotropy3");
Hist->fill2(3208,"08_kpx_kpz_Neon3",epx1,epz1,1.,"Measured
    electron momentum kx kz",400,-10.,10.,"kx [au]",400,-10.,10.,"
    kz [au]","Isotropy3");
Hist->fill2(3209,"09_kpz_kpy_Neon3",epz1,epy1,1.,"Measured
    electron momentum kz ky",400,-10.,10.,"kz [au]",400,-10.,10.,"
    ky [au]","Isotropy3");

Hist->fill2(3210,"10_kpx_kpy_Neon3",kpx12,kpy12,1.,"Calculated
    electron momentum kx ky",400,-10.,10.,"kx [au]",400,-10.,10.,"
    ky [au]","Isotropy3");
```

```
Hist->fill2(3211,"11_kpx_kpz_Neon3",kpx12,kpz12,1.,"Calculated
    electron momentum kx kz",400,-10.,10.,"kx [au]",400,-10.,10.,"
    kz [au]","Isotropy3");
Hist->fill2(3212,"12_kpz_kpy_Neon3",kpz12,kpy12,1.,"Calculated
    electron momentum kz ky",400,-10.,10.,"kz [au]",400,-10.,10.,"
    ky [au]","Isotropy3");

Hist->fill2(3213,"13_epx_epy_Neon3",epx2,epy2,1.,"2Measured
    electron momentum kx ky",400,-1.,1.,"ex [au]",400,-1.,1.,"ey [
    au]","Isotropy3");
Hist->fill2(3214,"14_epx_epz_Neon3",epx2,epz2,1.,"2Measured
    electron momentum kx kz",400,-1.,1.,"ex [au]",400,-1.,1.,"ez [
    au]","Isotropy3");
Hist->fill2(3215,"15_epz_epy_Neon3",epz2,epy2,1.,"2Measured
    electron momentum kz ky",400,-1.,1.,"ez [au]",400,-1.,1.,"ey [
    au]","Isotropy3");

Hist->fill1(3216,"16_Flat-photo_Cosx-hit1",epx2/epr2,1.,"Photo-
    Electron-Angular-Distribution",400,-1.,1.,"Cosx","Isotropy3");
Hist->fill1(3217,"17_Flat-photo_Cosx-corrected",epx2/epr2,1,"
    Photo-Electron-Angular-Distribution",400,-1.,1.,"Cosx","
    Isotropy3");

Hist->fill1(3218,"18_Photo-Electron-Energy_Neon3",eE2,1,"Photo-
    Electron Energy",350,0.5,2.5,"E [eV]","Isotropy3");
```

```
Hist->fill2(3219,"19_Cos_Energy",par2/epr2,eE2,1,"Cos_Energy
    ",100,-1.,1.,"cos(theta)",350,0.5,2.5,"Electron Energy [eV]","
    Isotropy3");
Hist->fill1(3220,"20_Energy-Photo-Proy",par2/epr2,1,"Energy
    ",350,0.5,2.5,"Electron Energy [eV]","Isotropy3");

Hist->fill1(3221,"21_Photo_Cosx_Neon3",epx2/epr2,1,"Auger Cosx
    ",100,-1.,1.,"Cos(#theta_{x})","Isotropy3");
Hist->fill1(3222,"22_Photo_Cosy_Neon3",epy2/epr2,1,"Auger Cosy
    ",100,-1.,1.,"cosy","Isotropy3");
Hist->fill1(3223,"23_Photo_Cosz_Neon3",epz2/epr2,1,"Auger Cosz
    ",100,-1.,1.,"cosz","Isotropy3");

Hist->fill1(3224,"24_Photo_Ne3",phi,1,"Photo-Electron Angle
    ",100,-pi,pi,"Photo-Electron [deg]","Isotropy3");
Hist->fill1(3225,"25_Photo_Ne2-corrected",phi*180./pi,weight3D(
    phi,parameter[1900]),"Photo-Electron Angle",100,-180.,180.,"
    Photo-Electron [deg]","Isotropy3");
//////////////

if (eE1<kE12) Hist->fill2(3301,"01_Auger_Energy_Sharing",eE1,kE12
    ,1,"Energy Sharing (Fast Electrons)",100,0.,900.,"Measured
    First Hit Electron [eV]",100,0.,900.,"Calculated Electron [eV
    ]","Energy3");
```

```
if (eE1<kE12) Hist->fill2(3301,"01_Auger_Energy_Sharing",kE12,eE1
    ,1,"Energy Sharing (Fast Electrons)",100,0.,900.,"Measured
    First Hit Electron [eV]",100,0.,900.,"Calculated Electron [eV
    ]","Energy3");

if (eE1+kE12>650. && eE1+kE12<900.) {//eE1+kE12>660. && eE1+kE12
    <760.
if (eE1<kE12) {//eE1<380.
Hist->fill2(3302,"02_Auger_Energy_Sharing_Gated",eE1,kE12,1,"
    Energy Sharing (Fast Electrons) Gated",100,0.,900.,"Measured
    First Hit Electron, [eV]",100,0.,900.,"Calculated First
    Electron, [eV]","Energy3");
Hist->fill1(3303,"Smile",eE1,1.,"Energy Sharing (Fast Electrons)
    ",50,0.,760.,"[eV]","Energy3");
Hist->fill1(3303,"Smile",760.-eE1,1.,"Energy Sharing (Fast
    Electrons)",50,0.,760.,"[eV]","Energy3");
if (eE1>g3 && eE1<g4) Hist->fill2(3304,"03_Energy_AP_Cosine",par4
    /epr2,eE2,1,"Energy vs. Cosine AP",50,-1.,1.,"Cosine
    ",50,0.,3.5,"Auger Energy, [eV]","Energy3");
Hist->fill2(3305,"04_Energy_AA_Cosine",par3a/epr1,eE1,1,"Energy
    vs. Cosine AA",50,-1.,1.,"Cosine",50,0.,380,"Auger Energy, [eV
    ]","Energy3");
if (eE1<5.5) Hist->fill2(3306,"05_Energy_AA_Cosine_low",par3b/
    epr1,eE1,1,"Energy vs. Cosine AP",50,-1.,1.,"Cosine
    ",50,0.,5.5,"Auger Energy, [eV]","Energy3");
}
```

```
if (eE1>g1 && eE1<g2){//Correlation between Calculated Auger and
    Photo-Electron
if(phi3-phi2<0.) Hist->fill1(3307,"angular_photo1",acos(par4/epr2
    )*180./pi,sin_inv4,"CosNe3sum",bin1,-180.,180.,"cos(theta)","
    Energy3");
if(phi3-phi2>0.) Hist->fill1(3307,"angular_photo1",-acos(par4/
    epr2)*180./pi,sin_inv4,"CosNe3sum",bin1,-180.,180.,"cos(theta)
    ","Energy3");
}

if (eE1>g2 && eE1<g3){
if(phi3-phi2<0.) Hist->fill1(3308,"angular_photo2",acos(par4/epr2
    )*180./pi,sin_inv4,"CosNe3sum",bin1,-180.,180.,"cos(theta)","
    Energy3");
if(phi3-phi2>0.) Hist->fill1(3308,"angular_photo2",-acos(par4/
    epr2)*180./pi,sin_inv4,"CosNe3sum",bin1,-180.,180.,"cos(theta)
    ","Energy3");
}

if (eE1>g3 && eE1<g4){
if(phi3-phi2<0.) Hist->fill1(3309,"angular_photo3",acos(par4/epr2
    )*180./pi,sin_inv4,"CosNe3sum",bin1,-180.,180.,"cos(theta)","
    Energy3");
if(phi3-phi2>0.) Hist->fill1(3309,"angular_photo3",-acos(par4/
    epr2)*180./pi,sin_inv4,"CosNe3sum",bin1,-180.,180.,"cos(theta)
    ","Energy3");
}
```

```
if (eE1>g1 && eE1<g2){//Correlation between Measured Auger and
    Photo-Electron
if(phi1-phi2<0.) Hist->fill1(3310,"angular_photo1a",acos(par1a/
    epr2)*180./pi,sin_inv1a*weight3D(phi,parameter[1900]),"
    CosNe3sum",bin1,-180.,180.,"cos(theta)","Energy3");
if(phi1-phi2>0.) Hist->fill1(3310,"angular_photo1a",-acos(par1a/
    epr2)*180./pi,sin_inv1a,"CosNe3sum",bin1,-180.,180.,"cos(theta
    )","Energy3");
}

if (eE1>g2 && eE1<g3){
if(phi1-phi2<0.) Hist->fill1(3311,"angular_photo2a",acos(par1a/
    epr2)*180./pi,sin_inv1a,"CosNe3sum",bin1,-180.,180.,"cos(theta
    )","Energy3");
if(phi1-phi2>0.) Hist->fill1(3311,"angular_photo2a",-acos(par1a/
    epr2)*180./pi,sin_inv1a,"CosNe3sum",bin1,-180.,180.,"cos(theta
    )","Energy3");
}

if (eE1>g3 && eE1<g4){
if(phi1-phi2<0.) Hist->fill1(3312,"angular_photo3a",acos(par1a/
    epr2)*180./pi,sin_inv1a,"CosNe3sum",bin1,-180.,180.,"cos(theta
    )","Energy3");
if(phi1-phi2>0.) Hist->fill1(3312,"angular_photo3a",-acos(par1a/
    epr2)*180./pi,sin_inv1a,"CosNe3sum",bin1,-180.,180.,"cos(theta
    )","Energy3");
```

```
}

if (eE1>g1 && eE1<g2){//Correlation between Calculated Auger and
    Auger Electron
if(phi3-phi1<0.) Hist->fill1(3313,"angular_Auger1",acos(par3a/
    epr1)*180./pi,sin_inv3b,"CosNe3sum",bin2,-180.,180.,"cos(theta
    )","Energy3");
if(phi3-phi1>0.) Hist->fill1(3313,"angular_Auger1",-acos(par3a/
    epr1)*180./pi,sin_inv3b,"CosNe3sum",bin2,-180.,180.,"cos(theta
    )","Energy3");
}

if (eE1>g2 && eE1<g3){
if(phi3-phi1<0.) Hist->fill1(3314,"angular_Auger2",acos(par3a/
    epr1)*180./pi,sin_inv3b,"CosNe3sum",bin2,-180.,180.,"cos(theta
    )","Energy3");
if(phi3-phi1>0.) Hist->fill1(3314,"angular_Auger2",-acos(par3a/
    epr1)*180./pi,sin_inv3b,"CosNe3sum",bin2,-180.,180.,"cos(theta
    )","Energy3");
}

if (eE1>g3 && eE1<g4){
if(phi3-phi1<0.) Hist->fill1(3315,"angular_Auger3",acos(par3a/
    epr1)*180./pi,sin_inv3b,"CosNe3sum",bin2,-180.,180.,"cos(theta
    )","Energy3");
```

```
if(phi3-phi1>0.) Hist->fill1(3315,"angular_Auger3",-acos(par3a/
    epr1)*180./pi,sin_inv3b,"CosNe3sum",bin2,-180.,180.,"cos(theta
    )","Energy3");
}

if (eE1>g1 && eE1<g2){//Correlation between kSum and Photo-
    Electron
if(phi3-phi1<0.) Hist->fill1(3316,"angular_kSum1",acos(par2/epr2)
    *180./pi,sin_inv2,"CosNe3sum",bin3,-180.,180.,"cos(theta)","
    Energy3");
if(phi3-phi1>0.) Hist->fill1(3316,"angular_kSum1",-acos(par2/epr2
    )*180./pi,sin_inv2,"CosNe3sum",bin3,-180.,180.,"cos(theta)","
    Energy3");
}

if (eE1>g2 && eE1<g3){
if(phi3-phi1<0.) Hist->fill1(3317,"angular_kSum2",acos(par2/epr2)
    *180./pi,sin_inv2,"CosNe3sum",bin3,-180.,180.,"cos(theta)","
    Energy3");
if(phi3-phi1>0.) Hist->fill1(3317,"angular_kSum2",-acos(par2/epr2
    )*180./pi,sin_inv2,"CosNe3sum",bin3,-180.,180.,"cos(theta)","
    Energy3");
}

if (eE1>g3 && eE1<g4){
```

```
if(phi3-phi1<0.) Hist->fill1(3318,"angular_kSum3",acos(par2/epr2)
    *180./pi,sin_inv2,"CosNe3sum",bin3,-180.,180.,"cos(theta)","
    Energy3");
if(phi3-phi1>0.) Hist->fill1(3318,"angular_kSum3",-acos(par2/epr2
    )*180./pi,sin_inv2,"CosNe3sum",bin3,-180.,180.,"cos(theta)","
    Energy3");
}
}
}
if (Neon3 && Elec2 && Elec3 && eE3<2.5 && Cone2){//Assumes 3rd
    hit is photo-electron
if (eE1<kE23) Hist->fill2(3301,"01_Auger_Energy_Sharing",eE2,kE23
    ,1,"Energy Sharing (Fast Electrons)",100,0.,900.,"Measured
    First Hit Electron [eV]",100,0.,900.,"Calculated Electron [eV
    ]","Energy3");
if (eE1<kE23) Hist->fill2(3301,"01_Auger_Energy_Sharing",kE23,eE2
    ,1,"Energy Sharing (Fast Electrons)",100,0.,900.,"Measured
    First Hit Electron [eV]",100,0.,900.,"Calculated Electron [eV
    ]","Energy3");
if (eE2+kE23>650. && eE2+kE23<900.) {//eE1+kE12>660. && eE1+kE12
    <760.
if (eE2<kE23) {//eE1<380.
Hist->fill2(3302,"02_Auger_Energy_Sharing_Gated",eE2,kE23,1,"
    Energy Sharing (Fast Electrons) Gated",100,0.,900.,"Measured
    First Hit Electron, [eV]",100,0.,900.,"Calculated First
    Electron, [eV]","Energy3");
```

```
Hist->fill1(3303,"Smile",eE2,1.,"Energy Sharing (Fast Electrons)
    ",50,0.,760.,"[eV]","Energy3");
Hist->fill1(3303,"Smile",760.-eE2,1.,"Energy Sharing (Fast
    Electrons)",50,0.,760.,"[eV]","Energy3");
}
}
}

//Pweight Section
g1=10.0;
g2=50.;
g3=280.;
g4=380.;
if (Neon3 && Elec1 && Elec2 && eE2<2.5 && Cone1 && eE1>10.0){//
    Assumes 2nd hit is photo-electron, 1st hit Auger
double weight = pweightalt(phi2,parameter[2001])*pweight2alt(epz2
    /epr2,parameter[2001]);
Hist->fill2(3401,"01_epx_epy_Neon3",epx2,epy2,weight,"Photo-
    Electron Momentum (Corrected)",100,-0.5,0.5,"Time-Axis [au
    ]",100,-0.5,0.5,"Jet-Axis [au]","Pweight3");
Hist->fill2(3402,"02_epy_epz_Neon3",epz2,epy2,weight,"Photo-
    Electron Momentum (Corrected)",100,-0.5,0.5,"Beam-Axis [au
    ]",100,-0.5,0.5,"Jet-Axis [au]","Pweight3");
Hist->fill2(3403,"03_epx_epz_Neon3",epx2,epz2,weight,"Photo-
    Electron Momentum (Corrected)",100,-0.5,0.5,"Time-Axis [au
    ]",100,-0.5,0.5,"Beam-Axis [au]","Pweight3");
```

```
Hist->fill1(3404,"04_Photo_Ellipticity_Ne3",phi2,weight,"Photo-
    Electron Angle (Corrected)",100,-pi,pi,"Photo-Electron [#phi_{
    TOF}]","Pweight3");

Hist->fill2(3405,"05_donut_cross_Neon3_unweighted",sqrt(epx2*epx2
     + epy2*epy2),epz2,(epr2/sqrt(epx2*epx2 + epy2*epy2)),"Cross
    Section of Photo-Electron Distribution",400,-1.,1.,"e#_{perp}
    [au]",400,-1.,1.,"ez [au]","Pweight3");
Hist->fill2(3406,"06_donut_cross_Neon3",sqrt(epx2*epx2 + epy2*
    epy2),epz2,weight*(epr2/sqrt(epx2*epx2 + epy2*epy2)),"Cross
    Section of Photo-Electron Distribution",400,-1.,1.,"e#_{perp}
    [au]",400,-1.,1.,"ez [au]","Pweight3");

Hist->fill1(3407,"07_counts_cosz",epz2/epr2,weight,"Photo-
    Electron Angle (Corrected)",100,-1,1,"Photo-Electron [#theta
    ]","Pweight3");

if (eE1<90.){//centroid of energy range is 34.1eV
Hist->fill1(3408,"08_photo_Auger34",acos(par1a/epr2)*180./pi,
    sin_inv1a*weight,"CosNe3sum",25,-180.,180.,"Cos(#theta)","
    Pweight3");
Hist->fill1(3408,"08_photo_Auger34",-acos(par1a/epr2)*180./pi,
    sin_inv1a*weight,"CosNe3sum",25,-180.,180.,"Cos(#theta)","
    Pweight3");
Hist->fill1(3409,"09_cos_photo_Auger34",par1a/epr2,weight,"
    cos_photo_Auger34",12,-1,1,"Events","Pweight3");
}
```

```
Hist->fill1(3410,"eE1_all_unweighted",eE1,1.,"Energy of Electron
    1",60,0,180,"Energy [eV]","Pweight3");
Hist->fill1(3411,"eE1_all",eE1,weight,"Energy of Electron
    1",60,0,180,"Energy [eV]","Pweight3");

Hist->fill1(3412,"eE1_zoom_unweighted",eE1,1.,"Energy of Electron
     1",60,0,90,"Energy [eV]","Pweight3");
Hist->fill1(3413,"eE1_zoom",eE1,weight,"Energy of Electron
    1",60,0,90,"Energy [eV]","Pweight3");

Hist->fill2(3414,"splish-splash_unweighted",par1a/epr2,eE1,1.,"
    Splash Effect",20,-1.,1.,"Cos(#theta)",17,10.,180.,"Auger
    Energy [eV]","Pweight3");
Hist->fill2(3415,"splish-splash",par1a/epr2,eE1,weight,"Splash
    Effect",20,-1.,1.,"Cos(#theta)",18,10.,90.,"Auger Energy [eV
    ]","Pweight3");

if (eE1>g1 && eE1<g2){//Correlation between Calculated Auger and
    Photo-Electron
Hist->fill1(3417,"angular_photo1",acos(par4/epr2)*180./pi,
    sin_inv4*weight,"CosNe3sum",bin1,-180.,180.,"Cos(#theta)","
    Pweight3");
 Hist->fill1(3417,"angular_photo1",-acos(par4/epr2)*180./pi,
     sin_inv4*weight,"CosNe3sum",bin1,-180.,180.,"Cos(#theta)","
     Pweight3");
}
```

```
if (eE1>g2 && eE1<g3){
Hist->fill1(3418,"angular_photo2",acos(par4/epr2)*180./pi,
    sin_inv4*weight,"CosNe3sum",bin1,-180.,180.,"Cos(#theta)","
    Pweight3");
Hist->fill1(3418,"angular_photo2",-acos(par4/epr2)*180./pi,
    sin_inv4*weight,"CosNe3sum",bin1,-180.,180.,"Cos(#theta)","
    Pweight3");
}

if (eE1>g3 && eE1<g4){
Hist->fill1(3419,"angular_photo3",acos(par4/epr2)*180./pi,
    sin_inv4*weight,"CosNe3sum",bin1,-180.,180.,"Cos(#theta)","
    Pweight3");
 Hist->fill1(3419,"angular_photo3",-acos(par4/epr2)*180./pi,
     sin_inv4*weight,"CosNe3sum",bin1,-180.,180.,"Cos(#theta)","
     Pweight3");
}

if (eE1>g1 && eE1<g2){//Correlation between Measured Auger and
    Photo-Electron
Hist->fill1(3421,"angular_photo1a",acos(par1a/epr2)*180./pi,
    sin_inv1a*weight,"CosNe3sum",bin1,-180.,180.,"Cos(#theta)","
    Pweight3");
Hist->fill1(3421,"angular_photo1a",-acos(par1a/epr2)*180./pi,
    sin_inv1a*weight,"CosNe3sum",bin1,-180.,180.,"Cos(#theta)","
    Pweight3");
```

```
}

if (eE1>g2 && eE1<g3){
Hist->fill1(3422,"angular_photo2a",acos(par1a/epr2)*180./pi,
    sin_inv1a*weight,"CosNe3sum",bin1,-180.,180.,"Cos(#theta)","
    Pweight3");
Hist->fill1(3422,"angular_photo2a",-acos(par1a/epr2)*180./pi,
    sin_inv1a*weight,"CosNe3sum",bin1,-180.,180.,"Cos(#theta)","
    Pweight3");
}

if (eE1>g3 && eE1<g4){
Hist->fill1(3423,"angular_photo3a",acos(par1a/epr2)*180./pi,
    sin_inv1a*weight,"CosNe3sum",bin1,-180.,180.,"Cos(#theta)","
    Pweight3");
Hist->fill1(3423,"angular_photo3a",-acos(par1a/epr2)*180./pi,
    sin_inv1a*weight,"CosNe3sum",bin1,-180.,180.,"Cos(#theta)","
    Pweight3");
}

if (eE1>g1 && eE1<g2){//Correlation between Calculated Auger and
    Auger Electron
Hist->fill1(3425,"angular_Auger1",acos(par3b/kpr12)*180./pi,
    sin_inv3b*weight,"CosNe3sum",bin2,-180.,180.,"Cos(#theta)","
    Pweight3");
```

```
Hist->fill1(3425,"angular_Auger1",-acos(par3b/kpr12)*180./pi,
    sin_inv3b*weight,"CosNe3sum",bin2,-180.,180.,"Cos(#theta)","
    Pweight3");
}

if (eE1>g2 && eE1<g3){
Hist->fill1(3426,"angular_Auger2",acos(par3b/kpr12)*180./pi,
    sin_inv3b*weight,"CosNe3sum",bin2,-180.,180.,"Cos(#theta)","
    Pweight3");
Hist->fill1(3426,"angular_Auger2",-acos(par3b/kpr12)*180./pi,
    sin_inv3b*weight,"CosNe3sum",bin2,-180.,180.,"Cos(#theta)","
    Pweight3");
}

if (eE1>g3 && eE1<g4){
Hist->fill1(3427,"angular_Auger3",acos(par3b/kpr12)*180./pi,
    sin_inv3b*weight,"CosNe3sum",bin2,-180.,180.,"Cos(#theta)","
    Pweight3");
Hist->fill1(3427,"angular_Auger3",-acos(par3b/kpr12)*180./pi,
    sin_inv3b*weight,"CosNe3sum",bin2,-180.,180.,"Cos(#theta)","
    Pweight3");
}

if (eE1>g1 && eE1<g2){//Correlation between kSum and Photo-
    Electron
Hist->fill1(3429,"angular_kSum1",acos(par2/epr2)*180./pi,sin_inv2
    *weight,"CosNe3sum",bin3,-180.,180.,"Cos(#theta)","Pweight3");
```

```
Hist->fill1(3429,"angular_kSum1",-acos(par2/epr2)*180./pi,
    sin_inv2*weight,"CosNe3sum",bin3,-180.,180.,"Cos(#theta)","
    Pweight3");
}

if (eE1>g2 && eE1<g3){
Hist->fill1(3430,"angular_kSum2",acos(par2/epr2)*180./pi,sin_inv2
    *weight,"CosNe3sum",bin3,-180.,180.,"Cos(#theta)","Pweight3");
Hist->fill1(3430,"angular_kSum2",-acos(par2/epr2)*180./pi,
    sin_inv2*weight,"CosNe3sum",bin3,-180.,180.,"Cos(#theta)","
    Pweight3");
}

if (eE1>g3 && eE1<g4){
Hist->fill1(3431,"angular_kSum3",acos(par2/epr2)*180./pi,sin_inv2
    *weight,"CosNe3sum",bin3,-180.,180.,"Cos(#theta)","Pweight3");
Hist->fill1(3431,"angular_kSum3",-acos(par2/epr2)*180./pi,
    sin_inv2*weight,"CosNe3sum",bin3,-180.,180.,"Cos(#theta)","
    Pweight3");
}
}

//adding in the 2nd 3rd hit events
if (Neon3 && Elec2 && Elec3 && eE3<2.5 && Cone2 && eE2>10.0){//
    Assumes 3rd hit is photo-electron, 2nd hit Auger
double weight = pweightalt(phi2a,parameter[2001])*pweight2alt(
    epz3/epr3,parameter[2001]);
```

```
Hist->fill2(3401,"01_epx_epy_Neon3",epx3,epy3,weight,"Photo-
    Electron Momentum (Corrected)",100,-0.5,0.5,"Time-Axis [au
    ]",100,-0.5,0.5,"Jet-Axis [au]","Pweight3");
Hist->fill2(3402,"02_epy_epz_Neon3",epz3,epy3,weight,"Photo-
    Electron Momentum (Corrected)",100,-0.5,0.5,"Beam-Axis [au
    ]",100,-0.5,0.5,"Jet-Axis [au]","Pweight3");
Hist->fill2(3403,"03_epx_epz_Neon3",epx3,epz3,weight,"Photo-
    Electron Momentum (Corrected)",100,-0.5,0.5,"Time-Axis [au
    ]",100,-0.5,0.5,"Beam-Axis [au]","Pweight3");

Hist->fill1(3404,"04_Photo_Ellipticity_Ne3",phi2a,weight,"Photo-
    Electron Angle (Corrected)",100,-pi,pi,"Photo-Electron [#phi_{
    TOF}]","Pweight3");

Hist->fill2(3405,"05_donut_cross_Neon3_unweighted",sqrt(epx3*epx3
     + epy3*epy3),epz3,(epr3/sqrt(epx3*epx3 + epy3*epy3)),"Cross
    Section of Photo-Electron Distribution",400,-1.,1.,"e#_{perp}
    [au]",400,-1.,1.,"ez [au]","Pweight3");
Hist->fill2(3406,"06_donut_cross_Neon3",sqrt(epx3*epx3 + epy3*
    epy3),epz3,weight*(epr3/sqrt(epx3*epx3 + epy3*epy3)),"Cross
    Section of Photo-Electron Distribution",400,-1.,1.,"e#_{perp}
    [au]",400,-1.,1.,"ez [au]","Pweight3");

Hist->fill1(3407,"07_counts_cosz",epz3/epr3,weight,"Photo-
    Electron Angle (Corrected)",100,-1,1,"Photo-Electron [#theta
    ]","Pweight3");
```

```
if (eE1<90.){//centroid of energy range is 34.1eV
Hist->fill1(3408,"08_photo_Auger34",acos(par1b/epr3)*180./pi,
    sin_inv1b*weight,"CosNe3sum",25,-180.,180.,"Cos(#theta)","
    Pweight3");
Hist->fill1(3408,"08_photo_Auger34",-acos(par1b/epr3)*180./pi,
    sin_inv1b*weight,"CosNe3sum",25,-180.,180.,"Cos(#theta)","
    Pweight3");
Hist->fill1(3409,"09_cos_photo_Auger34",par1b/epr3,weight,"
    cos_photo_Auger34",12,-1,1,"Events","Pweight3");
}

Hist->fill1(3410,"eE1_all_unweighted",eE2,1.,"Energy of Electron
    1",60,0,180,"Energy [eV]","Pweight3");
Hist->fill1(3411,"eE1_all",eE2,weight,"Energy of Electron
    1",60,0,180,"Energy [eV]","Pweight3");

Hist->fill1(3412,"eE1_zoom_unweighted",eE2,1.,"Energy of Electron
     1",60,0,90,"Energy [eV]","Pweight3");
Hist->fill1(3413,"eE1_zoom",eE2,weight,"Energy of Electron
    1",60,0,90,"Energy [eV]","Pweight3");

Hist->fill2(3414,"splish-splash_unweighted",par1b/epr3,eE2,1.,"
    Splash Effect",20,-1.,1.,"Cos(#theta)",17,10.,180.,"Auger
    Energy [eV]","Pweight3");
Hist->fill2(3415,"splish-splash",par1b/epr3,eE2,weight,"Splash
    Effect",20,-1.,1.,"Cos(#theta)",18,10.,90.,"Auger Energy [eV
    ]","Pweight3");
```

```
if (eE1>g1 && eE1<g2){//Correlation between Calculated Auger and
    Photo-Electron
Hist->fill1(3417,"angular_photo1",acos(par6/epr3)*180./pi,
    sin_inv6*weight,"CosNe3sum",bin1,-180.,180.,"Cos(#theta)","
    Pweight3");
Hist->fill1(3417,"angular_photo1",-acos(par6/epr3)*180./pi,
    sin_inv6*weight,"CosNe3sum",bin1,-180.,180.,"Cos(#theta)","
    Pweight3");
}

if (eE1>g2 && eE1<g3){
Hist->fill1(3418,"angular_photo2",acos(par6/epr3)*180./pi,
    sin_inv6*weight,"CosNe3sum",bin1,-180.,180.,"Cos(#theta)","
    Pweight3");
Hist->fill1(3418,"angular_photo2",-acos(par6/epr3)*180./pi,
    sin_inv6*weight,"CosNe3sum",bin1,-180.,180.,"Cos(#theta)","
    Pweight3");
}

if (eE1>g3 && eE1<g4){
Hist->fill1(3419,"angular_photo3",acos(par6/epr3)*180./pi,
    sin_inv6*weight,"CosNe3sum",bin1,-180.,180.,"Cos(#theta)","
    Pweight3");
Hist->fill1(3419,"angular_photo3",-acos(par6/epr3)*180./pi,
    sin_inv6*weight,"CosNe3sum",bin1,-180.,180.,"Cos(#theta)","
    Pweight3");
```

```
}

if (eE1>g1 && eE1<g2){//Correlation between Measured Auger and
    Photo-Electron
Hist->fill1(3421,"angular_photo1a",acos(par1b/epr3)*180./pi,
    sin_inv1b*weight,"CosNe3sum",bin1,-180.,180.,"Cos(#theta)","
    Pweight3");
Hist->fill1(3421,"angular_photo1a",-acos(par1b/epr3)*180./pi,
    sin_inv1b*weight,"CosNe3sum",bin1,-180.,180.,"Cos(#theta)","
    Pweight3");
}

if (eE1>g2 && eE1<g3){
Hist->fill1(3422,"angular_photo2a",acos(par1b/epr3)*180./pi,
    sin_inv1b*weight,"CosNe3sum",bin1,-180.,180.,"Cos(#theta)","
    Pweight3");
Hist->fill1(3422,"angular_photo2a",-acos(par1b/epr3)*180./pi,
    sin_inv1b*weight,"CosNe3sum",bin1,-180.,180.,"Cos(#theta)","
    Pweight3");
}

if (eE1>g3 && eE1<g4){
Hist->fill1(3423,"angular_photo3a",acos(par1b/epr3)*180./pi,
    sin_inv1b*weight,"CosNe3sum",bin1,-180.,180.,"Cos(#theta)","
    Pweight3");
```

```
Hist->fill1(3423,"angular_photo3a",-acos(par1b/epr3)*180./pi,
    sin_inv1b*weight,"CosNe3sum",bin1,-180.,180.,"Cos(#theta)","
    Pweight3");
}

if (eE1>g1 && eE1<g2){//Correlation between Calculated Auger and
    Auger Electron
Hist->fill1(3425,"angular_Auger1",acos(par5/kpr23)*180./pi,
    sin_inv5*weight,"CosNe3sum",bin2,-180.,180.,"Cos(#theta)","
    Pweight3");
Hist->fill1(3425,"angular_Auger1",-acos(par5/kpr23)*180./pi,
    sin_inv5*weight,"CosNe3sum",bin2,-180.,180.,"Cos(#theta)","
    Pweight3");
}

if (eE1>g2 && eE1<g3){
Hist->fill1(3426,"angular_Auger2",acos(par5/kpr23)*180./pi,
    sin_inv5*weight,"CosNe3sum",bin2,-180.,180.,"Cos(#theta)","
    Pweight3");
Hist->fill1(3426,"angular_Auger2",-acos(par5/kpr23)*180./pi,
    sin_inv5*weight,"CosNe3sum",bin2,-180.,180.,"Cos(#theta)","
    Pweight3");
}

if (eE1>g3 && eE1<g4){
```

```
Hist->fill1(3427,"angular_Auger3",acos(par5/kpr23)*180./pi,
    sin_inv5*weight,"CosNe3sum",bin2,-180.,180.,"Cos(#theta)","
    Pweight3");
Hist->fill1(3427,"angular_Auger3",-acos(par5/kpr23)*180./pi,
    sin_inv5*weight,"CosNe3sum",bin2,-180.,180.,"Cos(#theta)","
    Pweight3");
}

if (eE1>g1 && eE1<g2){//Correlation between kSum and Photo-
    Electron
Hist->fill1(3429,"angular_kSum1",acos(par3/epr3)*180./pi,sin_inv3
    *weight,"CosNe3sum",bin3,-180.,180.,"Cos(#theta)","Pweight3");
Hist->fill1(3429,"angular_kSum1",-acos(par3/epr3)*180./pi,
    sin_inv3*weight,"CosNe3sum",bin3,-180.,180.,"Cos(#theta)","
    Pweight3");
}

if (eE1>g2 && eE1<g3){
Hist->fill1(3430,"angular_kSum2",acos(par3/epr3)*180./pi,sin_inv3
    *weight,"CosNe3sum",bin3,-180.,180.,"Cos(#theta)","Pweight3");
Hist->fill1(3430,"angular_kSum2",-acos(par3/epr3)*180./pi,
    sin_inv3*weight,"CosNe3sum",bin3,-180.,180.,"Cos(#theta)","
    Pweight3");
}

if (eE1>g3 && eE1<g4){
```

```
Hist->fill1(3431,"angular_kSum3",acos(par3/epr3)*180./pi,sin_inv3
    *weight,"CosNe3sum",bin3,-180.,180.,"Cos(#theta)","Pweight3");
Hist->fill1(3431,"angular_kSum3",-acos(par3/epr3)*180./pi,
    sin_inv3*weight,"CosNe3sum",bin3,-180.,180.,"Cos(#theta)","
    Pweight3");
}
}

if (Neon3 && Elec1 && Elec3 && eE3<2.5 && Cone1 && eE1>10.0){//
    Assumes 3rd hit is photo-electron, 1st hit Auger
double weight = pweightalt(phi2a,parameter[2001])*pweight2alt(
    epz3/epr3,parameter[2001]);
Hist->fill2(3401,"01_epx_epy_Neon3",epx3,epy3,weight,"Photo-
    Electron Momentum (Corrected)",100,-0.5,0.5,"Time-Axis [au
    ]",100,-0.5,0.5,"Jet-Axis [au]","Pweight3");
Hist->fill2(3402,"02_epy_epz_Neon3",epy3,epz3,weight,"Photo-
    Electron Momentum (Corrected)",100,-0.5,0.5,"Jet-Axis [au
    ]",100,-0.5,0.5,"Beam-Axis [au]","Pweight3");
Hist->fill2(3403,"03_epx_epz_Neon3",epx3,epz3,weight,"Photo-
    Electron Momentum (Corrected)",100,-0.5,0.5,"Time-Axis [au
    ]",100,-0.5,0.5,"Beam-Axis [au]","Pweight3");

Hist->fill1(3404,"04_Photo_Ellipticity_Ne3",phi2a,weight,"Photo-
    Electron Angle (Corrected)",100,-pi,pi,"Photo-Electron [#phi_{
    TOF}]","Pweight3");
```

```
Hist->fill2(3405,"05_donut_cross_Neon3_unweighted",sqrt(epx3*epx3
    + epy3*epy3),epz3,(epr3/sqrt(epx3*epx3 + epy3*epy3)),"Cross
    Section of Photo-Electron Distribution",400,-1.,1.,"e#_{perp}
    [au]",400,-1.,1.,"ez [au]","Pweight3");
Hist->fill2(3406,"06_donut_cross_Neon3",sqrt(epx3*epx3 + epy3*
    epy3),epz3,weight*(epr3/sqrt(epx3*epx3 + epy3*epy3)),"Cross
    Section of Photo-Electron Distribution",400,-1.,1.,"e#_{perp}
    [au]",400,-1.,1.,"ez [au]","Pweight3");

Hist->fill1(3407,"07_counts_cosz",epz3/epr3,weight,"Photo-
    Electron Angle (Corrected)",100,-1,1,"Photo-Electron [#theta_{
    TOF}]","Pweight3");

if (eE1<90.){//centroid of energy range is 34.1eV
Hist->fill1(3408,"08_photo_Auger34",acos(par1c/epr3)*180./pi,
    sin_inv1c*weight,"CosNe3sum",25,-180.,180.,"Cos(#theta)","
    Pweight3");
Hist->fill1(3408,"08_photo_Auger34",-acos(par1c/epr3)*180./pi,
    sin_inv1c*weight,"CosNe3sum",25,-180.,180.,"Cos(#theta)","
    Pweight3");
Hist->fill1(3409,"09_cos_photo_Auger34",par1c/epr3,weight,"
    cos_photo_Auger34",12,-1,1,"Events","Pweight3");
}

Hist->fill1(3410,"eE1_all_unweighted",eE1,1.,"Energy of Electron
    1",60,0,180,"Energy [eV]","Pweight3");
```

```
Hist->fill1(3411,"eE1_all",eE1,weight,"Energy of Electron
    1",60,0,180,"Energy [eV]","Pweight3");

Hist->fill1(3412,"eE1_zoom_unweighted",eE1,1.,"Energy of Electron
     1",60,0,90,"Energy [eV]","Pweight3");
Hist->fill1(3413,"eE1_zoom",eE1,weight,"Energy of Electron
    1",60,0,90,"Energy [eV]","Pweight3");

Hist->fill2(3414,"splish-splash_unweighted",par1c/epr3,eE1,1.,"
    Splash Effect",20,-1.,1.,"Cos(#theta)",17,10.,180.,"Auger
    Energy [eV]","Pweight3");
Hist->fill2(3415,"splish-splash",par1c/epr3,eE1,weight,"Splash
    Effect",20,-1.,1.,"Cos(#theta)",18,10.,90.,"Auger Energy [eV
    ]","Pweight3");

if (eE1>g1 && eE1<g2){//Correlation between Calculated Auger and
    Photo-Electron
Hist->fill1(3417,"angular_photo1",acos(par4a/epr3)*180./pi,
    sin_inv4a*weight,"CosNe3sum",bin1,-180.,180.,"Cos(#theta)","
    Pweight3");
Hist->fill1(3417,"angular_photo1",-acos(par4a/epr3)*180./pi,
    sin_inv4a*weight,"CosNe3sum",bin1,-180.,180.,"Cos(#theta)","
    Pweight3");
}

if (eE1>g2 && eE1<g3){
```

```
Hist->fill1(3418,"angular_photo2",acos(par4a/epr3)*180./pi,
    sin_inv4a*weight,"CosNe3sum",bin1,-180.,180.,"Cos(#theta)","
    Pweight3");
Hist->fill1(3418,"angular_photo2",-acos(par4a/epr3)*180./pi,
    sin_inv4a*weight,"CosNe3sum",bin1,-180.,180.,"Cos(#theta)","
    Pweight3");
}

if (eE1>g3 && eE1<g4){
Hist->fill1(3419,"angular_photo3",acos(par4a/epr3)*180./pi,
    sin_inv4a*weight,"CosNe3sum",bin1,-180.,180.,"Cos(#theta)","
    Pweight3");
Hist->fill1(3419,"angular_photo3",-acos(par4a/epr3)*180./pi,
    sin_inv4a*weight,"CosNe3sum",bin1,-180.,180.,"Cos(#theta)","
    Pweight3");
}

if (eE1>g1 && eE1<g2){//Correlation between Measured Auger and
    Photo-Electron
Hist->fill1(3421,"angular_photo1a",acos(par1c/epr3)*180./pi,
    sin_inv1c*weight,"CosNe3sum",bin1,-180.,180.,"Cos(#theta)","
    Pweight3");
Hist->fill1(3421,"angular_photo1a",-acos(par1c/epr3)*180./pi,
    sin_inv1c*weight,"CosNe3sum",bin1,-180.,180.,"Cos(#theta)","
    Pweight3");
}
```

```
if (eE1>g2 && eE1<g3){
Hist->fill1(3422,"angular_photo2a",acos(par1c/epr3)*180./pi,
    sin_inv1c*weight,"CosNe3sum",bin1,-180.,180.,"Cos(#theta)","
    Pweight3");
Hist->fill1(3422,"angular_photo2a",-acos(par1c/epr3)*180./pi,
    sin_inv1c*weight,"CosNe3sum",bin1,-180.,180.,"Cos(#theta)","
    Pweight3");
}

if (eE1>g3 && eE1<g4){
Hist->fill1(3423,"angular_photo3a",acos(par1c/epr3)*180./pi,
    sin_inv1c*weight,"CosNe3sum",bin1,-180.,180.,"Cos(#theta)","
    Pweight3");
Hist->fill1(3423,"angular_photo3a",-acos(par1c/epr3)*180./pi,
    sin_inv1c*weight,"CosNe3sum",bin1,-180.,180.,"Cos(#theta)","
    Pweight3");
}

if (eE1>g1 && eE1<g2){//Correlation between Calculated Auger and
    Auger Electron
Hist->fill1(3425,"angular_Auger1",acos(par3c/kpr13)*180./pi,
    sin_inv3c*weight,"CosNe3sum",bin2,-180.,180.,"Cos(#theta)","
    Pweight3");
Hist->fill1(3425,"angular_Auger1",-acos(par3c/kpr13)*180./pi,
    sin_inv3c*weight,"CosNe3sum",bin2,-180.,180.,"Cos(#theta)","
    Pweight3");
}
```

```
if (eE1>g2 && eE1<g3){
Hist->fill1(3426,"angular_Auger2",acos(par3a/kpr13)*180./pi,
    sin_inv3b*weight,"CosNe3sum",bin2,-180.,180.,"Cos(#theta)","
    Pweight3");
Hist->fill1(3426,"angular_Auger2",-acos(par3a/kpr13)*180./pi,
    sin_inv3b*weight,"CosNe3sum",bin2,-180.,180.,"Cos(#theta)","
    Pweight3");
}

if (eE1>g3 && eE1<g4){
Hist->fill1(3427,"angular_Auger3",acos(par3a/kpr13)*180./pi,
    sin_inv3b*weight,"CosNe3sum",bin2,-180.,180.,"Cos(#theta)","
    Pweight3");
Hist->fill1(3427,"angular_Auger3",-acos(par3a/kpr13)*180./pi,
    sin_inv3b*weight,"CosNe3sum",bin2,-180.,180.,"Cos(#theta)","
    Pweight3");
}
}

if (Neon4 && Elec1 && Elec2 && Elec3){
Hist->fill2(4001,"01_epx1_epy1_Neon4",epx1,epy1,1.,"Electron
    momentum epx epy Hit 1",400,-10.,10.,"epx [au]",400,-10.,10.,"
    epy [au]","Momentum4");
Hist->fill2(4002,"02_epx1_epz1_Neon4",epx1,epz1,1.,"Electron
    momentum epx epz Hit 1",400,-10.,10.,"epx [au]",400,-10.,10.,"
    epz [au]","Momentum4");
```

```
Hist->fill2(4003,"03_epz1_epy1_Neon4",epz1,epy1,1.,"Electron
    momentum epz epy Hit 1",400,-10.,10.,"epz [au]",400,-10.,10.,"
    epy [au]","Momentum4");

Hist->fill2(4004,"04_epx2_epy2_Neon4",epx2,epy2,1.,"Electron
    momentum epx epy Hit 2",400,-6.,6.,"epx [au]",400,-6.,6.,"epy
    [au]","Momentum4");
Hist->fill2(4005,"05_epx2_epz2_Neon4",epx2,epz2,1.,"Electron
    momentum epx epz Hit 2",400,-6.,6.,"epx [au]",400,-6.,6.,"epz
    [au]","Momentum4");
Hist->fill2(4006,"06_epz2_epy2_Neon4",epz2,epy2,1.,"Electron
    momentum epz epy Hit 2",400,-6.,6.,"epz [au]",400,-6.,6.,"epy
    [au]","Momentum4");

Hist->fill2(4007,"07_epx3_epy3_Neon4",epx3,epy3,1.,"Electron
    momentum epx epy Hit 3",400,-6.,6.,"epx [au]",400,-6.,6.,"epy
    [au]","Momentum4");
Hist->fill2(4008,"08_epx3_epz3_Neon4",epx3,epz3,1.,"Electron
    momentum epx epz Hit 3",400,-6.,6.,"epx [au]",400,-6.,6.,"epz
    [au]","Momentum4");
Hist->fill2(4009,"09_epz3_epy3_Neon4",epz3,epy3,1.,"Electron
    momentum epz epy Hit 3",400,-6.,6.,"epz [au]",400,-6.,6.,"epy
    [au]","Momentum4");

Hist->fill2(4010,"10_r4px_r4py_Neon4",r4px,r4py,1.,"Recoil
    momentum px py",400,-10.,10.,"px [au]",400,-10.,10.,"py [au
    ]","Momentum4");
```

```
Hist->fill2(4011,"11_r4px_r4pz_Neon4",r4px,r4pz,1.,"Recoil
    momentum px pz",400,-10.,10.,"px [au]",400,-10.,10.,"pz [au
    ]","Momentum4");
Hist->fill2(4012,"12_r4pz_r4py_Neon4",r4pz,r4py,1.,"Recoil
    momentum pz py",400,-10.,10.,"pz [au]",400,-10.,10.,"py [au
    ]","Momentum4");

Hist->fill2(4013,"13_kpx123_kpy123_Neon4",kpx123,kpy123,1.,"
    Calculated electron momentum kx123 ky123",400,-10.,10.,"kx [au
    ]",400,-10.,10.,"ky [au]","Momentum4");
Hist->fill2(4014,"14_kpx123_kpz123_Neon4",kpx123,kpz123,1.,"
    Calculated electron momentum kx123 kz123",400,-10.,10.,"kx [au
    ]",400,-10.,10.,"kz [au]","Momentum4");
Hist->fill2(4015,"15_kpz123_kpy123_Neon4",kpz123,kpy123,1.,"
    Calculated electron momentum kz123 ky123",400,-10.,10.,"kz [au
    ]",400,-10.,10.,"ky [au]","Momentum4");

Hist->fill1(4016,"16_E1_Neon4-small",eE1,1.,"Electron Energy Hit
    1",100,0.,3.5,"E [eV]","Momentum4");
Hist->fill1(4017,"17_E1_Neon4-large",eE1,1.,"Electron Energy Hit
    1",300,0.,1200.,"E [eV]","Momentum4");
Hist->fill1(4018,"18_E2_Neon4-small",eE2,1.,"Electron Energy Hit
    2",75,0.,3.,"E [eV]","Momentum4");
Hist->fill1(4019,"19_E2_Neon4-large",eE2,1.,"Electron Energy Hit
    2",300,0.,1200.,"E [eV]","Momentum4");
Hist->fill1(4020,"20_E3_Neon4-small",eE3,1.,"Calculated Electron
    Energy Hit 3",100,0.,3.5,"E [eV]","Momentum4");
```

```
Hist->fill1(4021,"21_E3_Neon4-large",eE3,1.,"Calculated Electron
    Energy Hit 3",300,0.,1200.,"E [eV]","Momentum4");
Hist->fill1(4022,"22_kE123_Neon4-large",kE123,1.,"Calculated
    Electron Energy",300,0.,1200.,"E [eV]","Momentum4");

Hist->fill1(4023,"23_r1tof_Neon4",r1tof,1.,"Recoil TOF Neon 4+
    (3-ehit)",200,21872.,22172.,"TOF [ns]","Momentum4");
Hist->fill2(4024,"24_r1x_r1tof_Neon4",r1tof,r1x,1.,"Recoil x-fish
     Neon 4+ (3-ehit)",400,21872.,22172.,"r1tof [ns
    ]",200,-5.,20.,"x-position [mm]","Momentum4");

Hist->fill1(4025,"25_e1tof_Neon4",e1tof,1.,"e1tof Neon 3+ (3-ehit
    )",200,0.,120.,"e1tof [ns]","Momentum4");
Hist->fill1(4026,"26_e2tof_Neon4",e2tof,1.,"e2tof Neon 3+ (3-ehit
    )",200,0.,120.,"e2tof [ns]","Momentum4");
Hist->fill1(4027,"27_e3tof_Neon4",e3tof,1.,"e3tof Neon 3+ (3-ehit
    )",200,0.,120.,"e3tof [ns]","Momentum4");

Hist->fill2(4028,"28_e1tof_e2tof_Neon4",e1tof,e2tof,1.,"e2tof vs
    e1tof Neon 3+ (3-ehit)",400,0.,120.,"e1tof [ns]",400,0.,120.,"
    e2tof [ns]","Momentum4");
Hist->fill2(4029,"29_e2tof_e3tof_Neon4",e2tof,e3tof,1.,"e3tof vs
    e2tof Neon 3+ (3-ehit)",200,0.,120.,"e2tof [ns]",400,0.,120.,"
    e3tof [ns]","Momentum4");
Hist->fill2(4030,"30_e3tof_e1tof_Neon4",e1tof,e3tof,1.,"e3tof vs
    e1tof Neon 3+ (3-ehit)",400,0.,120.,"e1tof [ns]",400,0.,120.,"
    e3tof [ns]","Momentum4");
```

```
}

//************************************** end of analysis part
    ************************************************
//
//-------------------------------------------------------------------------------------------------


if(WriteNTuple) {
Hist->NTupleD(9999,"Data","Ne2","r1x:r1y:r1tof:r1flag:e1x:e1y:
    e1tof:e1flag:e2x:e2y:e2tof:e2flag:e3x:e3y:e3tof:e3flag:
    bunch_cleaning", 32000, NTupleData);
Ueber->eventswritten++;
}

if(parameter[57]>0.5) {
if(Ueber->eventswritten > unsigned int(parameter[56]+0.1)) {
Ueber->start_new_file = true;
Ueber->eventswritten = 0;
Hist->Reset();
} else {
Ueber->start_new_file = false;
}
}       else {
Ueber->start_new_file = false;
}
return 0;
```

```
}
```